INELASTIC H-COLUMN PERFORMANCE AT HIGH AXIAL LOADS

A Thesis submitted for the degree of
Doctor of Philosophy
in the Faculty of Engineering of the
University of London

by

Tapan Kumar Sen, B.Tech., M.C.E.

Imperial College of Science & Technology
London

January 1976

To My Parents

ABSTRACT

As very little information, experimental or theoretical, was available about elasto-plastic behaviour of columns at high axial loads of 0.6 to 0.9 times the squash load, a limited full scale test programme on beam columns was undertaken. This was then followed by a theoretical study. The problem investigated is that often encountered in practice of major axis asymmetrical bending with minor axis imperfections.

Ultimate load tests were carried out on a series of 8 ins x 8 ins (203 mm x 203 mm) Universal Columns to investigate their out-of-plane stability at high axial loads under a major axis moment applied at one end only. The tests covered columns of short to intermediate slenderness on which high axial loads could be sustained and in effect explored plastic hinge rotation capacity in this load range. The load path followed in most tests was full axial load applied first, followed by major axis end moment to failure. Except for the one test on a longer column (weaker axis slenderness ratio = 74) the columns were maintained in a pin-ended condition about the minor axis.

All the columns were of grade 50B steel (nominally 340 N/mm^2) and the three tests on the short columns (weaker axis slenderness ratio = 45) showed that they remained stable in-plane while undergoing plastic hinge type deformations towards one end of the column. The tests on the medium slenderness (weaker axis slenderness ratio = 60) showed that minor axis imperfections significantly influenced behaviour. The columns failed by the formation of a biaxial hinge at about the third point of the column after which they became unstable out-of-plane. The series of tests indicated that there is a slenderness limit at high axial loads for columns to remain stable in plane and which could perhaps be equal to 55 (weaker axis slenderness).

The theoretical work covered torsional effects and asymmetric bending. Numerical methods were adopted and a general biaxial program in Fortran IV language was developed covering initial curvature, residual stress and a non-linear stress-strain curve.

The theoretical model was utilised to highlight the important parameters influencing lateral instability. This included exploring slenderness limits for unbraced columns with normal levels of initial imperfection subjected to high axial loads and one major axis bending moment so that lateral torsional instability is avoided. The particular results obtained are compared with one set of existing charts (BCSA Publication No. 23).

The beneficial effects of minor axis restraint are well known and an attempt has been made to explore this aspect quantitatively. The results obtained have been compared again with the above-mentioned publication and conclusions drawn.

ACKNOWLEDGEMENT

The work reported in this thesis was carried out under the active supervision and guidance of Dr. A.R. Gent, to whom the author is grateful. His encouragement and expert advice throughout was a source of inspiration.

The author is indebted to Professor S.R. Sparkes, formerly Professor of Engineering Structures, for the opportunity to work on the project and generously making available all the laboratory facilities.

A special tribute must be paid to the skill, patience and help of Mr. E.J. Secker, working under the direction of Mr. J. Neale, in carrying out the full scale testing reported in this thesis.

The author would like to take this opportunity of expressing his deep sense of gratitude to the Secretary, Ministry of Education, Government of India, for sponsoring the author's research at this College. The author would also like to express his gratitude to Professor S.R. Sparkes for making available the supplementary grant and to Professor B.G. Neal for its continuation.

The author has had the benefit of many discussions with colleagues who freely gave their time over the period of this study, including Dr. K.S. Virdi, Dr. M. Raz-Nahan, Mr. F.M. Moolani and Mr. A.M. Joharzadeh.

The generous help offered by Mr. S.K. Guha in preparing the diagrams is gratefully acknowledged.

Thanks are also due to Miss Joyce Gurr who carefully processed the photographs and the Computer Program Advisory Service for their valuable suggestions.

Finally a special word of thanks is reserved for Miss E. Niblock for typing the thesis.

CONTENTS

		Page
Abstract	....	3
Acknowledgements	....	5
CHAPTER I	INTRODUCTION	
1.1	General	9
1.2	Outline of Previous Theoretical Work	10
1.3	Summary of Research and Formulation of the Problem	21
CHAPTER II	EXPERIMENTAL PROGRAMME	
2.1	Introduction	24
2.2	Details of Test Programme	24
	2.2.1 Details of Cross-Section	24
	2.2.2 Parameters Varied	24
	2.2.3 Parameters Not Varied	25
2.3	Material Tests	25
2.4	Load Path Followed During Tests	26
2.5	Outline of the Loading Rig	27
	2.5.1 Details of the Loading Rig	28
2.6	Note on Support Conditions	29
2.7	Instrumentation	30
	2.7.1 The Load Cells	30
	2.7.2 The Deflection Rig	32
	2.7.3 Recording End Rotations	32
2.8	Test Procedure	33
2.9	Units Used	34
2.10	Test Results and Comments	34
	2.10.1 Mode of Failure	35
	2.10.2 Columns A1, A2 and A3 (Group A)	35
	2.10.3 Columns B1, B2, B3 and B4 (Group B)	37
	2.10.4 Column C1 (Group C)	38
2.11	Conclusions	40
CHAPTER III	THEORY: MOMENT-THRUST-CURVATURE RELATIONSHIPS	
3.1	Introduction	43
3.2	Assumptions	43
3.3	Steel Stress-Strain Curve Adopted	45

		Page
3.4	Residual Stresses	45
3.5	Expressions for Moment-Thrust-Curvature Relations	47
3.6	Computational Procedure	48
CHAPTER IV	THEORY: FAILURE LOADS OF COLUMNS AND GENERAL EQUATIONS OF EQUILIBRIUM	
4.1	Introduction	51
4.2	General Computational Principles	51
	4.2.1 Outline of Computational Procedure	53
4.3	General Equations of Equilibrium	55
	4.3.1 Assumptions	55
	4.3.2 Elastic Columns	55
	4.3.3 Restrained Elastic Columns	59
CHAPTER V	THEORY: INELASTIC RESTRAINED COLUMNS	
5.1	Introduction	61
5.2	Inelastic Stiffnesses	61
5.3	Computation of Torsional Resistance	63
5.4	Inelastic Form of Equations of Equilibrium	66
5.5	Finite Difference Form of Equations	68
5.6	Method of Solution of Equilibrium Equations	69
5.7	Convergence Criteria	71
5.8	Computational Procedure	72
CHAPTER VI	COMPARISON WITH THEORETICAL AND EXPERIMENTAL RESULTS	
6.1	Introduction	75
6.2	Verification of the Moment-Thrust-Curvature Relations	76
6.3	Verification of the Biaxial Bending Equations in the Elastic Range	76
6.4	Comparison of Theoretical and Experimental Results	77
CHAPTER VII	APPLICATION, DISCUSSION AND CONCLUSION	
7.1	Introduction	85
7.2	What Constitutes LTB Failure?	85
7.3	Ultimate Load Design Predictions	91
	7.3.1 Exploratory Calculations	92
	7.3.2 Comparison with Deisgn Charts (BCSA Publication No. 23)	93

		Page
7.4	Effect of Minor Axis End Restraint	95
	7.4.1 Ultimate Load Design Predictions with Minor Axis Restraint	97
7.5	Concluding Remarks on the Experimental Programme	98
	7.5.1 Conclusion and Summary of Theoretical Work	99
Appendix A	....	101
Notations	....	104
Bibliography	....	107
Tables I - X	....	111
Figures 2.1 - 7.15	....	120.

CHAPTER I
INTRODUCTION

1.1 General

Research activity has been very intense in the field of inelastic column stability for the past three decades and various numerical methods have recently been developed for predicting the strength and behaviour of H-columns subjected to axial load and strong axis bending moments[20],[21],[24]. These methods assume that the out-of-plane deformations and hence lateral instability can be effectively prevented by lateral bracing so that deformations are confined in the plane of the applied moments. Design procedures for this type of building column have been formulated[22],[23], and apply to columns subjected to a wide range of axial loads.

However, most columns in practice are not braced against lateral deformations. In such cases their ultimate load behaviour, involving the magnification of minor axis imperfections in the presence of axial load, is likely to be affected by lateral buckling or lateral torsional buckling, a type of instability which involves twisting and out-of-plane deformations. Columns with high axial loads are more likely to be affected by this type of instability, but design aids for such unbraced columns are few[16],[17],[36]. There seems to be very little information, experimental or theoretical, about elasto-plastic behaviour in the high axial load range, i.e. columns subjected to 0.6 to 0.9 of squash load. A better understanding of elasto-plastic behaviour in this high axial load range is necessary for more rational and efficient design of columns. The present study seeks to achieve this.

In the past, research in the field of inelastic stability was inhibited as an exact theoretical elastic-plastic solution of the biaxially loaded column problem is virtually impossible. This explains the lack of adequate design recommendations and charts for such columns. Use of numerical methods along with high speed digital computers has now made progress possible.

The study reported herein may be regarded as an attempt to explore design limits for unbraced columns with normal levels of initial imperfection subjected to a high axial load and one major axis bending moment so that lateral torsional instability is avoided. The particular results obtained are compared with one set of existing charts[16] which were calculated on the basis of the severe limitation of restricting spread of plasticity along the member by the condition that the yield stress shall not be reached near the centre of column length. However, before the problem considered is presented in greater detail, a brief review of theoretical work is outlined.

1.2 Outline of Previous Theoretical Work

In the space available it would be impossible to present a comprehensive survey of research on steel columns because of the enormous quantity of work which has been done. A very brief outline of relevant inelastic work will only be given here.

In order to avoid confusion about the problems to which methods discussed in this chapter are applicable, it is desirable to define clearly the phenomenon of 'in-plane buckling' and 'lateral buckling'. In-plane buckling is considered to have taken place when the plane of actual buckling is identical with the plane of the applied moment or eccentricity or the plane of lateral forces. When buckling occurs out of plane to the plane of the applied moments it is termed lateral buckling.

The first to consider successfully the in-plane buckling loads of eccentrically loaded inelastic columns as a stability problem was von Karman who in 1910 gave a general and exact theory for the determination of the buckling loads of such columns loaded beyond the material's elastic limit. He solved the problem of a rectangular column with equal eccentricities of loading at each end. This was an outstanding contribution and consequently was to form the foundation of considerable future research including this thesis.

Since von Karman's work, Westergaard and Osgood in 1928 provided a simple solution to eccentrically loaded compression members. The method is based upon the same equations as were used by von Karman but assumes the deflected centre line of the column to be part of a cosine curve, thereby simplifying von Karman's method without impairing the practical accuracy of the results.

Jezek in 1934 gave an analytical solution to the in-plane buckling problem employing bilinear stress-strain curve for steel and showed that the results agreed well with the real stress-strain solution.

An excellent account of the development of the theory of eccentrically loaded inelastic columns covering the further work since von Karman referred to briefly above is given by Bleich[1].

Several years later Neal[2] in 1950 provided solutions to the problem of the inelastic lateral torsional buckling of rectangular beams under uniform bending. Wittrick[3] extended the work to include strain hardening in the computations.

About a decade later Galambos[4] in 1959 provided solutions for the inelastic lateral torsional buckling of wide flange beam columns under uniaxial uniform bending. Lateral torsional buckling of H-columns is complicated by the occurrence of twisting and warping of the column cross-section. Analytical solutions for inelastic lateral torsional buckling of columns are also difficult to obtain owing to the non-linearity of the governing differential equations as may be seen in Chapter V, equations (5.19)-(5.21). In Galambos' work the effect of residual stresses was considered. Unlike beams subjected to equal end moments, the bending and torsional stiffnesses of a beam column in the inelastic range vary along its length because of the variation of moments along the length due to primary deflections in the presence of axial load. For simplicity Galambos assumed in his solutions a beam column of uniform stiffness, the magnitude of which was equal to that at the column ends. An upper bound solution was thus achieved. It would have been possible to obtain a lower bound solution by evaluating the moments along the length of the

column. However to evaluate these, recourse would have had to be taken to some form of numerical technique to establish the equilibrium shape of the beam column under a given loading. This equilibrium shape of the beam-column in the inelastic range may be determined by a number of iterative methods. In the United States the Column Deflection Curve method[5] has been widely used to find equilibrium shapes in the plane of bending as would have been necessary in this case.

More accurate solutions for lateral torsional buckling of beam-columns under major axis bending were then developed in the United States by Galambos and Fukomoto[6]. In this work they have reported the solution for the one end moment case, i.e. the ratio of end moments $\beta = 0$. The governing equations of bending and torsion were derived for this case and an eigen value solution of lateral torsional buckling was achieved. The eigen value approach is discussed more fully later in Chapter VII. The finite difference technique was used to solve these equations for the critical moment which indicated initiation of lateral torsional buckling. The stiffness terms occurring in the finite difference equations were constant as long as the member was elastic. With yielding these terms changed their value and because yielding was a function of the bending moment distribution along the length of the member, the stiffnesses were not the same at every pivotal point. The solution of the problem was one of trial and error. For a given beam column an axial force and an end moment was specified first. The corresponding deflected shape and moment diagram was then computed with the help of CDC's (Column Deflection Curves). The inelastic regions of the column were then determined and from this knowledge the coefficients of the finite difference equations. If the originally chosen combination of axial load and end moment were also the critical combination for the start of lateral torsional buckling, then the determinant of the coefficients of the finite difference equations would be equal to zero.

Employing a similar technique to that outlined above Lim and Lu[7] studied the occurrence of inelastic lateral torsional buckling of laterally unsupported beam columns restrained against weak axis bending and warping at the column ends. Both the tangent modulus and the reduced modulus solutions were provided. The same technique was extended to cover the case of inelastic lateral torsional buckling problems in continuous beam columns with warping and weak axis bending restraints at the joints.

The research work briefly summarised above was all restricted to uniaxial bending of the beam columns and the problems of lateral torsional buckling were treated as eigen value problems.

Less work has been done on biaxial bending and very few solutions have been reported for biaxial eccentric loading covering torsion.

The first general solution for pin-ended biaxially loaded columns was reported by Birnstiel and Michalos[8] and was based on a successive trial and correction procedure. This procedure was improved by Harstead, Birnstiel and Leu[9] and a systematic correction procedure introduced. The analytical procedure requires the calculation of increments of internal or resisting moments and axial force corresponding to changes of strain distribution over the cross-section at a particular station. This was achieved by dividing the column cross-section into a number of small elements. The changes in resisting moments and axial force were computed by summing up the effects of all these small elements.

Successive equilibrium positions of the biaxially loaded column were determined from each incremental increase in the deformations on the column. The axial strain, the bending curvatures about the two principal axes and the twisting curvature were chosen to be the controlling deformations. The external bending and twisting moments and the axial force were unknown at the start. A trial and error procedure had to be followed to obtain the equilibrium position of the column corresponding to each increment of deformations. The total increment of strain distribution over the

section was assumed to be the sum of the small increments of strain caused by the bending and twisting curvatures and the axial strain. The total strain at each point of the section was then obtained by superimposing the total strain increment on the previously established strain corresponding to an equilibrium configuration. Curvature and strain relationship was assumed to vary linearly, i.e. plane sections remain plane after loading. The superposition of each incremental strain distribution resulted in a change in stress distribution over the section and also an additional deflection of the column. The initially assumed incremental deformations were adjusted at this stage until equilibrium was achieved, and hence the new deflected shape determined. In the analysis the effect of shearing stresses on the plastic yielding of the material was neglected as in all work to date by subsequent authors and only the normal stress in the axial direction was considered. The main feature of this work may be outlined as follows:

(a) The analysis was for pin-ended biaxially loaded columns with equal eccentricities of load at each end producing symmetrical bending. Extension of the work to include bending restraints and cover asymmetrical bending would involve major changes in the computational scheme.

(b) The stress-strain curve assumed was bilinear, i.e. elastic-perfectly plastic. Residual stresses were however included in the analysis.

(c) The shift of the position of the shear centre due to progressive yielding was considered. The location of the shear centre was based on the assumption that imposition of the warping strains did not result in any change of axial force or any bending moment about any axis. The external and internal torsional moments were computed about this shear centre and torsional equilibrium satisfied.

(d) The unloading path of the load deformation curve was obtained.

Theoretical work on restrained columns under symmetrical biaxial bending was first reported by Milner[10]. A finite difference scheme was employed to solve the differential equations of equilibrium. Exact analytical expressions for evaluating the internal forces at a particular cross-section were derived. This was possible because a bilinear stress-strain curve (i.e. elastic-perfectly plastic) was assumed and the stress blocks occurring due to a particular strain distribution over the cross-section could be evaluated analytically. Solution of these internal forces involved three non-linear algebraic equations and these were solved iteratively using the Newton-Raphson algorithm. The column length was divided into a number of small divisions. The external and internal forces were computed at each of these divisions to satisfy equilibrium. Finite difference expressions for curvature were based on these subdivisions. The standard Newmark iterative procedure was used to obtain the initial deflected shape neglecting torsional deformations at this stage. Once the initial deflected shape was obtained, torsional calculations were introduced separately to maintain torsional equilibrium. The position of the shear centre of the partially yielded cross-section was determined approximately. The internal and external torsional moments were computed about this approximate shear centre.

Subsequent deflected shapes were obtained by incrementing curvature at the mid-height of the column. From the finite difference expressions a trial deflected shape of the column was obtained and external and internal moments compared. Corrections were applied to the central curvature until equilibrium within specified accuracy was obtained and this iteration was again based on Newton-Raphson algorithm. As pointed out earlier, torsional calculations were introduced after obtaining the major and minor axes deflected configuration. Thus torsional calculations were always one step behind the basic equilibrium shape calculations. Milner's work was different in another aspect from Birnstiel's work, briefly reviewed earlier, in that the column was not subjected to proportional loading. Also, amongst other things, the influence of elastic unloading and strain hardening were investigated. The main features of this work were:

(a) The analysis was for biaxially loaded restrained columns producing symmetrical bending about both axes. The loading was not proportional.

Extension of the work to include asymmetrical bending would involve major modifications in the computational scheme. The procedure of incrementing curvatures at mid-height of the column to obtain subsequent deflected shapes is not applicable to asymmetrical bending. A different numerical approach would have to be adopted.

(b) The stress-strain curve assumed was bilinear (i.e. elastic-perfectly plastic). The analytical method developed to evaluate the internal forces could not be extended to include residual stresses and these were not considered in the computations.

(c) The torsional calculations were very approximate due to two reasons:

(i) torsional calculations were one step behind equilibrium shape calculations about the other two axes.

(ii) the position of the shear centre was determined approximately

(d) The unloading path of the load deformation curve was obtained.

A detailed review of existing literature covering theoretical and experimental work on biaxial bending of columns has been presented by Chen and Santathadaporn[11]. This gives a comprehensive survey of research on the inelastic behaviour of biaxially loaded columns up to 1968. Some of the numerical techniques adopted for solution were also briefly discussed.

A more approximate method of analysis for biaxially loaded restrained columns has been described by Santathadaporn and Chen[12]. The solution was again for symmetrical loading. The deflected shape of the column was assumed to be a combination of a sine function and

a second order polynomial. The analytical procedure required calculation of the internal forces including torsional moments of the elastic-plastic cross-section. For this the column cross-section was divided into a number of small elements and numerical integration was performed by summing up the effect of all the elements. The equations were expressed in a different form and were derived for the rate of change of internal forces. It is convenient to interpret rate of change of forces as variables denoting infinitesimal increment. Similarly the rate of change of external forces at mid-span of the column were developed. Yielding and instability effects were incorporated in the tangent stiffness matrix[13] which can be interpreted as the tangent of the load deformation curve. The actual solution process was iterative and equilibrium was only satisfied at mid-height of the column. The tangent stiffness method may be viewed as a modification of the widely-used Newton-Raphson iterative algorithm for solution of a system of 'n' non-linear equations involving 'n' variables and utilises the same underlying concepts for evaluating the correction vectors. They are thus similar in a philosophical sense. The main feature of this approximate method are as follows:

(a) The analysis was for biaxially loaded restrained columns producing symmetrical bending only.

(b) The deflected shape of the column was assumed to be a combination of a sine function and a second order polynomial. Extension of the method to cover asymmetry is virtually impossible. Equilibrium was only satisfied at mid-column height.

(c) Boundary conditions prevailing due to elastic restraints at the ends were not properly satisfied and the failure loads obtained were slightly different to other solutions. It was reported, however, that the failure loads obtained were slightly lower than the more accurate theory developed by Harstead, Birnstiel and Leu[9].

(d) The stress-strain curve was assumed to be bilinear i.e. elastic-perfectly plastic.

(e) Torsional calculations were approximate as the shift of the shear centre due to yield was neglected. Also the warping torsional rigidity was assumed to be directly proportional to the ratio of the remaining elastic area to the total area of the cross-section.

(f) The unloading path of the load-deformation curve was obtained.

The Newton-Raphson iterative approach was extended to solve the general case of asymmetrical biaxial bending of pin-ended columns by Virdi[14]. The theory was developed in connection with studies on composite concrete columns, but is equally applicable to bare steel columns. However, it did not cover torsional deformations.

For evaluating the internal forces the column cross-section was subdivided into a number of small elements as was adopted by Harstead, Birnstiel and Leu[9]. Moment-thrust-curvature relationships were computed by summing up the effects of all the small elements and using an interpolation technique. In computing these relationships the exact nature of the stress-strain curve was accounted for by idealising it as a multilinear curve. Residual stresses could also be incorporated.

A finite difference scheme was again employed to obtain the deflected shape. A set of trial deflections was assumed along the column length and curvatures computed. Moment-thrust-curvature relations were then computed for the given axial load. External moments were then calculated and compared with the internal moments. The solution process was iterative and the Newton-Raphson correction procedure was set up at this stage for obtaining the new deflected shape. Subsequent deflected shapes were obtained for increasing axial load applied eccentrically. The main features of this work were:

(a) The solution was for a general case of asymmetrical biaxial bending of pin-ended columns. The program was modified later to include end restraints.

(b) Exact stress-strain relationships were used for computing the moment-thrust-curvature relationships.

(c) Torsionsal stability was not considered.

(d) Calculation of the unloading path was included subsequently.

This numerical technique may be extended to include torsional calculations. But a linear iterative technique was adopted in the study reported in this thesis and this is discussed in Chapter IV, Section 4.2.

The important aspects of the major computational efforts in biaxial bending to trace the complete load-deformation path up to collapse, discussed above, are now summarised below:

Details of Numerical work \ Authors	Harstead, Birnstiel and Leu[9]	Milner[10]	Santathadaporn and Chen[12]	Virdi[14]
End condition	pin-ended	restrained	restrained	restrained (modified subsequently)
β value	$+1$ symmetrical bending	$+1$ symmetrical bending	$+1$ symmetrical bending	$\neq +1$ asymmetrical bending
Torsional calculations	accurate shift in shear centre considered	approximate	approximate	not included
Stress-strain curve used	bilinear	bilinear	bilinear	multi-linear
Unloading path	reported	reported	reported	reported (modified subsequently)

All the numerical procedures discussed above have been programmed on digital computers and the correlation with experiments whenever reported have been largely favourable. For various reasons, including economic factors, very few parametric studies have been undertaken and very little design data for predicting column behaviour is available.

Horne[15] has provided some design data. In 1964 he published theoretical solutions based on modification to an elastic analysis for beam columns subjected to any end moment ratio with both ends free to warp and simply supported about the strong and weak axes. The stability criteria were that plastic hinges may form at either end of the column but that yield stress must not be reached at mid-column height. Governing equations for bending and torsion involving minor axis imperfections were reduced to a set of six non-linear equations. These were solved iteratively to give the maximum safe axial load in terms of major and minor axis slenderness ratios, the torsional parameter T[15] and the end moment ratio β for which the above mentioned stability criteria were satisfied. The theory is based however on equivalent moment approach which assumes that the behaviour of a beam column under axial load P and two different end moment ratios about the strong axis M_x' and M_x'' is the same as a beam column subjected to an axial load P and a uniform strong axis moment M_x'/m where m is a function of the end moment ratio. The presence of the residual stresses were not considered. Extensive sets of design charts were produced based on this approach[16].

In a more recent work Wood[17] has suggested that an exact ultimate load analysis of continuous elastic plastic columns restrained by minor axis beams against buckling, is in effect intractable because of the large number of independent variables involved. He has proposed a 'semi-intuitive' approach to design of elastic plastic columns restrained by elastic minor axis beams in building frames. The major axis beams are designed by plastic theory and the minor axis beams are designed to remain elastic. In Wood's design method plasticity is allowed in columns. While no attempt is made to outline precisely the plastic zones, their extent is controlled in order

to limit the reduction in stiffness of the column. Control on the plastic zone is achieved by limiting the applied major axis end moment, so that only one flange is fully plastic at a particular cross-section. The axial collapse load is estimated on the basis of the stiffness of the elastic plastic column. This approach is analogous to the concept of deteriorated elastic critical load, a concept originally suggested by Wood[18] for calculating the critical load of elastic plastic frames. The collapse load is defined by the formula

$$P = C' \cdot R'_x \cdot P_E$$

where C' depends on the minor axis beam/column stiffness ratio and may be read from charts ($1.0 < C' < 4.0$).

The stiffness reduction coefficient R'_x depends on the magnitude of the ratio of end moments and the axial load. P_E is the Euler critical load about the weaker axis. Intuitive formulae are proposed by Wood for the calculation of R'_x coefficients

1.3 Summary of Research and Formulation of the Problem

Although a substantial amount of work both experimental and theoretical has been done on the problem of bare steel columns under general conditions of loading, relatively little information is available about column behaviour in the high axial load range, i.e. columns subjected to 0.6 - 0.9 times the squash load.

A recent review[19] of the large number of eccentrically loaded column tests which have been performed on rolled sections showed that very few of these gave information regarding column behaviour in this range of axial loads. Theoretical results presented from previous computer programs developed elsewhere gave no indication regarding lateral torsional instability and end deformation capacity at high axial loads.

Most of the tests performed to date have invariably been under conditions which preclude high axial loads. The beam colums were loaded at such eccentricities that the resulting magnitude of

end moments ruled out any possibilities of high axial loads being sustained. The results were also not typical from another aspect. For experimental convenience the lightest rollings of the particular column size being tested were mostly selected. The sections were thus torsionally weak and prone to local buckling.

Due to the paucity of results and information available the limited full scale test programme on beam columns reported in this thesis was undertaken. The primary purpose was to explore the ultimate end moment deformation capacity and column stability in the high axial load range. The range of slendernesses selected covered the short to intermediate range. Torsionally strong as well as torsionally weak sections were included. All the tests were carried out under the condition of major axis moment gradient ($\beta = 0.15$). This was considered to be more typical of load conditions in practice, than the extreme situation of equal end moments applied at both ends ($\beta = + 1.0$).

The tests were also of interest from the point of view of exploring the validity of the 'short column' concept at high axial loads for H-sections. In early work on the steel section of Bridge Code BS.116 an attempt was made to frame design provisions which would, amongst other things, permit advantage to be taken of the high ultimate load capacity of many beam columns. The tests were thus relevant to BS.116.

To complement the experimental study, theoretical work was undertaken to develop a program to correlate with the experimental results. Torsional effects were included. The theoretical model developed was then utilised to highlight the important parameters influencing lateral instability. This included developments of typical column curves for giving slenderness limits which preclude lateral instability.

The beneficial effects of restraints from minor axis beams on column stability have long been recognised. These effects have been incorporated in the semi-intuitive column design approach by Wood[17] which was briefly summarised in the preceding section.

Although some studies on restrained inelastic columns[10], [12] have been reported, there seems to be no clear indication of the range of slendernesses (in combination with axial loads) in which end restraints are particularly helpful. Also the extent of practical benefit to be derived is not clear. An attempt has been made to explore this aspect quantitatively. The increase in permitted slenderness ratios with end restraints which preclude lateral instability for a particular column range are compared with a predicted column curve with no end restraints.

All the predicted typical column curves are compared with the curves in BCSA Publication No. 23[16] presented by Professor Horne. Professor Horne's design curves are seen to be conservative. Some ideas are presented in an attempt to clarify the vexing question whether the column behaviour (load deformation characteristics) in presence of imperfections represents in-plane failure or lateral torsional buckling failure. It appears that there is an intermediate range in which it is difficult to distinguish the type of failure.

CHAPTER II

EXPERIMENTAL PROGRAMME

2.1 Introduction

This limited full scale test programme on eccentrically loaded steel columns was originally proposed to explore column behaviour at high axial loads as discussed in the previous chapter. They were intended to fill in a gap in the available results for eccentrically loaded columns.

2.2 Details of Test Programme

Eight full scale tests were conducted on 8 ins. - 8 ins. (203 mm - 203 mm) Universal Column sections of varying lengths and weights. The details of the test programme are summarised in Table I.

All the tests were under minor axis pin-ended condition and major axis moment gradient ($\beta = 0.15$), except the last test (column C1) in which minor axis restraint was introduced. The sequence of columns in Table I also reflects the chronological order of the test programme. The columns were all tested to establish their load deformation characteristics in the inelastic range.

2.2.1 Details of Cross-section

The U C sections which were tested are:

i) 8 ins - 8 ins @ 48 lb (203 mm - 203 mm @ 71 Kg/m)
ii) 8 ins - 8 ins @ 35 lb (203 mm - 203 mm @ 52 Kg/m)
iii) 8 ins - 8 ins @ 31 lb (203 mm - 203 mm @ 46 Kg/m)

2.2.2 Parameters Varied

The parameters which were varied during the tests are:

i) Slenderness ratio
ii) Axial load
iii) Torsional stiffness - i.e. T value[16] or Wagner pure

torsion critical stress σ_w

where $T = \frac{AGK_T}{Z_x^2}$

and $\sigma_w = GK/Ip$

A = area of cross section

G = elastic shear modulus (5000 tons/sq. in.)

K_T = the St. Venant torsion constant

Z_x = elastic modulus of section about the major axis

Ip = Polar moment of inertia of the section

iv) Minor axis restraint

Columns of three different lengths - 90 ins., 123 ins and 153 ins. were tested. These lengths were chosen to cover the range of slenderness ratios at which high axial loads could be sustained. Specimens of the same length were tested under varying axial loads.

2.2.3 Parameters not varied

The parameters which were not varied are:

i) The major axis moment gradient (the ratio β).
It was equal to 0.15 in all the tests.

ii) Major axis restraint condition.
All the tests were under pin-ended conditions about the major axis.

2.3 Material Tests

Tensile test specimens were taken from extra lengths of the rolled sections to obtain typical stress-strain properties. Four specimens were cut from each of the cross-sectional sizes shown in Figure 2.13. The specimens were 178 mm long and of diameter 12 and 5 mm. This choice was dictated by the jaws available on the tensile testing machine. The test results are shown in Figures 2.14 - 2.16.

It is of interest to note that except for the 8 ins. - 8 ins. @ 31 lb section, the stress-strain curves showed no distinct yield point and immediate strain hardening. Also the stress-strain properties were different for the flanges and webs. In the theoretical work reported later, these exact stress-strain curves as obtained experimentally have been used for the computations. An extra check on the material properties was made in the case of column B2 by cutting a test specimen from the actual column from the smaller moment end after the test. Residual stresses were not measured as they are unreliable being often altered locally by cold straightening.

2.4 Load Path Followed During Tests

All the columns (except columns B4 and C1) were tested under full axial load applied first followed by end moment to failure.

After the first six tests it was decided to test column stability under a different load path as discussed later in Section 2.10.3. Columns B4 and C1 were therefore tested in the following manner:

i) Moderate axial load applied first

ii) Major axis moment increased holding the axial load constant

iii) With the end joint rotation held approximately constant the axial load is increased to failure

Column C1 however had minor axis restraint. The load path followed for these two tests is also shown in Figures 2.33 and 2.39.

2.5 Outline of the Loading Rig

The loading rig basically consisted of an arrangement whereby the axial load was applied first by means of a large capacity hydraulic jack. The end moments were applied through a moment arm and a separate hydraulic jack. The pin-ended condition of the tests was achieved by applying the load through bridge bearings. Two spherical PTFE Glacier bearings were used for this purpose.

Photographs showing a general view of the entire loading rig are reproduced in Figures 2.1 and 2.2. The tie rod arrangement to take up the reaction was built around the two concrete blocks at the ends. To produce the major axis moment gradient desired during the tests, another tie rod arrangement was devised. Minor axis flexing arms were provided to flex the bearings and test the stability of the columns about the minor axis during tests and the arrangement has been reproduced in Figure 2.3. A small minor axis moment was always maintained during the tests for this purpose. Loads and moments in the inelastic range were measured directly using purpose-designed load cells made of Maraging steel attached to the ends of the columns as may be seen in Figures 2.3 and 2.5. The elastic limit of the Maraging steel was around 100 tons/in^2. Thus the load cells were well inside the elastic range during the failure stages of the test columns. Also any friction that existed in the jack or spherical bearings did not affect the test results. A schematic diagram of the loading rig is shown in Figures 2.7 and 2.8.

The columns were all tested in the horizontal position for the following reasons. Firstly a vertical rig was not available to test columns up to twelve feet in length, and it would have been expensive to construct one. Secondly, a horizontal position is very convenient regarding instrumentation, recording and overall observation.

2.5.1 Details of the Loading Rig

Two concrete blocks of dimensions 5 ft. - 2 ft. - 2 ft were used at each end to provide end supports and may be seen in Figures 2.1 and 2.2. Eight tie rods of high tensile steel material and 1 1/2 inches diameter extending over the entire length of the rig, were used to take up the loading of the jack. The tie rods can be seen in Figures 2.1, 2.2, 2.7 and 2.8. They were held in place by two thick metal plates positioned across the back of the concrete block surface (Figure 2.9). The details of the jack end are shown in Figures 2.3, 2.4 and 2.9. These details are basically similar at the other end, as shown in the photographs reproduced in Figures 2.5 and 2.6.

By using eight tie rods it was possible to limit the maximum extension of these, when the loading was applied, to a small value (approximately 1/2 in.). The concrete blocks were so positioned that they could slide on the floor and accommodate the extension of the tie rods. To ensure that the concrete blocks moved in the desired direction of applied jack loading only, guide bars were placed along the length of the concrete blocks which prevented any lateral movements. These guide bars were firmly fixed to the laboratory floor by means of tensioned floor bolts.

As mentioned earlier, the pin-ended condition of the tests was simulated by applying the load through two spherical PTFE Glacier bridge bearings. The diameter and radius of curvature of the bearings were 15 inches. At the main hydraulic jack end the bearing was connected to the face of the ram by means of two 1 inch thick square plates. The square plates, which were fixed to the bearing and the face of the ram, were bolted together. The details are shown in Figure 2.9.

As shown in Figures 2.1, 2.2, 2.6 and 2.8, the major axis moment was applied by a separate hydraulic jack of 60 tons capacity. The heavier moment arm was built up by welding 55 in. - 8 in. - 1 5/8 in thick steel plates to a square billet of size 12 in. - 12 in. - 4 in. thick. The billet was bolted to the bearing. Some idea of the details may be obtained from the photograph showing the heavier moment arm and reproduced in Figure 2.5.

The minor axis moment arm at each end was provided by a 4 in. - 4 in. tube section welded to the square billets mentioned above. This is shown in Figures 2.4 and 2.5. These minor axis moment arms were primarily provided so that the column could be flexed about its minor axis. This ensured that the bearings did not restrain the column about its minor axis in any way. A small positive moment was always maintained during the tests.

The major axis moment gradient required for the tests was achieved through another tie rod arrangement as shown in Figures 2.1, 2.2 and 2.7. This tie rod was provided with knuckle joints (joints providing freedom of movement about X and Y axes but not about Z axis). This system of applying moments was adopted to make the system self-equilibrating, i.e. to make sure that the PTFE bearings were not required to resist any lateral shear. It is believed that (from the trial runs conducted before the present turnbuckle arrangement was introduced) the performance of these bearings was adversely affected if called upon to resist lateral shear.

2.6 Note on Support Conditions

The ends of the columns (except column C1) were pin-ended and supports considered to be prevented from translating with respect to each other. The twist at the ends was also considered to be prevented. The knuckle joints were provided for this reason. Great care was taken to achieve these conditions as far as possible. The effective pin-ended length of the column was the distance between the centre of rotations of the bearings. This centre of rotation was located in the middle of the load cell mentioned earlier and, as may be seen from the construction of the rig in Figures 2.4, 2.5 and 2.6, warping was restrained for all practical purposes at the ends. Partial minor axis restraint was introduced for column C1, other things remaining the same.

2.7 Instrumentation

Instrumentation methods were devised for the tests to cover the following aspects:

i) Record axial load, major and minor axis moments in the inelastic range

ii) Record deflections along the length of the column about major and minor axes. Deflections of both the flanges about the minor axis were recorded to give twist results.

iii) Record end rotations of the column at the larger moment end.

The details of each of these aspects are now given:

2.7.1 The Load Cells

As referred to earlier, the axial load and the end moments applied to the column in the inelastic range were recorded with the aid of specially fabricated H-section load cells. These were connected at each end of the column and the results obtained were not affected by friction in the PTFE bearings or the hydraulic jack. The details of the H-section load cell are shown in Figures 2.3, 2.5 and 2.10, and they were built up by welding Maraging steel plates. The load cells were indirectly calibrated by carefully measuring its dimensions and the axial and bending strains were recorded from electrical resistance strain gauges fixed on the load cell. Sixteen such strain gauges were positioned on the load cell, as shown in Figure 2.11, to pick up the axial and bending strains. One set of eight strain gauges was connected to a digital Compulog for automatic recording and the other set to Peekel instruments for manual recording. This was necessary to monitor the loads during the tests. No strain gauges were placed on the test column.

To ensure satisfactory working of the strain gauges, it was necessary to prevent them from coming into contact with moisture. The following procedure was adopted:

i) The tip of the flange and the location in the web was cleared of all dirt

ii) The adhesive resin was applied on the metal surface and the strain gauge stuck in position

iii) The strain gauge circuit was tested using a Peekel instrument

iv) A protective covering was placed over the gauge and the strain gauge circuit tested once again.

The strain gauges used were of 10 mm length with a gauge factor of 2.10. The strain measuring circuit included dummy strain gauges fixed on an unstressed piece of Maraging steel. The temperature of the laboratory was assumed to be uniform.

Thus a reliable device for recording the forces and moments in the inelastic range was obtained. Maraging steel was chosen for this purpose because it is linear elastic up to $100 t/in^2$ after hardening. It is a special alloy steel which has been developed to meet the requirements of high strength with good ductility, toughness and weldability. The most common of the Maraging steels are those of 18% Nickel type having Cobalt and Molybdenum as the major alloying elements with the addition of Titanium and Aluminium to promote further hardening. Composition of the alloying elements of Telmar 90 used for the load cells is given below:

Alloying element %	Ni	Co	Mo	Ti
Telmar 90	17 - 19	8 - 9	3.0 - 3.5	0.15 - 0.25

The main advantages of this alloy steel are:

i) Ease of fabrication

ii) Simplicity of heat treatment with lack of distortion

iii) Considerable safety margin against brittle failure

iv) High tensile strength and toughness

The welding procedure adopted was Tungsten Inert Gas welding. In this case the inert gas was Argon. This welding process was thought to create less distortion during welding as well as providing purer welds with respect to impurities attracted compared with the normal flux coated electrode process. After welding the H-section pieces were maraged (heat treated) for 3 hours at 430°C and allowed to cool slowly. The Vickers hardness test after heat treatment revealed a strength of 100 tons/in^2. As pointed out earlier, the load cells were well inside the elastic range during the failure stages of the column.

2.7.2 The Deflection Rig

The deflections of the columns under load were measured using dial gauges. These dial gauges were supported on a rig running parallel to the column. The deflection rig was isolated from the loading rig - thus the observed deflections were absolute. Since there was a major axis moment gradient the dial gauge spacings were varied about the stronger axis - more dial gauges near the larger moment end than the other end. About the minor axis the dial gauges were evenly spaced on both flanges and deflections recorded at mid-span, quarter-span and end points. The differential bending of the two flanges gave the measure of twist. The end gauge stations were intended primarily to detect any slip and rigid body movements of the rig and were duly considered in obtaining the deflected profile. The gauges had an accuracy of 0.001 in. and a travel of 1 - 2 inches. All the dial gauges were read manually at each increment of load.

2.7.3 Recording End Rotations

To record the end rotations of the larger moment end a mirror was set up at the column end. The mirror reflected the readings from a stationary illuminated scale placed at an appropriate distance to give reasonable magnification of movements. The movements were viewed through a telescope after each increment of load. The arrangement is sketched in Figure 2.12.

All the columns were white-washed before testing to indicate the extent of yield zones.

2.8 Test Procedure

Trial runs on the test rig were necessary to obtain proper functioning. The PTFE spherical bearings were being employed for the first time so the performance of these bearings under these conditions was unknown. Results from trial runs indicated that introducing lateral shear into the bearings adversely affected their performance. The turnbuckle arrangement described earlier was therefore devised to eliminate this. The shortest 8 in - 8 in @ 58 lb column (column A1) was chosen for all the trial runs. First, only axial loads up to 100 tons and then 200 tons were applied a few times and unloaded. This was done to ensure that the bearings were properly 'bedded in'. The load cell instrumentation was checked with the axial load applied. The instrumentation being satisfactory, the eccentricity of applied loading was studied carefully. At this stage major and minor axis moments were recorded by the load cells. This called for proper alignment of the column. The positioning of the column with respect to the bearings, although carried out very carefully, still required minor adjustments. The columns rested on supports which could be adjusted and these were removed once the axial load was applied. Although a time-consuming process, the supports could be adjusted till the eccentricity of the load, as indicated by the load cell, was quite negligible. This initial adjustment of supports to align the column properly was carried out for all the subsequent tests.

All initial dial gauge readings were recorded before the start of the test. The axial load was then applied after proper alignment of the column. Another set of readings was recorded at this stage, which included all strain gauge readings, the major and minor axis dial gauge readings and the mirror reading for the end rotation. Major axis moments were then applied in small increments. After each increment the column was flexed about its minor axis to check out-of-plane stability and a small moment was always maintained. A complete set of readings was also recorded. The axial load applied

was held constant by monitoring the Amsler load control cabinet. As mentioned earlier, the major axis moments were applied through a smaller hydraulic jack. The load from this jack was added to the column and therefore the axial load from the main jack was reduced accordingly to maintain a constant axial load.

As the growth of deflections with applied moment indicated an increasing degree of non-linearity, the increment of moment was progressively reduced. During this stage steady deflections were obtained after some time, while the load was maintained at constant value. The time interval needed to obtain a steady deflection reading tended to increase with higher values of load, beginning initially with instant equilibrium. When the moment reached near the failure moment the interval became as much as 4 - 6 minutes. Beyond this stage therefore, the testing procedure was modified slightly.

The observations were recorded not for increasing loads, but for increasing deflections and end rotations during the final phase. After the previous equilibrium state the load was increased slightly and the column allowed to deflect progressively. Attempts were made to record the unloading portion of the load-deflection curve, but severe growth of deflections at this stage sometimes made this difficult and unobtainable. Although the load path for columns B4 and C1 were different, the testing procedure was similar to that outlined above.

2.9 Units Used

Since the dial gauges and the jack were calibrated in inches and tons, Imperial Units have been used throughout in discussion. Tables on column test results and data are repeated in SI units as well.

2.10 Test Results and Comments

The experimental research programme undertaken conveniently divides itself into two main groups according to slenderness ratios. The columns may be grouped as follows: (see Table I)

GROUP A Short columns - slenderness ratio $l/r_y \approx 45$

Group B Intermediate columns - slenderness ratio $l/r_y \approx 60$

Only one column of greater slenderness has been tested (slenderness ratio ≈ 74) and this has been labelled column C1. All the experimental results are presented graphically. The major and minor axis deflections and twist values plotted are for mid-column height only.

2.10.1 Mode of Failure

It was interesting to note that the mode of failure of the columns in Groups A and B were different. All the columns under Group A failed in the plane of the applied moment.

The failure of all the columns under Group B followed a standard pattern. Whilst no noticeable out-of-plane deformations were recorded in the early stages of loading, the final collapse was due to a combination of lateral bending and twisting.

Although light minor axis restraint was introduced for column C1, it also ultimately failed due to a combination of lateral bending and twisting.

A summary of the test results is given in Table II.

2.10.2. Columns A1, A2 and A3 (Group A)

As referred to earlier (Section 2.8), the shortest 8 ins - 8 ins @ 48 lb column (column A1) was tested first. This column was associated with the rig during the trial runs and subsequent modifications to the rig to eliminate lateral shear from the PTFE bearings. The end moment - end rotation curve for this column is shown in Figure 2.17. In view of the repeated number of loading and unloading operations that had to be undertaken, the experimental end moment - end rotation curve obtained for this column is presented with reservations regarding its accuracy and should not be chosen for any comparison. Also, although the experiment was conducted till a large joint rotation was reached, the failure moment was not reached. Nevertheless, it

reflects broadly the moment-rotation characteristics of the column and the behaviour at this high axial load was interesting and observed carefully during all the loading operations. A tangent modulus analysis based on the stress-strain curve of Figure 2.14 predicted an ultimate axial load of about 330 tons. The tangent modulus load P_{crit} is defined as

$$P_{crit} = \frac{\pi^2 E_T I_y}{L^2}$$

where E_T = reduced elastic modulus
I_y = minor axis moment of inertia
L = column length.

An axial load of 300 tons therefore represents the equivalent of 0.9 P_{crit} where P_{crit} is the tangent modulus load. During the experiment the column showed no tendency to out-of-plane buckling. Small minor axis end moments producing single curvature bending were maintained throughout the experiment to test the stability of the column about the minor axis.

Columns A2 and A3 were lighter rolling - 8 ins. - 8 ins. @ 31 lb sections. These again performed in accordance with short column concepts and formed a plastic hinge and failed in the plane of applied moment without any tendency to lateral torsional buckling. The axial loads applied represented 0.805 and 0.665 P_{squash} based on Y_s = 24 tons/in^2. Figures 2.18 and 2.19 show the end moment vs. end rotation and end moment vs. major and minor axis deflections plots for column A2. Figures 2.20 and 2.21 are similar plots for column A3. Also no local buckling was observed during the tests. The results were interesting as this section is often classified as being prone to local buckling. As twisting deformations were insignificant during the experiment, these values have not been plotted for these cases. Flaking of white-wash with progressive yielding was observed and can be seen in Figures 2.22 and 2.23. A fairly localised hinge is indicated spreading over about 12 - 18 inches. The material of these columns had a distinct yield point (see Figure 2.16) and so a more normal plastic hinge behaviour was observed.

2.10.3 Columns B1, B2, B3 and B4 (Group B)

All the columns in this group ($l/r_y \approx 60$) performed in a different manner to that observed previously. Columns B1 and B2 were of the heaviest rolling and classified as torsionally stiff, having a T value of 75.2 tons/in^2. These two columns were tested at axial loads of 230 and 200 tons respectively. As indicated earlier, the material properties plotted in Figure 2.14 showed no distinct yield point. The axial loads therefore represented approximately 0.8 and 0.7 P_{crit} where P_{crit} is again the tangent modulus load (defined earlier) evaluated graphically.

The columns were initially stable about the minor axis under axial loads only and then during the early stages of the application of the major axis moment, the out-of-plane minor axis deflections were small. These progressively increased however at a faster rate as the major axis moments were increased and eventually equalled the magnitude of the major axis deflections. The twisting deformations recorded also increased progressively. The final collapse was due to a combination of lateral bending and twisting. Figures 2.24, 2.25 and 2.26 show end moment vs. end rotation, end moment vs. major and minor axis deflections and end moment vs. twist values for column B1. Figures 2.27, 2.28 and 2.29 are similar plots for column B2. It is believed that significant interaction between out-of-plane bending effects associated with imperfections and high axial load and in-plane bending had taken place. This evidently produced biaxial deterioration of stability and subsequent failure in the mode described above.

Column B3 was of a lighter rolling 8 in. - 8 in. @ 35 lb section and it performed in an almost similar manner to columns B1 and B2. The end moment vs. end rotation, end moment vs. major and minor axis deflections and end moment vs. twist plots are shown in Figures 2.30, 2.31 and 2.32.

In view of the performance of column B3, it was decided at this stage to test another column of the same cross-section but starting from a reduced axial load. The primary objective was to investigate the out-of-plane buckling limits as the axial load was

increased. Initially an axial load of 100 tons was applied. The column remained stable while a major axis moment of 400 t. in. was applied. The end joint rotation sustained at this stage was 0.016 radians approximately. The load path followed during the test is shown in Figure 2.33. The results for this part of the test are covered by Figures 2.34, 2.35 and 2.36. It may be pointed out that column B3 at 160 tons was laterally unstable when a joint rotation of approximately 0.02 radians was reached.

The end joint rotation was then held approximately constant at 0.02 radians while the axial load was increased to failure. The results for this part of the test are shown in Figure 2.37. Referring back to Figure 2.33 the experiment demonstrates at full scale the phenomenon of 'moment shedding'[25] in the plastic range. As the axial load is increased the column can remain stable and in effect move round the interaction curve as shown in Figure 2.38(a) from position 1 to 2. The column eventually became unstable out-of-plane at about 160 tons. In Figure 2.38(b) is shown the variation of $M_x - \theta_b$ curves with axial load. In increasing the axial load from 100 tons (position 1) to 160 tons (position 2) one is checking stability under end moment for all intermediate loads.

2.10.4 Column C1

It was clear from previous tests that colum C1, which was 153 inches long, could not sustain high axial loads under pin-ended conditions. This column was of the heavier rolling section (8 in. - 8 in. @ 48 lb). Provision of restraint was not originally provided for in the rig and so only light restraining effects could be devised. Also an accurate estimate of the stiffness of the end-restraints could not be made. An approximate value of 3100 t. in./radian was recorded and is considered relatively light compared to typical three-dimensional frames in practice. The axial load of 150 tons applied initially represented 0.58 P_{crit}. The column initially carried this axial load pin-ended about the minor axis, but would almost certainly have failed by out-of-plane buckling at 150 tons as major axis moment was applied; this at a relatively low joint

rotation and small end moment. In the event with only light minor axis end restraint it sustained a major axis end joint rotation of 0.02 radians approximately at 150 tons with only small out-of-plane deformations. The major axis moment applied was about 540 t. in. With this major axis end rotation held constant, the axial load was then increased as the purpose of these tests was to explore column behaviour at high axial loads. At 200 Tons the column began to develop significant out-of-plane bending and twisting deformations. Major axis 'moment shedding'[25] was observed during this stage of the test. Therefore the column could sustain this moment at an axial load of 200 tons and joint rotation of 0.02 radians. It finally failed by lateral torsional buckling as the axial load was increased to 220 tons. Reference to the results of tests B1 and B2 on the same column section show close agreement on failure loads, indicating that the effect of minor axis restraint on the 153 inches column was to make its performance equivalent to that of the 123 inches ones. More twist was however developed at failure for the longer column. This test has therefore established that moderate minor axis end restraint can make more slender columns behave as short columns in-plane. This aspect will be explored further later in the thesis.

The test results are plotted on Figures 2.39 - 2.44. Figure 2.39 shows the load path followed to failure and to facilitate the presentation of other data the initial increase of axial load has been termed phase 1, the application of M_x - major axis moment, phase 2, and further increase of axial load holding the major axis end rotation approximately constant, phase 3. The application of further major axis end joint rotation and moment at 200 tons, i.e plastic hinge rotation, was explored but the increase of minor axis deflections indicated that this would soon have produced failure. The decrease of major axis end moment with increase of axial load with end joint rotation held constant during phase 3 indicates plastic 'moment shedding'[25] as the axial load is increased to failure at 220 tons. On Figure 2.40 is plotted the end moment vs. end joint rotation curve. The major and minor axis mid-column height deflections and twist values

during phase 2 are plotted on Figures 2.41 and 2.42. Figures 2.43 and 2.44 show the minor axis end restraining moments developed during the test, and the major and minor axis deflections during phase 3.

2.11 Conclusions

A summary of the test results is given in Tables I and II. It may be seen that columns in Group A with slenderness ratio $l/r_y \approx 45$ sustained high axial loads and performed in-plane, i.e. failure was in the plane of applied moments.

The columns in Group B performed differently. The high axial load conditions produced a lateral torsional buckling mode failure.

Also given in Table II are the M_{pc} values, i.e. the plastic moment capacity of the section as modified by axial loads. These values were obtained from a computer program developed to compute moment-thrust-curvature relations and discussed later. The stress-strain curves used to compute the M_{pc} values are taken from Figures 2.14 - 2.16 and the curves marked 2 and 3 were used for the flanges and web respectively for the 8 in. - 8 in. @ 48 lb and 8 in. - 8 in. @ 35 lb sections. For the 8 in. - 8 in. @ 31 lb section curves marked 1 and 3 were used for the flanges and web. The computations were carried on until a large value of curvature was reached, e.g. $\rho = 0.06$ in.$^{-1}$ The moment corresponding to this value of curvature should be very close to the actual reduced fully plastic moment capacity.

The full plastic moment capacity M_p of all the sections was computed from data from steel tables and an average yield stress of 30.0, 25.0 and 24.0 t/in^2 for the 8 in. - 8 in. @ 48 lb, 8 in. - 8 in. @ 35 lb and 8 in. - 8 in. @ 31 lb sections respectively.

At very high axial loads the moment carrying capacity of a column is small. This is clearly seen from the typical axial load-moment interaction diagram shown in Figure 2.38(a). A slight variation in material properties of the section causes a significant

change in moment carrying capacity. At such high axial loads this change would be a large fraction of the calculated moment carrying capacity. This is reflected in Table II in the values of M_f/M_{pc} for columns A2 and A3 where M_f = experimental failure moment and M_{pc} = plastic moment capacity modified by axial load. Under such conditions of high axial loads a more realistic estimate of the total carrying capacity of the column is given by the radial vector to the interaction diagram, as shown in Figure 2.38(a). This radial vector is simply given in non-dimensional form by

$$\left[\left(\frac{P}{P_s}\right)^2 + \left(\frac{M_x}{M_p}\right)^2 \right]^{\frac{1}{2}}$$

It is realistic to compare experimentally obtained carrying capacity with calculated short column carrying capacity in this manner.

The experimental strength of all the columns considering axial load and failure moment may now be expressed as

$$\left[\left(\frac{P}{P_T}\right)^2 + \left(\frac{M_f}{M_p}\right)^2 \right]^{\frac{1}{2}}$$

where P → axial load at failure

P_T → ultimate axial load - either tangent modulus load obtained from stress-strain data, or the squash load for bilinear stress-strain curves

M_f → experimental failure moment

M_p → fully plastic moment capacity

On the same basis the calculated short column strength of all the columns considering axial load and reduced plastic moment capacity is

$$\left[\left(\frac{P}{P_T}\right)^2 + \left(\frac{M_{pc}}{M_p}\right)^2 \right]^{\frac{1}{2}}$$

where M_{pc} → plastic moment capacity of the section as reduced by the axial load.

The ratios of

experimental total strength/calculated short column total strength

are shown in Table II. It may be seen that the shorter columns in Group A reached a very high proportion of the calculated short column total strength. These columns also failed in-plane.

The experimental strength of the columns in Groups B and C were lower by about 10%. These columns became laterally unstable and failure was in the lateral torsional buckling mode. This had affected the ultimate moment carrying capacity and this was confirmed by the detailed calculations reported and discussed in Chapter VI, Section 6.4. It can therefore be concluded that columns of this slenderness and above cannot be expected to carry high axial loads and major axis bending moments and remain stable in-plane. Also shown in Table II are the ratios of

experimental failure moment/plastic moment capacity as reduced by axial load.

These results also reflect the reduction in moment carrying capacity for columns in Groups B and C which failed out-of-plane.

Axial load seemed to be one of the dominant parameters influencing lateral torsional buckling. Another important aspect to emerge out of the last test (column C1) was that relatively light minor axis restraint is effective in delaying lateral instability and may make slender columns with suitable restraints behave as short columns in-plane.

To investigate the above-mentioned effects more fully and provide a clearer picture of column behaviour under these conditions, the theoretical work reported in the next three chapters was undertaken.

CHAPTER III

THEORY: MOMENT-THRUST-CURVATURE RELATIONSHIPS

3.1 Introduction

A basic requirement for studying inelastic beam columns is the generation of moment-thrust-curvature relations of the cross-section, i.e. determining values of θ, ρ and Z_n for particular values of P, M_x and M_y. These are defined with reference to Figure 3.4 where

θ - is the inclination of the neutral axis

ρ - is the curvature of the section

Z_n - is the depth of the neutral axis

P - is the axial load on the section

M_x - is the major axis moment applied

M_y - is the minor axis moment applied

In the elastic region, for a constant thrust, the variation of moments with curvature is linear and depends only on the shape of the cross-section. In the inelastic region they are non-linear and affected by the presence of residual stresses. Analytical evaluation of these relations is very involved, if not altogether impossible, and recourse must be had to numerical integration procedures.

The numerical integration method adopted here is similar to the one suggested by Birnstiel[8] and others[26], [14], whereby the cross section is sub-divided into small elemental areas for the purpose of computing the internal forces as shown in Figure 3.3. The method is very general and steel columns having any stress-strain relationship may be analysed with equal ease. Incorporating residual stresses into the calculations is fairly straight-forward and any type of residual stress pattern may be included. Residual stresses are recognised as one of the major sources of imperfections affecting ultimate load of structural members and the ease with which this may be accounted for in the numerical integration procedure is a great advantage.

3.2 Assumptions

To include all known effects in a program for biaxial bending of steel columns would be almost impossible without recourse to certain simplifications and idealisations. The major assumptions

are as follows:

(a) Elastic unloading is not covered, i.e. the stress-strain relationship for steel is assumed to be reversible.

Most calculations follow a direct load path to failure and elastic unloading is unlikely to be a dominant effect until the later stages of failure.

(b) When calculating the stiffness properties of the cross-section, it is necessary to solve the cross-sectional equations, i.e. establish values of curvature, neutral axis depth, and angle of inclination of the neutral axis for a particular combination of axial load, major and minor axes moments. In solving these cross-sectional equations the usual assumption of plane sections remaining plane has been made.

This assumption is not strictly correct, except when the bending is about an axis of symmetry. In all other cases the section is subjected to torsion which results in warping of the section. Theoretically moment-thrust-curvature relations should take account of warping stresses.

(c) The effect of shear stresses on the yielding of the section is neglected, i.e. only longitudinal direct stresses are considered to produce yield on the section.

This effect was considered to be relatively small and thus no attempts were made to introduce the concept of yield criteria into the calculations.

(d) The shear modulus G is assumed to retain its full elastic value after yield has taken place. The variation of the shear modulus in the inelastic region is a complex phenomenon and a thorough understanding of the problem is lacking. However, certain considerations have been forwarded by Professor Horne justifying the retention of an elastic value for G after yield for situations arising

in most beam columns[27]. He has suggested that the shear stress is usually small when plastic yield starts in a member under thrust and moment and under such conditions plastic potential theory shows that the elastic value is correctly used for initial deformations. Secondly, he has suggested that since the column is torsionally flexible, large shear stresses cannot be introduced in the practical range of deformations, and it therefore follows that the effective shear modulus does not fall significantly below the elastic value. Any fall-off that occurs is probably compensated for by the complete neglect of warping rigidity in the plastic regions.

3.3 Steel Stress-Strain Curve Adopted

In most of the previous studies briefly referred to in the first chapter the stress-strain relations have been idealised for computational purposes. The idealisation adopted was an elastic-perfectly plastic bilinear curve for steel, ignoring the effect of strain hardening.

In view of the stress-strain relations obtained from specimen tests for grade 50B steel, it was necessary to develop the computational procedure in a way so as to take account of the exact stress-strain curve. This was necessary because nearly all grades of high tensile steel seem to exhibit a smooth stress-strain curve like the ones shown in Figures 2.14 and 2.15. In the computational procedure the experimentally obtained curve was specified as a multilinear curve. By choosing data points at sufficiently close intervals, the observed curve can be reproduced accurately. In the computer program any pattern of stress-strain relationship can be specified as a multilinear curve.

3.4 Residual Stresses

Residual stresses are introduced into a member during the manufacturing process because of uneven cooling of different parts of the section after the hot rolling process. The magnitude and distribution of these stresses across the section are highly

variable, depending on the shape and size of the section and the nature of the manufacturing process. They may also be affected by subsequent cold rolling to straighten the member. The net effect of these residual stresses present in rolled sections subjected to compressive load is to delay or accelerate the process of yielding in different parts of the section depending upon the stress being tensile or compressive respectively. Various investigators have attempted to obtain generalised patterns for the residual stress distribution across the section. Currently two patterns of residual stress pattern are frequently considered. They are

(a) The AISC pattern[28]

This is shown in Figure 3.1. In the computational results reported later only the AISC stress pattern was considered wherever indicated. The tensile residual stress σ_{rt} in the web is

$$\sigma_{rt} = \sigma_{rc} \left\{ \frac{bt}{bt + w(d-2t)} \right\}$$

where b = flange width
t = flange thickness
d = depth of the section
w = width of the web

This is obtained from the condition that residual stresses are self-equilibrating.

(b) The Cambridge pattern[29]

This is shown in Figure 3.2. The variation is parabolic with compressive residual stresses in the web.

The residual stresses present cannot be directly used in considering their effect on the column behaviour. The stress pattern is first converted to residual strain pattern. During the actual manufacturing process it

is the locked-in residual strains that produce residual stresses. The strains due to applied loads are then superimposed on the residual strains. The net strains so obtained are then used to determine the net stresses using the particular stress-strain relationship adopted for the problem.

3.5 Expressions for Moment-Thrust-Curvature Relations

The column cross-section is subdivided into a grid of small size rectangular elements, as shown in Figure 3.3. The axes of reference chosen are shown in Figure 3.4. Thus the value of θ - the inclination of the neutral axis with the X-axis would lie between 0 and $\pi/2$. It is also assumed that the point 0 is always under maximum compression. Suitable transformation of axes can be easily made if some other corner goes under maximum compression. The moment-thrust-curvature relationship for biaxial bending consists of relation between six quantities, viz. P, M_x, M_y, θ, ρ, and Z_n, which are as defined in Section 3.1.

In principle by assigning values to any three of the variables the other three can be determined. It is, however, most convenient computationally if values of θ, ρ, and Z_n are specified. P, M_x and M_y are then directly computed. In general P, M_x and M_y are non-linear functions of θ, ρ, and Z_n. In order to determine the value of θ, ρ, and Z_n for certain specific values of P, M_x and M_y, an iterative procedure is necessary. With the curvature ρ, and the neutral axis depth Z_n being assumed the strain distribution across the section is obtained. This follows directly from the assumption about plane sections remaining plane stated earlier. Thus

$$\varepsilon_o = \rho \cdot Z_n$$

where ε_o - is the strain at the origin 0 (Figure 3.4).

The strain in any element of area Δa_i whose centroid is (x_i, y_i) is given by

$$\varepsilon_i = \varepsilon_o \, (1 - z_i/z_n)$$

where Z_i is the perpendicular distance of an axis, passing through the centroid of the element and parallel to the neutral axis, from the origin 0. The value of the strain obtained is modified at this stage to take account of residual strains.

With this value of strain existing at the element, the stress σ_i in the elemental area can be obtained from the stress-strain relationship appropriate to the material of the area. In general stress-strain relations may be different in the flanges and web.

The elemental force is given by

$$\Delta P_i = \Delta a_i \cdot \sigma_i$$

where Δa_i represents elemental area.

Summing up for all the elements, the axial force P in the section is obtained. Thus

$$P = \sum_{i=1}^{i=n} \Delta a_i \cdot \sigma_i \qquad \ldots (3.1)$$

where n is the total number of elements in the section.

Similarly the moments about X and Y axes are obtained.

$$M_x = \sum_{i=1}^{i=n} \Delta a_i \cdot \sigma_i \cdot y_i \qquad \ldots (3.2)$$

$$M_y = \sum_{i=1}^{i=n} \Delta a_i \cdot \sigma_i \cdot x_i \qquad \ldots (3.3)$$

where x_i and y_i are the respective lever arms for the X and Y axes.

3.6 Computational Procedure

In order to establish the stiffness properties of the section due to applied loading, it is necessary as already stated to obtain solutions of θ, ρ, and Z_n for a specific set of values of P, M_x and M_y. Values of θ, ρ, and Z_n are assumed - these are

the starting values to solve the cross-sectional equations giving the internal forces. For the position of the neutral axis assumed, the strain, the stress and the force in each elemental area are computed taking into account the appropriate stress-strain characteristics. Summation of these forces over the section gives the resultant axial force. Summation of these elemental forces times the lever arm over the section gives the moments about the two axes (Equations (3.2) and (3.3)). The values of P, M_x and M_y obtained are not the same as the specified values. In order to obtain correction terms for θ, ρ, and Z_n, a generalised form of Newton-Raphson iterative technique[30] is employed, as described below.

In case of biaxial bending P, M_x, M_y may in general be written in the form

$$P = f_1 (\rho, Z_n, \theta) \qquad \ldots (3.4)$$

$$M_x = f_2 (\rho, Z_n, \theta) \qquad \ldots (3.5)$$

$$M_y = f_3 (\rho, Z_n, \theta) \qquad \ldots (3.6)$$

where f_1, f_2, f_3 are in general non-linear functions of the three unknown quantities ρ, Z_n and θ. Now if h_1, k_1 and l_1 are the corrections to be applied to ρ, Z_n and θ, then it may be shown that for necessary conditions of convergence, the correction terms may be calculated by the solution of the following equations:

$$\begin{bmatrix} \frac{\delta f_1}{\delta \rho} & \frac{\delta f_1}{\delta Z_n} & \frac{\delta f_1}{\delta \theta} \\ \frac{\delta f_2}{\delta \rho} & \frac{\delta f_2}{\delta Z_n} & \frac{\delta f_2}{\delta \theta} \\ \frac{\delta f_3}{\delta \rho} & \frac{\delta f_3}{\delta Z_n} & \frac{\delta f_3}{\delta \theta} \end{bmatrix} \begin{bmatrix} h_1 \\ k_1 \\ l_1 \end{bmatrix} = \begin{bmatrix} P - f_1 (\rho, Z_n, \theta) \\ M_x - f_2 (\rho, Z_n, \theta) \\ M_y - f_3 (\rho, Z_n, \theta) \end{bmatrix} \qquad \ldots (3.7)$$

so that at convergence the right hand side of the equation vanishes.

The partial derivatives required are calculated numerically by giving a small increment (0.1%) of the value to ρ, Z_n and θ in turn keeping the others constant. Convergence is normally achieved within three to four cycles. Success of this iterative procedure depends on how close the chosen initial values are to the final values. If the assumed values are far outside, the process may fail to converge even if there is a solution. In the computer program iteration was continued till the differences between external and internal forces were less than $1.0 * 10^{-5}$. For summing up the forces each flange was subdivided into 100 elemental areas and the web into 40 elemental areas.

Once the cross-sectional equations are solved (Equations (3.4) - (3.6)), the inelastic properties of the section are computed easily. Thus the procedure described above may be used to determine the failure loads of columns in biaxial bending described later.

It is of interest to note that while this method of numerical integration and solution of cross-sectional equations is very general, it requires extensive computer time. Milner[10] provided exact solutions for the internal forces for partially yielded H-sections for a bilinear stress-strain curve, i.e. elastic-perfectly plastic. The analytical equations given are quite involved, but are much more economical for computer solution. Milner's method was attractive for this purpose but has the limitation that only bilinear stress-strain curves can be introduced. Inclusion of residual stresses would make the analytical equations extremely complicated. Numerical integration techniques offer greater versatility from this aspect.

CHAPTER IV

THEORY - FAILURE LOADS OF COLUMNS AND GENERAL EQUATIONS OF EQUILIBRIUM.

4.1 Introduction

A procedure for computing moment-thrust-curvature relations for column elements under biaxial bending has been described in the previous chapter. Such moment-thrust-curvature relations can be used to generate moment-thrust interaction surfaces corresponding to infinite curvature for different cross-sections. The failure loads of short, stocky columns lie very close to these interaction surfaces which provide sufficient information for this case. The failure of longer columns, however, is influenced by slenderness and the deformed geometry and consideration of their flexural and torsional stability is essential.

A typical load vs. deflection diagram for a column in uniaxial bending under constant axial load is shown in Figure 4.1. The curve is characterised by a peak moment and a descending unstable equilibrium path. For a biaxially loaded column it is basically the same as shown in Figure 4.2. The column will continue to deform under increasing load until instability occurs. Thereafter unloading begins with further deformation. The deformations along X and Y axes, the twisting deformation and the end rotation take place simultaneously. The rate of increase of these deformations is not the same and the failure moment is the peak of all these deformations. Some of the underlying principles used in the computation of column failure loads and the broad considerations for the particular numerical procedure adopted are now discussed breifly.

4.2 General Computational Principles

The most important aspects of the major previous computational work on biaxial bending were summarised in Chapter I. It may be recalled that these previous efforts were not for the general asymmetrical case of biaxial loading and were restrictive in certain aspects as mentioned. It was the object of the work

reported herein to develop general computational procedures to cover the following aspects:

(a) to analyse biaxially loaded restrained H-columns

(b) to cover the general case of asymmetrical bending about both axes, i.e. $\beta \neq 1.0$

(c) to include torsional calculations accurately

(d) to include the exact stress-strain relationships

It was appreciated that inclusion of all the above-mentioned aspects in the computational procedures would involve much solution time on the computer. The numerical approach adopted had therefore to be chosen with regard to computational efficiency and some of the points considered in adopting an efficient, linear iterative scheme rather than a second order iterative scheme are now mentioned.

The Newton-Raphson iterative approach was extended to solve the general case of asymetrical biaxial bending by Virdi[14]. Torsional stability was not considered in the above-mentioned work. The method may be extended to include torsion in a similar manner to that outlined for biaxial bending but at the expense of a large increase in computer time. Concerning computer solution time, it should be noted that most of the solution time is consumed in calculating the internal forces, i.e. moment-thrust-curvature relationships. The correction vector in the Newton-Raphson iterative technique involves formation of an 'n x n' Jacobian matrix where 'n' is the number of unknown variables at a point. For biaxial bending 'n' is 2. For biaxial bending covering torsion 'n' would be 3. Calculation of each of these elements of the Jacobian matrix involves calculation of the internal forces. This calculation would have to be repeated for each cycle of iteration at each subdivision along the column. It was felt that extension of the method to include torsion would be computationally uneconomic. The linear iterative technique reported herein was adopted for this reason.

4.2.1 Outline of the Computational Procedure

As discussed previously and noting that the failure load is associated with the peak of all the deformation curves, the following procedure may be adopted for computing the failure load of columns under biaxial bending with constant axial load. The load path followed is:

a) Axial load applied first and held constant

b) End moments increased to failure.

The computational procedure starts with calculating the deflected shape when particular values of axial load, major and minor axes moments are applied. The deflected shape is obtained by adjusting the values of all the three displacements simultaneously to satisfy the equilibrium of forces. The axial load is then kept constant and the end moments increased to obtain subsequent deflected shapes. Due account is taken of the extent of plasticity in the section and consequent reduction in stiffnesses.

In classical theory the torsional displacements take place about a point S known as the centre of twist or shear centre. For an elastic member cross-section this point may be found from established theories. In an elastic-plastic cross-section the location of this point is extremely complicated and intractable when there are no precise yield zones. A rigorous analysis of elastic plastic warping is not available. As mentioned in the previous chapter the mement-thrust-curvature relationships for biaxial bending are affected by warping stresses. Due to its extremely complicated nature the idealisation regarding plane sections remaining plane was made in establishing these relationships. As discussed earlier in Chapter I, previous efforts[8], [9], [10] in determining the average centre of twist was based on the assumption that imposition of warping strains on the strains due to bending do not result in a force in the ζ direction (see Figure 4.3) nor moments about ξ and η axes. When the position of this average centre of twist was located the internal and external torque were computed about an axis parallel to the ζ axis and passing through the above-mentioned centre of twist, and equilibrium satisfied. This is a somewhat tedious process and

much of this is eliminated by a different approach. In this thesis no effort is made to locate the average centre of twist. Instead all the torsional moments external and internal are computed about the ζ axis passing through the centroid and equilibrium established. Further details are given later.

The actual process of satisfying equilibrium is by adjusting the displacements. As discussed previously, a first order iterative procedure was used to solve the variable-coefficient differential equations presented later. An iterative procedure is necessary because with the onset of twisting deformations the external forces about the two principal axes are changed slightly. In fact if all the displacements could be known in advance no such iteration would be required. The process of iteration is continued until the difference between assumed displacements and final displacements are less than a specified small amount. In the inelastic range the various stiffness properties depend upon the spread of plasticity which in turn depends upon the deflections. Once a deflected shape has been obtained for a fixed set of stiffness values at each point but varying along the length of the column, a new set of stiffness coefficients may be calculated. This leads to another deflected shape. Another iterative cycle is set up at this stage. Equilibrium at a particular load level is achieved when the values of the assumed deflected shape differ by less than a small specified amount. Further details are given later.

For successively higher values of load level the displacements are obtained corresponding to the equilibrium of the twisted flexural shape. With increasing load level, the rate of change of deflection also increases, and finally a given load fails to result in an equilibrium shape. This load is sufficiently close to the peak load, as depicted in Figure 4.2. It is thus possible to compute the failure load as the peak of such a load-deflection response in the case of biaxial bending and compression.

4.3 General Equations of Equilibrium

To calculate the equilibrium configuration of a column subject to axial load P and moments about the X and Y axes taking into account the secondary forces arising from member displacements, it is necessary to compute and equate internal and external forces at a general displaced section, as shown in Figure 4.3. The right hand screw rule has been adopted for positive moments. To formulate the equations certain assumptions have been made. These assumptions are in addition to those listed earlier in Chapter III.

4.3.1 Assumptions

a) Deflections are small, so that curvature can be represented by the second derivative of the deflections.

b) The column is an as-rolled wide flange or H-section but torsional imperfections are neglected. Major and minor axis imperfections and residual stresses are considered.

c) The axial load acts along the original centroidal axis of the column and remains so throughout the loading.

d) No transverse loads are considered between the ends of the column.

e) The cross-section is uniform over the length of the column

4.3.2 Elastic Columns

For the displaced cross-section shown in Figure 4.3 the moments acting about the two principal axes of the section ξ and η and the ζ axis are M_ξ, M_η and M_ζ respectively. The geometric relationship that exists may be derived from Figure 4.4. The element of the column starts initially from position 1, then under action of u and v displacements moves to position 2 and finally by twisting about an axis through S it moves to position 3. Displacements u and v, the twist ϕ and the coordinates of S, viz.

x_o and y_o are all positive as shown. The quantities u, v and ϕ are small so that geometry of small displacements applies.

As the result of twisting the axes ξ and η rotate relative to the X and Y axes through an angle ϕ and the displacement components of the centroid change from u and v to u_c and v_c where

$$u_c = u + \phi \cdot y_o \qquad \ldots \quad (4.1)$$

$$v_c = v - \phi \cdot x_o \qquad \ldots \quad (4.2)$$

Another geometric change that takes place during the member displacement is the inclination of the ζ axis to the original Z axis caused by du/dz and dv/dz. Thus twisting of the column together with u and v displacements means that forces computed in the X, Y, Z coordinate system differ from the ξ, η and ζ system. The details of the forces are now given. These are well established and are given in any standard text[31]. The procedure to relate all forces to the principal axes of the deformed cross-section is shown in Figures 4.5, 4.6 and 4.7, and using vector symbols, ϕ being a small angle, it may be assumed that $\cos \phi = 1$ and $\sin \phi = \phi$.

With reference to Figure 4.3, the forces acting in the Z-X and the Z-Y plane are shown in Figure 4.5. The applied moments at a distance z from the lower end of the member (Figure 4.3) are:

$$M_x = - M_{BX} + R_y \cdot z + P \cdot v_c \qquad \ldots \quad (4.3)$$

$$M_y = - M_{BY} + R_x \cdot z - P \cdot u_c \qquad \ldots \quad (4.4)$$

where M_{BX} = applied major axis bending moment at end 0
M_{TX} = applied major axis bending moment at end L
M_{BY} = applied minor axis bending moment at end 0
M_{TY} = applied minor axis bending moment at end L
$R_y = (M_{BX} + M_{TX})/L$
$R_x = (M_{BY} + M_{TY})/L$

and u_c and v_c are as defined above. Transformation of the moments to the new axes ξ and η have to be carried out and referring to

Figure 4.6 we get by vector addition

$$M_\xi = M_x + \phi M_y \qquad \ldots \quad (4.5)$$

and

$$M_\eta = M_y - \phi M_x \qquad \ldots \quad (4.6)$$

In addition to the components of M_x and M_y along the ξ and η axes, they also have components along the ζ axis which is perpendicular to the cross-section and is inclined from the Z axis. These components result in a twisting moment, as shown in Figure 4.7

$$M_{\zeta_1} = M_x \, du/dz + M_y \, dv/dz \qquad \ldots \quad (4.7)$$

where the relationships $\sin \frac{du}{dz} = \frac{du}{dz}$ and $\sin \frac{dv}{dz} = \frac{dv}{dz}$ are used.

A second contribution to M_ζ is due to end shears, as shown in Figure 4.8

$$M_{\zeta_2} = - R_x \cdot v - R_y \cdot u \qquad \ldots \quad (4.8)$$

A third contribution to M_ζ is caused by the fact that two cross-sections d_ζ apart will warp with respect to each other and therefore a small stress element is inclined to the ζ axis. This has been derived elsewhere[32].

$$M_{\zeta_3} = \overline{K} \cdot \frac{d\phi}{dz} \qquad \ldots \quad (4.9)$$

where $\overline{K} = \int \sigma a^2 \, dA$

where σ = stress in a small element

a = distance of the element from the centre of twist.

A fourth contribution arises due to components $P\frac{du}{dz}$ and $P\frac{dv}{dz}$ acting through the centroid. Therefore the fourth contribution of torque about the centre of twist is

$$P\frac{du}{dz} \cdot y_o - P\frac{dv}{dz} \cdot x_o \qquad \ldots \quad (4.10)$$

The total twisting moment is the sum of all the components or

$$M_\zeta = M_x \frac{du}{dz} + M_y \frac{dv}{dz} - R_x \cdot v - R_y \cdot u + \bar{K} \frac{d\phi}{dz} + P\frac{du}{dz} \cdot y_o - P\frac{dv}{dz} \cdot x_o \quad \ldots (4.11)$$

The moments which are acting at any location along the Z axis are M_ξ, M_η and M_ζ and can now be equated to the internal resistance of the member.

In terms of stiffnesses and deformation, the moments M_ξ, M_η and M_ζ are approximately equal to

$$M_\xi \simeq - EI_\xi \frac{d^2v}{dz^2} \quad \ldots (4.12)$$

$$M_\eta \simeq EI_\eta \frac{d^2u}{dz^2} \quad \ldots (4.13)$$

$$M_\zeta \simeq GK_T\frac{d\phi}{dz} - EI_w \frac{d^3\phi}{dz^3} \quad \ldots (4.14)$$

Where E = Elastic modulus

I_η = Moment of inertia about η axis

I_ξ = Moment of inertia about ξ axis

G = Shearing modulus

$K_T \simeq$ Pure torsion constant or St. Venant's term

$\simeq \sum \frac{t^3 \cdot \ell}{3}$ where t is the thickness and ℓ the length of a typical element. The summation is for all elements.

I_w = Warping rigidity[32].

Combining equations (4.3) - (4.11) and equating them to equations (4.12) - (4.14), we have

$$M_{BX} - \frac{z}{L}(M_{BX}+M_{TX}) - P\cdot v_c + \phi\{M_{BY} - \frac{z}{L}(M_{BY}+M_{TY}) + P\cdot u_c\} = EI_\xi \frac{d^2v}{dz^2} \quad \ldots (4.15)$$

$$M_{BY} - \frac{z}{L}(M_{BY}+M_{TY}) + P\cdot u_c - \phi\{M_{BX} - \frac{z}{L}(M_{BX}+M_{TX}) - P\cdot v_c\} = - EI_\eta \frac{d^2u}{dz^2} \quad \ldots (4.16)$$

$$(GK_T-\bar{K})\frac{d\phi}{dz} - EI_w\frac{d^3\phi}{dz^3} = \{-M_{BX}+\frac{z}{L}(M_{BX}+M_{TX}) + P\cdot v_c + P\cdot y_o\}\frac{du}{dz}$$

$$+\{-M_{BY}+\frac{z}{L}(M_{BY}+M_{TY}) - P\cdot u_c - P\cdot x_o\}\frac{dv}{dz} - (M_{BY}+M_{TY})/L\cdot v - (M_{BX}+M_{TX})/L\cdot u \quad \ldots (4.17)$$

4.3.3 Restrained Elastic Columns

The equations (4.15) - (4.17) describe the equilibrium position of a displaced cross-section shown in Figure 4.3. The equations do not include the effect of initial imperfections and end restraints. The modified equations to include the effects covered in this work namely minor axis end restraints, are now given.

The modified equations for H-sections will only be given. For a symmetrical elastic H-section the points S and C in Figure 4.4 coincide.

The forces in the X-Z plane of a restrained column with imperfections are shown in Figure 4.9. Similar imperfections are present in the Y-Z plane, but no restraints are present. From Figure 4.9 the boundary conditions become:

$$M_{cyb} = M_{BY} - M_{ryb} \quad \ldots (4.18a)$$

and

$$M_{ryb} = K_{byb}\cdot\frac{du_c}{dz}\ (z=0) \quad \ldots (4.18b)$$

$$M_{cyt} = M_{TY} - M_{ryt} \quad \ldots (4.18c)$$

and

$$M_{ryt} = K_{byt}\cdot\frac{du_c}{dz}\ (z=L) \quad \ldots (4.18d)$$

where M_{BY} and M_{TY} are as defined above

M_{cyb} = column end moment at end 0

M_{cyt} = Column end moment at end L

K_{byb} = Stiffness of the restraining beam at end 0 (t.in/radian)

K_{byt} = Stiffness of the restraining beam at end L (t.in/radian)

The modified equation of bending about the strong axis (Equation (4.15)) becomes

$$M_{BX}-\frac{z}{L}(M_{BX}+M_{TX}) - P(v_c+v_{imp}) + \phi\{M_{BY}-K_{byb}\cdot\frac{du_c}{dz}(z=0) - \frac{z}{L}$$
$$(M_{BY}-K_{byb}\cdot\frac{du_c}{dz}(z=0) + M_{TY}-K_{byt}\cdot\frac{du_c}{dz}(z=L)) + P(u_c+u_{imp})\} = EI_\xi\frac{d^2v_c}{dz^2}$$

... (4.19)

The weak axis bending equation becomes

$$M_{BY}-K_{byb}\cdot\frac{du_c}{dz}(z=0) - \frac{z}{L}(M_{BY}-K_{byb}\cdot\frac{du_c}{dz}(z=0) + M_{TY}-K_{byt}\cdot\frac{du_c}{dz}(z=L))$$
$$+ P(u_c+u_{imp}) - \phi\{M_{BX}-\frac{z}{L}(M_{BX}+M_{TX}) - P(v_c+v_{imp})\} = -EI_\eta\frac{d^2u_c}{dz^2}$$

... (4.20)

The torsional equation becomes

$$(GK_T-\bar{K})\frac{d\phi}{dz} - EI_w\frac{d^3\phi}{dz^3} = \{-M_{BX}+\frac{z}{L}(M_{BX}+M_{TX}) + P(v_c+v_{imp})\}\cdot\frac{d}{dz}(u_c+u_{imp})$$
$$+ \{-M_{BY}+K_{byb}\cdot\frac{du_c}{dz}(z=0) + \frac{z}{L}(-M_{BY}+K_{byb}\cdot\frac{du_c}{dz}(z=0) - M_{TY}+K_{byt}\cdot\frac{du_c}{dz}(z=L))$$
$$- P(u_c+u_{imp})\}\cdot\frac{d}{dz}(v_c+v_{imp}) - (\frac{M_{BX}+M_{TX}}{L})\cdot(u_c+u_{imp}) - \{M_{BY}-K_{byb}\cdot\frac{du_c}{dz}(z=0)$$
$$+ M_{TY}-K_{byt}\cdot\frac{du_c}{dz}(z=L)\}/L\cdot(v_c+v_{imp}) \quad \ldots (4.21)$$

These three differential equations (4.19) - (4.21) describe the equilibrium of any cross-section in the member shown in Figure 4.3 but restrained about minor axis by elastic beams as depicted in Figure 4.9. As can be seen, the equations are not independent of each other. Equation (4.19) which represents bending about the strong axis, for example, depends also on the angle of twist ϕ. The equations are also not linear with respect to the three deformations u_c, v_c and ϕ. A closed form analytical solution does not exist to the Author's knowledge for these coupled non-linear differential equations and therefore a numerical solution based on centre finite difference is used in this study. The inelastic form of these equations is considered in the next chapter.

CHAPTER V

THEORY - INELASTIC RESTRAINED COLUMNS

5.1 Introduction

Establishing equilibrium between internal and external forces at a column cross-section in the inelastic range is not straight-forward. This is because the internal forces have to be evaluated taking into account the inelastic zones which in turn depend upon the deflected shape. An iterative procedure is therefore necessary to obtain the correct deflected shape.

5.2 Inelastic Stiffnesses

The details of computing moment-thrust-curvature relationships were described in Chapter III. The iterative procedure to calculate θ, ρ and Z_n for a particular set of external forces P, M_x and M_y was outlined. Residual stresses may also be included in solving the above cross-sectional equations. Once the values of θ, ρ and Z_n are obtained the various stiffness values pertinent to the cross-section may be computed. A typical strain diagram due to biaxial bending is shown in Figure 3.4.

If curvatures along ξ and η axes are represented by ρ_ξ and ρ_η we have

$$\rho = \sqrt{\rho_\xi^2 + \rho_\eta^2} \qquad \ldots (5.1)$$

$$\theta = \tan^{-1} (\rho_\eta / \rho_\xi) \qquad \ldots (5.2)$$

From this the deteriorated stiffness about the ξ axis may be obtained by summing up the moments in the following manner:

$$X_\xi = \sum_{i=1}^{i=n} \Delta a_i \cdot \sigma_i \cdot \eta_i / \rho_\xi \qquad \ldots (5.3)$$

where Δa_i - an elemental area

σ_i - stress in an elemental area

η_i - lever arm of the elemental area from the ξ axis

n - total number of elemental areas in the cross-section.

Similarly about the η axis the stiffness becomes:

$$Y_\eta = \sum_{i=1}^{i=n} \Delta a_i \cdot \sigma_i \cdot \xi_i/\rho_\eta \qquad \ldots (5.4)$$

The Wagner effect term $\overline{K}$ in equation (4.9) may be similarly computed from

$$\overline{K} = \sum_{i=1}^{i=n} \Delta a_i \cdot \sigma_i \cdot \omega_i^2 \qquad \ldots (5.5)$$

where ω_i = distance from the elemental area Δa_i to the centre of twist.

Similarly, if the stiffnesses of the compression and tension flanges are denoted by C_{cf} and C_{tf} then

$$C_{cf} = \sum_{j=1}^{j=s} \Delta a_j \cdot \sigma_j \cdot \xi_j/\rho_\eta \qquad \ldots (5.6)$$

$$C_{tf} = \sum_{k=1}^{k=s} \Delta a_k \cdot \sigma_k \cdot \xi_k/\rho_\eta \qquad \ldots (5.7)$$

where s = number of elemental areas in the compression and tension flange.

These stiffnesses represent various points on the respective moment-thrust-curvature plots, as shown in Figure 5.1. In biaxial bending these plots are dependent on each other and as M_ξ and M_η change, the point as shown on the curve moves to another position on a different M_ξ-P-ρ_ξ and M_η-P-ρ_η curve. Thus in order to calculate the deteriorated stiffness corresponding to the new M_ξ-P-ρ_ξ curve, the iterative procedure for soliving the cross-sectional equations discussed in Chapter III has to be repeated.

5.3 Computation of Torsional Resistance

In establishing equilibrium between internal and external forces at any cross-section, discretion may be exercised concerning the choice of axes about which moments are taken so that computing efforts are minimised. In this work, M_ξ and M_η have been taken about the ξ and η axes through the centroid of the section as usual.

As mentioned in the previous chapter, in satisfying equilibrium of torsional moments, the classical approach has been to compute the moments about an axis parallel to the ζ axis and passing through the centre of twist called S. The torsional resistance offered by a section about such an axis is due to the combined effects of a pure torsion or St. Venant's term and the warping torque resistance offered by the differential flange bending. The evaluation of St.Venant's term is straight-forward and is based upon assumptions mentioned earlier in Chapter III.

It is in the evaluation of the warping torque term that the discretion regarding choice of axis is significant. In this thesis the external and internal torsional moments have been computed about an axis parallel to ζ axis and passing through the centroid of the section. The reasons for this are two-fold:

a) Even for the case of a bilinear stress-strain curve (i.e. elastic-perfectly plastic) where yield zones of the section are clearly defined, computing the exact centre of twist based on the assumptions mentioned earlier is a difficult and time-consuming process. When a stress-strain curve such as the one in Figure 2.14 is used, the yield zones of the section are not clearly defined and location of the centre of twist becomes extremely involved.

b) There are only advantages in taking moments about the shear centre when attempting an analytical solution of the differential equations for general elastic problems. In classical elastic theory the internal warping resistance is expressed in terms of the warping

rigidity. This warping rigidity for a particular cross-section was derived from the considerations of warping displacements and rotation of the cross-section about the centre of twist and is treated exhaustively by Timoshenko[32]. This approach facilitated the direct solution of the differential equations of equilibrium as it separated warping and bending effects.

In dealing with inelastic cross-sections there are no advantages in the above-mentioned classical approach and it is inconvenient and clumsy from the computational point of view. It is necessary in this case to review the basic phenomenon of warping torque resistance. This is offered by the introduction of differential shears. These flange shears may be computed directly and the moments taken about the centroidal axis to produce the warping torque resistance about that axis. The warping torque resistance in this case is different from the classical warping rigidity term mentioned previously. The external torsional moments calculated about the centroidal axis are altered as well from those calculated previously in Chapter IV and this follows from equations (4.1) and (4.2).

The displacements of the centroid, with rotation about the shear centre or centre of twist are (equations (4.1) and (4.2)):

$$u_c = u + \phi y_o$$

$$v_c = v - \phi x_o$$

The external moments as calculated previously are:

$$M_x = - M_{BX} + R_y \cdot z + P\ (v - \phi x_o)$$

$$M_y = - M_{BY} + R_x \cdot z - P\ (u + \phi y_o)$$

In computing moments about the centroid and considering twist about that axis, the terms ϕx_o and ϕy_o do not exist and they become

$$M_x = - M_{BX} + R_y \cdot z + P \cdot v \qquad \ldots (5.8)$$

$$M_y = - M_{BY} + R_x \cdot z - P \cdot u \qquad \ldots (5.9)$$

The warping torque resistance of the cross-section about the centroid may now be derived as follows (see Figures 4.3 and 5.2)

Total flange displacements are:

$$u + \phi\frac{D}{2} \text{ - Compression flange} \qquad \ldots (5.10)$$

$$u - \phi\frac{D}{2} \text{ - Tension flange} \qquad \ldots (5.11)$$

The curvatures of compression and tension flange are:

$$\rho_{comp} = \frac{d^2u}{dz^2} + \frac{D}{2}\frac{d^2\phi}{dz^2} \qquad \ldots (5.12)$$

$$\rho_{ten} = \frac{d^2u}{dz^2} - \frac{D}{2}\frac{d^2\phi}{dz^2} \qquad \ldots (5.13)$$

If C_{cf} and C_{tf} are the stiffnesses of the compression and tension flanges respectively, then flange bending moments are:

$$M_{fc} = C_{cf}\left(\frac{d^2u}{dz^2} + \frac{D}{2}\frac{d^2\phi}{dz^2}\right) \qquad \ldots (5.14)$$

$$M_{ft} = C_{tf}\left(\frac{d^2u}{dz^2} - \frac{D}{2}\frac{d^2\phi}{dz^2}\right) \qquad \ldots (5.15)$$

The respective flange shears after neglecting certain product of small quantities become:

$$V_{fc} = C_{cf}\left(\frac{d^3u}{dz^3} + \frac{D}{2}\frac{d^3\phi}{dz^3}\right) \qquad \ldots (5.16)$$

$$V_{ft} = C_{tf}\left(\frac{d^3u}{dz^3} - \frac{D}{2}\frac{d^3\phi}{dz^3}\right) \qquad \ldots (5.17)$$

Resisting warping torque about C

$$= \frac{D}{2}\frac{d^3u}{dz^3}(C_{tf} - C_{cf}) - \frac{D^2}{4}\cdot\frac{d^3\phi}{dz^3}(C_{cf} + C_{tf}) \qquad \ldots (5.18)$$

In computing $\overline{K}$ the distance ω_i in equation (5.5) is taken as the distance of the elemental area Δa_i from the centroid.

Here it may be pointed out that in the computations the flange shears have been assumed to act in the middle of the flange. Refinements in computing the warping torque could be introduced by dividing the flange into thin strips and computing the shear in each of these. This is shown in Figure 5.3.

5.4 Inelastic Form of Equations of Equilibrium

The equations of equilibrium (4.19) - (4.21) which were derived in the previous chapter will now be modified for inelastic bending.

The strong axis bending equation (4.19) becomes:

$$M_{BX} - z/L\,(M_{BX}+M_{TX}) - P(v+v_{imp}) + \phi\,\{M_{BY}-K_{byb}\cdot\frac{du}{dz}(z=0) - z/L\,(M_{BY}-K_{byb}\cdot\frac{du}{dz}(z=0) + M_{TY} - K_{byt}\cdot\frac{du}{dz}(z=L)) + P(u+u_{imp})\} = \frac{d^2v}{dz^2}\cdot \sum_{i=1}^{i=n}\Delta a_i\cdot\sigma_i\cdot\eta_i/\rho_\xi \qquad \cdots (5.19)$$

where the summation denotes the deteriorated stiffness discussed earlier in Section 5.2.

The weak axis bending equation (4.20) becomes:

$$M_{BY} - K_{byb}\cdot\frac{du}{dz}(z=0) - z/L\,(M_{BY}-K_{byb}\cdot\frac{du}{dz}(z=0) + M_{TY}-K_{byt}\cdot\frac{du}{dz}(z=L)) + P(u+u_{imp}) - \phi\,\{M_{BX} - z/L\,(M_{BX}+M_{TX}) - P(v+v_{imp})\} = -\frac{d^2u}{dz^2}\cdot \sum_{i=1}^{i=n}\Delta a_i\cdot\sigma_i\cdot\xi_i/\rho_\eta \qquad \ldots (5.20)$$

The torsional equation (4.21) becomes:

$$\{- M_{BX} + z/L\ (M_{TX}+M_{BX}) + P(v+v_{imp})\} \cdot \frac{d}{dz}(u+u_{imp}) + \{- M_{BY}+K_{byb} \cdot \frac{du}{dz}(z=0) + z/L\ (- M_{BY}+K_{byb} \cdot \frac{du}{dz}(z=0) - M_{TY}+K_{byt} \cdot \frac{du}{dz}(z=L)) - P(u+u_{imp})\} \cdot \frac{d}{dz}(v+v_{imp}) - (M_{TX}+M_{BX})/L \cdot (u+u_{imp}) - \{M_{BY}-K_{byb} \cdot \frac{du}{dz}(z=0) + M_{TY}-K_{byt} \cdot \frac{du}{dz}(z=L)\} \cdot (v+v_{imp}) = (GK_T-\bar{K}) \cdot \frac{d\phi}{dz} - \{\frac{d^3\phi}{dz^3} \cdot \frac{D^2}{4} (\sum_{j=1}^{j=s} \Delta a_j \cdot \sigma_j \cdot \xi_j/\rho_\eta + \sum_{k=1}^{k=s} \Delta a_k \cdot \sigma_k \cdot \xi_k/\rho_\eta) - \frac{d^3u}{dz^3} \cdot \frac{D}{2} (\sum_{k=1}^{k=s} \Delta a_k \cdot \sigma_k \cdot \xi_k/\rho_\eta - \sum_{j=1}^{j=s} \Delta a_j \cdot \sigma_j \cdot \xi_j/\rho_\eta)\} \quad \ldots \quad (5.21)$$

where the respective flange stiffnesses are explained in Section 5.2.

These three differential equations are coupled and non-linear and the various stiffness properties vary along the length of the column. The forces being dependent upon the assumed deflected shape, they are best solved by iterative methods. A numerical solution based on centre finite difference has been used in this study and the method employed was Successive Over Relaxation[33]. Other first order methods of iterative solution could have been employed and dynamic relaxation was explored for an elastic beam column problem but it was found to be slower in convergence and the equations more cumbersome to handle than the S.O.R. method. The latter method was adopted and is particularly suitable for a diagonally dominant system of equations with very few coefficients outside the diagonally banded area. Because of the non-symmetric bending it is necessary to calculate the column deflections along the entire length. In the following sections a general procedure for computing deflections at a number of discrete points along a column under biaxial bending is outlined.

5.5 Finite Difference Form of Equations

The equations (5.19) - (5.21) may be expressed in finite difference form. Let the column length be divided into 'r' equal segments. The station points are identified as shown in Figure 5.4.

Equation (5.19) in finite difference form becomes:

$$X_{\xi_i}(v_{i-1} - 2v_i + v_{i+1})/h^2 + P(v_i + v_{imp_i}) = M_{BX} - z_i/L(M_{BX}+M_{TX})$$

$$+ \phi_i\{M_{BY}-K_{byb}(u_1-u_3)/2h - z_i/L(M_{BY}-K_{byb}(u_1-u_3)/2h + M_{TY}-K_{byb} \cdot$$

$$(u_{j-1}-u_{j+1})/2h) + P(u_i+u_{imp_i})\} \qquad \ldots (5.22)$$

where X_{ξ_i} is as defined earlier in Section 5.2

'h' is the length of each segment

subscript 'i' denotes any station in the column

subscript 'j' denotes the end station as shown in Figure 5.4.

Using the following notation for the bending moments at station 'i'

$$M_{xx_i} = M_{BX} - z_i/L(M_{BX}+M_{TX}) \qquad \text{and}$$

$$M_{yy_i} = M_{BY} - K_{byb}(u_1-u_3)/2h - z_i/L(M_{BY}-K_{byb}(u_1-u_3)/2h$$

$$+ M_{TY} - K_{byt}(u_{j-1} - u_{j+1})/2h)$$

The above equation becomes:

$$X_{\xi_i}(v_{i-1}-2v_i + v_{i+1})/h^2 + P \cdot v_i = M_{xx_i} + \phi_i(M_{yy_i}$$

$$+ P(u_i+u_{imp_i})) - P \cdot v_{imp_i}$$

Then after rearrangement we have:

$$(Ph^2/X_{\xi_i} - 2.0)v_i = h^2/X_{\xi_i} \cdot M_{xx_i} + h^2/X_{\xi_i} \cdot \phi_i \cdot P(u_i+u_{imp_i})$$

$$+ h^2/X_{\xi_i} \cdot \phi_i \cdot M_{yy_i} - v_{i-1}-v_{i+1} - h^2/X_{\xi_i} \cdot v_{imp_i} \cdot P \qquad \ldots (5.23)$$

Equations (5.20) and (5.21) may be expressed in similar form and the details are given in Appendix A. They become:

$$(Ph^2/Y_{\eta_i} - 2.0)\, u_i = - h^2/Y_{\eta_i} \cdot M_{yy_i} - h^2/Y_{\eta_i} \cdot P \cdot u_{imp_i} + h^2/Y_{\eta_i} \cdot \phi \cdot \{M_{xx_i} - P\,(v_i + v_{imp_i})\} - u_{i-1} - u_{i+1} \quad \ldots (5.24)$$

and

$$(2C_{T_i} h^2 + 6\,\frac{D^2}{4} \cdot C_{cf_i} + 6\,\frac{D^2}{4}\, C_{tf_i})\, \phi_i = \{-M_{xx_i} + P\,(v_i + v_{imp_i})\} \cdot h^2 \cdot (u_{i-1} + u_{imp_{i-1}} - 2.0\,(u_i + u_{imp_i}) + u_{i+1} + u_{imp_{i+1}}) + \{-M_{yy_i} - P\,(u_i + u_{imp_i})\} \cdot h^2 \cdot (v_{i-1} + v_{imp_{i-1}} - .2.0\,(v_i + v_{imp_i}) + v_{i+1} + v_{imp_i}) - (\frac{D}{2}\, C_{cf_i} - \frac{D}{2}\, C_{tf_i})\,(u_{i-2} - 4.0\, u_{i-1} + 6.0\, u_i - 4.0\, u_{i+1} + u_{i+2}) - (\frac{D^2}{4} \cdot C_{cf_i} + \frac{D^2}{4} \cdot C_{tf_i})\, \phi_{i-2} + (D^2\, C_{cf_i} + D^2 \cdot C_{tf_i} + C_{T_i} \cdot h^2) \cdot \phi_{i-1} + (D^2\, C_{cf_i} + D^2\, C_{tf_i} + C_{T_i} h^2)\, \phi_{i+1} - (\frac{D^2}{4}\, C_{cf_i} + \frac{D^2}{4}\, C_{tf_i}) \cdot \phi_{i+2} \quad \ldots (5.25)$$

5.6 Method of Solution of Equilibrium Equations

As already stated, the three equations (5.23) - (5.25) may be solved by successive over relaxation. The total number of unknown variables depends on 'r' - the number of equal segments into which the column is divided. The new values of the deflections u_i, v_i and ϕ_i are determined as the sum of the old value plus the difference between the value given by equations (5.23) - (5.25) and the old value times an over relaxation factor. Expressing the value of v for the $(n+1)^{th}$ iterative cycle, equation (5.23), in terms of values of v for the n^{th} iterative cycle and assuming nodes to be taken from the end O to end L of the column in order, we have:

$$v_i^{(n+1)} = v_i^{(n)} + \frac{\alpha}{a_1} \{h^2/X_{\xi_i} \cdot M_{xx_i} + h^2/X_{\xi_i} \cdot \phi_i^{(n)} \cdot M_{yy_i}$$

$$+ h^2/X_{\xi_i} \cdot \phi_i^{(n)} \cdot P \cdot (u_i^{(n)} + u_{imp_i}) - v_{i-1}^{(n+1)} - v_{i+1}^{(n)} - a_1 \cdot v_i^{(n)}$$

$$- h^2/X_{\xi_i} \cdot P \cdot v_{imp_i}\} \qquad \ldots (5.26)$$

where $a_1 = Ph^2/X_{\xi_i} - 2.0$

and α = the relaxation factor determining the degree of over relaxation and controlling the rate of convergence.

Similar expressions for u and ϕ are given in Appendix A. α, λ and γ are the three relaxation parameters. For a particular set of values of these parameters, different for every problem, the convergence rate has maximum efficiency. There is no simple method of determining the optimum values except by trial and error, but they will always lie between 1.0 and 2.0. Suitable values were chosen on the basis of exploratory calculations, a typical result of which is shown in Figure 5.5.

It is seen that equation (5.26) which gives improved values of v also involves values of u and ϕ and similarly the equations for u and ϕ. In the iterative cycle set up to solve these three equations simultaneously, the following procedure was adopted:

a) The iteration for obtaining improved values of v was carried out from node 3 to node j-1 taken in order (see Figure 5.4)

b) The iteration for u was then carried out from node 3 to node j-1, introducing in the process the improved values of v obtained in Step (a).

c) The iteration for ϕ was then carried out using the new values of u and v obtained in Steps (a) and (b).

This completes one cycle of iteration towards the solution of the equations.

d) The iteration from Step (a) to Step (c) was then repeated with the improved values of v, u and ϕ obtained from the last iterative cycle. This process is continued until satisfactory convergence is achieved.

5.7 Convergence Criteria

The finite difference form of the differential equations are given in Section 5.5 (equation 5.22 and Appendix A). The matrix form of the equations although coupled was found to be basically diagonally dominant. For this type of matrix the following convergence criterion was found to be suitable in terms of accuracy and computer time.

Let δv_i, δu_i and $\delta \phi_i$ represent the difference in values obtained for the deflections at station 'i' for the n^{th} and $(n+1)^{th}$ iterations. The magnitude of the cumulative error of all the stations was controlled and was less than a small fraction μ of the cumulative values of deflections of all the stations.

This is expressed as:

$$\frac{\sum_{i=3}^{i=j-1} |\delta v_i|}{\sum_{i=3}^{i=j-1} |v_i|} \leq \mu$$

$$\frac{\sum_{i=3}^{i=j-1} |\delta u_i|}{\sum_{i=3}^{i=j-1} |u_i|} \leq \mu$$

$$\frac{\sum_{i=3}^{i=j-1} |\delta \phi_i|}{\sum_{i=3}^{i=j-1} |\phi_i|} \leq \mu$$

The quantity μ was assigned the small value of 1.0×10^{-7}.

5.8 Computational Procedure

Based on the above-mentioned procedures for computing the stiffnesses and then solving the equations of equilibrium, the following computational procedure was adopted.

Step 1 Read in column length, cross-sectional data, stress-strain characteristics of the material of the column, residual stress and imperfection data.

Step 2 Read in the minor axis restraint data.

Step 3 Read in trial values of the deflections, i.e. v, u and ϕ for all the nodes including the imaginary node 1 and node (j+1). These deflections can be assumed to be zero at the beginning.

Step 4 Read in the constant axial load value and the starting values of major axis moment and minor axis moment for end 0.

Step 5 Read in the ratio of end moments.

Step 6 Compute the initial deflections due to imperfections.

Step 7 Compute the total external moments at all the nodes from node 2 to node j from equations (4.5) and (4.6).

Step 8 Solve the cross-sectional equations at each node, i.e. find values of θ, ρ and Z_n at each node as described in Chapter III.

Step 9 Compute the stiffness properties at each cross-section from equations (5.3) - (5.7).

Step 10 Using the stiffnesses obtained from Step 9, solve the equilibrium equations for the deflected shape of the column by the iterative technique discussed in Section 5.6.

If the solution fails to converge according to the convergence criteria adopted after a specified large number of iterations or the values start diverging, then it is assumed that a stable deflected shape does not exist. One then proceeds to Step 15.

If the solution converges proceed to Step 11.

Step 11 From this new deflected shape compute the total external moments as described in Step 7.

Step 12 Repeat Steps 8, 9 and 10 so that another set of deflections is obtained.

Step 13 Compare the deflections obtained from Step 12 with those obtained previously.

If the values of the deflections differ by less than a specified amount at each node a satisfactory stable deflected shape has been obtained. One may then proceed to Step 14. Otherwise it is necessary to go back to Step 11. If a stable deflected shape is not obtained after repeating this process for a specified number of cycles it is assumed that a stable deflected shape does not exist. One then proceeds to Step 15.

Step 14 Increase the major axis moment by a specified amount keeping axial load and minor axis moment fixed, and repeat from Step 7.

Step 15 If no convergence is obtained either in Step 10 or Step 13 within a specified number of cycles, the major axis moment increment may be reduced by a certain ratio and Steps 7 - 13 may be repeated until the value of the increment diminishes to a specified small value.

Step 16 The highest value of the major axis moment for which a stable deflected shape is obtained is taken as the failure moment of the column for the specified axial load and minor axis moment.

Certain intuitive ideas have been introduced in order to obtain fast convergence. In Step 10 the iterative technique employed to calculate the deflected shape is based on the stiffnesses calculated previously. The stiffnesses change slightly as one moves from one moment-thrust-curvature plot to another. Since the changes in minor axis moments due to deflection effects are small and

the axial load is kept constant, an attempt is made to modify the major axis stiffness after each iteration. This is shown in Figure 5.6 where ΔM is the change in major axis moment due to the improved deflection values obtained after a single iteration. The slope of the $M_\xi - \rho_\xi$ is approximately equal to the true $M_\xi - \rho_\xi$ curve slope since changes in M_η are negligible. On the basis of this $M_\xi - \rho_\xi$ slope at that point the modified stiffness is found by linear extrapolation, as shown in Figure 5.6. This has resulted in a fair improvement in solution time.

Another intuitive idea introduced is indicated in Figure 5.7. The assumed deflections for the next major axis moment increment are obtained by linear extrapolation from the two previous solutions. These deflections are fairly close to the true solution and this has resulted in a significant reduction in solution time.

CHAPTER VI

COMPARISON OF THEORETICAL & EXPERIMENTAL RESULTS

6.1 Introduction

Based on the procedures outlined in the foregoing chapters, two computer programs were developed for use on the CDC 6400/7600 computers. The first program was developed for solving the cross-sectional equations for any given multilinear stress-strain relationship for the flanges and web and the iterative technique outlined in Chapter III formed the basis. The first program is also incorporated in the second program in the form of a subroutine. The second program follows the computational steps outlined in Section 5.8 of Chapter V and traces the load deflection response of an H-column, i.e. major and minor axes deflections and twist, in biaxial bending till failure. The program calculates the actual deflected shape and asymmetrical bending along the column is taken into account. Residual stresses may be included in both the programs. Initial imperfections about the major and minor axes can be considered in the form of cosine waves. The program has been recently modified to include torsional imperfections and could also be altered to cover other end conditions and load paths.

An example is given to demonstrate the accuracy of the program for the solution of the cross-sectional equations by comparing results with another existing program.

Several examples are given where solutions to the differential equations governing biaxial bending with torsion in the elastic range are compared with existing published solutions.

Theoretical results from the second program are compared with the experimental results described in Chapter II.

6.2 Verification of the Moment-Thrust-Curvature Relationships

To check the validity of the program a comparison was made with results obtained from an existing moment-thrust-curvature relations program developed by Virdi and described elsewhere[14]. The details of the example chosen are as follows:

(a) Section 8 in x 8 in @ 48 lb

(b) Axial load: 200 tons

(c) Stress-strain relationships: Those obtained from material tests shown in Figure 2.14 were used. The curves marked 2 and 3 were used for the flanges and web respectively.

(d) No residual stress was introduced.

The moment-thrust-curvature relations obtained by Virdi were based on the Lagrangian interpolation technique and the results are shown in Figure 6.1. It may be seen that there is very close agreement with the results from the Author's program.

6.3 Verification of the Biaxial Bending Equations in the Elastic Range

The differential equations governing bending and torsion are Equations (5.19) - (5.21). The accuracy of the accelerated iterative technique described previously for solving the above differential equations was examined with Culver's solutions. Culver[34] has provided solutions for symmetrical biaxial bending in the elastic range and obtained analytical solutions to the differential equations of equilibrium. The published results are thus accurate from this aspect. The examples chosen for comparison are Prob.2 and Prob.4 of the above-mentioned publication, so that both free warping and restrained warping cases are covered. The cross-sectional properties of the examples chosen are summarised in Table III. The results of the 'warping free' case (Prob.2) due to Culver are compared with those from the program and are summarised in Table IV and Figure 6.2. The results for the 'restrained warping' case (Prob.4) are summarised in Table V and Figure 6.3.

It may be seen that the results are in close agreement with those of Culver and slight differences are probably attributable to the differences in numerical approach.

Syal and Sharma[35] have provided numerical solutions to asymmetrical elastic biaxial bending equations. This includes the case of double curvature biaxial bending. The solution of the differential equations of equilibrium was simplified by assuming a power series solution. The various constants at a particular load level were evaluated from the boundary conditions and considering equilibrium at the quarter points and mid-point along the length of the column.

Since the iterative technique developed is for asymmetric bending, solutions of an elastic problem are compared with those given by Syal and Sharma. The example chosen is Column 15 in the paper mentioned above. The cross-sectional properties of the example chosen are tabulated in Table VI. The results obtained are summarised in Tables VII- IX and Figure 6.4. It is seen that the results are identical within the range of numerical accuracies.

6.4 Comparison of Theoretical and Experimental Results

One of the aims of the theoretical study was to simulate the experimental conditions and attempt to correlate between theory and experiment. The experimental results of the tests have been discussed in Chapter II, Sections 2.10 and 2.11. Theoretical correlation with the results will be considered in this Section.

Full-scale experiments involve uncertainties, some of which are mentioned below:

(a) Variations in stress-strain relations in different parts of the column.

(b) Magnitude of residual stress and variation.

(c) Simulating theoretical support conditions and loading.

(d) Variations of initial imperfections along the column length not being the normally assumed cosine wave.

(e) Variations in cross-sectional dimensions along the length.

(f) Presence of torsional imperfections.

A possible combination of several of these effects can make accurate correlation with experimental results unlikely. Therefore only a general correlation with experimental results was sought. It is not possible for example to cover all possibilities under (a) and (b) and therefore an exhaustive study of material properties was not considered justified. As already mentioned, cold straightening of the column length could have totally altered the residual stress distribution over a critical length. Residual stresses were therefore generally not included in the theoretical calculations for correlation with experiments, but their effect was investigated for one of the columns and this is discussed. Material properties obtained were different for flanges and webs and these were taken into account in the theoretical calculations. The material properties across the flanges were considered uniform, but in actual practice they vary along the width of the flange. To account for these variations, even if relevant data were available, would involve excessive solution time on the computer.

Initial imperfections were measured at mid-point of the column and assumed to vary as a cosine wave along the length of the column.

Cross-sectional dimensions were measured at three points in the column and the average of the dimensions was used in the theoretical calculations.

Computer results were obtained for all the test columns described in Chapter II, except column A1. The load path followed in the calculations was the same as that described for those experiments. The minor axis bending moment in the calculations was kept constant, except in the case of the restrained column, C1, at a value of 4.0 t.in. and was considered to be applied at both ends to produce single curvature bending. All the theoretical results have been expressed graphically along with experimental

points. The theoretical and experimental results are summarised in Table X.

In view of the repeated number of loadings and unloadings undertaken in testing column A1, and therefore certain doubts about the reliability of the results as already mentioned in Chapter II, Section 2.10.2, no theoretical calculations have been made for this column.

Column A2

This was a short column and the lightest rolling 8 in x 8 in @ 31 lbs (203 mm x 203 mm @ 46 Kg). The axial load was 0.805 P/P_s with the weaker axis slenderness ratio being 43. The theoretical curve and experimental plots are shown in Figures 6.5 and 6.6. Torsional deflections are not shown as these were negligible in the experiment and calculations. The theoretical collapse moment indicated is 162 t.in. which is approximately 18% higher than the experimental value. The stress-strain curves for this type of cross-section are shown in Figure 2.16 and the higher yield stress of 24 t/in^2 was used in the calculations. Residual stresses could have been present and their effect was not investigated. A combination of the above two factors may be the cause of the lower experimental collapse moment. The concept of total column strength was discussed in Chapter II, Section 2.11. Considered in terms of total column strength, the correlation of 0.99 was very satisfactory.

The significant aspect of column behaviour to be noted from this experiment is the in-plane behaviour at this high axial load with low slenderness value. The calculations also predicted this type of behaviour and in this respect correlation is good. These computer results clearly indicate in-plane behaviour with small minor axis deflections. In the presence of imperfections, the definition of in-plane behaviour is not however always clear and this point is considered in the next chapter.

The experimental minor axis deflection results show somewhat peculiar behaviour and consequently some discrepancies with the theoretical result. This was however not followed up, being relatively insignificant in the overall context. The correlation with experimental end rotation values and major axis deflections are in general reasonable.

Column A3

This was another short column of the lightest rolling 8 in x 8 in @ 31 lb (203 mm x 203 mm @ 46 Kg). The axial load was 0.665 P/P_s with the weaker axis slenderness ratio being 43. The theoretical and experimental plots are shown in Figures 6.7 and 6.8. Torsional deflections again are not shown as these were very small. The theoretical collapse load for this column, using the higher yield stress of 24 t/in^2, is 272.0 t.in. This is only 5% lower than the experimental value, and considering overall column strength, the correlation of 1.01 is good.

This column again performed in an in-plane manner and this aspect of correlation with experiments is also good. There are some discrepancies between theoretical and experimental minor axis deflections, but this was not followed up any further. Theretical major axis deflections and end rotation correlate reasonably well with experiments.

Column B1

This column was a heavier rolling of the section - 8 in x 8 in @ 48 lb (203 mm x 203 mm @ 71 Kg). The axial load was 0.8 P/P_T with the weaker axis slenderness ratio being 59. The theoretical and experimental plots are shown in Figures 6.9 - 6.11. In the theoretical calculations the stress-strain curve marked 2 in Figure 2.14 was considered for the flanges and the curve marked 3 for the web. The curve marked 2 was idealised as a multilinear curve with ten divisions. The theoretical collapse moment without any residual stresses was 600.0 t.in. This is 11% higher than the experimental value. The effect of residual stresses was investigated for this column and it is the only case in which this was done. As mentioned earlier in Chapter III, the AISC residual stress pattern [28] was used with $\sigma_{rc} = 5.0\ t/in^2$. The theoretical results obtained are also shown in Figures 6.9 - 6.11 with dotted lines. It can be seen that the theoretical collapse load is then 544.0 t.in. which is only 0.8%

higher than the theoretical collapse load. For this column and other columns of Series B, considering overall column strength shown in Table X, the correlation is good, and the effect of residual stress viewed in this perspective is small. The significant aspect of column behaviour to be noted is the gradual increase of out-of-plane deformations and the final collapse by a combination of excessive minor axis deflections and twisting. The general pattern of correlation with experimental values is good. The theoretical minor axis deflections follow the experimental trend of increasing more rapidly than the major axis deflections and consequently produce out-of-plane failure. The computer results thus indicate out-of-plane failure. Correlation with experimental end rotation, major and minor axes deflections and twist are good for the theoretical curve with residual stress.

Column B2

This column was also the heavier rolling of the section - 8 in x 8 in @ 48 lb (203 mm x 203 mm @ 71 Kg). The axial load was 0.7 P/P_T with the weaker axis slenderness ratio being 59. The theoretical curves and experimental points are shown in Figures 6.12 to 6.14. For this column another set of material tests was carried out on specimens cut from the small-moment-end of the column and this is the only instance where this was done. The stress-strain relationships were basically similar to the ones shown in Figure 2.14 with slight variations and are therefore not reproduced again. The theoretical collapse load, with the stress-strain relationship for the flange and web as obtained, was 686.0 t.in. This is approximately 16% higher than the experimental collapse load. Residual stress was not included in the calculations. One possible explanation may be that quite high residual stresses were present in this column. Also stress-strain relations could vary along the length of the column.

For this column as well, the behaviour was marked by the gradual increase of out-of-plane deformations and the final collapse by a combination of these deformations. The general pattern of

correlation with experimental values is good. The computer results indicate out-of-plane failure. Correlation with experimental end rotation and major axis deflections are good but there are discrepancies in the minor axis deflections and twist. These may be due to variation in the initial imperfections.

Column B3

This column was of a lighter rolling - 8 in x 8 in @ 35 lb (203 mm x 203 mm @ 52 Kg). The axial load was 0.69 P/P_T with the weaker axis slenderness ratio being 61. The theoretical curves and experimental points are shown in Figures 6.15 - 6.17. The stress-strain relationships used in the calculations are shown in Figure 2.15 and were introduced into the computer program in the same way as mentioned previously. The theoretical collapse load is 306 t.in. This is only 2% higher than the experimental collapse load. No residual stress was included in the calculations. This column also failed by a combination of minor axis bending and twisting. The general pattern of correlation with experimental values is good, the computer results indicating similar behaviour. Correlation with experimental end rotation, major and minor axes deflections are good. Correlation with twist values recorded, however, shows some discrepancies.

Column B4

This column was of the same rolling section and length as B3. As discussed previously this column was tested under a reduced axial load of 100 tons, to investigate out-of-plane stability. When the end rotation of 0.16 radians was reached during the experiments, the axial load was increased keeping the end joint rotation constant. The load path followed during the experiment is shown in Figure 2.33. The theoretical curves and experimental points for the first phase of the test when the axial load was kept constant are shown in Figures 6.18 - 6.20. The stress-strain relationship included in the calculations was the same as the previous column B3. No residual stress was included in the calculations. The correlation

with experimental major and minor axes deflections is good while there are discrepancies in the end rotation and twist values.

As the axial load was increased plastic 'moment shedding' [25] occurred. This is depicted in Figure 2.34. The computer program was modified to obtain stable deflected shapes under increasing axial loads with major and minor axes moments held constant. The ultimate theoretical axial load obtained was 140 t.in. and the major axis moment was 380 t.in. The theoretical axial load is 12.5% lower than the experimental value, but this is to be expected because plastic 'moment shedding' occurred during the tests. Considering overall colum strength, the correlation of 1.016 (Table X) is good. Theoretical plots for this part of the test (axial load increased) are not shown.

Column C1

This was the longest column tested from the heavier rolling section - 8 in x 8 in @ 48 lb (203 mm x 203 mm @ 71 Kg). The slenderness ratio about the weaker axis was 74. As discussed previously in Chapter II this column could not be expected to sustain high axial loads. Accordingly, minor axis restraint was introduced into this test. The minor axis restraint estimated after the test was approximately 3100 t.in/rad. This value was used for the theoretical calculations. The column was tested initially at an axial load of 150 tons. This part of the test has been termed phase 2 in Chapter II. The stress-strain curves included for computations were the same as those for column B1. Residual stresses were not considered for calculations. The load path followed is shown in Figure 2.39. The theoretical curves and experimental points for phase 2 are shown in Figures 6.21 - 6.23. Correlation with experimental end rotation, major and minor axes deflections and twist is good.

The next part of the test, phase 3, consisted of increasing the axial load till failure. As depicted in Figures 2.39 and 2.40 plastic 'moment shedding' occurred. At 200 tons the major axis

moment was increased by a small amount and then again axial load was increased till failure which occurred at 220 tons. The computer program was modified, as in the case of column B4, to obtain stable deflected shapes under increasing axial loads with major and minor axes moments held constant. Theoretical curves for major and minor axes deflections and experimental points for this part of the test are shown in Figure 6.24. The slight increase in major axis moment when the value of the axial load was 200 tons was not considered in the computer program. The theoretical collapse load is 208 t.in. This is approximately 6% lower than the experimental value. This is quite expected because in the computer program the major axis support conditions are "pin-ended", and plastic 'moment shedding'[25] cannot occur. Again, considering total column strength, Table X, the correlation of 1.017 was good. The experimental points, Figure 6.24, indicate smaller deflection values, but this is thought to be a direct consequence of plastic moment shedding during the experiment. The restraining moments developed about the minor axis, both theoretical and experimental, are shown in Figure 6.25. The theoretical curve is for the end-moment end while experimental points for both ends of the column are shown. Higher restraining moments were developed during the experiment than predicted theoretically. This has contributed towards the higher experimental collapse load.

A typical analysis, for calculating the collapse moment of these columns, took about 1000 seconds on the CDC 6400 computer.

CHAPTER VII

APPLICATIONS, DISCUSSION AND CONCLUSION

7.1 Introduction

It was observed in Chapter II that the failure modes of columns in Groups A and B were different. The columns in the former group failed in plane while those in the latter group failed by lateral torsional buckling. The question of what is a lateral torsional buckling mode failure for a column with imperfections is not always clear, and this chapter starts with a general discussion of this type of failure, with suggestions on possible criteria to identify it.

The steps in the development of the computer program for calculating failure loads of columns in biaxial bending have been described in the previous chapters. The torsionally stiff section 8 ins x 8 ins @ 48 lb ($T = 75.2$ t/in^2) which has been recommended as being suitable for plastic action[16] with grade 50B steel was then chosen for a theoretical study to explore safe slenderness limits for in-plane behaviiur. Results of the theoretical calculations obtained from the program are compared with one existing set of published charts[16] presented by Professor Horne.

The computer program developed also included minor axis end restraint. The effect of minor axis restraint on the ultimate failure moment and its influence on lateral torsional buckling mode failure is explored next. Theoretical calculations on the same (8 ins x 8 ins @ 48 lb) section were carried out with the objective of exploring the effective increase in slenderness limits for in-plane behaviour. These are again compared with the previously mentioned charts[16] presented by Professor Horne. Concluding remarks on the experimental programme and a summary of the theoretical work are finally given.

7.2 What Constitutes LTB Failure?

The theoretical approach to date adopted towards the lateral torsional buckling problem has been the mathematically correct eigen value approach. In this approach lateral torsional buckling is a clearly defined bifurcation point on the equilibrium

path. A perfectly straight wide flange member which is subjected to an axial force and to end moments about the strong axis of the member will deflect in the plane of the applied moments as long as the moments and axial force are below certain critical values. At the instant of attainment of the critical condition bifurcation of equilibrium will take place and failure is initiated by lateral deflection and twisting of the member.

Typical idealized inelastic beam-column behaviour is illustrated in Figure 7.1(a), where the schematic relationship between the applied end moment, M_x and the resulting end slope, θ_o, is shown for a wide flange member bent about its strong axis. The axial force, P, and the end moment ratio, β, are assumed to remain constant as the moment M_x is increased from zero to its maximum value and past the maximum moment into the unloading zone.

Failure, i.e. unloading of the moment capacity, may be attributed to two major causes:

(a) If lateral torsional buckling is prevented by suitable bracings placed at appropriate intervals within the span of the member, failure will be due to excessive bending in the plane of applied moment[20]. This is the optimum expected performance of the beam-column and the resulting $M_x - \theta_o$ curve is the upper branch of the curve in Figure 7.1(a). The corresponding maximum moment is $M''_{x_{max}}$.

(b) If no lateral bracing is provided, failure may be due to lateral torsional buckling, and the resulting maximum moment $M'_{x_{max}}$ (see lower branch of the curve in Figure 7.1(a)) will be lower than $M''_{x_{max}}$. The maximum point on this curve is reached after bifurcation of the equilibrium occurs at a moment equal to $M_{x_{cr}}$. At the attainment of $M_{x_{cr}}$, it is possible for the member to be in two infinitely close equilibrium positions:

(i) where the deformations lie all in the original plane of bending

(ii) where the member is also twisted and deformed in the lateral direction.

The value of $M_{x_{cr}}$ for inelastic beam columns may be determined numerically from an eigen value solution. The case of one end moment (end moment ratio $\beta = 0$) has been solved by Galambos and Fukomoto[6]. The details of this work have been summarised in Chapter I and therefore are not repeated here.

The above theoretical approach assumes that the column member is perfectly straight. However, a practical beam column is bent about the major axis with imperfections about the minor axis and this in the presence of axial load gives rise to minor axis bending and out-of-plane deformations. This transforms the problem into one of biaxial bending. There is no buckling in this situation and the eigen value approach can no longer be used. The column $M_x - \theta_o$ deformation curve in this case is characterised only by a failure moment and to determine this one has to trace the complete load-deformation characteristics from the initiation of plasticity.

As may be seen from equations (4.25) - (4.27) in Chapter IV, the differential equations of equilibrium for the biaxial problem are coupled. This implies that all the three deformations, i.e. major and minor axes deflections and twisting, would be present from the very initiation of loading in the presence of imperfections and theoretically there cannot be an in-plane failure. However, such an imperfect column loaded in the manner stated above, depending upon the axial load and slenderness, may either develop severe minor axis bending and twisting and fail in a distinctly lateral torsional buckling mode or, alternatively, it may predominantly deform in plane. The problem of differentiating the 'primarily in-plane' failure from the 'lateral torsional buckling mode' failure arises in such cases and is now considered.

Deterioration of the lateral and torsional stiffnesses during major axis bending is the primary cause of out-of-plane instability where this is dominant. Viewed from the deterioration of stiffness point of view, there exists an elastic critical moment for out-of-plane instability based on the deteriorated lateral stiffnesses. The behaviour, for the idealised case with no imperfections, is illustrated in Figure 7.1(b). At various points 1, 2, 3, 4, along the in-plane deflection curve there exists a set of deteriorated lateral stiffnesses and the corresponding elastic critical moments are shown as M_1, M_2, M_3 and M_4. It is seen that as the lateral stiffnesses deteriorate, the critical moments diminish and they can approach the situation reflected in Figure 7.1(a) where lateral instability occurs before the maximum in-plane strength is reached.

If, however, lateral imperfections are present in the column, this situation is modified. Out-of-plane deformations are present from the initiation of loading and the growth or magnification of these deformations prior to failure is dependent on the prevailing lateral stiffnesses. These stiffnesses in turn are reduced as a result of the biaxial forces associated with these magnified imperfections. Therefore a column which could in theory have remained stable and failed in-plane may, in the presence of imperfection, change its failure mode to lateral torsional buckling. Considering behaviour in general, except for very stocky columns, minor axis and torsional imperfections will always be magnified prior to failure and the problem is to decide where these are significant. If the elastic critical moment is high as failure is approached the failure will be predominantly in-plane but for lower values there will be a gradual transition to lateral torsional buckling failure.

The range of possible cases is illustrated in Figures 7.2 to 7.4, where typical deflection curves for beam-columns with imperfections are shown. The schematic relationship between the applied major axis end moment M_x and the resulting end rotation θ_o, the major and minor axes deflections, v and u, and the twist ϕ are

shown for the load case - axial load P held constant and major axis moments increased to failure.

In Figure 7.2 the behaviour of a beam column which may for all practical purposes be called in-plane failure is demonstrated. It is characterised by these features

(a) During the application of the major axis moment increments the growth of the minor axis deflections is small - the minor axis deflection curve being nearly vertical.

(b) The slope of the major axis deflection curve near the peak, $\frac{dM_x}{dv}$, is less than the slope of the minor axis deflection curve, $\frac{dM_x}{du}$, indicating predominantly major axis bending.

(c) The growth of the twisting deformations is also small.

A column with this type of load deformation characteristics would continue to deform essentially in-plane beyond the peak of the $M_x - \theta_o$ curve. As mentioned earlier in Chapter II, the columns in Group A failed in the plane of applied moments. The load deformation characteristics were very similar to that shown in Figure 7.2. These columns are likely to reach a high proportion of the total column strength as also discussed in Chapter II, Section 2.11. The experimental results also indicate this (Table II).

In Figure 7.4 is shown the behaviour of a column which is clearly a lateral torsional buckling mode failure. The characteristics are distinctly different from those shown in Figure 7.2 and the main features are:

(a) During increase of the major axis moment, the increase of minor axis deflections is initially small but they progressively increase at a faster rate with further increase of major axis moments. The slope of the minor axis deflection curve near failure is less than the slope of the major axis deflection curve. This indicates predominantly out-of-plane failure.

(b) The growth of the twisting deformations is excessive and near the peak the slope of the curve is nearly zero, indicating very little torsional resistance.

The columns in Group B failed in this mode, as reported in Chapter II, and the load-deformation characteristics were very similar to those shown in Figure 7.4. Columns of this type are not likely to reach as high a proportion of the total column strength as those in Group A (see Table II).

In Figure 7.3 is shown the behaviour of a column which may be said to be on the boundary of in-plane failure. The characteristics lie somewhat in the middle of the two cases illustrated earlier in Figures 7.2 and 7.4. To be able to classify column behaviour for design purposes, it is obviously necessary to establish criteria defining limits for what is essentially in-plane behaviour, even though no clear theoretical demarcation exists.

It may be seen from Figures 7.2 and 7.4 that the slope of the curves near failure is an indication regarding its mode of failure, i.e. $\frac{dM_x}{du}$, $\frac{dM_x}{dv}$ and $\frac{dM_x}{d\phi}$. Therefore two possible criteria can be on the basis of:

(i) an absolute value on the ratio of the slope of the minor axis deflection to the major axis deflection near failure

(ii) an absolute value on the ratio of the slope of the twisting deformations of the initial part of the loading to that near failure.

Thus for primarily in-plane behaviour ($0 \leq \beta \leq +1.0$) the following criteria are suggested:

(a) $$\left(\frac{dM_x}{du}\right)_{failure} \geq K_d \left(\frac{dM_x}{dv}\right)_{failure}$$

where u = minor axis deflection (mid-column height)

v = major axis deflection (mid-column height)

M_x = major axis end moment

K_d = empirical constant, suggested value 1.5.

(b) $$\left(\frac{dM_x}{d\phi}\right)_{failure} \leq K_\phi \left(\frac{dM_x}{d\phi}\right)_{initial}$$

where ϕ = twisting deformation (mid-column height)

M_x = major axis end moment

K_ϕ = empirical constant, suggested value 30.0

In calculations the slope of the twist curve of the initial part is taken as the average up to half the failure moment.

Based on this approach calculated beam column cases have been identified as in-plane failure or lateral torsional buckling.

7.3 Ultimate Load Design Predictions

The failure modes of beam columns, with minor axis imperfections and subjected to major axis bending, were discussed in the preceding section. Lateral torsional buckling limits for such beam columns are clearly of importance in relation to ultimate load design. This is particularly the case in methods of design based on the estimation of collapse loads, where the concept of in-plane behaviour with possible plastic hinge action at either or both ends is being considered.

The full scale tests, reported earlier, at high axial loads had confirmed the importance of slenderness as a key parameter affecting out-of-plane stability. If plastic hinge action is to occur in an H-section member subjected to major axis bending without premature collapse due to lateral torsional buckling, the level of axial load permitted must be controlled in relation to the weaker axis slenderness ratio. In an effort to explore such out-of-plane buckling limits for various combinations of axial load and slenderness ratio, the following set of theoretical calculations were undertaken. Also the effect of minor axis restraint in raising these limits was examined.

7.3.1 Exploratory Calculations

The torsionally stiff section 8 ins x 8 ins @ 48 lb ($T = 75.2$ t/in^2), which has been recommended as being suitable for plastic action[16] with grade 50B steel was selected for the theoretical calculations. Other details are:

(a) stress-strain relationship: bilinear (i.e. elastic-perfectly plastic) for the flanges and web

(b) yield stress - $Y_s = 22.5$ t/in^2

(c) residual stress: AISC pattern: $\sigma_{rc} = 4.5$ t/in^2 (see Chapter III, Section 3.4).

(d) end moment ratio (major axis): $\beta = 0.15$ (single curvature bending)

(e) minor axis disturbing moment: 4.0 t. in. (maintained constant) with end moment ratio $\beta = 1.0$ (single curvature bending).

(f) initial imperfections: L/1400 - minor axis
L/2000 - major axis
(approximately)

For this type of beam column it has been mentioned earlier that there was no precise bifurcation of equilibrium point and certain criteria were suggested to identify 'primarily in-plane' failure from lateral torsional buckling. A large number of calculations, which gave the complete load deflection response of the beam columns, was undertaken and classified by this criteria. The combination of mean axial stress, p, and slenderness ratio, ℓ/ry, which have been identified as giving 'primarily in-plane' failure are given below:

	p (t/in^2)	ℓ/ry
(a)	14.9	43
(b)	7.1	59
(c)	4.96	74
(d)	2.48	100

In Figure 7.5 are shown the load deflection characteristics to failure as obtained from the computer program, for $\ell/ry = 74$ and axial stress $p = 4.96$ t/in^2. This is considered to represent 'primarily in-plane' failure. The load deflection characteristics for the other cases (a), (b) and (d) are similar to those shown in Figure 7.5 and are therefore not reproduced. The main features are:

(a) Minor axis deflections are not excessive and the slope of the minor axis deflection curve near the peak is more than the slope of the major axis deflection curve indicating predominantly major axis bending. The value of K_d, the empirical constant defined earlier, is more than 1.5 in all the cases.

(b) Twisting deformations are small. The value of K_ϕ is less than the suggested value of 30.0 in all the cases.

Based on these load deformation paths, which show no tendency towards lateral torsional buckling mode failure, is drawn the predicted slenderness limits for in-plane behaviour as shown in Figure 7.6. This curve would provide limits for the safe combination of axial load and slenderness under which columns may develop plastic hinge action without premature lateral torsional buckling. It should be emphasised that this predicted curve is conservative in the high axial load range and only tentative being based on the in-plane failure criteria defined in the preceding section.

7.3.2 Comparison with Design Charts (BCSA Publication No. 23)

Professor Horne has provided similar design charts[16] for deriving the maximum permissible mean axial stress for plastic hinge action at either or both ends. These charts were derived, as reviewed earlier in Chapter I, on the basis that plastic hinges may form at either or both ends of the column but the yield stress must not be reached at mid-column height. This was a severe limitation and hence the apparently conservative nature of

Professor Horne's curves, for the appropriate β and T value, as shown in Figure 7.6 is not surprising. His charts excluded the effect of residual stresses. In the calculations described earlier, the AISC pattern of residual stress was considered.

In the absence of any computer program to calculate lateral beam instabilities, (i.e. the limiting case when axial load is zero) the limiting slenderness for zero axial load as suggested by Professor Horne is accepted and the predicted curve extended to that point.

Another set of exploratory calculations, based on an exactly similar approach to those already described was undertaken for the $\beta = 0.4$ case. These were intended to explore the sensitivity of the slenderness limits to variation of end moment ratio β for a case approaching more uniform single curvature bending. Professor Horne's curves are sensitive in this range (i.e. $0.0 \leqslant \beta \leqslant +1.0$) and it was thought that this would be a direct consequence of the stability criteria of not exceeding the yield stress at mid-column height. The theoretically predicted curve for this case ($\beta = 0.4$) is shown on Figure 7.7 along with Professor Horne's prediction and again confirms the conservative nature of his approach. Also shown are the curves for the $\beta = 0.15$ case for comparison and it is seen from the predicted curves that the sensitivity to β value is not so severe as indicated by Professor Horne's design curves.

The effect of variation of T value has not, however, been investigated theoretically and this could have as much effect as the level of axial load in establishing slenderness limits.

Slenderness limits for the $\beta = +1.0$ case have not been established. Nevertheless, it appears from Figure 7.7 that in the high axial load range ($P/P_s > 0.4$) the slenderness limits are almost insensitive to β values. It seems to indicate that one slenderness limit could cover all the cases between $0 < \beta < 1.0$ and would be significant from the design point of view.

7.4 Effect of Minor Axis End Restraint

It was mentioned in Chapter II that Column C1 was tested with minor axis restraint. Although the ultimate failure was in the lateral torsional buckling mode, it sustained higher moments than it would have done without the restraint. This was achieved, as pointed out, with relatively light restraint. This phenomenon has been confirmed by a series of theoretical calculations on the same Column C1. The stress-strain relations used are those from Figure 2.14, the curve marked '2' being used for the flange and the one marked '3' being used for the web. Calculations for the pin-ended case are presented first for easier comparison. All the major and minor axes deflections and twist results now presented are for mid-column height only. Figure 7.8 shows the load-deflection characteristics up to failure for the above-mentioned column with an axial load of 150 tons under pin-ended conditions and $\beta = 0.15$. A small minor axis moment of 2.0 t. in. producing symmetrical single curvature bending about this axis was maintained constant throughout the computer calculations. The results as may be seen from Figure 7.8, indicate lateral torsional buckling failure at a moment of 750 t. in. The slope of the minor axis deflection curve, $\frac{dM_x}{du}$, near the peak is nearly zero and is less than the major axis deflection curve slope, $\frac{dM_x}{dv}$. Twisting deformations are large and the slope of the curve near the peak is virtually zero. The value of K_ϕ (the empirical constant defined earlier) is approximately 198.2 which implies excessive torsional deformation.

The results for the same column with minor axis restraints are shown in Figures 7.9 and 7.10. Calculations with minor axis beam stiffnesses of 12,000 ($K_{byb}/K_C = 0.58$) and 20,000 t. in./radian ($K_{byb}/K_C = 0.97$) are shown. The net result is an increase in the failure moment by nearly 30%. As may be seen from Figures 7.9 and 7.10, the minor axis deflections are very much reduced compared to those in Figure 7.8. It can be seen that a minor axis restraint of 12,000 t. in./radian ($K_{byb}/K_C = 0.58$) is not effective in preventing twisting deformations at mid-column height. Twist values are large and a situation of torsional buckling is indicated. The

value of K_ϕ for this end restraint case ($K_{byb}/K_C = 0.58$) is approximately 67. This is greater than the suggested value of 30.0 and implies excessive torsional deformation.

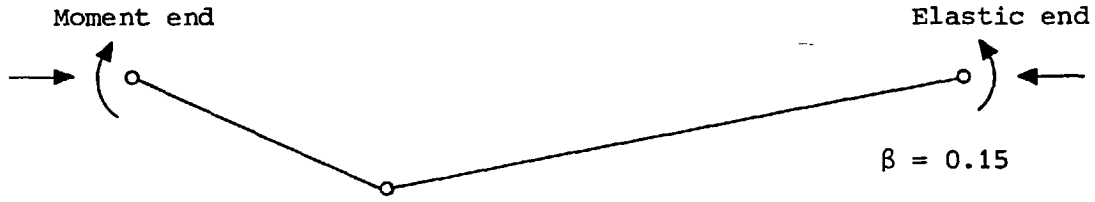
The effect of a stiffer restraint of 20,000 t.in./radian ($K_{byb}/K_C = 0.97$) is shown by the dotted lines in Figures 7.9 and 7.10. Although the ultimate moment is not increased, the failure is essentially in-plane. Torsional deformations are much smaller and the value of K_ϕ is less than 30.0. The calculations for this case therefore suggest that higher restraints would be necessary to obtain satisfactory in-plane performance than would be necessary to obtain the optimum ultimate moment capacity.

In the above example the presence of minor axis end restraints of 12,000 and 20,000 t. in./radian resulted in an increase of the failure moment by about 30%. It was obviously of interest to know the minimum amount of restraint which could provide full fixity regarding collapse moment for all practical purposes. This was investigated by varying the minor axis end restraint and the variation of ultimate moment associated with this is shown in Figure 7.11. The distinct improvement in the moment carrying capacity due to quite small restraint emerges quite clearly from the left part of the curve (Figure 7.11). A restraint of only 7,000 t.in./radian ($K_{byb}/K_C = 0.34$) seems to give nearly the maximum moment obtainable. The curve then becomes almost horizontal, indicating that little further benefit can be derived by increasing the restraint.

In the same plot (Figure 7.11) is shown the benefit to be derived when the restraint is applied at one end only. It can be seen that restraint at the greater moment end is more effective than restraint applied at the smaller end ($\beta = 0.15$ for the beam column under discussion). This can be explained as following:

Pin-ended beam columns at failure would develop a partial plastic hinge somewhere inside the column and would produce a collapse mechanism. Now the position of this plastic hinge is dependent upon the loading conditions. Symmetric single curvature bending ($\beta = + 1.0$) would produce this partial plastic hinge

at mid-point of the column. In the example considered above, the beam column was subjected to a major axis moment gradient ($\beta = 0.15$). Coupled with this was the condition of high axial load and minor axis moments associated with imperfections. This resulted in the formation of a partial biaxial hinge at about the third point of the column. The hinge formation is far from complete, as one flange only is plastic and the other elastic. Nevertheless, it would produce a possible collapse mechanism shown below:



Column Collapse Mechanism

It is now obvious that providing restraint at the end nearer to the hinge would be more effective and invariably delay the formation of this partial biaxial hinge at about the third point. Restraint provided at the far end would have much less influence on the formation of this hinge, and hence this would produce a lower collapse moment than the other case of restraint at the nearer end. The theoretical results (Figure 7.11) confirm this view.

7.4.1 Ultimate Load Design Predictions With Minor Axis Restraint

The slenderness limits for 'primarily in-plane' behaviour for pin-ended columns were investigated in the preceding section. The effect of minor axis restraint on these slenderness limits will now be discussed. The previously illustrated case of $\beta = 0.15$ with minor axis restraint at both ends is chosen again for the theoretical calculations. Other details are exactly similar to the example described in Section 7.3.1, except that no minor axis moments are applied in this case.

The minor axis restraint stiffness was 20,000 t. in./ radian and was selected as a typical value on the horizontal part of the curve in Figure 7.11 (discussed earlier) and which would provide the maximum ultimate moment.

Since there is no direct way of determining the slenderness limits which conform to the in-plane criteria mentioned earlier, a large number of calculations were again undertaken. The complete load deflection response of each beam column was compared with the 'primarily in-plane'failure criteria. The results of a typical restrained column behaviour are shown in Figure 7.12. These curves are considered to represent 'primarily in-plane' behaviour. The predicted design limit curve with minor axis restraint is shown in Figure 7.13. Also shown is the pin-ended curve and Professor Horne's predicted pin-ended curve[16] for comparison. The improvement in permissible slenderness is readily seen. Columns in the middle slenderness range ($\ell/ry \approx 50\text{-}90$) are seen to benefit most from the restraint.

The range of increase in slenderness ratios as indicated in Figure 7.12 also suggests that the effective length approach if applied to restrained columns could be unsatisfactory for elastic plastic behaviour. It should also be pointed out that perhaps with very high restraint the permissible slenderness ratios could be increased safely a little further, but this is a matter of discretion.

7.5 Concluding Remarks on the Experimental Programme

A limited series of full scale tests on H-columns at high axial loads, carried out to explore their out-of-plane stability under a major axis moment gradient, were reported.

The tests have shown that there are severe limits to the slenderness at which pin-ended H-columns under high axial loads can develop a simple major axis plastic hinge at one end and remain stable in-plane while sustaining high joint rotations. This has been supported by subsequent calculations.

In columns under high axial loads and major axis moment applied at one end plasticity spreads significantly down the column length. This is demonstrated by the deflected shape of the column. As a typical example of spread of plasticity, the deflected shapes about the major and minor axes at the maximum joint rotation attained for Column B1 are plotted in Figures 7.14 and 7.15. They indicate plastic deformations spreading through most of the column length and the absence of any localised hinge. The short columns tested with $\ell/ry \approx 45$ (Group A) behaved in-plane, but for the more slender columns minor axis moments, associated with the imperfections, resulted in a reduction of the column strength below their in-plane value. Columns tested with $\ell/ry \approx 60$ (Group B) appeared to develop a biaxial plastic hinge about a third of the way down the column and like a laterally unsupported simple beam, failed out-of-plane without developing significant further in-plane rotation capacity. The hinge is far from complete in that only one flange goes plastic with the other remaining elastic; but the resulting loss of minor axis bending and warping stiffnesses leads to lateral torsional buckling.

At loads above about half the squash load and minor axis slenderness somewhere between Series A and Series B, the hinge tends to develop away from the column end initiating failure by out-of-plane lateral torsional buckling. This, however, does not occur until a joint rotation capacity in excess of 0.02 radians has been achieved at the end at which the major axis moment is applied. These tests also suggest that for more slender H-columns ($\ell/ry \approx 60$) the torsional stiffness is not an important parameter influencing behaviour under pin-ended conditions.

7.5.1 Conclusion and Summary of Theoretical Work

The predicted slenderness limits for 'primarily in-plane' behaviour for pin-ended H-columns are shown in Figure 7.6. This predicted curve is conservative in the high axial load range and only tentative being based on the in-plane failure criteria defined earlier. Nevertheless, the shape of the left part of this curve

is nearly vertical and suggests that axial load has only moderate effect above about half the squash load. Slenderness is then the overriding parameter. This has been confirmed by Group A test columns. Although no calculations for the $\beta = +1.0$ case have been done, it appears from Figure 7.7 that in the high axial load range ($P/P_S > 0.4$) the slenderness limits are almost insensitive to β values. It seems to indicate that one slenderness value could cover all the cases between $0 \leqslant \beta \leqslant 1.0$. This is interesting as it could lead to the definition of a new class of short columns which under high axial loads would develop a simple major axis plastic hinge at one end and remain stable in-plane while sustaining high joint rotations.

The following points summarise the theoretical work and provide guidelines for future investigators:

(a) With the help of the theoretical work undertaken, it has been possible to trace the complete load deflection path for beam columns up to failure. Torsional effects are important and must be considered to obtain the true mode of failure under the loading conditions discussed earlier.

(b) Based on the load deflection characteristics, typical design curves have been presented defining slenderness for 'primarily in-plane' behaviour. These curves have been compared with one set of available design curves[16] which have been found to be conservative.

(c) Effects of minor axis end restraint have been studied. The benefits to be derived in terms of raising the slenderness limits for 'primarily in-plane' behaviour has again been presented as a typical design curve.

(d) From the above-mentioned design curve it appears that a direct effective length approach for restrained columns could be misleading regarding their true strength considering elasto-plastic behaviour.

APPENDIX A

Finite Difference form of Equations (5.20) and (5.21), Chapter V.

Equation (5.20) becomes

$$Y_{\eta i}\ (u_{i-1} - 2.0\ u_i + u_{i+1})/h^2 + P \cdot u_i$$

$$= - M_{YY_i} - P \cdot u_{imp_i} + \phi_i \{M_{XX_i} - P\ (v_i + v_{imp_i})\} \qquad \ldots\ (A1)$$

where M_{XX_i} and M_{YY_i} are as defined in Section 5.5.

Then after rearrangement we have

$$(P \tilde{\cdot} h^2/Y_{\eta_i} - 2.0)\ u_i = - h^2/Y_{\eta_i} \cdot (M_{YY_i} + P \cdot u_{imp_i}) + h^2/Y_{\eta_i} \cdot$$

$$\phi_i \cdot \{M_{XX_i} - P\ (v_i + v_{imp_i})\} - u_{i-1} - u_{i+1} \qquad \ldots\ (A2)$$

The torsional equation (5.21) contains first and third derivatives of ϕ with respect to z. In order to incorporate the boundary conditions in the relaxation technique it is necessary to differentiate the equation once more with respect to z.

Differentiating equation (5.21) and neglecting product of small quantities, we have after simplification

$$C_{Ti} \frac{d^2\phi}{dz^2} - \frac{d^4\phi}{dz^4} \left(\frac{D^2}{4} \cdot C_{cfi} + \frac{D^2}{4} \cdot C_{tfi}\right) = \{- M_{XX_i} + P\ (v_i + v_{imp_i})\} \cdot$$

$$\frac{d^2}{dz^2}\ (u_i + u_{imp_i}) + \{- M_{YY_i} - P\ (u_i + u_{imp_i})\} \cdot \frac{d^2}{dz^2}\ (v_i + v_{imp_i})$$

$$+ \frac{D}{2} \cdot C_{cf_i} \cdot \frac{d^4u}{dz^4} - \frac{D}{2} \cdot C_{tf_i} \cdot \frac{d^4u}{dz^4} \qquad \ldots\ (A3)$$

where $C_{T_i} = G \cdot K_T - \overline{K}_i$

In finite difference form this becomes

$$C_{T_i}(\phi_{i-1} - 2\phi_i + \phi_{i+1})/h^2 - (\frac{D^2}{4} C_{cf_i} + \frac{D^2}{4} C_{tf_i}) \cdot (\phi_{i-2} - 4\phi_{i-1} + 6\phi_i - 4\phi_{i+1} + \phi_{i+2})/h^4 = \{- M_{XX_i} + P(v_i + v_{imp_i})\} \cdot \{u_{i-1} + u_{imp_{i-1}} - 2(u_i + u_{imp_i}) + u_{i+1} + u_{imp_{i+1}}\}/h^2 + \{- M_{YY_i} - P(u_i + u_{imp_i})\} \cdot \{v_{i-1} + v_{imp_{i-1}} - 2(v_i + v_{imp_i}) + v_{i+1} + v_{imp_{i+1}}\}/h^2 + (\frac{D}{2} C_{cf_i} - \frac{D}{2} C_{tf_i}) \cdot (u_{i-2} - 4u_{i-1} + 6u_i - 4u_{i+1} + u_{i+2})/h^4 \quad \ldots (A4)$$

To determine values of u_i from equation (A2) the following iterative cycle may be set up

$$u_i^{(n+1)} = u_i^{(n)} + \frac{\lambda}{b_1} \cdot \{- h^2/Y_{\eta_i} \cdot M_{YY_i} + h^2/Y_{\eta_i} \cdot \phi_i^{(n)} \cdot M_{XX_i} - h^2/Y_{\eta_i} \cdot \phi_i^{(n)} \cdot P(v_i^{(n)} + v_{imp_i}) - h^2/Y_{\eta_i} \cdot P \cdot u_{imp_i} - u_{i-1}^{(n+1)} - u_{i+1}^{(n)} - b_1 \cdot u_i^{(n)}\} \quad \ldots (A5)$$

where $b_1 = P \cdot h^2/Y_{\eta_i} - 2.0$

λ = relaxation factor

n = iteration number

Similarly for determining the values of ϕ_i the following iterative cycle may be set up

$$\phi_i^{(n+1)} = \phi_i^{(n)} + \frac{\gamma}{d_1}\{- h^2 \cdot (M_{XX_i} - P \cdot (v_i + v_{imp_i}) \cdot$$

$$(u_{i-1}^{(n+1)} + u_{imp_{i-1}} - 2\,(u_i^{(n)} + u_{imp_i}) + u_{i+1}^{(n)} + u_{imp_{i+1}})$$

$$- h^2 \cdot (M_{YY_i} + P \cdot (u_i^{(n)} + u_{imp_i}) \cdot (v_{i-1}^{(n+1)} + v_{imp_{i-1}} - 2$$

$$(v_i^{(n)} + v_{imp_i}) + v_{i+1}^{(n)} + v_{imp_{i+1}}) - e_1\,(u_{i-2}^{(n+1)} - 4_{u-1}^{(n+1)} + 6u_i^{(n)}$$

$$- 4\,u_{i+1}^{(n)} + u_{i+2}^{(n)}) - f_1 \cdot \phi_{i-2}^{(n+1)} + g_1 \cdot \phi_{i-1}^{(n+1)} + g_1 \cdot \phi_{i+1}^{(n)}$$

$$- f_1 \cdot \phi_{i+2}^{(n)} - d_1 \cdot \phi_i^{(n)}\} \qquad \ldots(A6)$$

where $d_1 = 2C_{T_i} \cdot h^2 + 3 \cdot \frac{D^2}{2} C_{cf_i} + 3 \cdot \frac{D^2}{2} C_{tf_i}$

$e_1 = \frac{D}{2} \cdot C_{cf_i} - \frac{D}{2} C_{tf_i}$

$f_1 = \frac{D^2}{4} C_{cf_i} + \frac{D^2}{4} C_{tf_i}$

$g_1 = C_{T_i} \cdot h^2 + D^2 \cdot C_{cf_i} + D^2 \cdot C_{tf_i}$

γ = relaxation factor

n = iteration number.

NOTATIONS

The following notations have been used in the text. Any deviation or addition has been defined locally.

A	area of cross-section
a	distance of an elemental area from the centre of twist
b	flange width
C_{cf}	stiffness of the compression flange
C_{tf}	stiffness of the tension flange
C_T	$(G.K_T - \bar{K})$
D	distance between centre line of flanges
d	depth of section
E	elastic modulus = 13000 t/in^2
E_T	reduced elastic modulus
G	elastic shear modulus = 5000 t/in^2
h	length of a column segment
h_1	correction term for solving the cross-sectional equations
I_ξ	moment of inertia about the ξ axis
I_η	moment of inertia about the η axis
I_p	polar moment of inertia
I_w	warping rigidity
I_y	moment of inertia about the y-y axis (weak axis)
K_{byb}	stiffness of minor axis restraining beam at end O
K_{byt}	stiffness of minor axis restraining beam at end L
K_c	column rotational stiffness = $4\ EI_y/L$
K_d , K_ϕ	empirical constant for the in-plane behaviour
K_T	St. Venant torsion constant
$\bar{K}$	Wagner effect = $\int \sigma a^2 dA$
k_1	correction term for solving the cross-sectional equations
L , ℓ	length of column
M_{BX}	applied major axis moment at end O
M_{BY}	applied minor axis moment at end O
M_{cyb}	minor axis column end moment at end O (restrained column)
M_{cyt}	minor axis column end moment at end L (restrained column)
M_f	experimental failure moment
M_{fc}	compression flange bending moment
M_{ft}	tension flange bending moment

M_p	fully plastic moment capacity
M_{pc}	plastic moment capacity as reduced by axial load
M_{ryb}	minor axis restraining moment at end O
M_{ryt}	minor axis restraining moment at end L
M_{TX}	applied major axis moment at end L
M_{TY}	applied minor axis moment at end L
M_{th}	theoretical failure moment
M_x	major axis moment (as defined in the text)
$M''_{x\ max}$	maximum in-plane major axis moment
$M'_{x\ max}$	maximum major axis moment after bifurfaction of equilibrium
$M_{x_{cr}}$	critical major axis moment at bifurfaction of equilibrium
M_y	minor axis moment (as defined in the text)
n	iteration number in relaxation method
P	axial load
P_{crit}	tangent modulus load of a column (pin-ended condition)
P_s	squash load of a column
P_T	ultimate axial load either tangent modulus load or the squash load
p	axial stress
R_X	end shear in the X-direction
R_Y	end shear in the Y-direction
r_x	radius of gyration about X-axis
r_y	radius of gyration about Y-axis
T	torsional stiffness
t	flange thickness
u	minor axis displacement
u_c	minor axis displacement of the centroid
u_{imp_i}	minor axis imperfection at station 'i'
v	major axis displacement
v_c	major axis displacement of the centroid
v_{imp_i}	major axis imperfection at station 'i'
V_{fc}	compression flange shear
V_{ft}	tension flange shear
w	web thickness
x_o	x-coordinate of shear centre
X_ξ	stiffness of the section about the ξ axis
y_o	y-coordinate of shear centre
Y_s	yield stress of the material
Y_η	stiffness of the section about the η axis

z_i	distance of station 'i' from end O
z_n	depth of the neutral axis
z_x	elastic modulus of section.
α	relaxation factor for SOR method
β	end moment ratio (= +1.0 for uniform single curvature bending)
γ	relaxation factor for SOR method
Δa_i	an elemental area in the cross-section
δu_i	difference in u deflections at station 'i' for n^{th} and $(n+1)^{th}$ iteration
δv_i	difference in v deflections at station 'i' for n^{th} and $(n+1)^{th}$ iterations
$\delta \phi_i$	difference in ϕ values at station 'i' for n^{th} and $(n+1)^{th}$ iterations
ε	strain
η_i	lever arm of an elemental area from the ξ axis
θ	inclination of the neutral axis
θ_o	end roation
λ	relaxation factor for SOR method
μ	factor controlling the magnitude of the cumulative errors during iteration
ξ_i	lever arm of an elemental area from the η axis
σ_i	stress in an elemental area
σ_{rc}	compressive residual stress
σ_{rt}	tensile residual stress
σ_w	Wagner pure torsion critical stress
ρ	curvature of the section
ρ_η	curvature about the η axis
ρ_ξ	curvature about the ξ axis
ϕ	angle of twist of the section
ω_i	distance of an elemental area Δa_i from the centroid of the section.

Abbreviations

LTB	Lateral Torsional Buckling
S/C	single curvature
RES	compressive residual stress (figures 6.5 - 6.25)

BIBLIOGRAPHY

1. BLEICH, F. *Buckling Strength of Metal Structures,* McGraw Hill Book Company, New York, 1952.

2. NEAL, B.G. "The Lateral Instability of Yielded Mild Steel Beams of Rectangular Cross-Section". *Phil. Trans. of the Royal Society,* Series A, Vol. 242, January 1950.

3. WITTRICK, W.H. "Lateral Instability of Rectangular Beams of Strain-Hardening Material Under Uniform Bending". *Journal of Aeronautical Science,* Vol. 19, No.12, p.835, December 1952.

4. GALAMBOS, T.V. "Inelastic Lateral Torsional Buckling of Eccentrically Loaded Wide-Flange Columns". *Ph.D. Dissertation, Lehigh University,* 1959.

5. OJALVO, M. "Restrained Columns" *Proceedings, ASCE,* Vol.86, No. EM5, p.1, October 1960.

6. FUKUMOTO, Y. and GALAMBOS, T.V. "Inelastic Lateral Torsional Buckling of Beam Columns" *Journal of the Structural Division, ASCE,* Vol. 92, No. ST2, p.41, April 1966.

7. LIM, L.C. and LU, L.W. "The Strength and Behaviour of Laterally Unsupported Columns" *Fritz Engineering Laboratory Report* No. 329.5, June 1970.

8. BIRNSTIEL, C. and MICHALOS, J. "Ultimate Load of H-Columns Under Biaxial Bending" *Journal of the Structural Division, ASCE,* Vol. 89, No. ST2, April 1963.

9. HARSTEAD, G.A., BIRNSTIEL, C. and LEU, K.C. "Inelastic H-Columns Under Biaxial Bending" *Journal of the Structural Division, ASCE,* Vol. 94, No. ST9, October 1968.

10. MILNER, H.R. "The Elastic-Plastic Stability of Stanchions Bent About Two Axes" *Ph.D. Thesis, University of London,* December 1965.

11. CHEN, W.F. and SANTATHADAPORN, S. "Review of Column Behaviour Under Biaxial Loading" *Journal of the Structural Division, ASCE,* Vol. 94, No. ST12, December 1968.

12. SANTATHADAPORN, S. and CHEN, W.F. "Analysis of Biaxially Loaded Steel H-Columns" *Journal of the Structural Division, ASCE,* Vol. 99, No. ST3, p. 491, March 1973.

13. SANTATHADAPORN, S. and CHEN, W.F. "Tangent Stiffness Method for Biaxial Bending" *Journal of the Structural Division, ASCE,* Vol. 98, ST1, January 1972.

14. VIRDI, K.S. "Inelastic Column Behaviour - Its Application to Composite Columns in Biaxial Bending and Stiffened Plates in Compression" *Ph.D. Thesis, University of London,* October 1973.

15. HORNE, M.R. "Safe Loads on I-Section Columns in Structures Designed by Plastic Theory" *Proceedings, Institution of Civil Engineers,* Vol. 29, September 1964.

16. HORNE, M.R. "The Plastic Design of Columns" *British Constructional Steelwork Association,* London, Publication No. 23, 1964.

17. WOOD, R.H. "A New Approach to Column Design" *Her Majesty's Stationery Office,* 1974.

18. WOOD, R.H. "The Stability of Tall Buildings" *Proceedings, Institution of Civil Engineers,* Vol. 11, September 1958, pp 69 - 102.

19. KAVEH, A. "The Lateral Torsional Buckling of H-Section Beam Columns" *M.Sc. dissertation, Imperial College,* July 1970.

20. GALAMBOS, T.V. and KETTER, R.L. "Columns Under Combined Bending and Thrust" *Transactions, ASCE,* Vol. 126(I) 1961, p.1.

21. KETTER, R.L. "Further Studies on the Strength of Beam Columns" *Transactions, ASCE,* Vol. 127, Part II, 1962, p. 244.

22. DRISCOLL, G.C. "Plastic Design of Multi-Storey Frames" *Frizt Engineering Laboratory Report* No. 273, August 1965, Lehigh University.

23. PARIKH, B.P., DANIELS, J.H. and LU, L.W. "Plastic Design of Multi-Storey Frames - Design Aids" *Fritz Engineering Laboratory Report* No. 273.24, August 1965, Lehigh University.

24. YOUNG, B.W. "The In-plane Failure of Steel Beam Columns" *The Structural Engineer*, Vol. 51, January 1973, pp 27-35.

25. GENT, A.R., "Elastic-Plastic Column Stability and the Design of No-Sway Frames" *Proceedings, Institution of Civil Engineers*, Vol. 34, June 1966, pp 129 - 151.

26. GESUND, H. "Stress and Moment Distribution in Three-dimensional Frames Composed of Non-prismatic Members Made of Non-linear Material" *Space Structures*, Chapter 13, Blackwell, Oxford and Edinburgh, 1967, pp 145 - 153.

27. HORNE, M.R. "Failure of Columns Laterally Supported on One Flange" Discussion on Paper by Professor M.R. Horne and Dr. J.L. Ajmani" *The Structural Engineer*, Vol. 51, No. 7, July 1973, pp 255 - 256.

28. HUBER, A.W. and BEEDLE, L.S. "Residual Stress and the Compressive Strength of Steel" *The Welding Journal*, Vol.33, No. 12, December 1954.

29. YOUNG, B.W. "Residual Stresses in Hot-rolled Sections" *Cambridge University Report*, No. CUED/C - Struct/Tr.9 (1971).

30. HOUSEHOLDER, A.S. *Principles of Numerical Analysis* Chapter 3, McGraw Hill Book Company, Inc. 1953.

31. GALAMBOS, T.V. *Structural Members and Frames* Prentice-Hall Inc., Englewood Cliffs, N.J., 1968.

32. TIMOSHENKO, S.P. and GERE, J.M. *Theory of Elastic Stability* McGraw Hill Book Company, Inc. New York, 1961.

33. VIKTOVICH, D., ed. *Field Analysis* Van Nostrand, London 1966.

34. CULVER, C.G. "Exact Solution of the Biaxial Bending Equations" *Journal of the Structural Division, ASCE*, Vol. 92, No.ST2, April 1966.

35. SYAL, I.C. and SHARMA, S.S. "Elastic Behaviour of Biaxially Loaded Steel Columns" *Journal of the Structural Division ASCE*, Vol. 96, No. ST3, March 1970.

36. YOUNG, B.W. "Steel Column Design" *The Structural Engineer*, Vol. 51, No. 9, September 1973.

TABLE I COLUMN TEST RESULTS (IMPERIAL UNITS)

Column Number	U.C. Sections	Slenderness l/r_y	Col. Length Between Bearings (inches)	T Value t/in^2	Axial Loads tons	Failure Moment M_f t.ins	Mode of Failure
A1	8 in x 8 in @ 48 lb	43	90	75.2	300.0	---	In-plane
A2	8 in x 8 in @ 31 lb	45	90	32.8	175.0	137.0	In-plane
A3	8 in x 8 in @ 31 lb	45	90	32.8	145.0	284.0	In-plane
B1	8 in x 8 in @ 48 lb	59	123	75.2	230.0	540.0	L.T.B.
B2	8 in x 8 in @ 48 lb	59	123	75.2	200.0	588.0	L.T.B.
B3	8 in x 8 in @ 35 lb	61	123	41.5	160.0	304.0	L.T.B.
B4*	8 in x 8 in @ 35 lb	61	123	41.5	100/159.4	254.9	L.T.B.
C1*	8 in x 8 in @ 48 lb	74	153	75.2	150/220.0	431.4	L.T.B.

* These columns were tested under a different load path, see text.

TABLE I COLUMN TEST RESULTS (SI UNITS)

Column Number	U.C. Sections	Slenderness l/r_y	Col. Length Between Bearings (m)	T Value (N/mm^2)	Axial Loads (N)	Failure Moment M_f ($N.m$)	Mode of Failure
A1	203 mm x 203 mm @ 71 Kg	43	2.286	1162.3	298.8×10^4	--	In-plane
A2	203 mm x 203 mm @ 46 Kg	45	2.286	506.95	174.3×10^4	3.468×10^4	In-plane
A3	203 mm x 203 mm @ 46 Kg	45	2.286	506.95	144.4×10^4	7.186×10^4	In-plane
B1	203 mm x 203 mm @ 71 Kg	59	3.124	1162.3	229.1×10^4	13.66×10^4	L.T.B.
B2	203 mm x 203 mm @ 71 Kg	59	3.124	1162.3	199.2×10^4	14.87×10^4	L.T.B.
B3	203 mm x 203 mm @ 52 Kg	61	3.124	641.4	159.4×10^4	7.69×10^4	L.T.B.
B4*	203 mm x 203 mm @ 52 Kg	61	3.124	641.4	99.6×10^4 / 158.8×10^4	6.45×10^4	L.T.B.
C1*	203 mm x 203 mm @ 71 Kg	74	3.886	1162.3	149.4×10^4 / 219.1×10^4	10.915×10^4	L.T.B.

* These columns were tested under a different load path, see text.

TABLE II DATA ON TEST RESULTS (IMPERIAL UNITS)

Column Number	Slenderness l/r_y	Axial Loads at failure (tons)	$\frac{P}{P_T}$ *	Plastic Moment Capacity M_{pc} **(t.in)	$\frac{M_f}{M_{pc}}$	Experimental strength/ Calculated short column strength (see formula below***)	Failure Mode
A1	43	300	0.9	570.8	--	----	In-plane
A2	45	175.0	0.805	175.2	0.782	0.9843	In-plane
A3	45	145.0	0.665	289.3	0.982	0.994	In-plane
B1	59	230.0	0.8	843.3	0.640	0.8942	L.T.B.
B2	59	200.0	0.7	956.1	0.615	0.8437	L.T.B.
B3	61	160.0	0.69	422.6	0.719	0.9161	L.T.B.
B4	61	159.4	0.69	422.6	0.603	0.8879	L.T.B.
C1	74	220.0	0.85	880.6	0.49	0.86	L.T.B.

* P_T denotes tangent modulus load, see text, section 2.10

** See text, section 2.11

*** $$\left[\left(\frac{P}{P_T}\right)^2 + \left(\frac{M_f}{M_p}\right)^2 \Big/ \left(\frac{P}{P_T}\right)^2 + \left(\frac{M_{pc}}{M_p}\right)^2 \right]^{\frac{1}{2}}$$

TABLE II DATA ON TEST RESULTS (SI UNITS)

Column Number	Slenderness $1/r_y$	Axial Loads at failure (N)	$\frac{P}{P_T}$ *	Plastic Moment Capacity M_{pc} **(N.M)	$\frac{M_f}{M_{pc}}$	Experimental strength/ calculated short column strength (see formula below ***)	Failure Mode
A1	43	298.8×10^4	0.9	14.44×10^4	--	----	In-plane
A2	45	174.3×10^4	0.805	4.43×10^4	0.782	0.9843	In-plane
A3	45	144.4×10^4	0.665	7.32×10^4	0.982	0.994	In-plane
B1	59	229.1×10^4	0.8	21.34×10^4	0.640	0.8942	L.T.B.
B2	59	199.2×10^4	0.7	24.19×10^4	0.615	0.8437	L.T.B.
B3	61	159.4×10^4	0.69	10.69×10^4	0.719	0.9161	L.T.B.
B4	61	158.8×10^4	0.69	10.69×10^4	0.603	0.8879	L.T.B.
C1	74	219.1×10^4	0.85	22.28×10^4	0.49	0.86	L.T.B.

* P_T denotes tangent modulus load, see text, section 2.10

** see text, section 2.11

*** $$\left[\left(\frac{P}{P_T}\right)^2 + \left(\frac{M_f}{M_p}\right)^2 \Big/ \left(\frac{P}{P_T}\right)^2 + \left(\frac{M_{pc}}{M_p}\right)^2\right]^{\frac{1}{2}}$$

TABLE III CROSS-SECTIONAL PROPERTIES OF EXAMPLES 2 AND 4 IN REF. (34)

Problem	Column	A in^2	r_o^2 in^2	I_x in^4	I_y in^4	K_T in^4	I_w in^6	σ_y K/in^2	l/r_y	Loading e_x	Loading e_y	Boundary Conditions
2	14 WF43	12.65	37.5	429.0	45.1	1.06	1950.0	33	140	5	5	Simply supported Warping free
4		12.65	37.5	429.0	45.1	1.06	1950.0	33	140	5	5	Simply supported Warping restrained

TABLE IV COMPARISON WITH CULVER'S SOLUTIONS - REF(34)

Problem	Load P Kips	Mid-Column Height Deflections u (minor axis) ins		v (major axis) ins		ϕ(twist) radians		Boundary Conditions
		Culver	Author	Culver	Author	Culver	Author	
2	20	0.7267	0.7273	0.0686	0.0686	0.0033	0.003424	Simply Supported Warping Free
	40	1.6683		0.1373		0.0160		
	60	2.9607		0.2035		0.0449		
	80	4.8906	4.929	0.2607	0.2596	0.1044	0.1088	
	100	8.1848	8.306	0.2927	0.2892	0.2314	0.2423	

TABLE V COMPARISON WITH CULVER'S SOLUTIONS - REF(34)

Problem	Load P Kips	Mid-Column Height Deflections u ins		v ins		ϕ radians		Boundary Conditions
		Culver	Author	Culver	Author	Culver	Author	
	20	0.7254	0.7259	0.0687	0.06872	0.0012	0.00129	
	40	1.6583		0.1386		0.0057		Simply
4	60	2.8894		0.2088		0.0155		Supported
	80	4.6238	4.652	0.2777	0.2772	0.0343	0.03661	Warping
	100	7.2512	7.327	0.3420	0.3405	0.0696	0.07458	Restrained

TABLE VI CROSS-SECTIONAL PROPERTIES OF EXAMPLE 15 IN REF(35)

Specimen	Column	Cross-Sectional Properties									Eccentricities of Loading			
		Length	Flange Width	Flange Thickness	Depth	Web Thickness	Area of Cross-Section	Moment of Inertia	Moment of Inertia	Yield Stress				
		L ins	B ins	t_f ins	H ins	t_w ins	A in^2	I_{xx} in^4	I_{yy} in^4	σ_y K/in^2	e_{ox} ins	$e_{\ell x}$ ins	e_{oy} ins	$e_{\ell y}$ ins
15	5x5H	120.0	5.06	0.34	5.04	0.25	4.53	21.1	7.4	65	1.75	-1.47	2.96	-2.96

TABLE VII COMPARISON WITH SYAL & SHARMA'S SOLUTIONS - REF(35)

Specimen	Station	Load P Kips	u (Minor Axis) ins		v (Major Axis) ins		ϕ (twist) radians		Boundary Conditions
			Syal & Sharma	Author	Syal & Sharma	Author	Syal & Sharma	Author	
15	B ($\frac{1}{4}$ point)	10	-0.0257		-0.0106		0.0001425		Simply Supported Warping Free
		20	-0.05335	-0.05340	-0.02128	-0.02129	0.000603	0.000617	
		30	-0.0833		-0.03209		0.001442		
		40	-0.116	-0.1164	-0.04301	-0.04303	0.002727	0.002743	
		50	-0.152		-0.0540		0.004549		

TABLE VIII COMPARISON WITH SYAL & SHARMA'S SOLUTIONS - REF(35)

Specimen	Station	Load P Kips	u ins		v ins		ϕ radians		Boundary Conditions
			Syal & Sharma	Author	Syal & Sharma	Author	Syal & Sharma	Author	
15	C (mid-point)	10	-0.01217		0.0000006		0.0001776		Simply Supported Warping Free
		20	-0.0262	-0.02626	0.0000059	0.00000607	0.000752	0.0007615	
		30	-0.0427		0.0000219		0.001794		
		40	-0.0621	-0.0622	0.0000571	0.00005733	0.003388	0.003381	
		50	-0.0854		0.0001229		0.00564		

TABLE IX COMPARISON WITH SYAL & SHARMA'S SOLUTION - REF(35)

Specimen	Station	Load P Kips	u ins		v ins		ϕ radians		Boundary Conditions
			Syal & Sharma	Author	Syal & Sharma	Author	Syal & Sharma	Author	
15	E ($\frac{3}{4}$ point)	10	0.0075		0.01058		0.000131		Simply Supported Warping Free
		20	0.0142	0.01427	0.02129	0.02130	0.000553	0.000564	
		30	0.020		0.0321		0.001314		
		40	0.0243	0.02435	0.0431	0.04312	0.00247	0.00248	
		50	0.02639		0.05419		0.004091		

TABLE X COMPARISON OF EXPERIMENTAL & THEORETICAL RESULTS

Column Number	Slenderness l/r_y	Axial Loads (Tons)	Plastic Moment Capacity M_{pc}*	Failure Moment (Experiment) (M_f)	Failure Moment (Theory) (M_{th})**	Experimental Strength / Theoretical Strength (See formula below)***	Comments
A1	43	300	570.8				In-plane
A2	45	175	175.2	137.0	162.0	0.990	In-plane
A3	45	145	289.3	284.0	272.0	1.01	In-plane
B1	59	230	843.3	540.0	600.0/544.0	0.98/0.998	L.T.B.
B2	59	200	956.1	588.0	686.0	0.96	L.T.B.
B3	61	160	422.6	304.0	306.0	0.998	L.T.B.
B4	61	159.4	422.6	254.9	140.0t/380.0	1.016	L.T.B.
C1	74	220.0	880.6	431.4	208.0t/540.0t.in	1.017	L.T.B.

* See text, Section 2.11

** Theoretical ultimate moment obtained from computer program

*** $$\left[\left(\frac{P}{P_T}\right)^2 + \left(\frac{M_f}{M_p}\right)^2 \Big/ \left(\frac{P}{P_T}\right)^2 + \left(\frac{M_{th}}{M_p}\right)^2 \right]^{\frac{1}{2}}$$

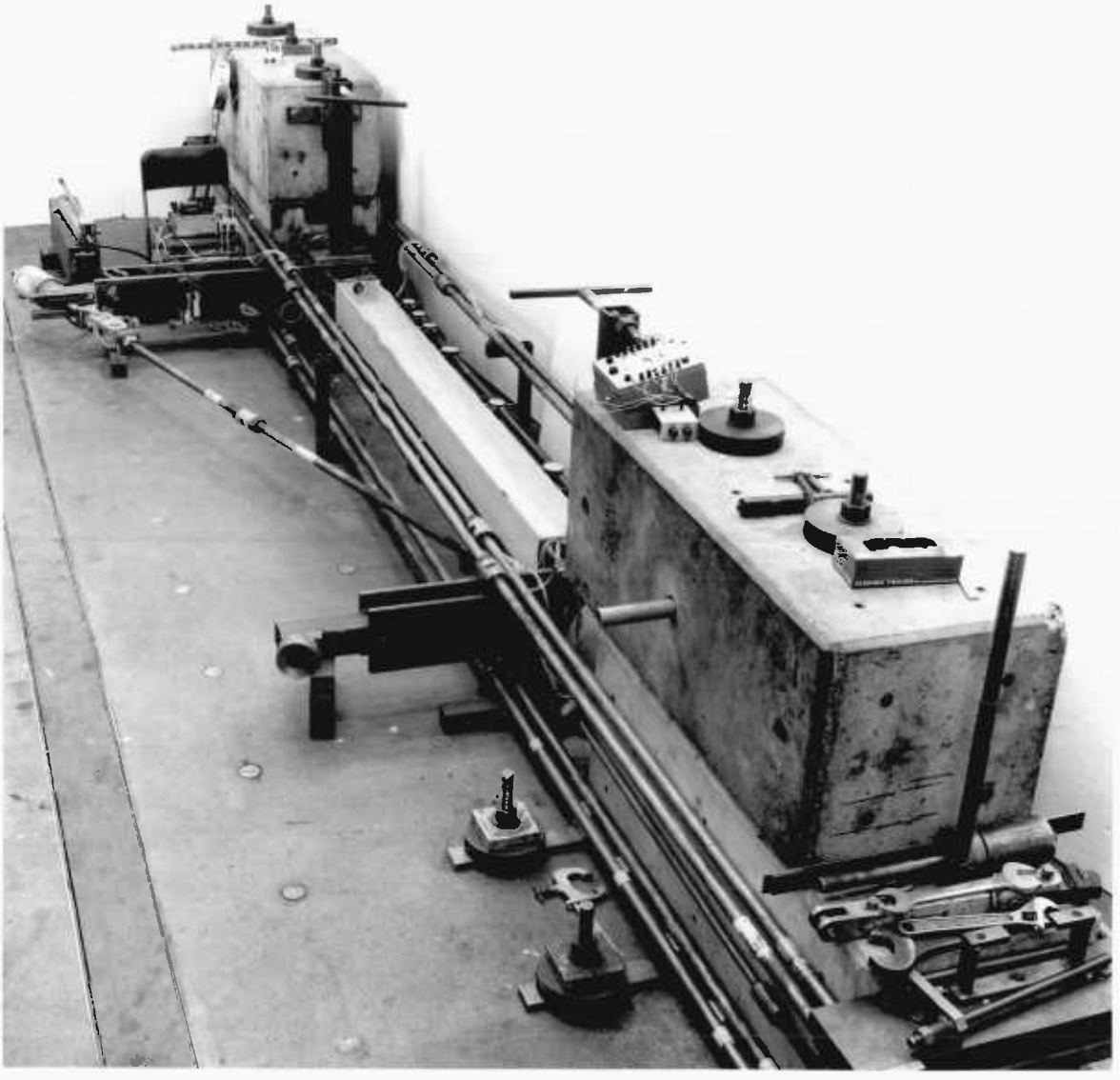


Fig. 2.1 General view of the entire rig (viewed from the jack end)

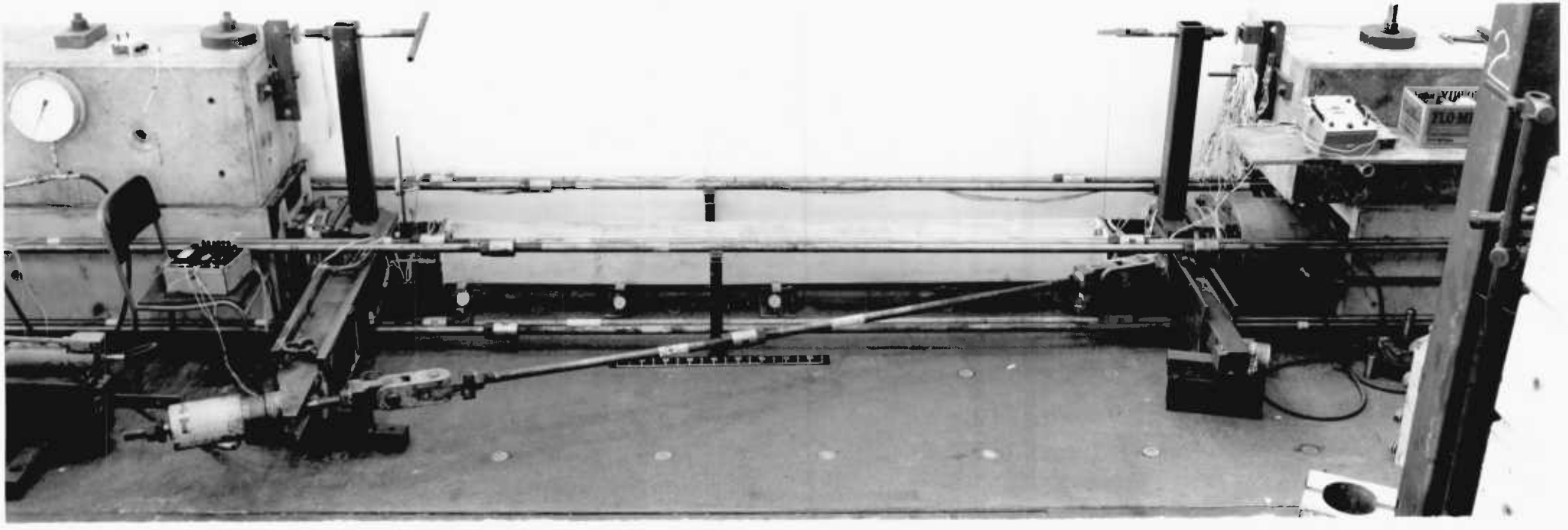


Fig. 2.2 Side view of the entire rig

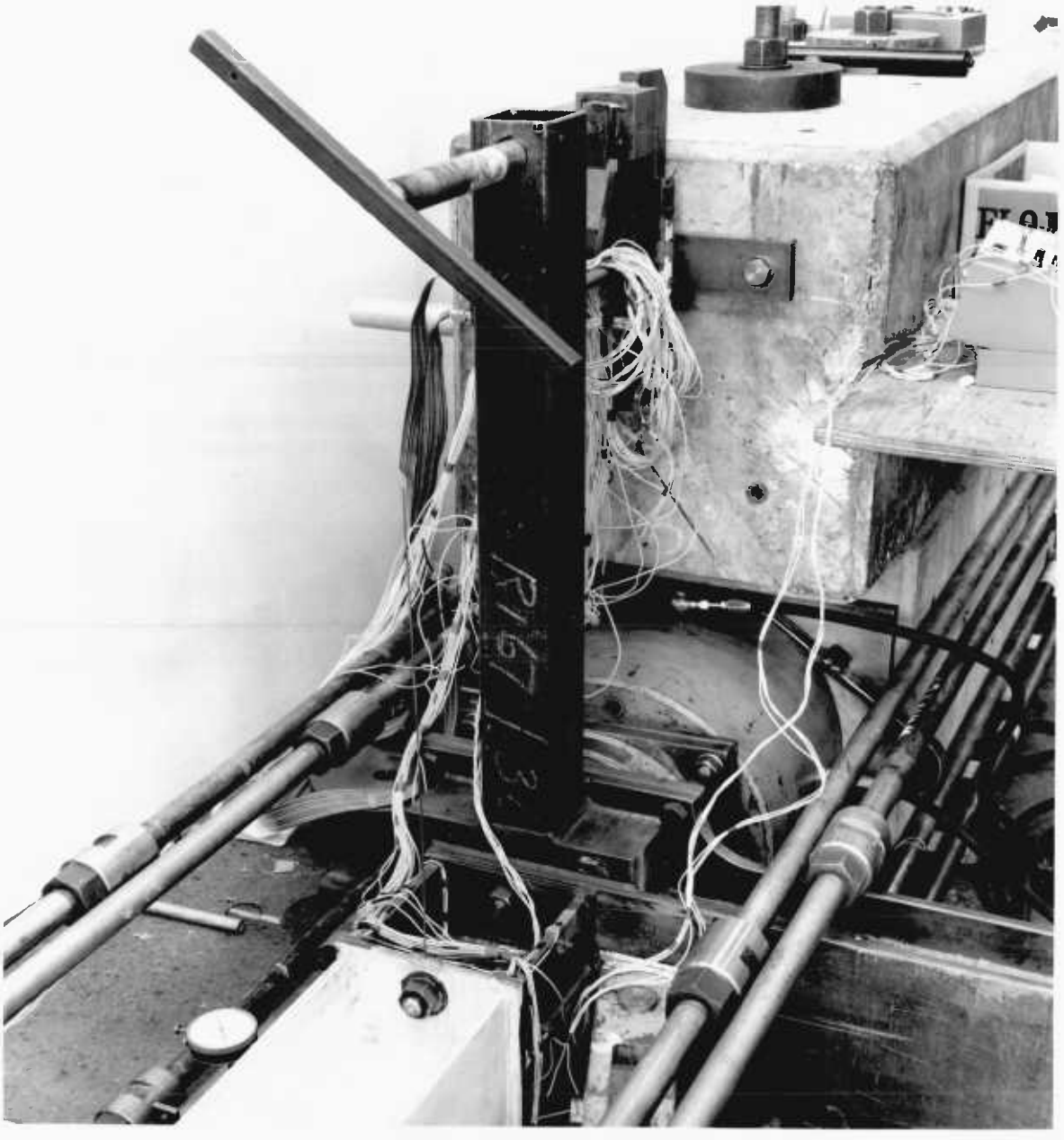


Fig. 2.3 Close up view showing the load cell position (jack end)

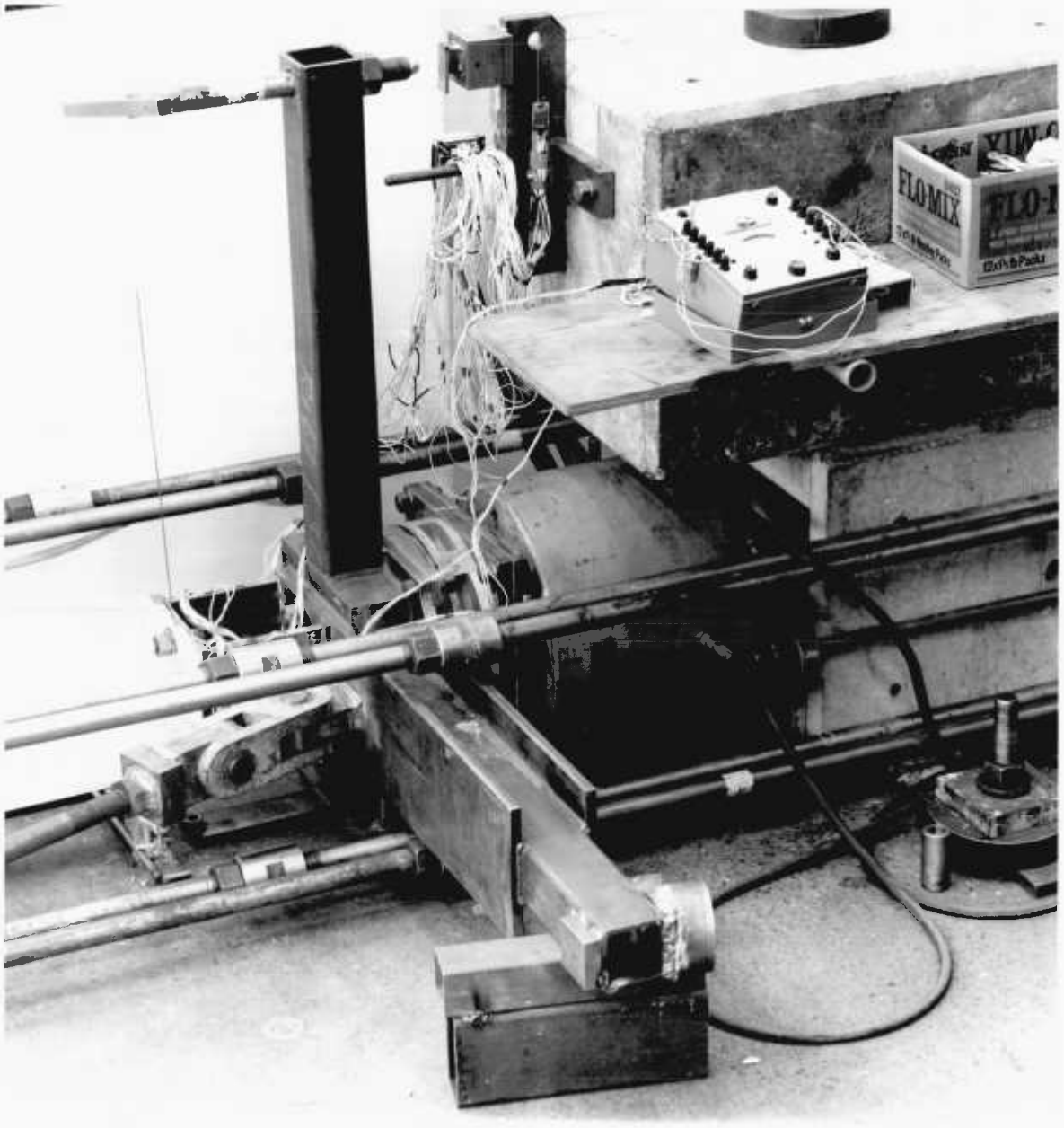


Fig. 2.4 Close up view showing details of the jack end

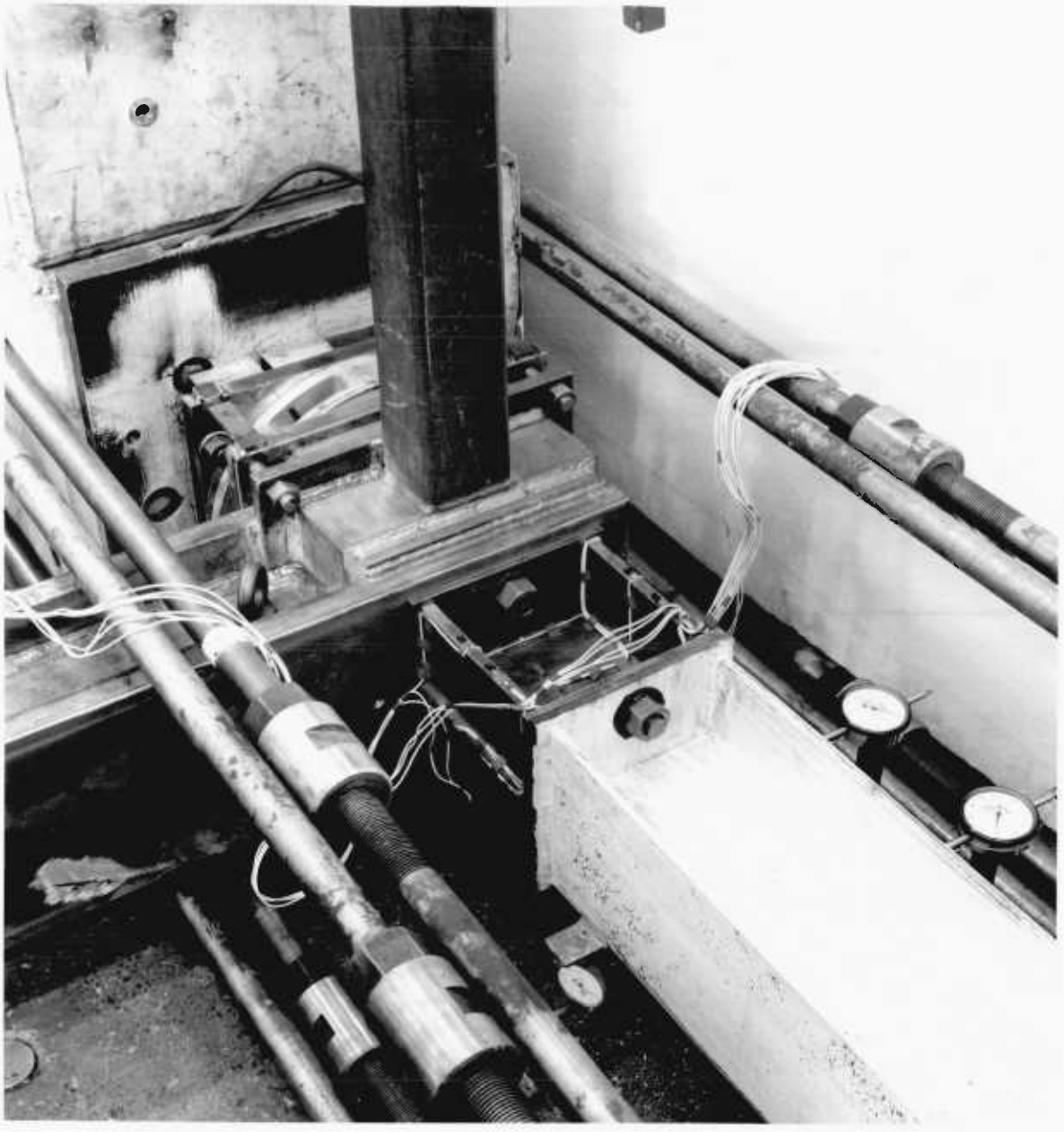


Fig. 2.5 Close up view showing details of the end moment end

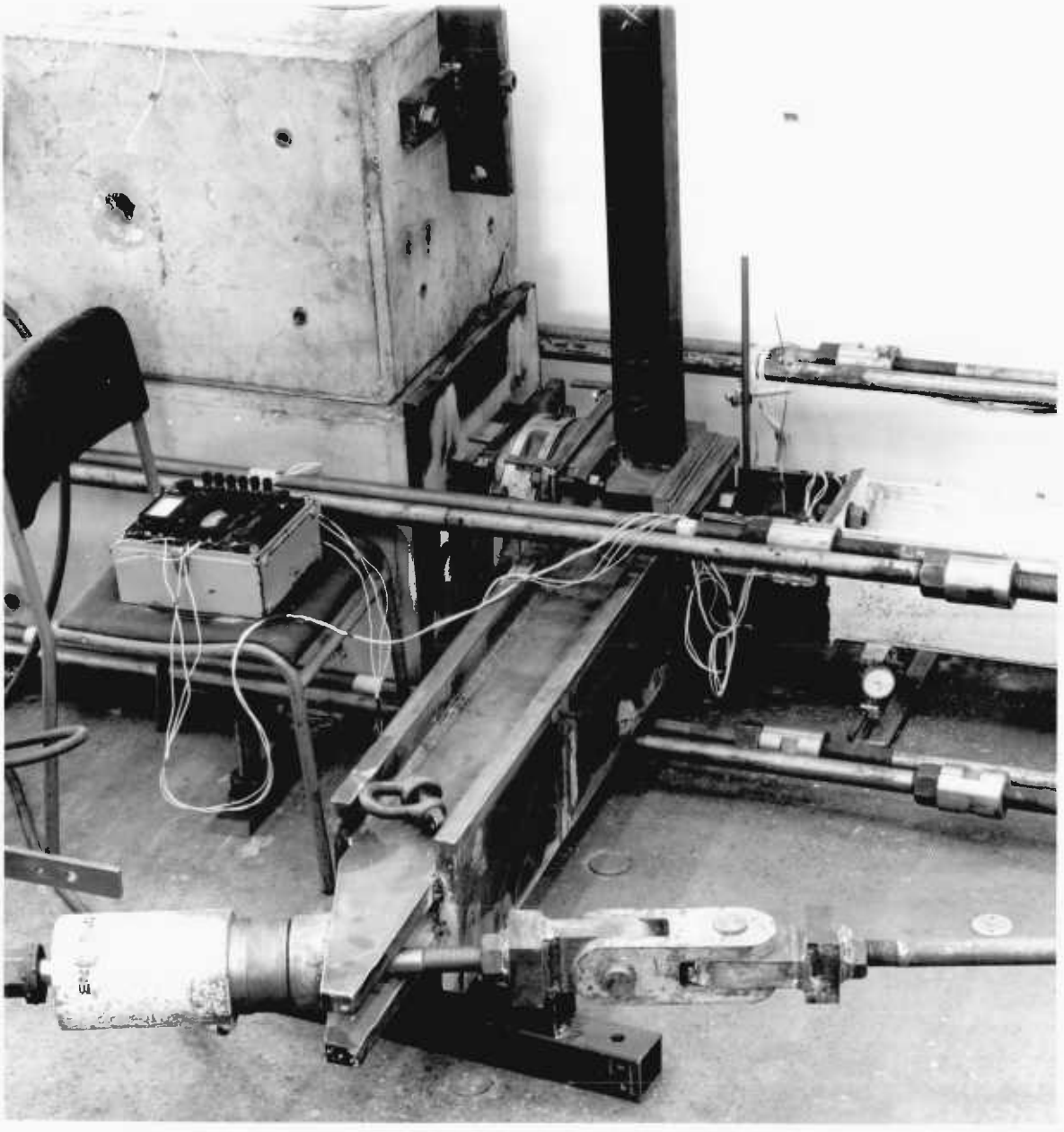


Fig. 2.6 Close up view showing details of the major axis moment arm arrangement

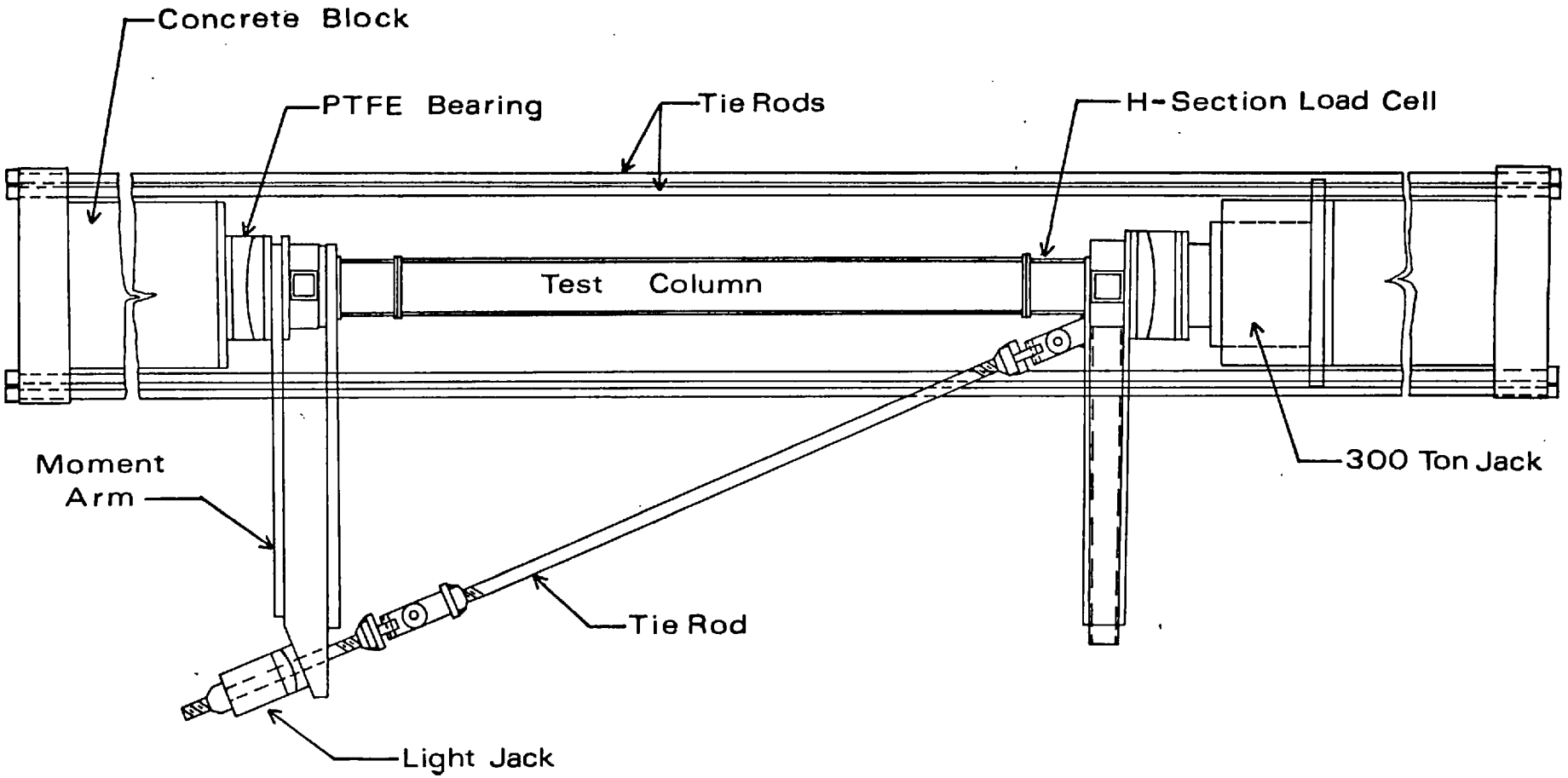


Fig. 2.7 THE TEST RIG (PLAN)

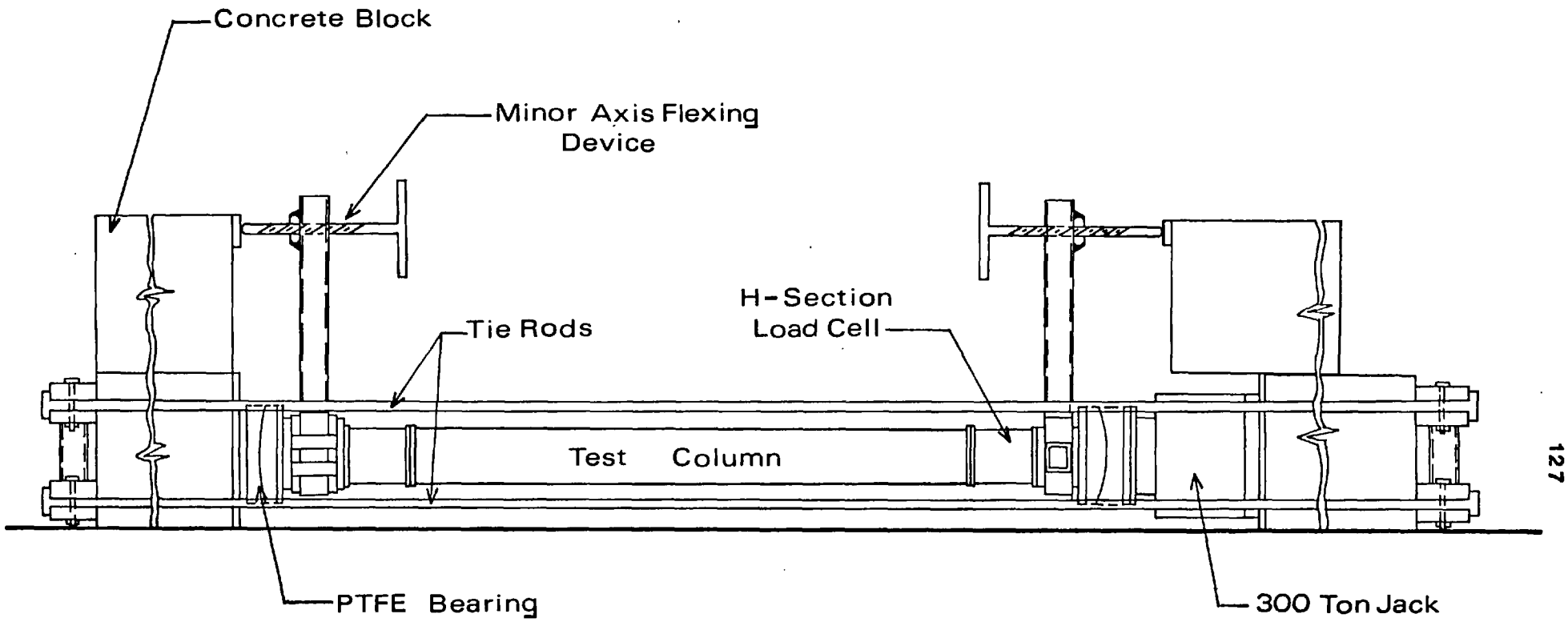


Fig. 2.8 THE TEST RIG (ELEVATION)

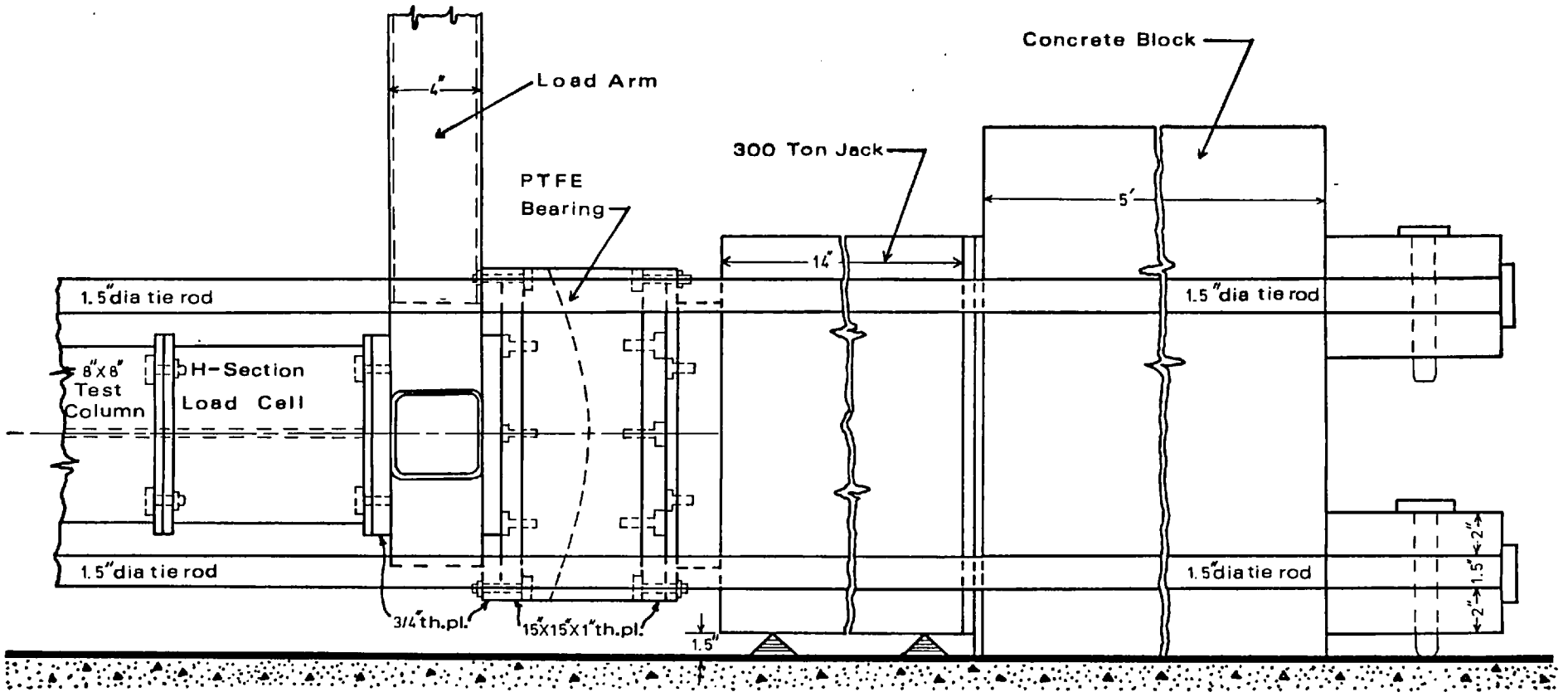
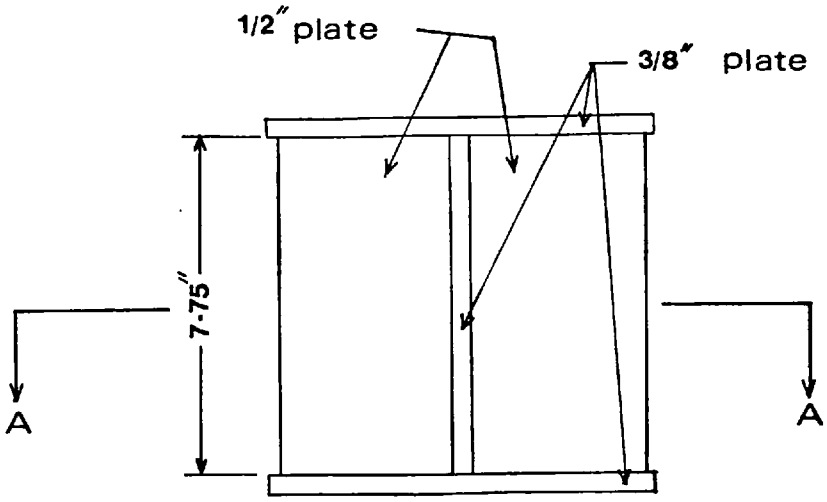
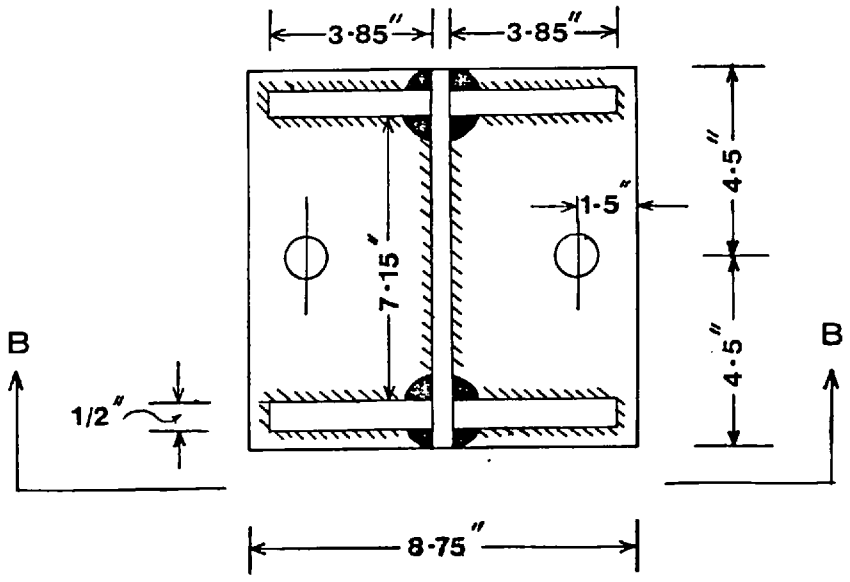


Fig. 2.9 CONNECTION DETAILS AT THE JACK END

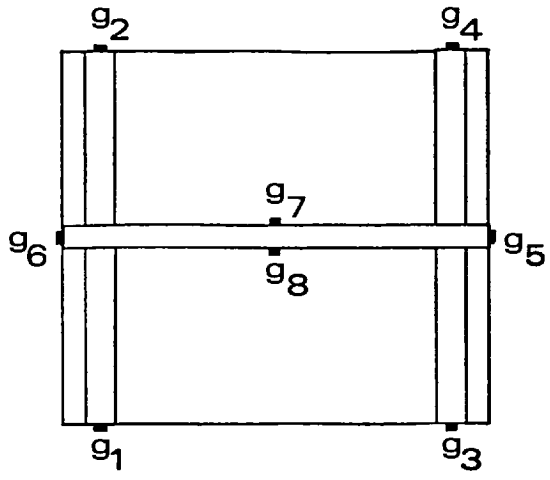


ELEVATION B-B

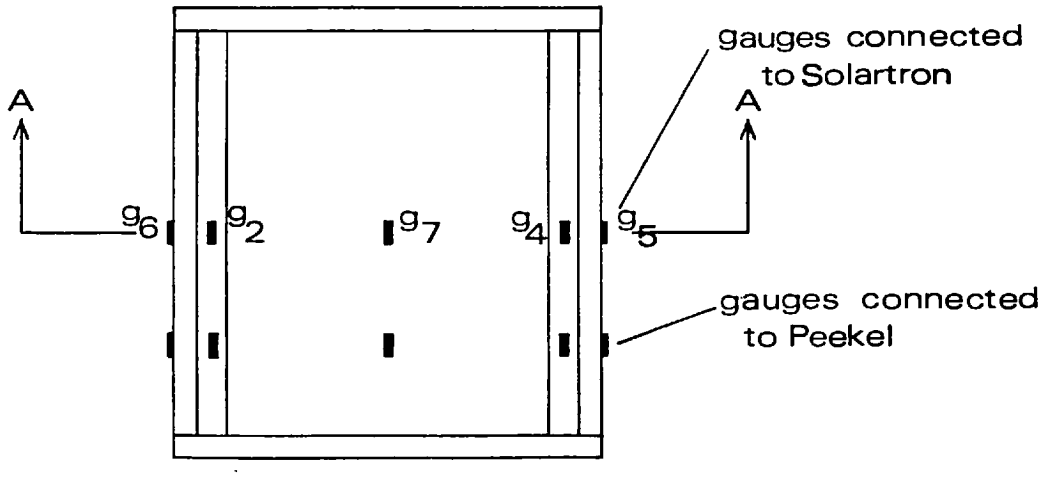


PLAN A-A

Fig.2.10 Diagram of the Load Cell (Maraging Steel)



Section A-A



P L A N

Fig. 2.11 Position of the gauges on the Load Cell

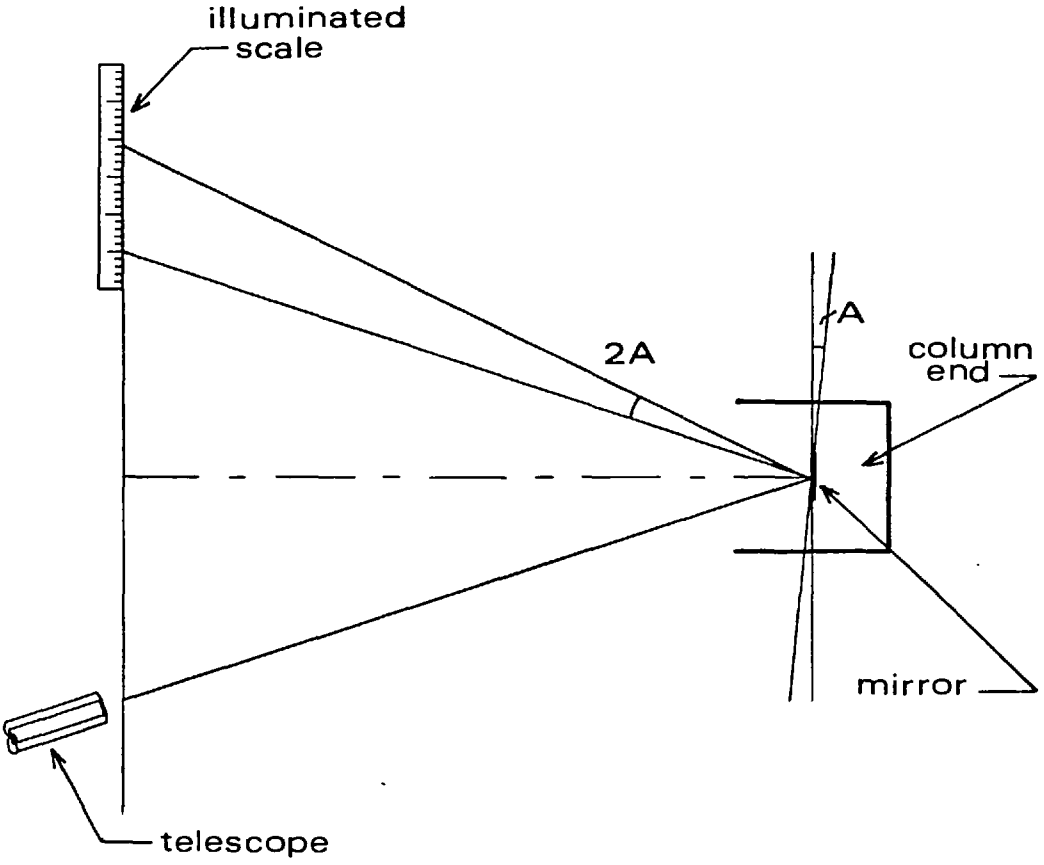


Fig. 2.12 Mirror arrangement to record end rotation

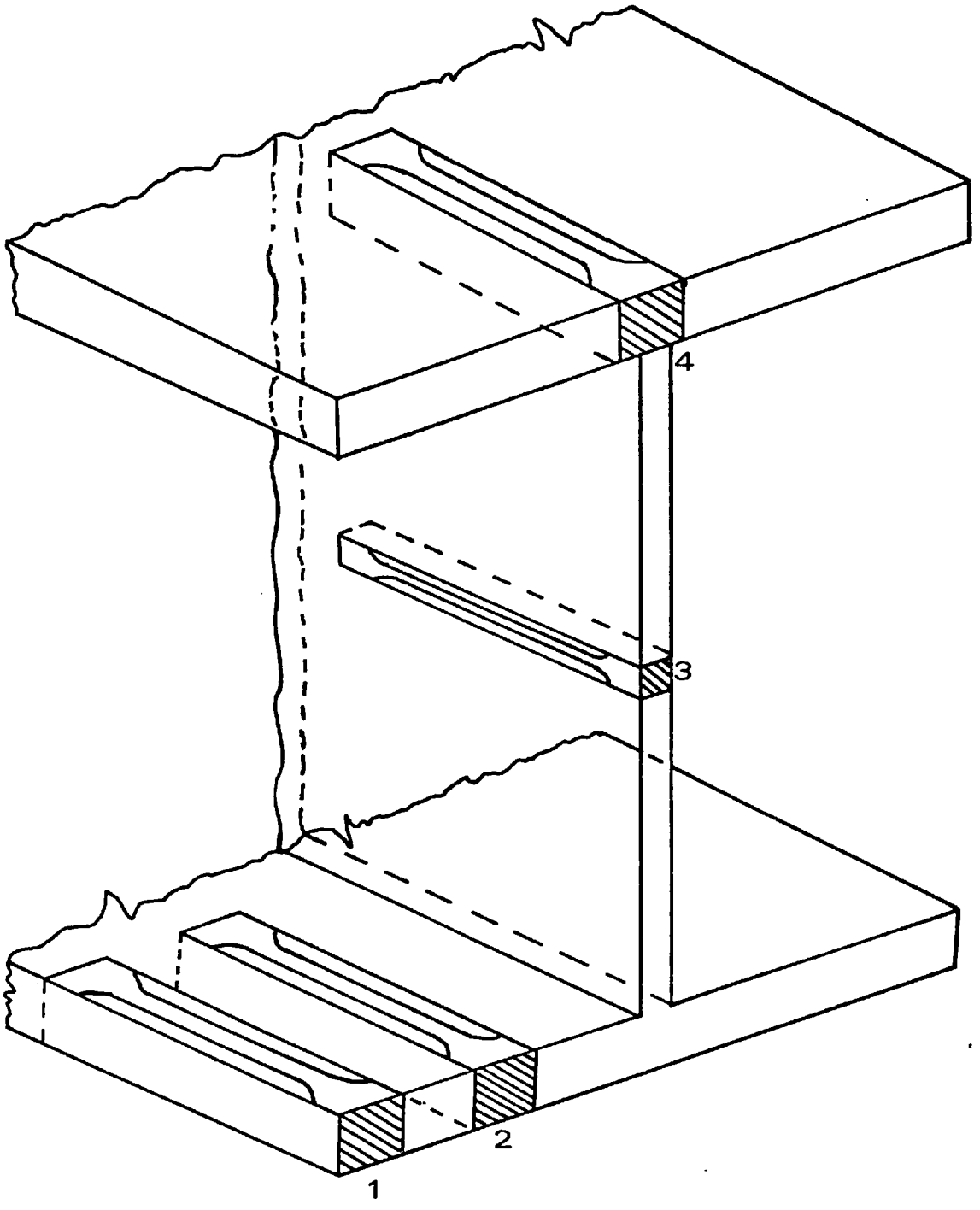


Fig. 2.13 Tensile Test Specimen Location

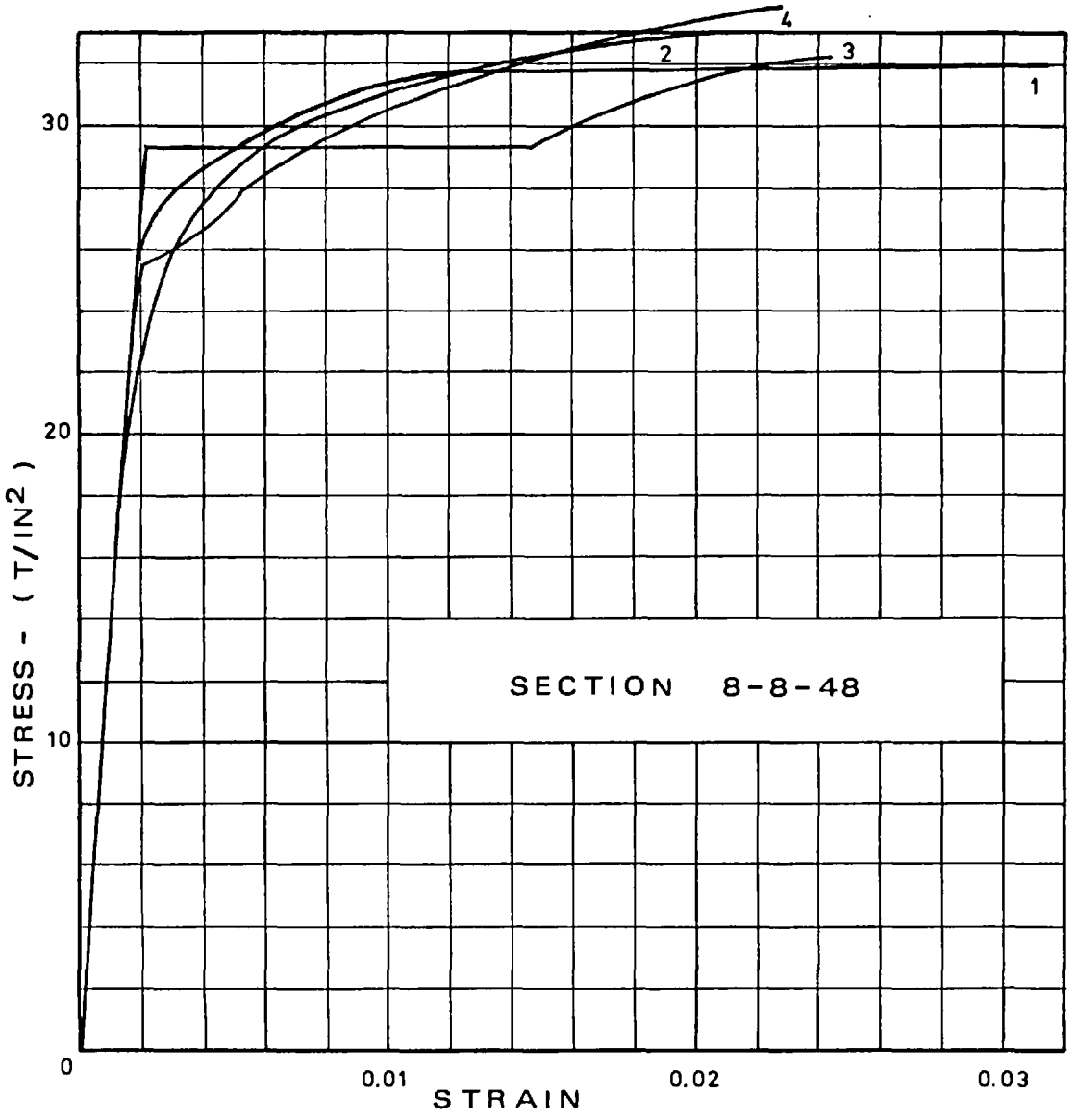


Fig. 2.14 EXPERIMENTAL STRESS-STRAIN CURVE

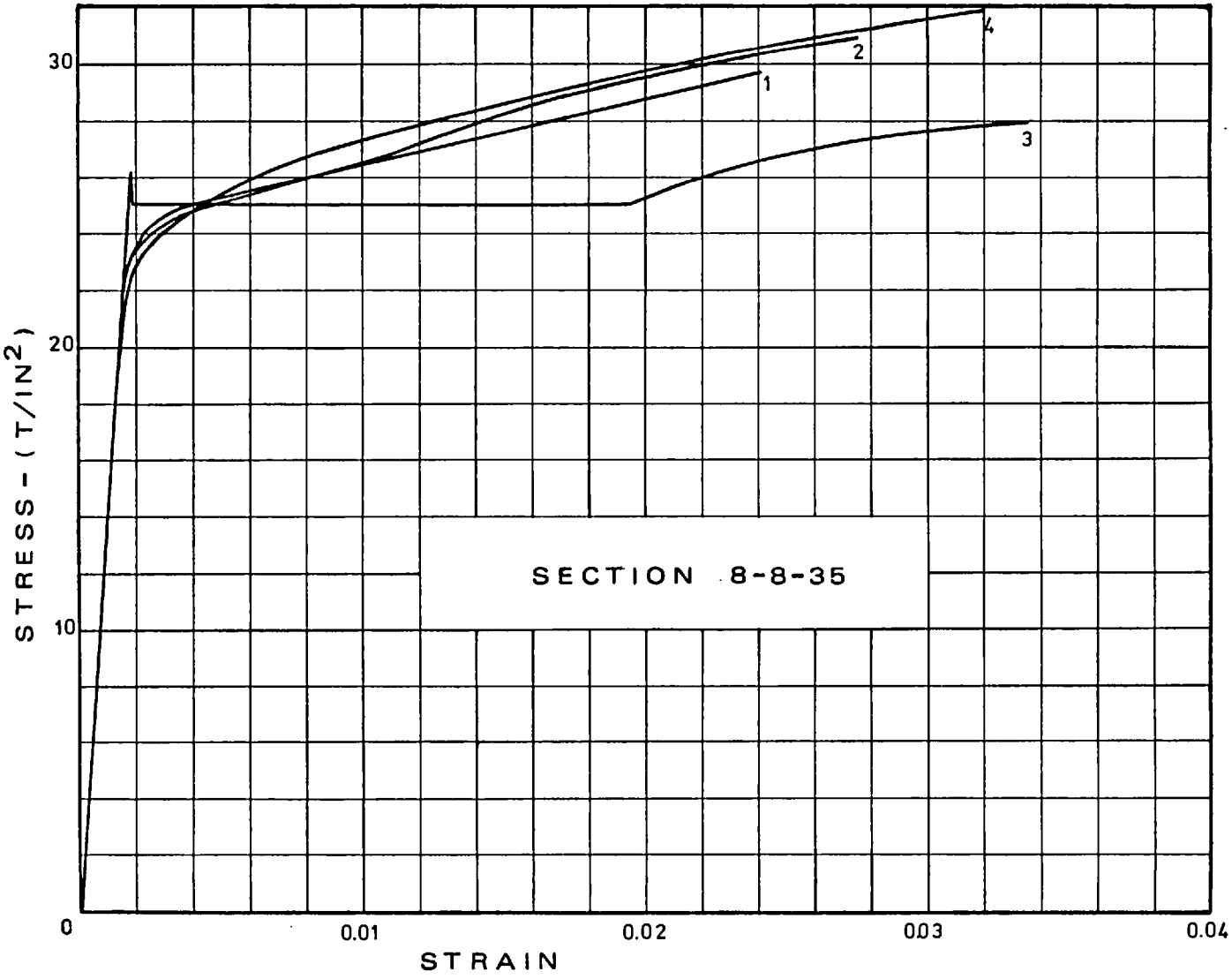


Fig. 2.15 EXPERIMENTAL STRESS-STRAIN CURVE

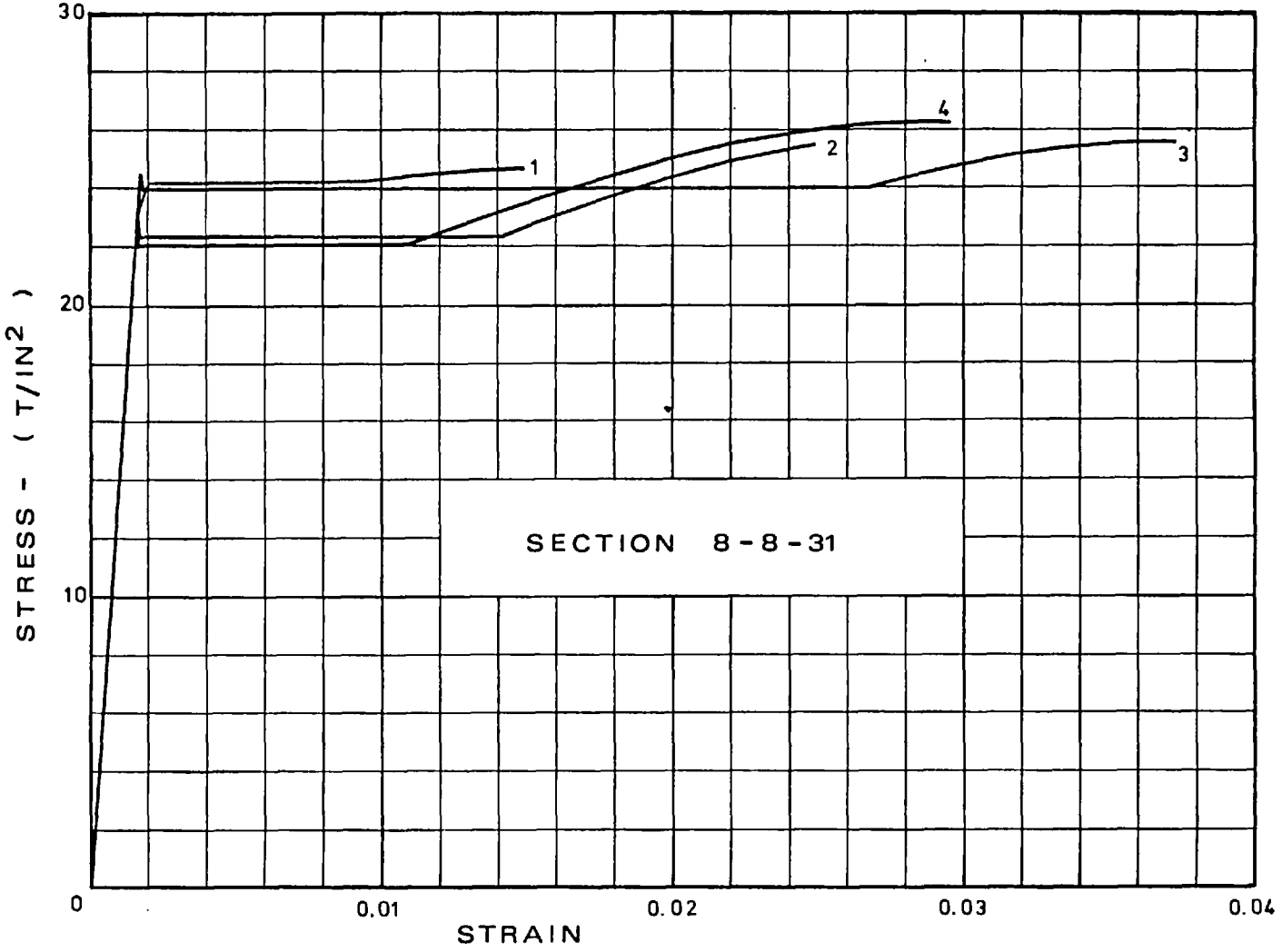


Fig. 2.16 EXPERIMENTAL STRESS-STRAIN CURVE

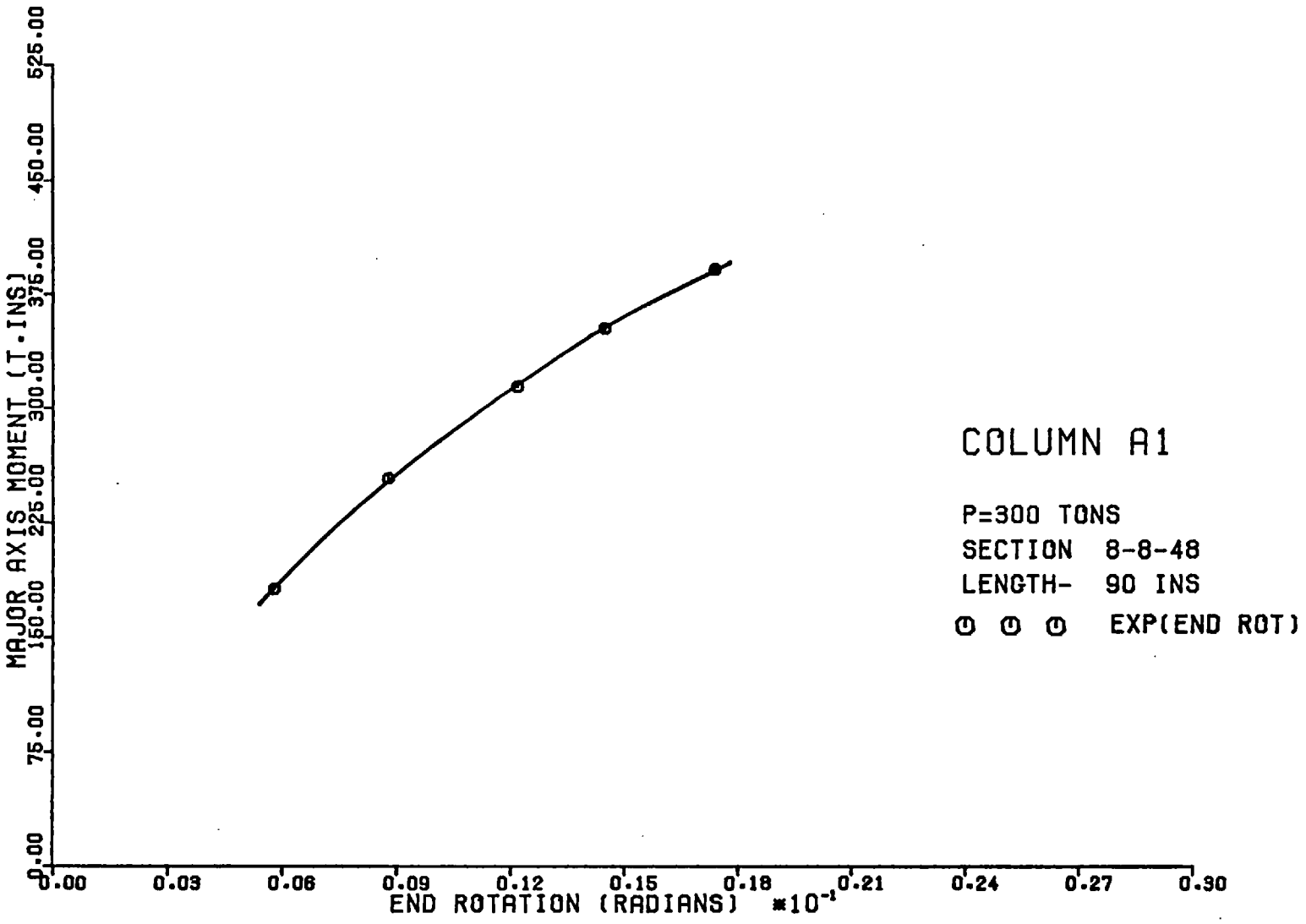


FIG. 2.17 EXPERIMENTAL MOMENT-END ROTATION PLOT

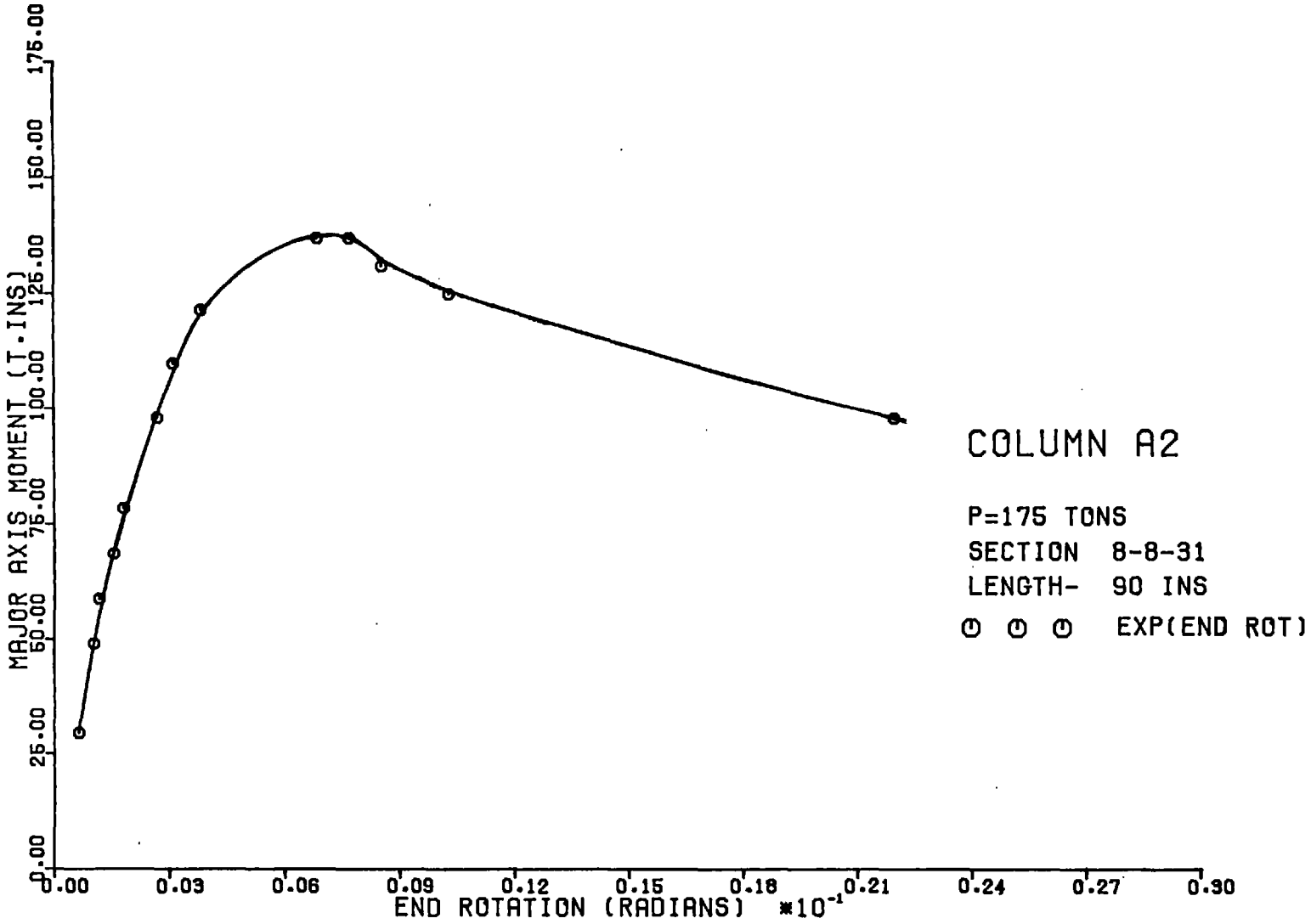


FIG. 2.18 EXPERIMENTAL MOMENT-END ROTATION PLOT

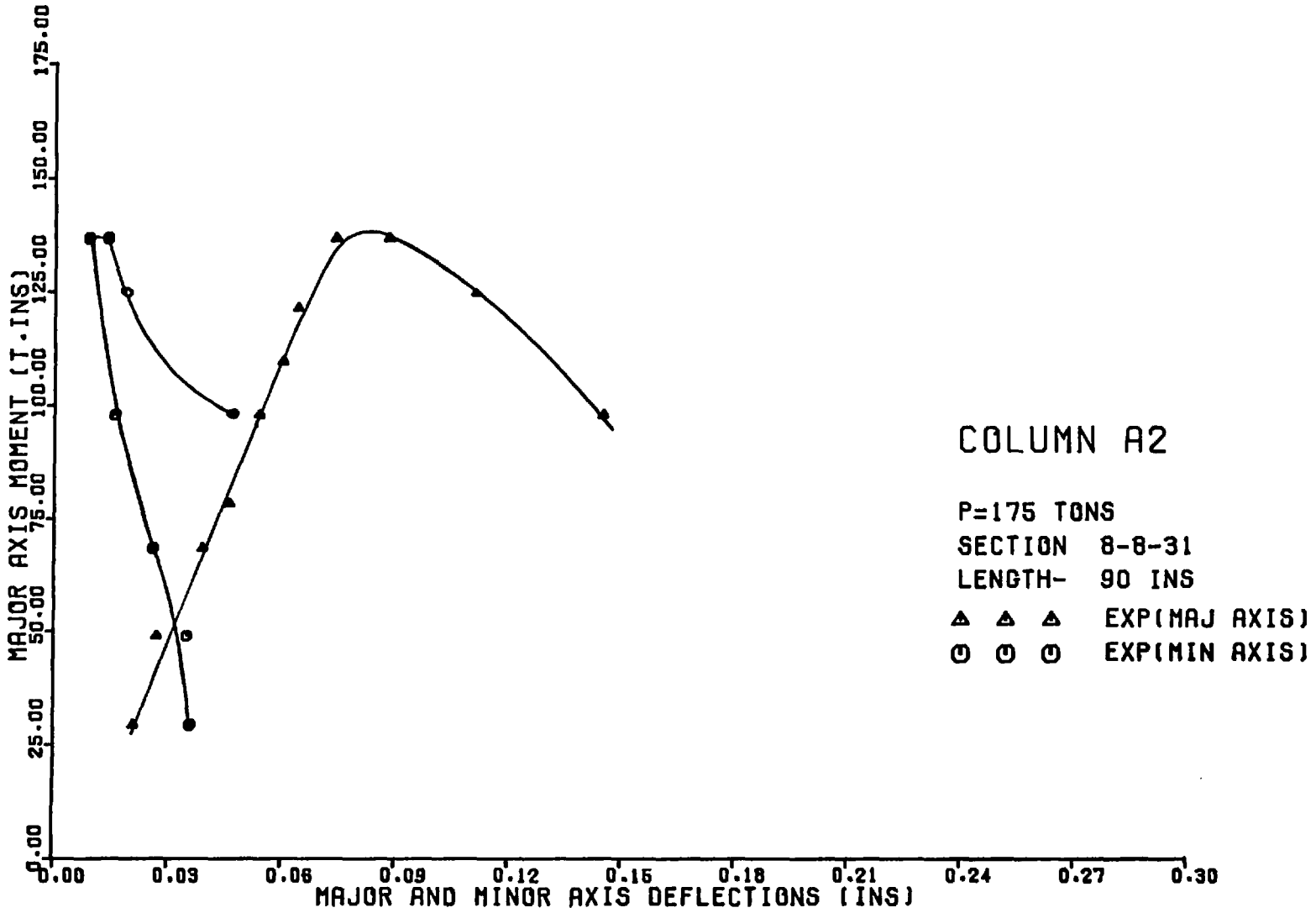


FIG. 2.19 EXPERIMENTAL MOMENT-MID COLUMN HEIGHT DEFLECTION PLOT

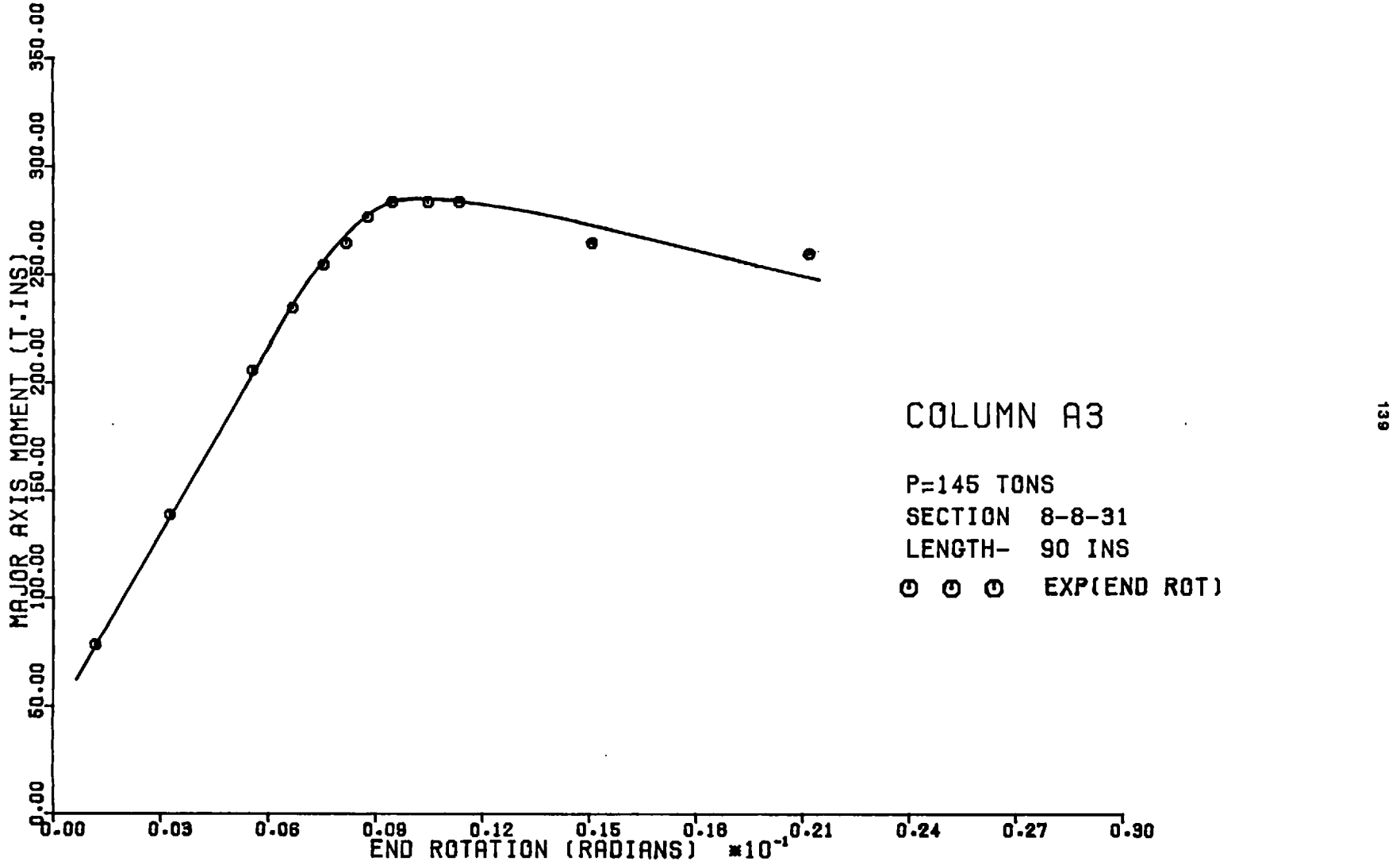


FIG. 2.20 EXPERIMENTAL MOMENT-END ROTATION PLOT

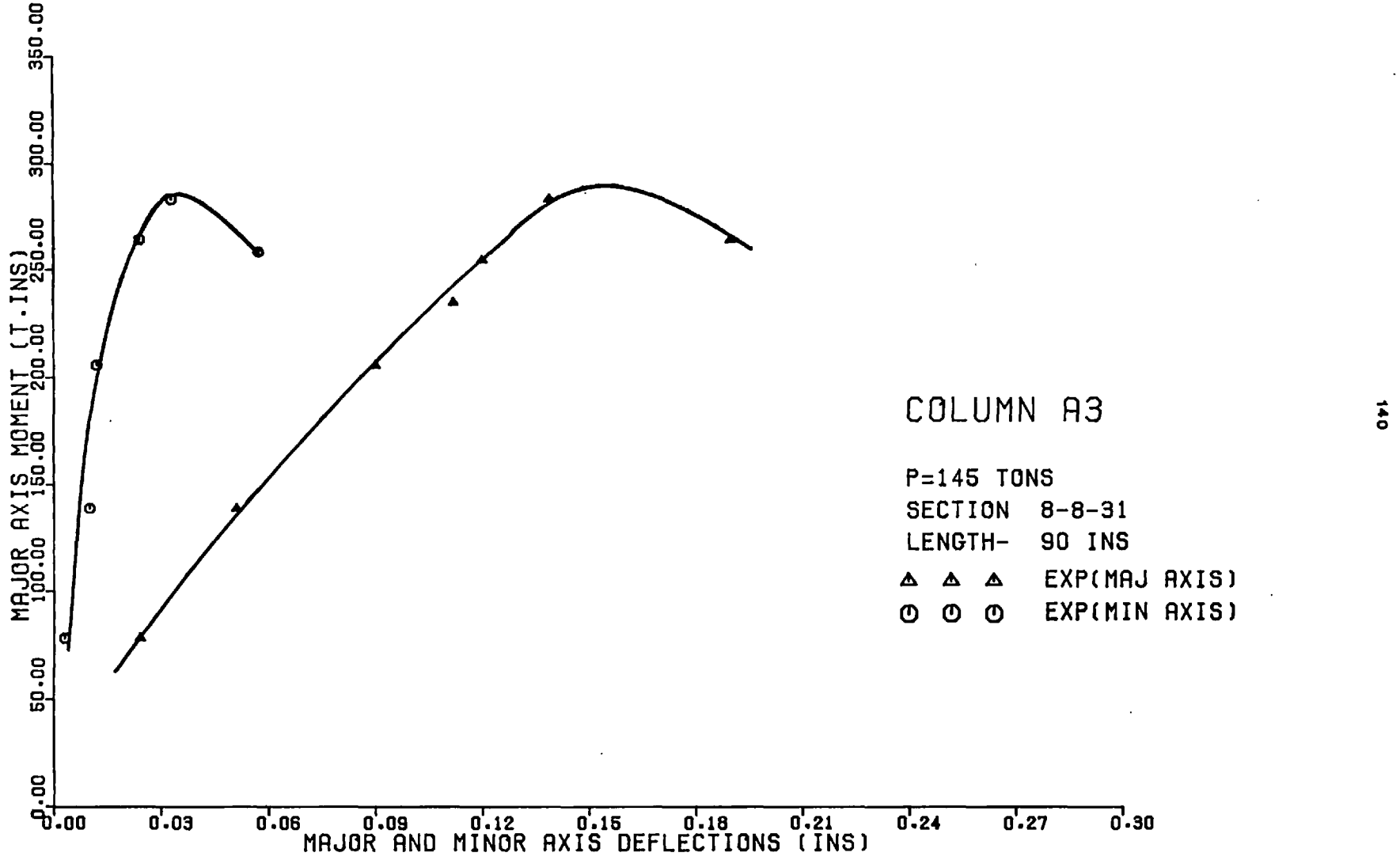


FIG. 2.21 EXPERIMENTAL MOMENT-MID COLUMN HEIGHT DEFLECTION PLOT

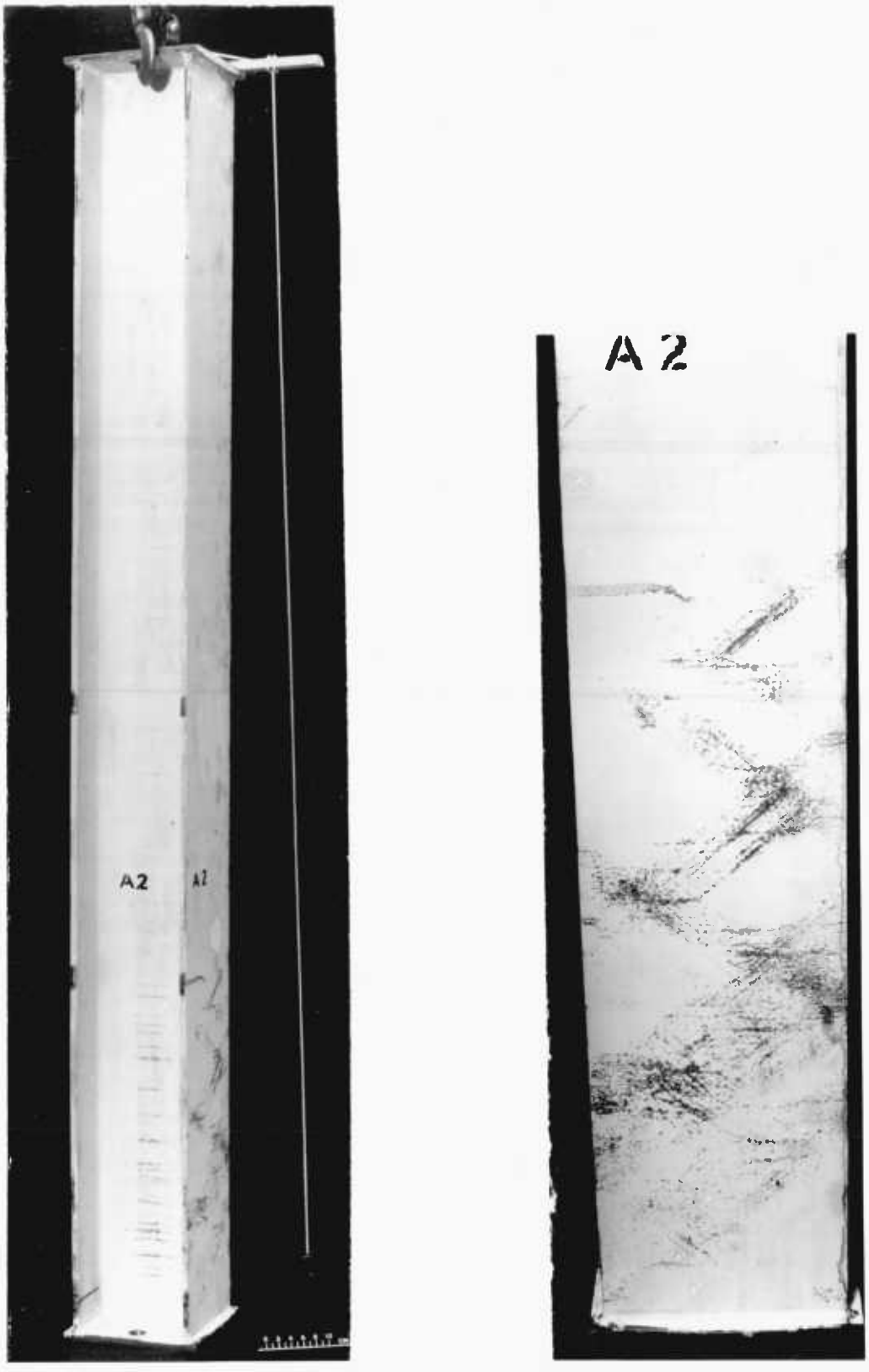


Fig. 2.22 Yield zones on the compression flange (Column A2)



Fig. 2.23 Yield zones on the compression flange (Column A3)

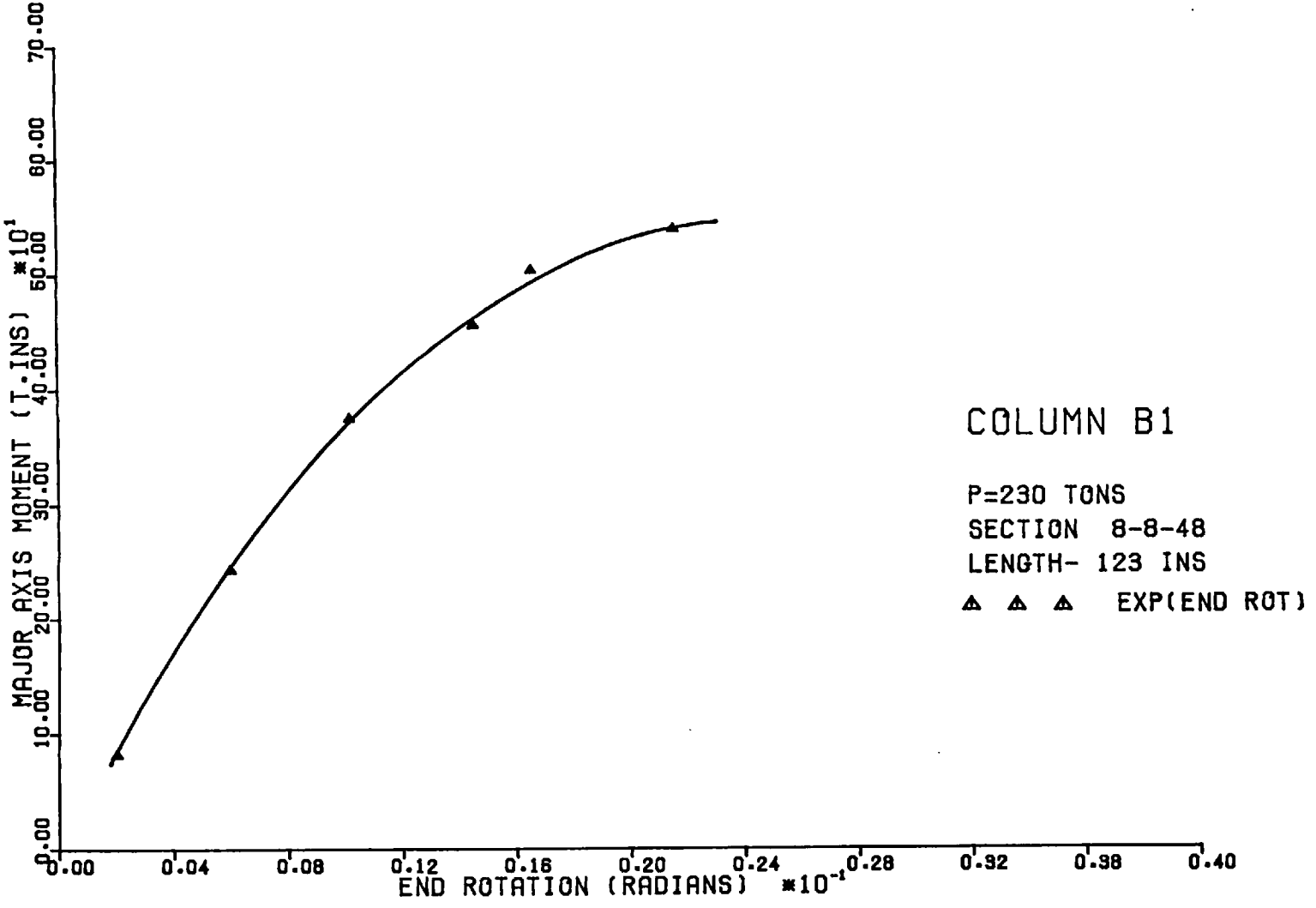


FIG. 2.24 EXPERIMENTAL MOMENT-END ROTATION PLOT

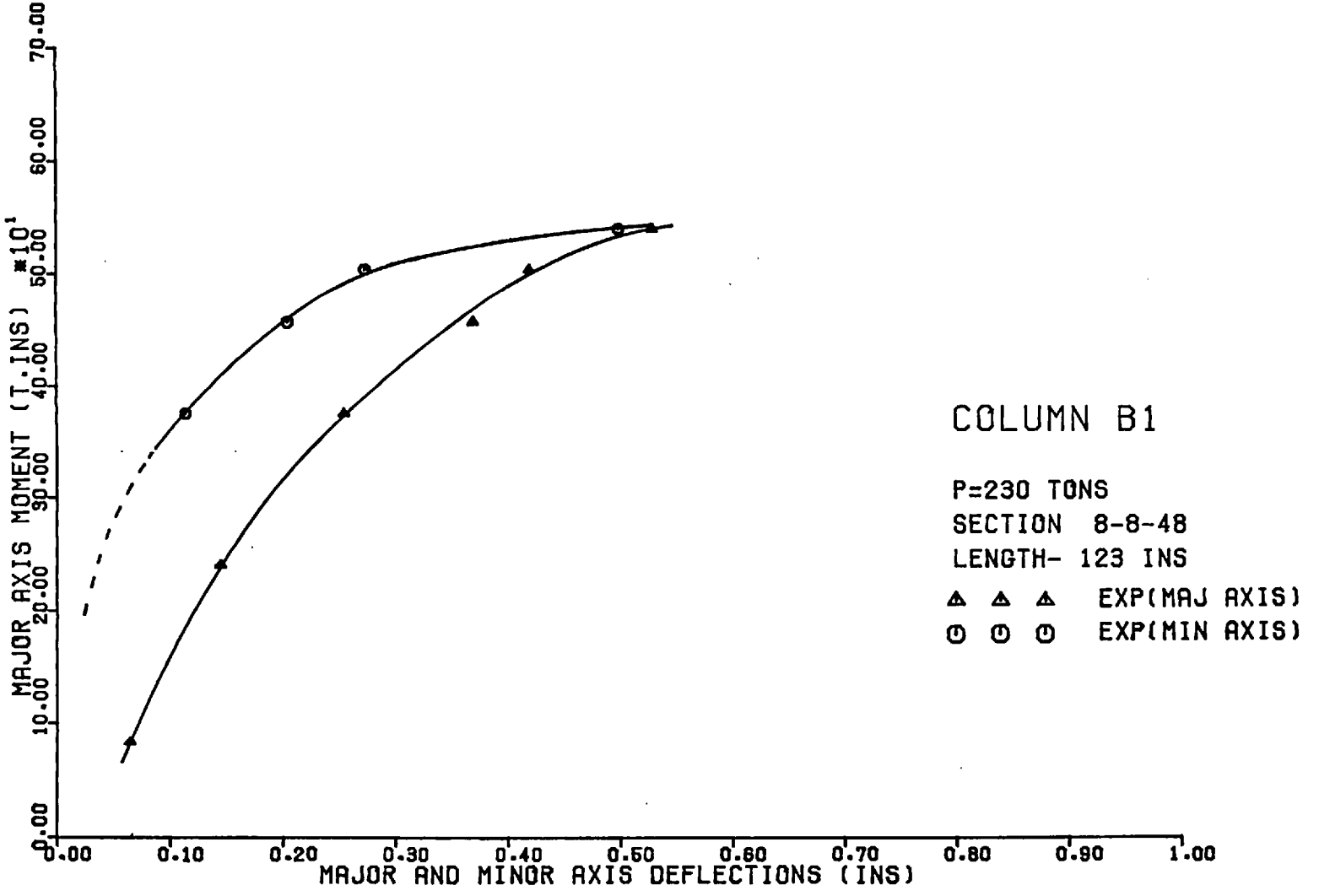


FIG. 2.25 EXPERIMENTAL MOMENT-MID COLUMN HEIGHT DEFLECTION PLOT

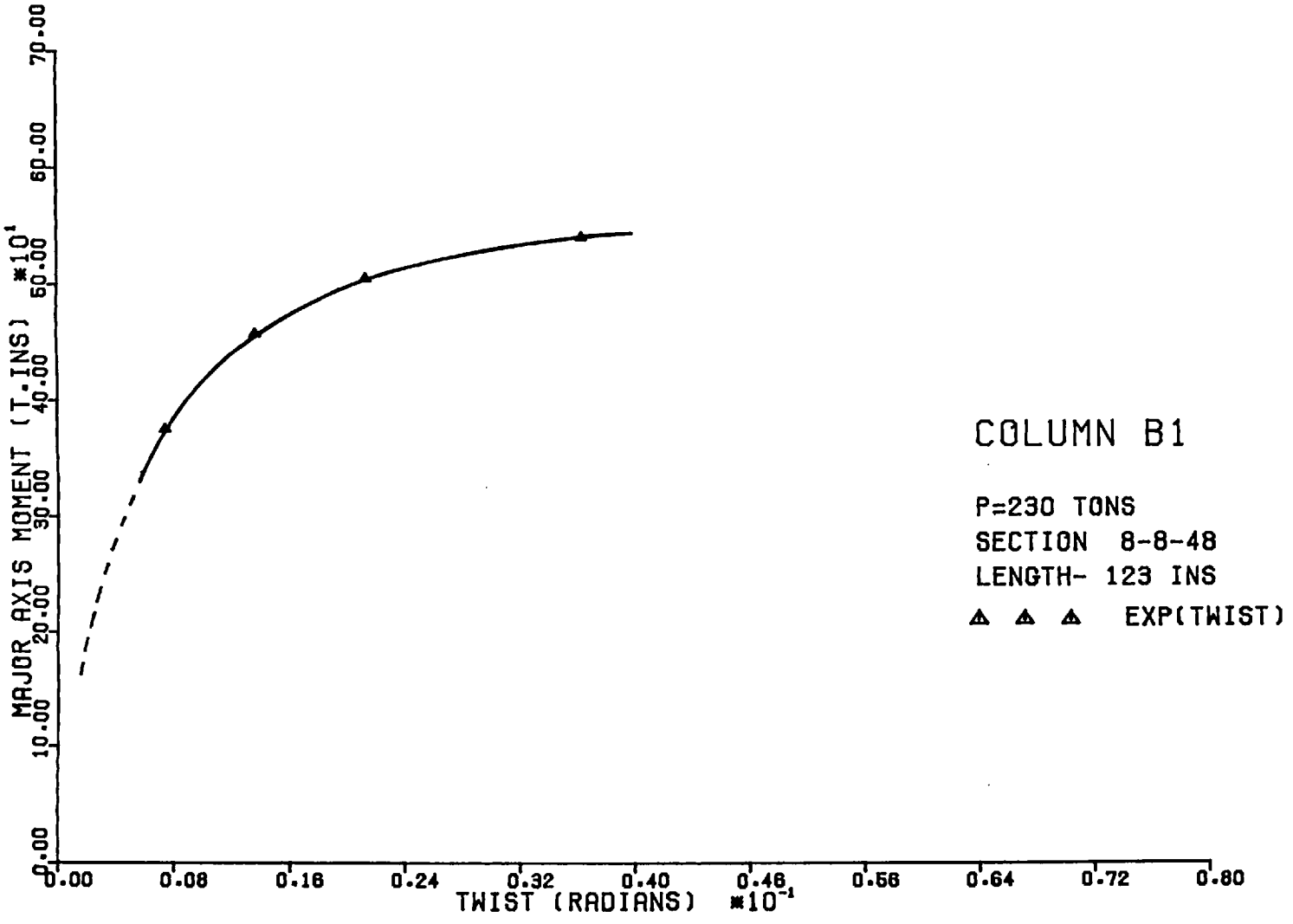


FIG. 2.26 EXPERIMENTAL MOMENT-MID COLUMN HEIGHT TWIST PLOT

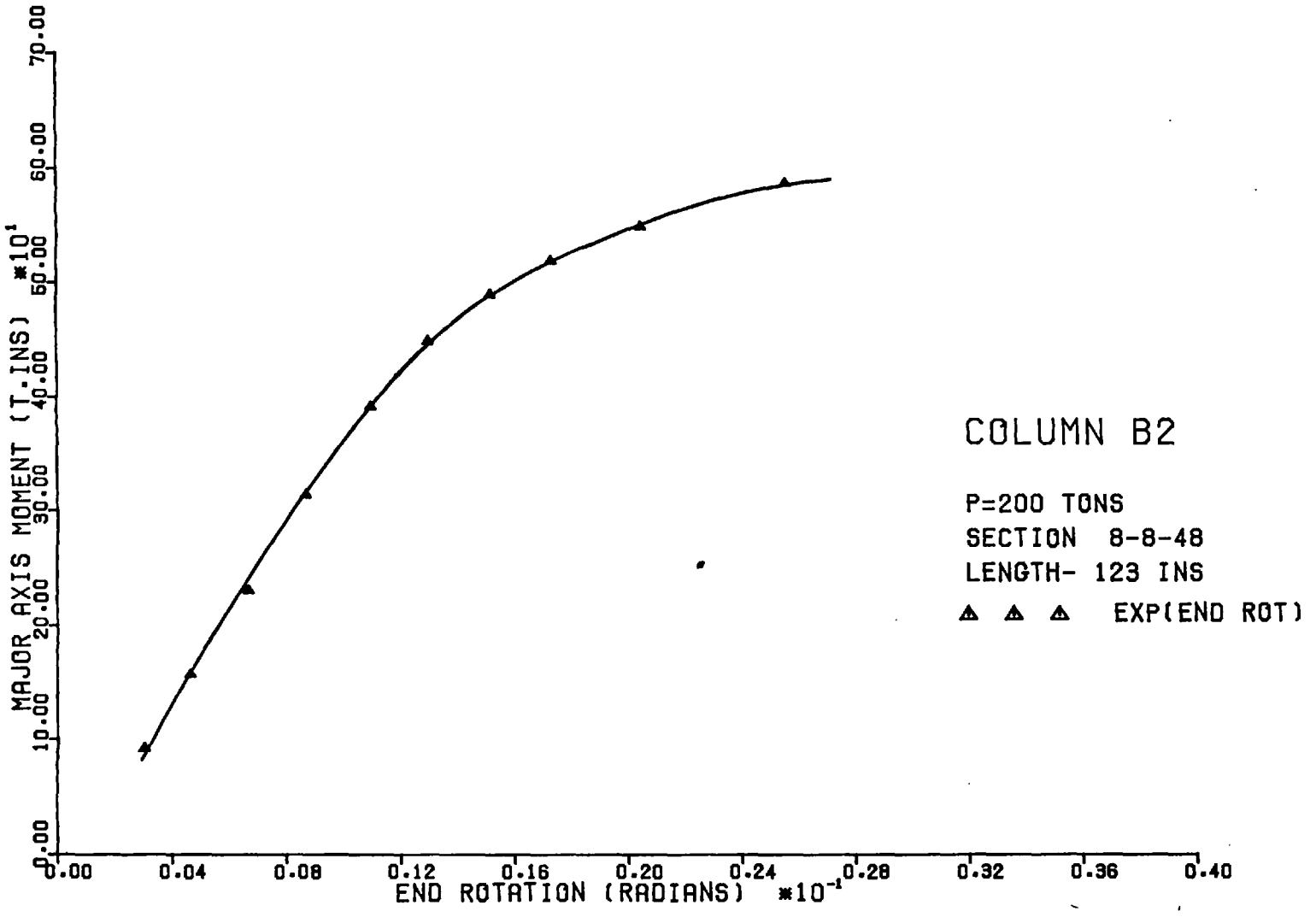


FIG. 2.27 EXPERIMENTAL MOMENT-END ROTATION PLOT

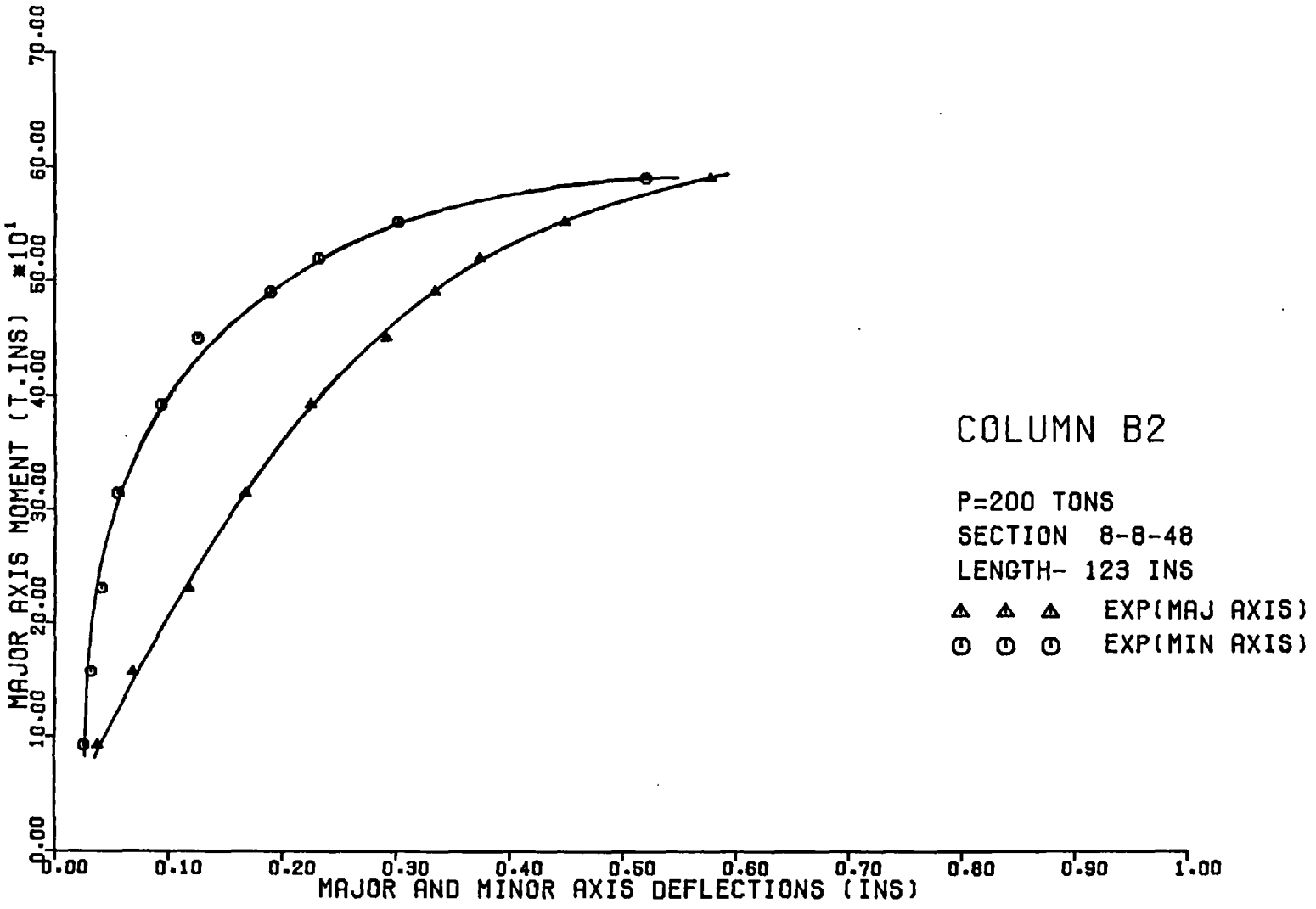


FIG. 2.28 EXPERIMENTAL MOMENT-MID COLUMN HEIGHT DEFLECTION PLOT

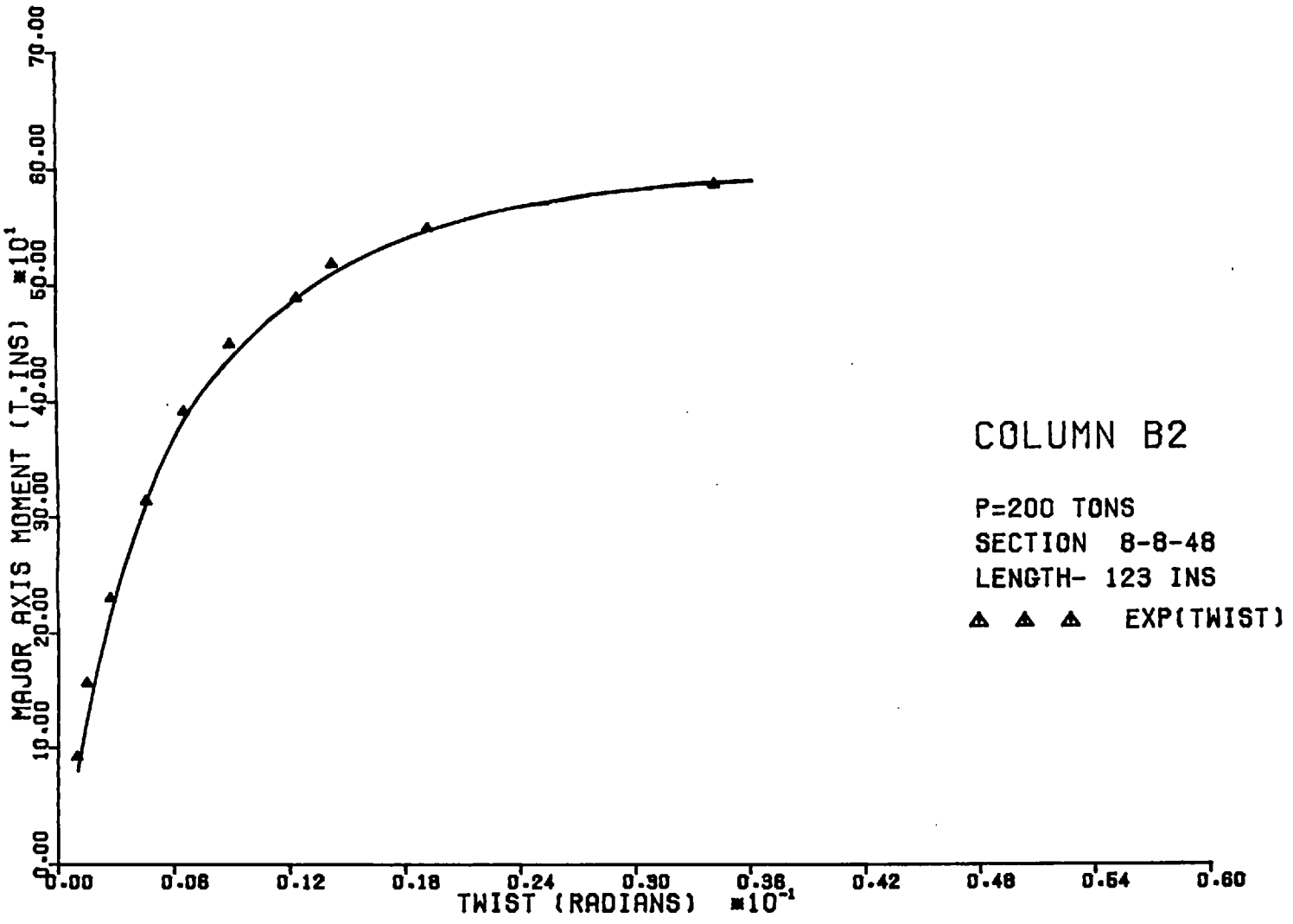


FIG. 2.29 EXPERIMENTAL MOMENT-MID COLUMN HEIGHT TWIST PLOT

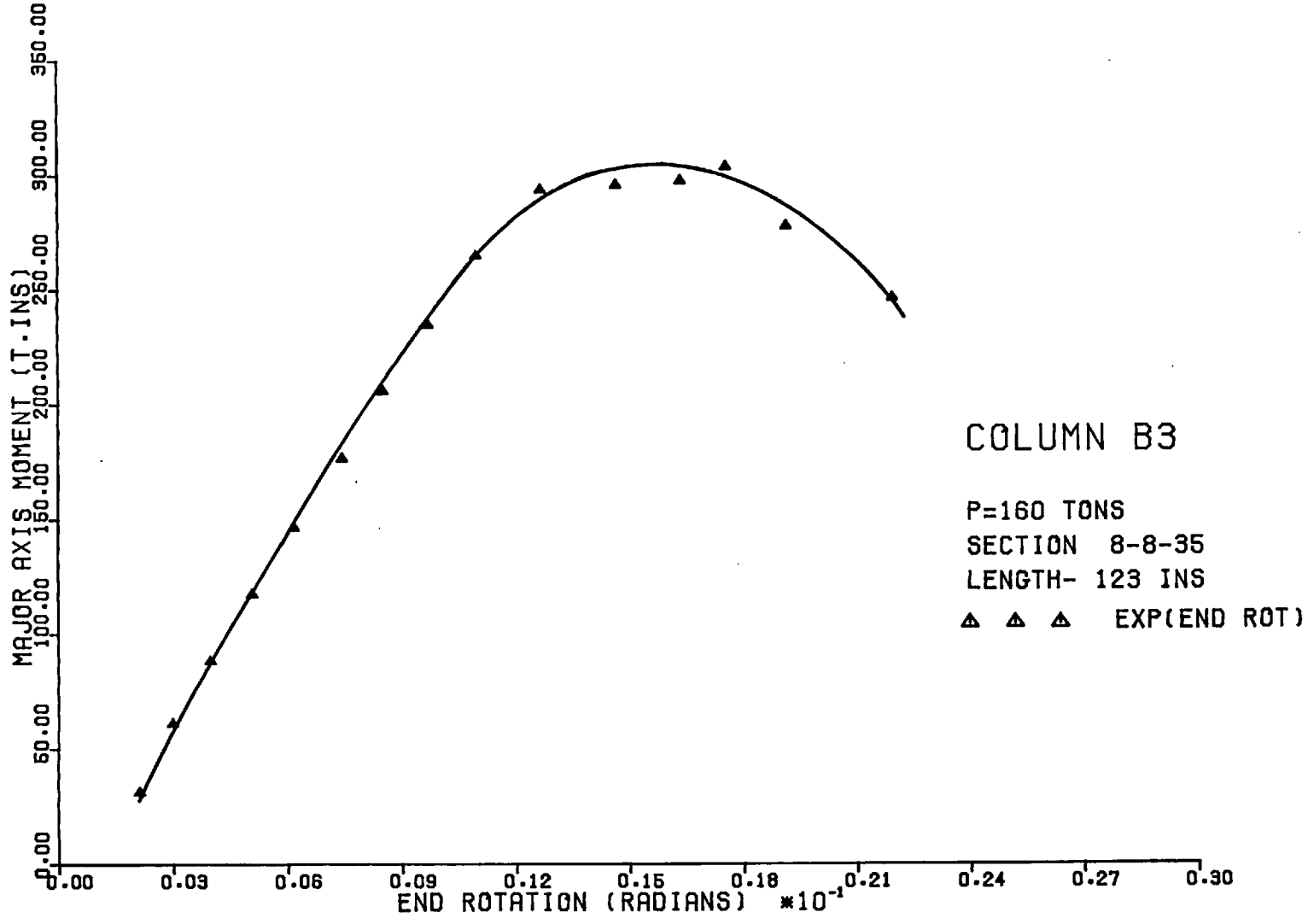


FIG. 2.30 EXPERIMENTAL MOMENT-END ROTATION PLOT

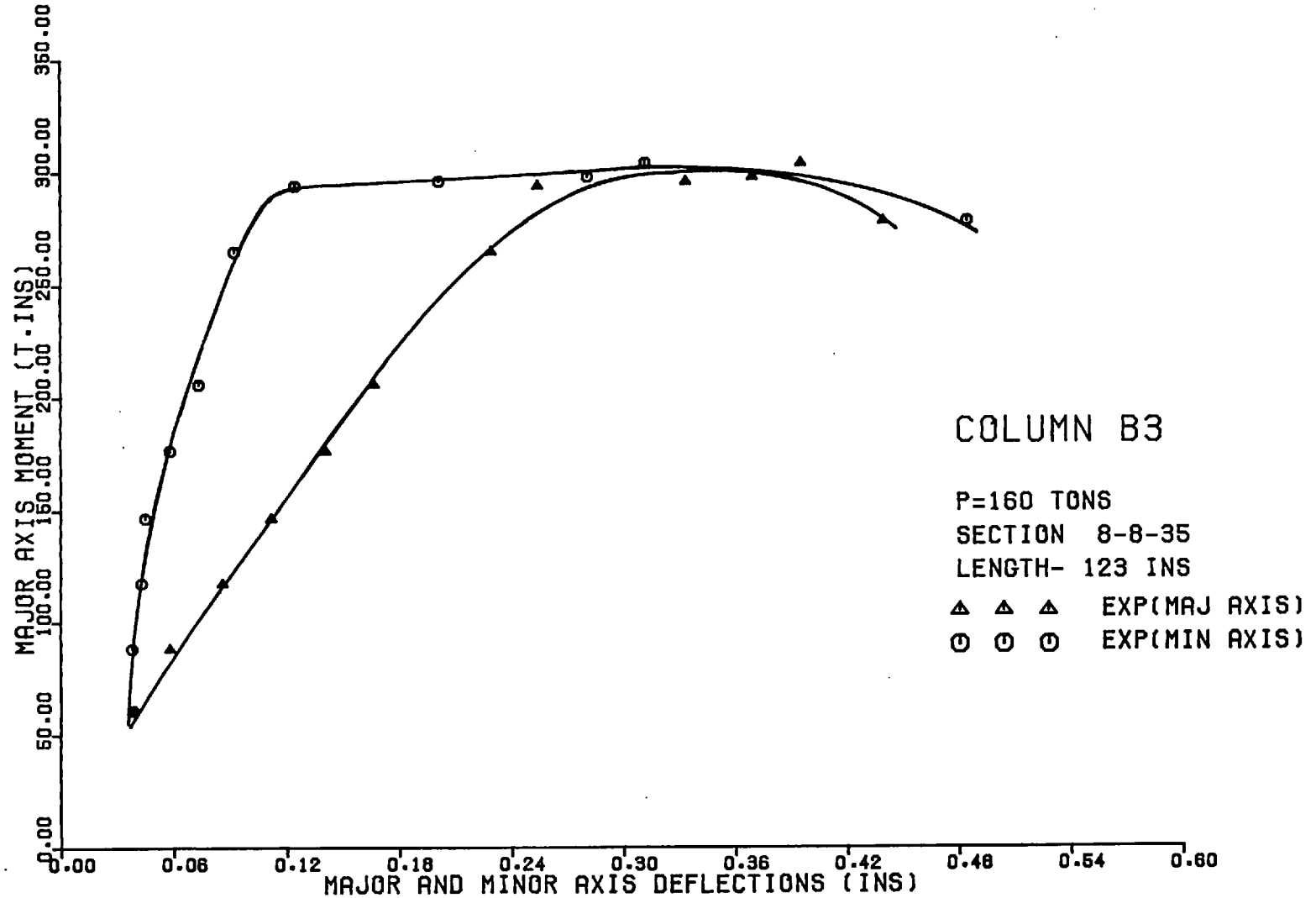


FIG. 2.31 EXPERIMENTAL MOMENT-MID COLUMN HEIGHT DEFLECTION PLOT

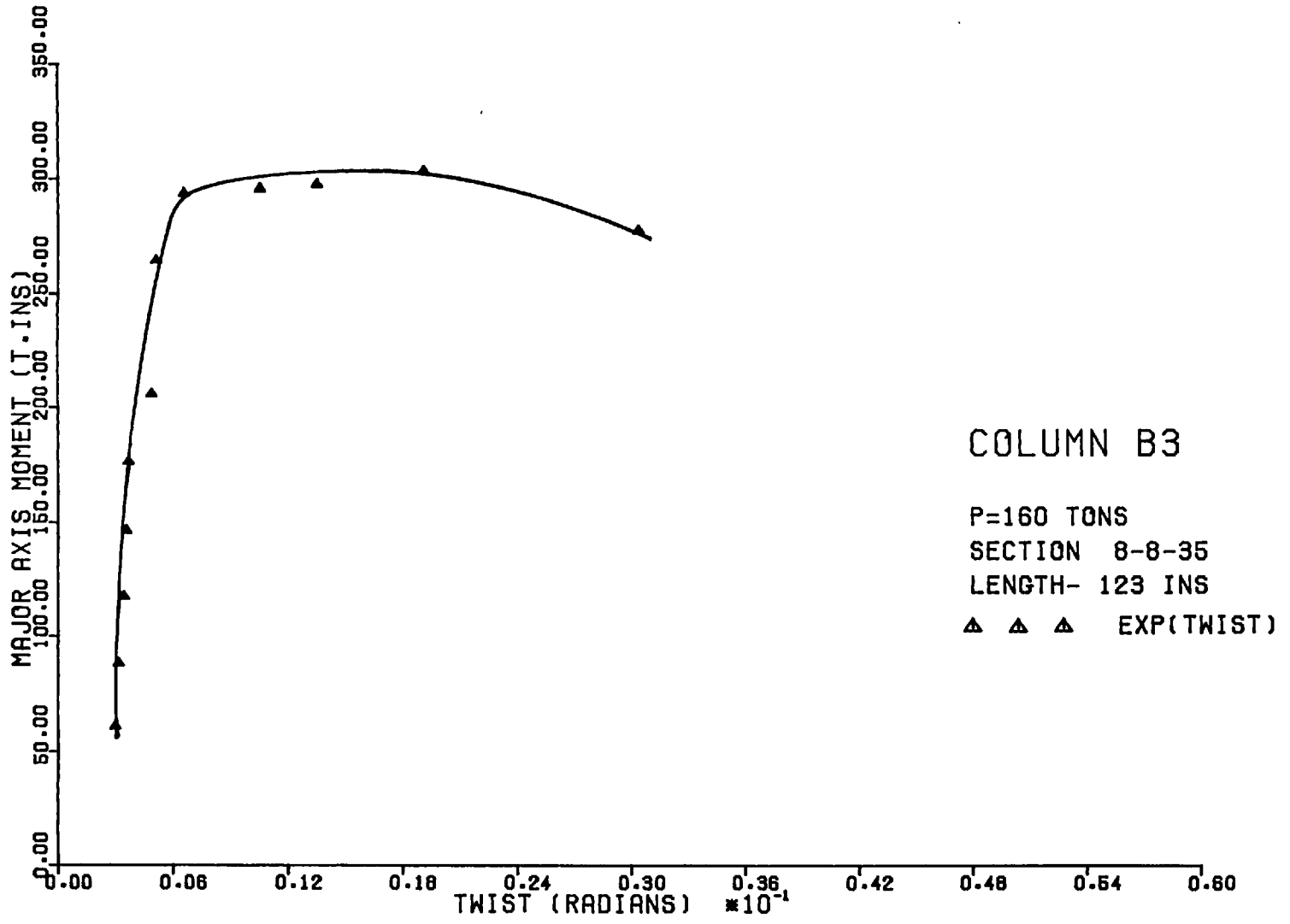


FIG. 2.32 EXPERIMENTAL MOMENT-MID COLUMN HEIGHT TWIST PLOT

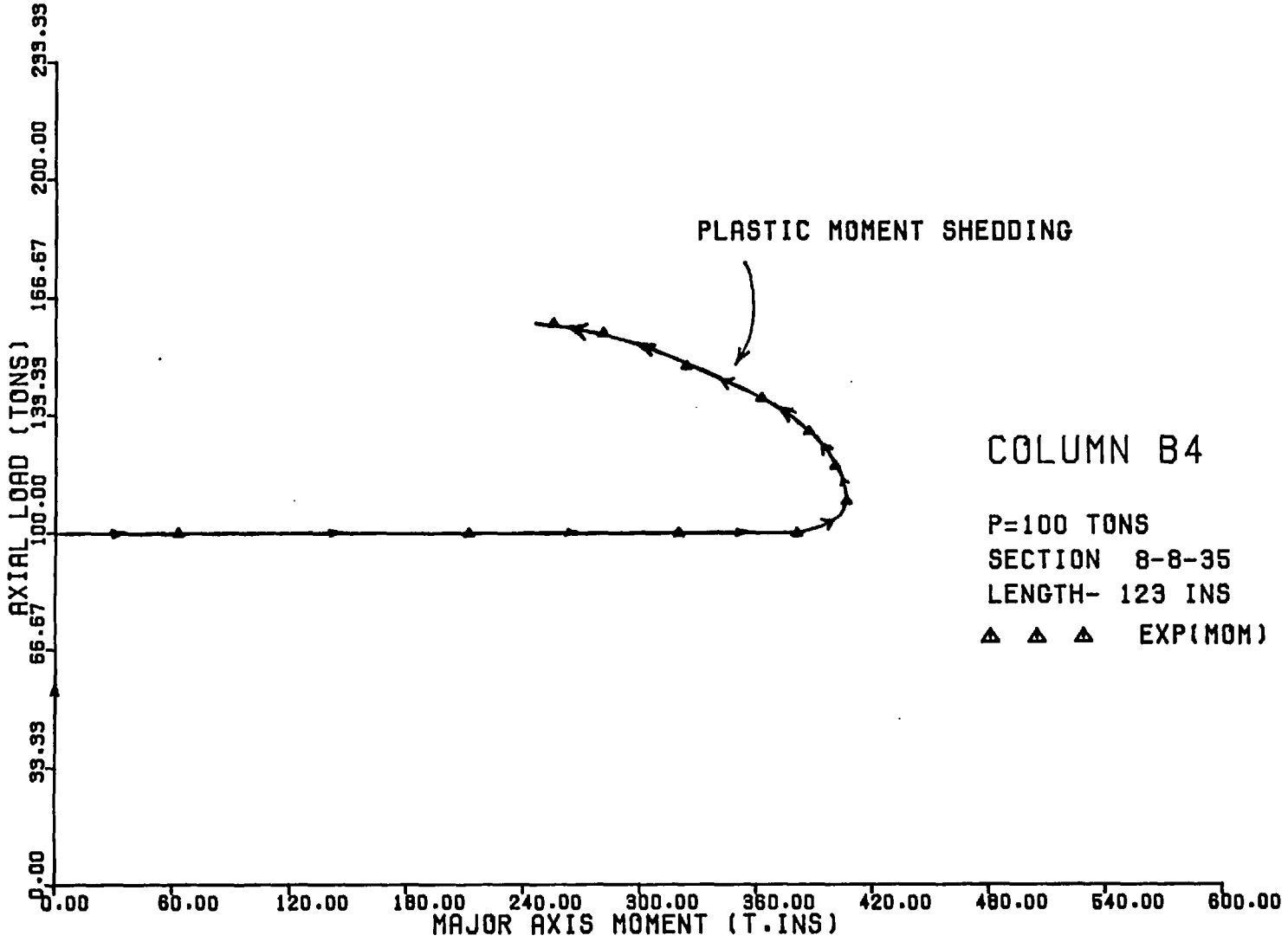


FIG. 2.33 THE LOAD PATH FOLLOWED DURING TEST

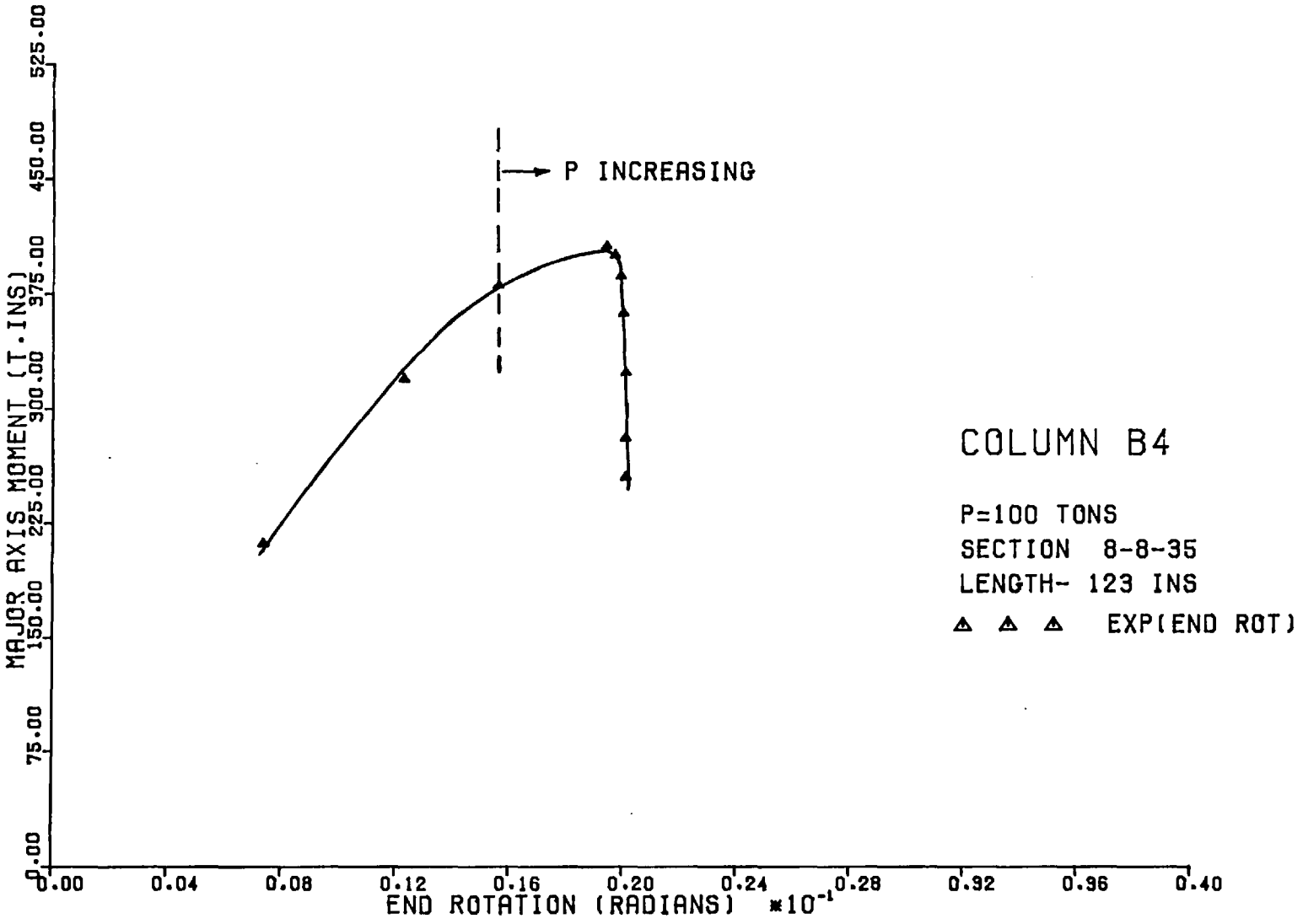


FIG. 2.34 EXPERIMENTAL MOMENT-END ROTATION PLOT

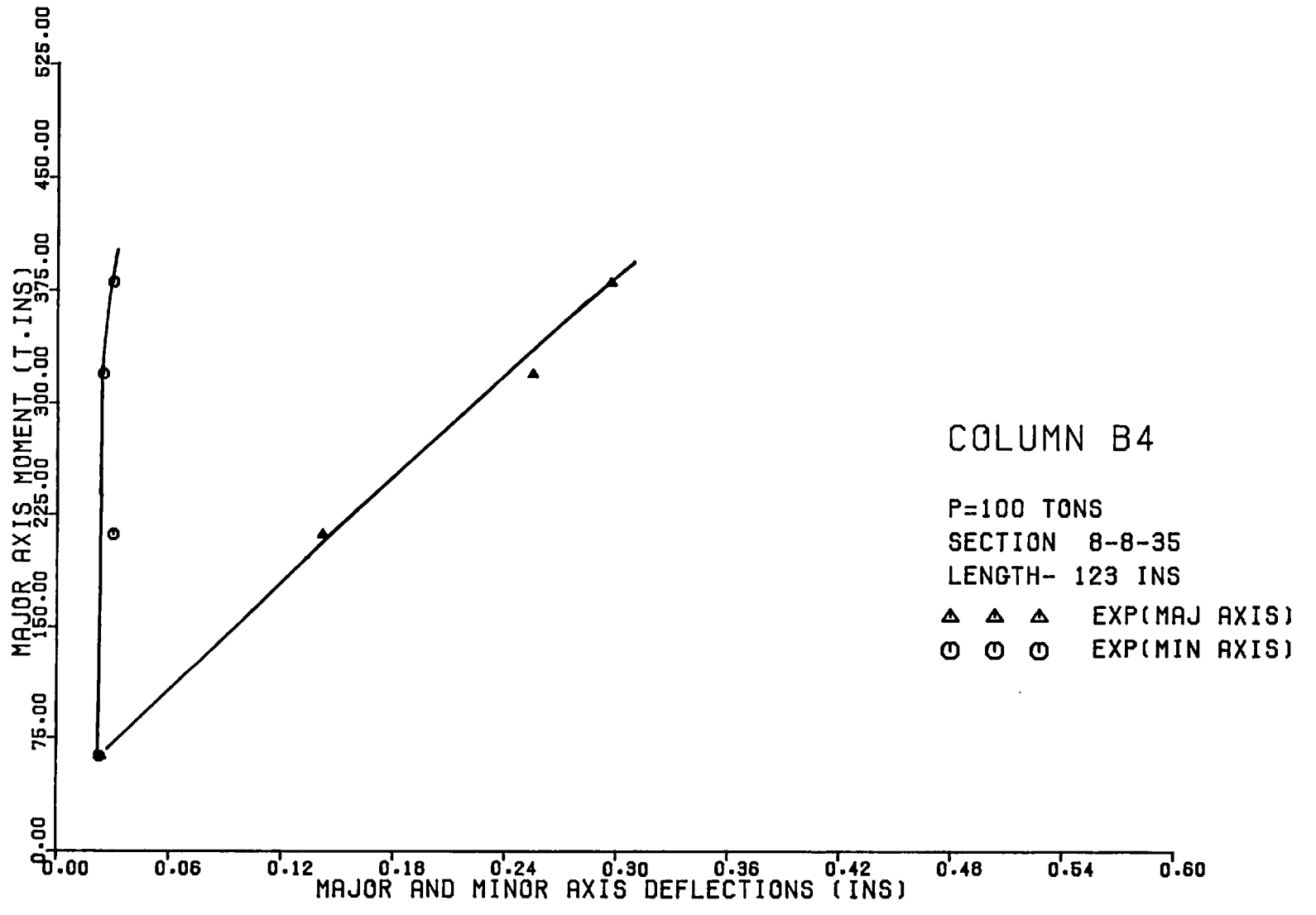


FIG. 2.35 EXPERIMENTAL MOMENT-MID COLUMN HEIGHT DEFLECTION PLOT

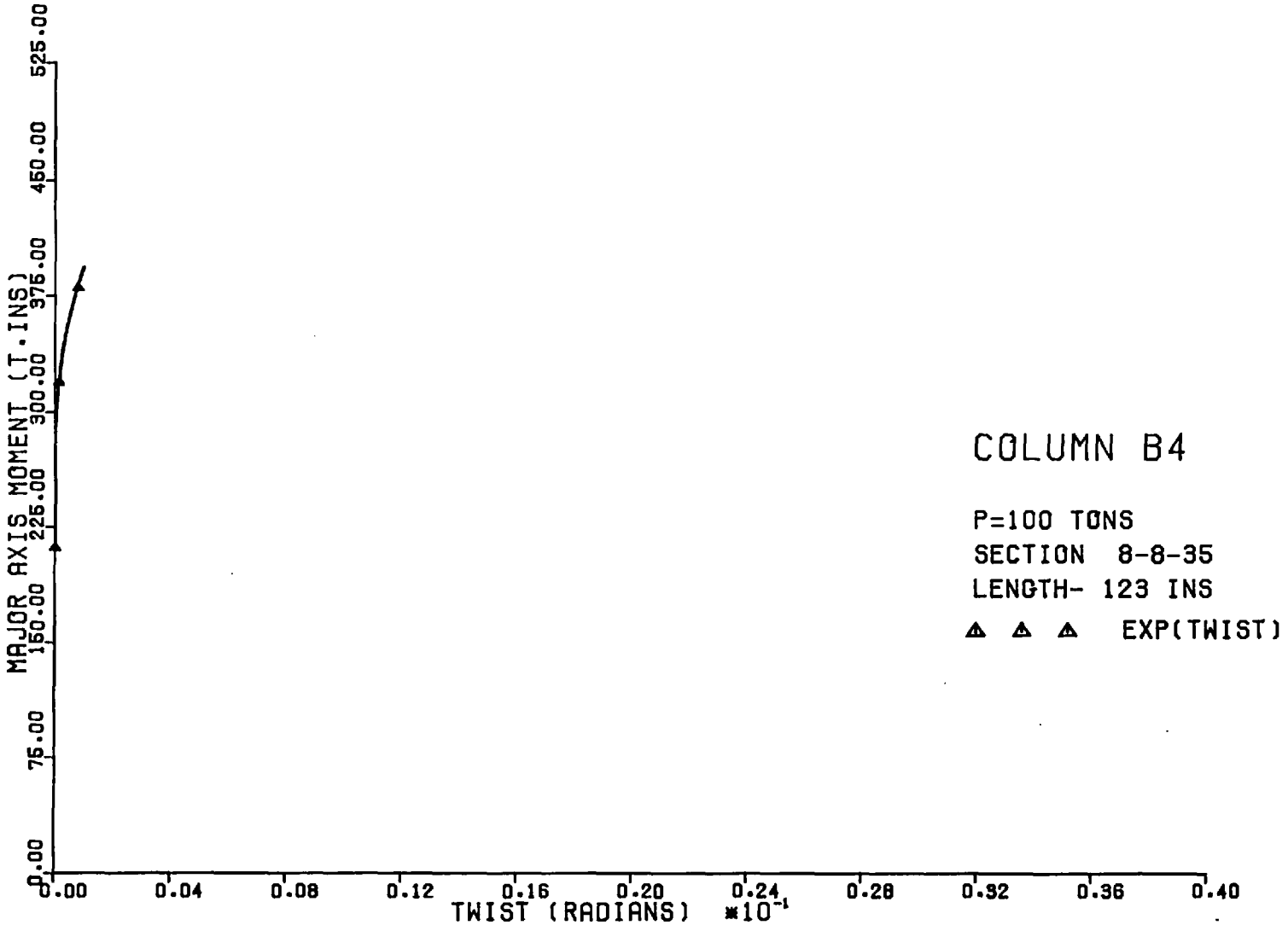


FIG. 2.36 EXPERIMENTAL MOMENT-MID COLUMN HEIGHT TWIST PLOT

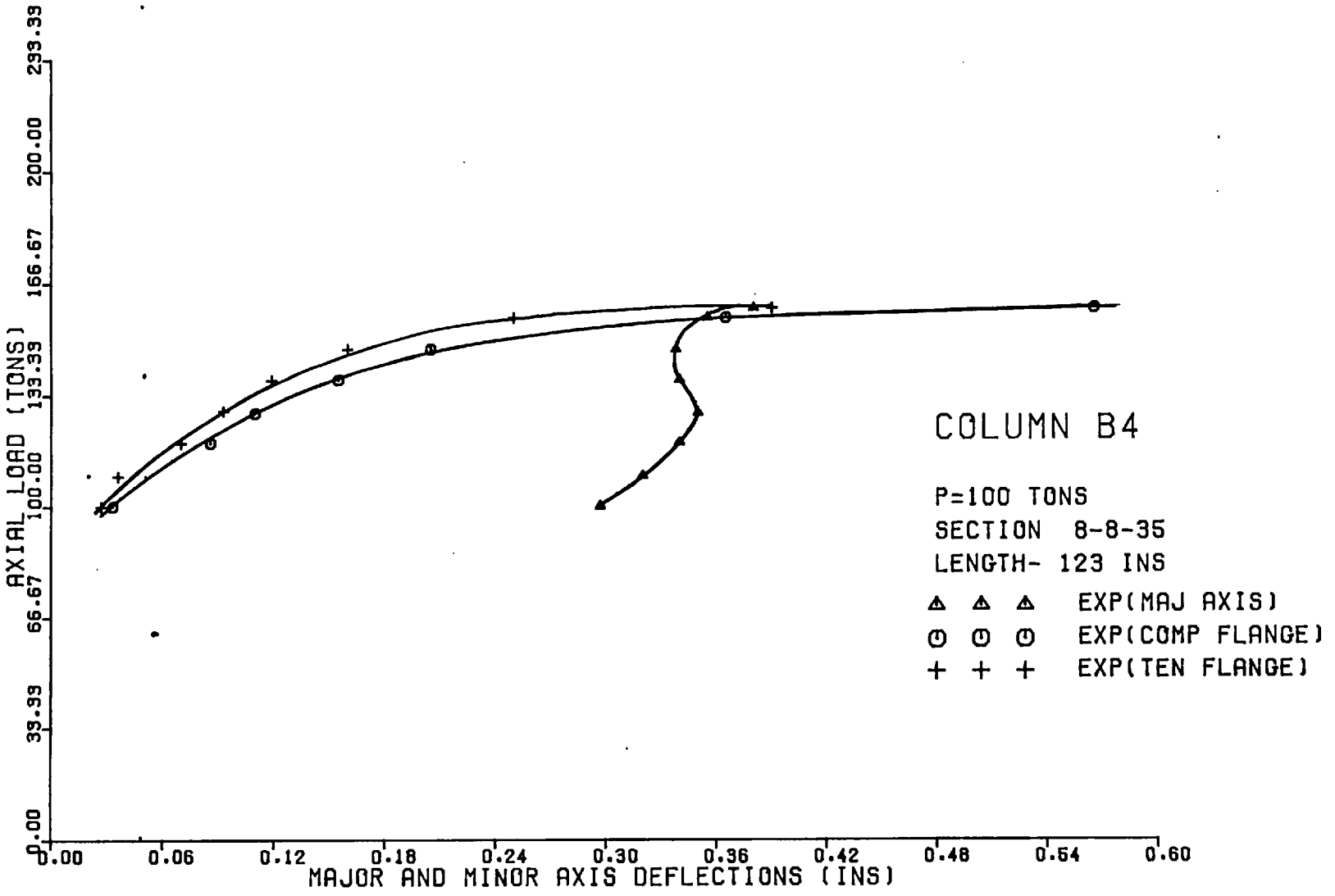


FIG. 2.37 EXPERIMENTAL AXIAL LOAD-MID COLUMN HEIGHT DEFLECTION PLOT

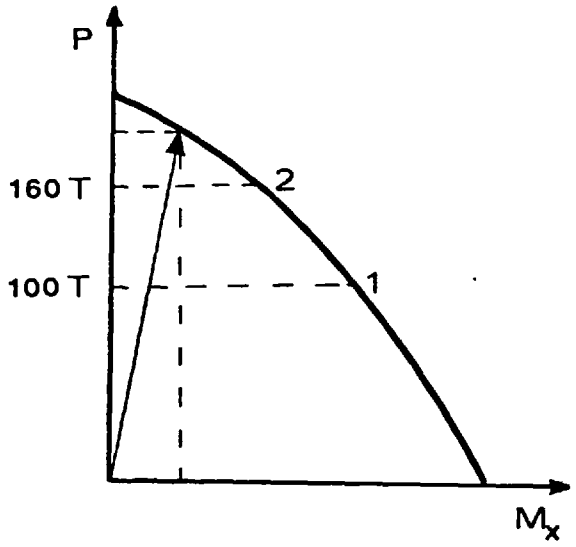


Fig.2.38a Typical Interaction Curve for Axial Load and Moment

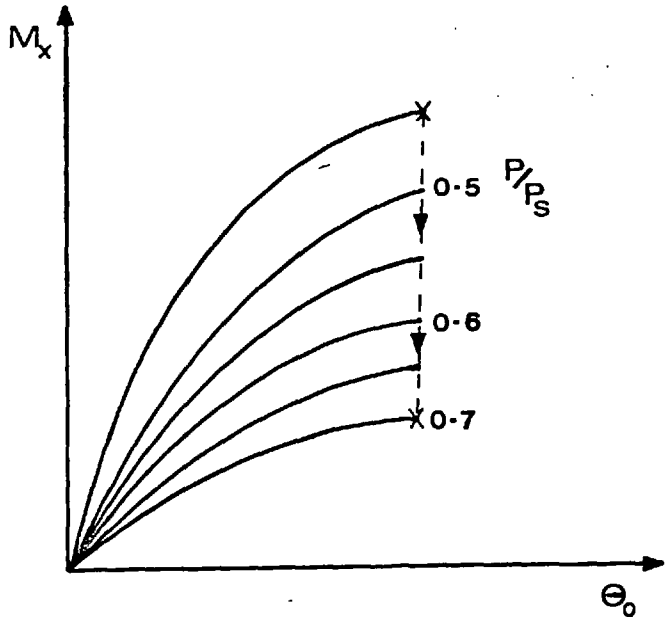


Fig.2.38b Typical Moment - End Rotation Curves at Various Axial Loads

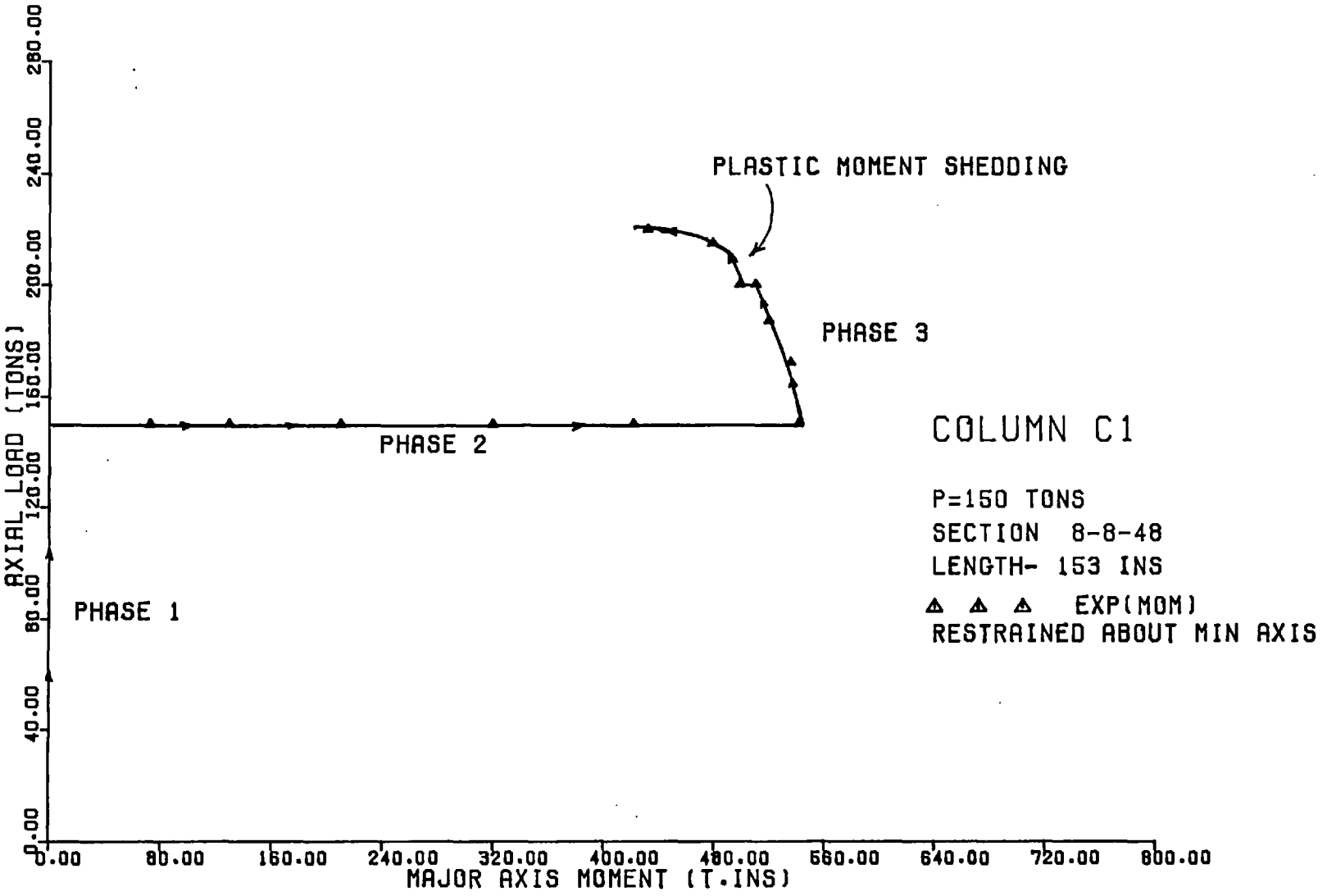


FIG. 2.39 THE LOAD PATH FOLLOWED DURING TEST

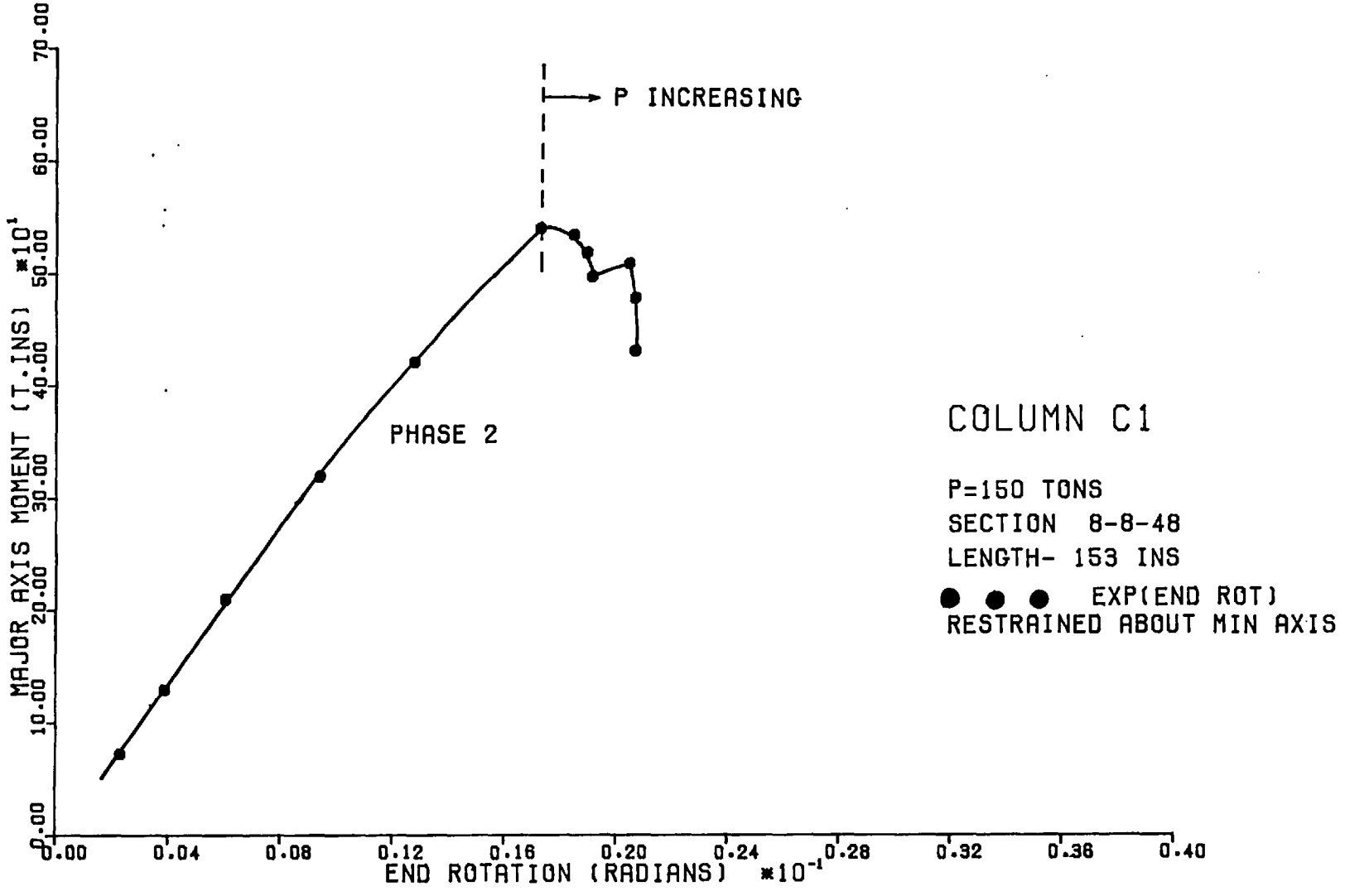


FIG. 2.40 EXPERIMENTAL MOMENT-END ROTATION PLOT

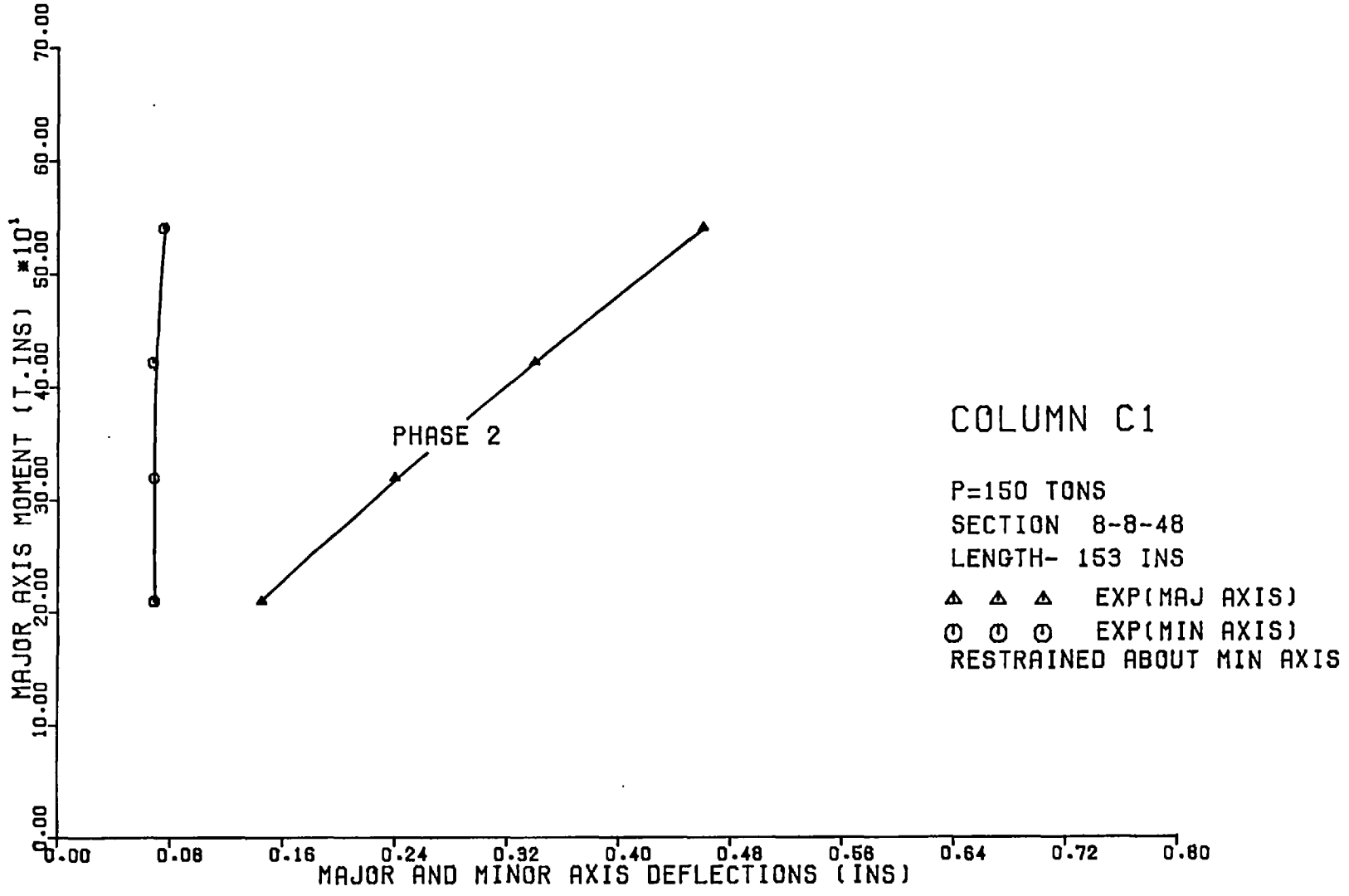


FIG. 2.41 EXPERIMENTAL MOMENT-MID COLUMN HEIGHT DEFLECTION PLOT

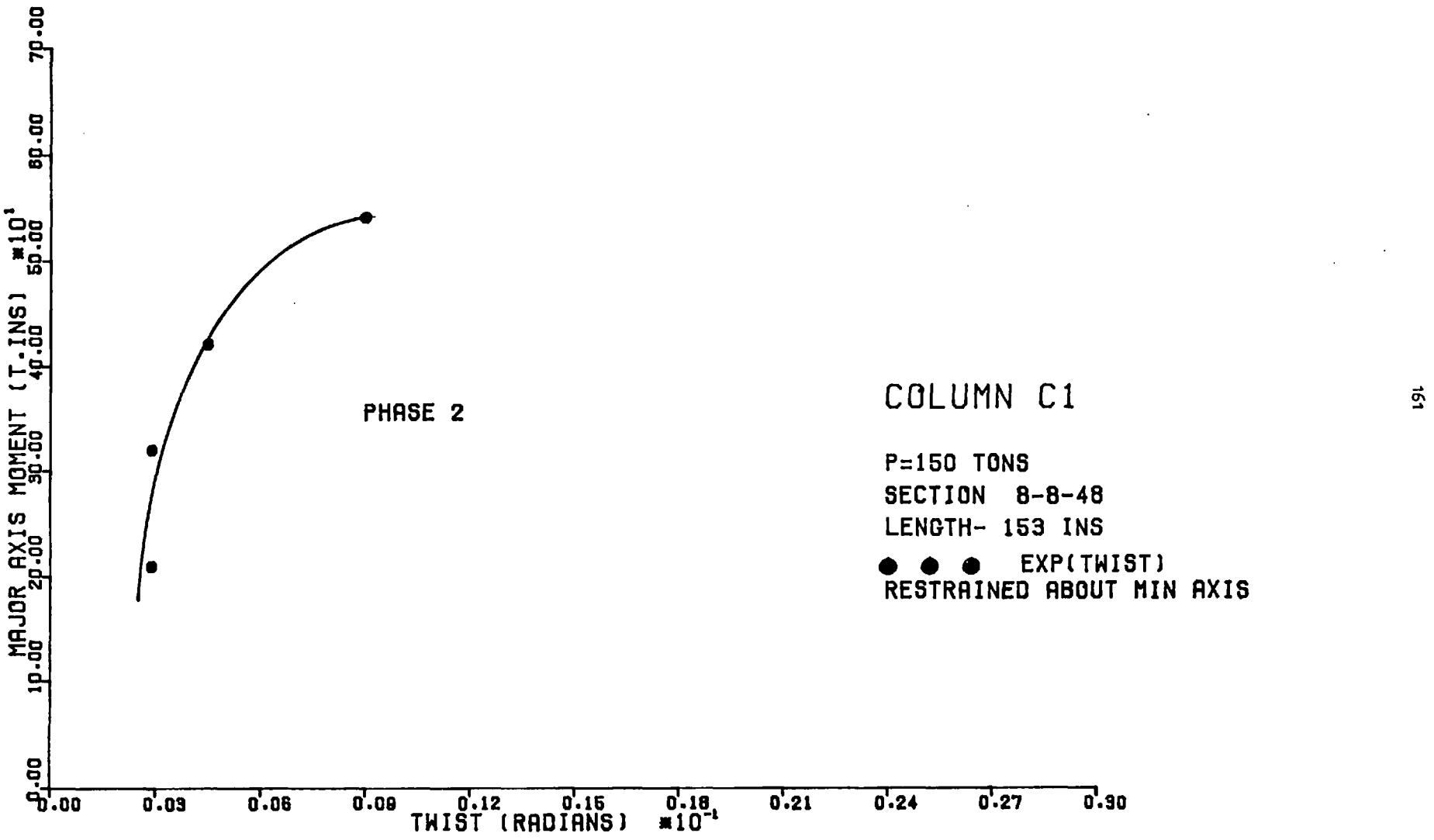


FIG. 2.42 EXPERIMENTAL MOMENT-MID COLUMN HEIGHT TWIST PLOT

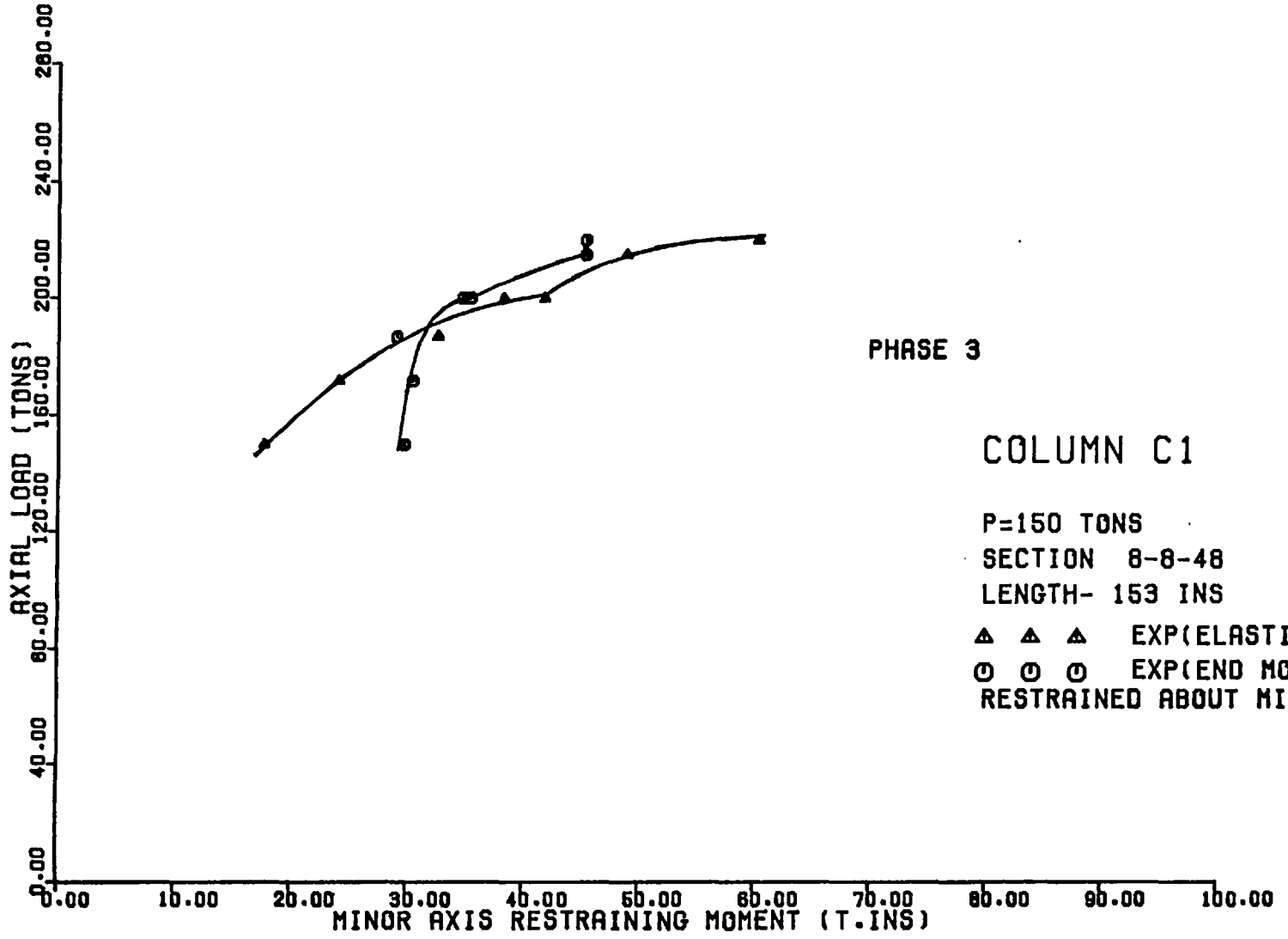


FIG. 2.43 EXPERIMENTAL AXIAL LOAD-MINOR AXIS RESTRAINING MOMENT PLOT

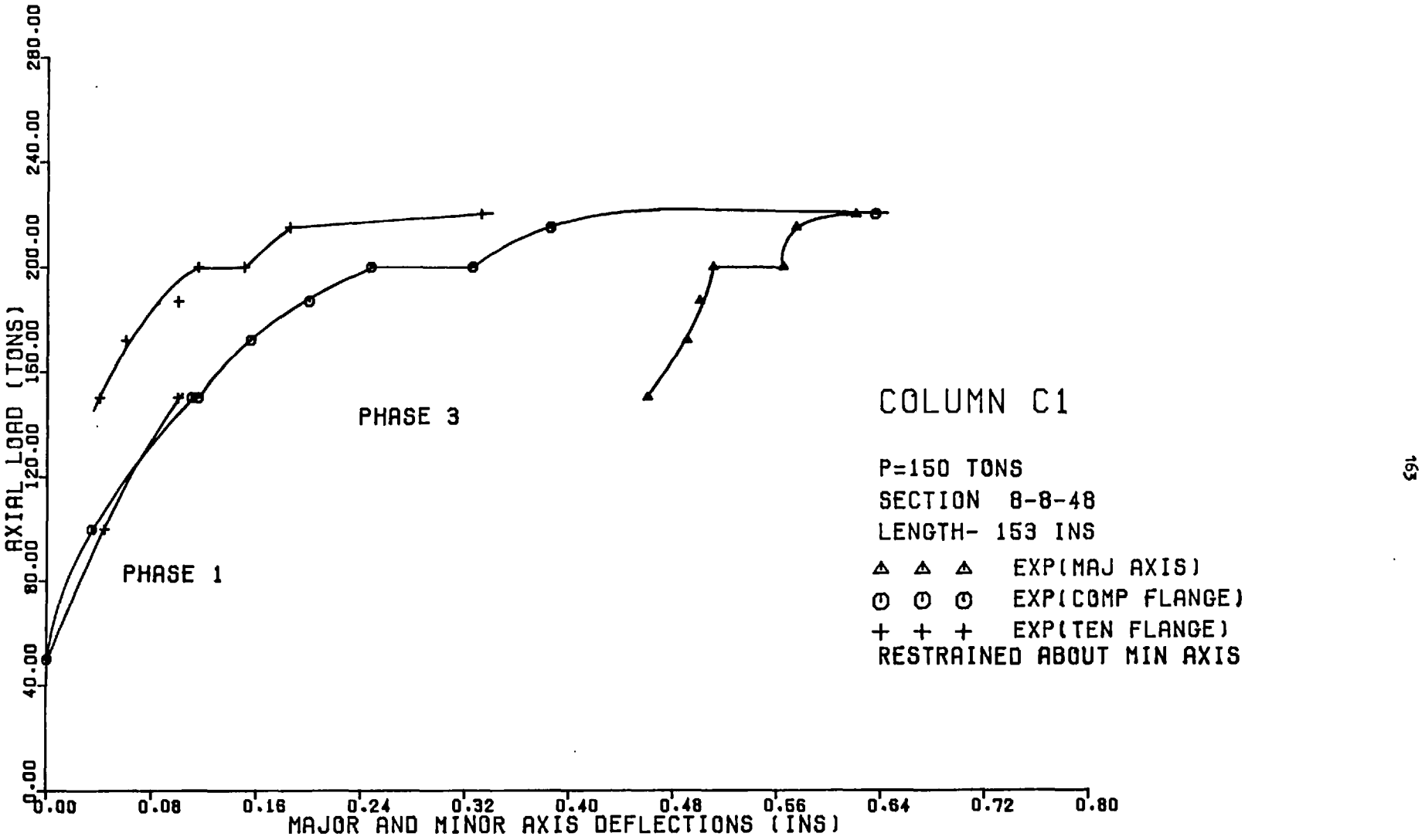


FIG. 2.44 EXPERIMENTAL AXIAL LOAD-MID COLUMN HEIGHT DEFLECTION PLOT

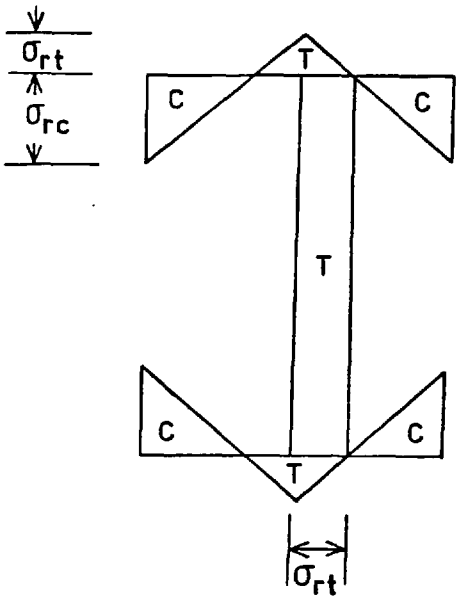


Fig. 3.1 Linear Residual Stress Distribution Pattern

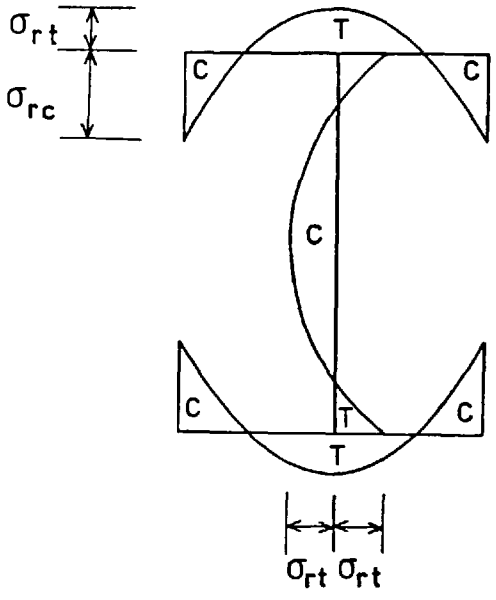


Fig. 3.2 Parabolic Residual Stress Distribution Pattern

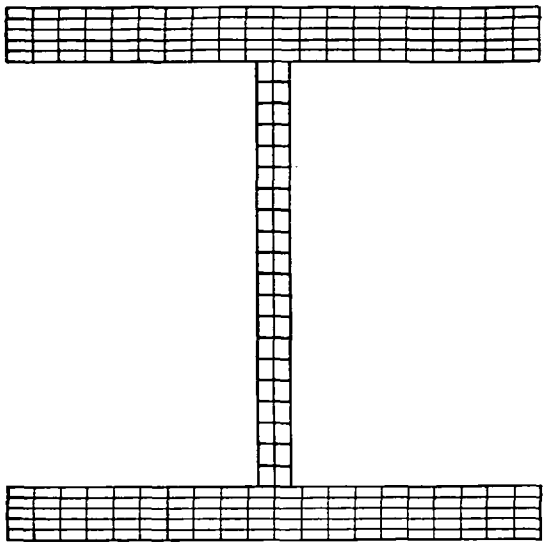


Fig. 3.3 SUBDIVISION OF COLUMN CROSS SECTION

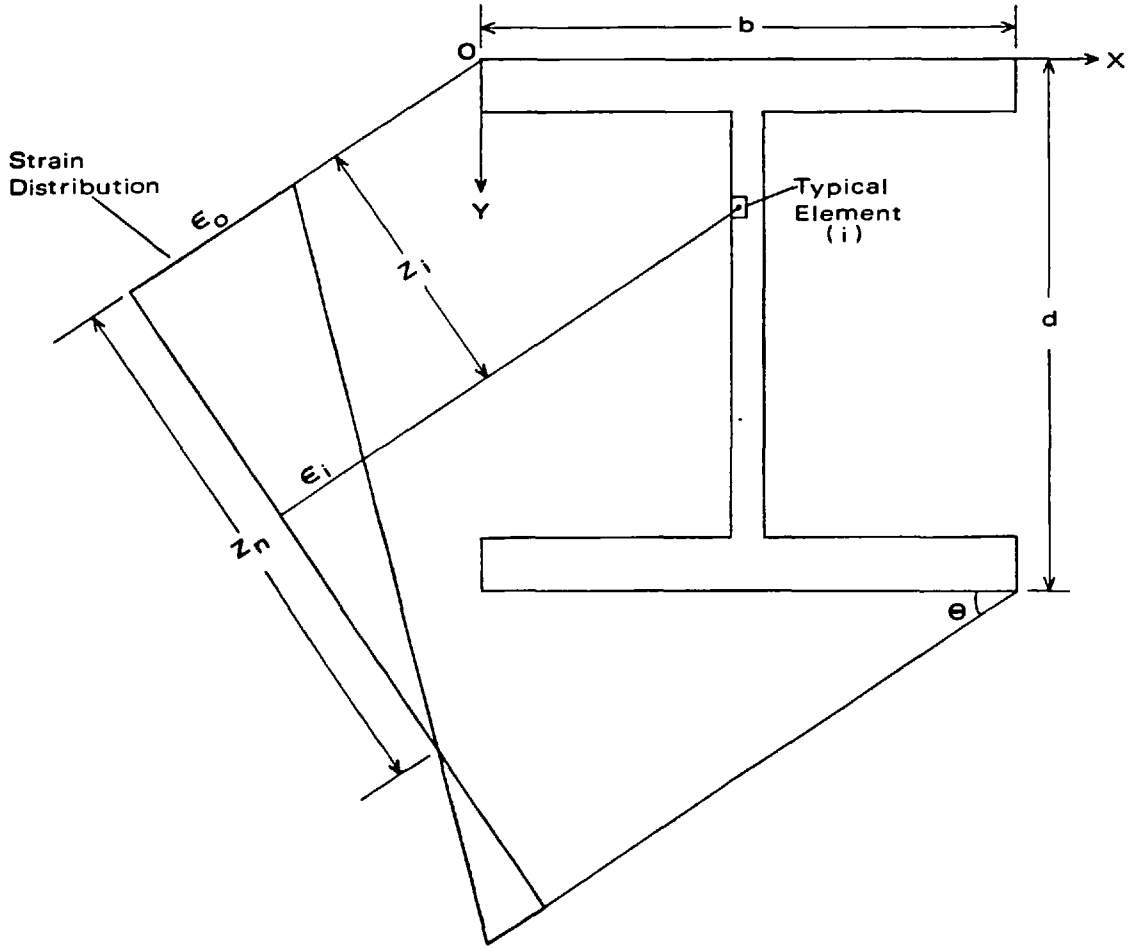


Fig. 3.4 SIGN CONVENTION USED IN THE ANALYSIS

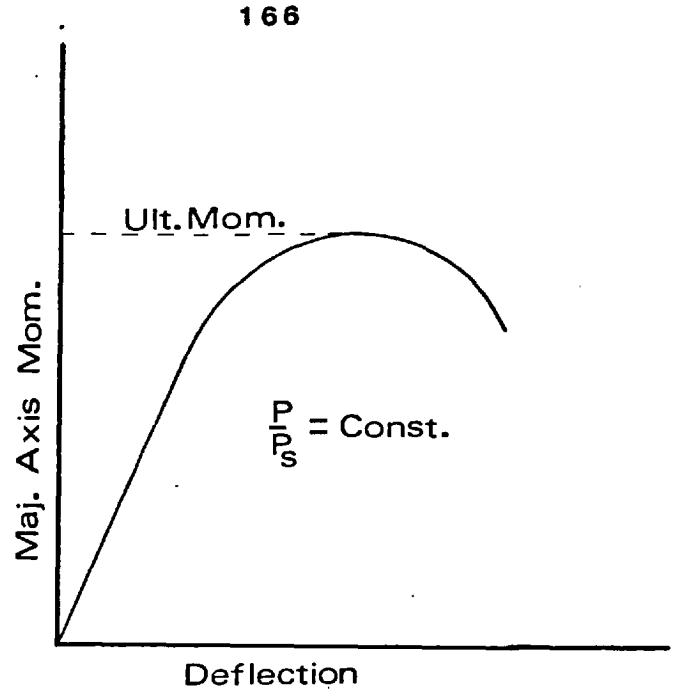


Fig. 4.1 Typical Load-Deflection Plot for a Column in Uniaxial Bending Under Constant Axial Thrust

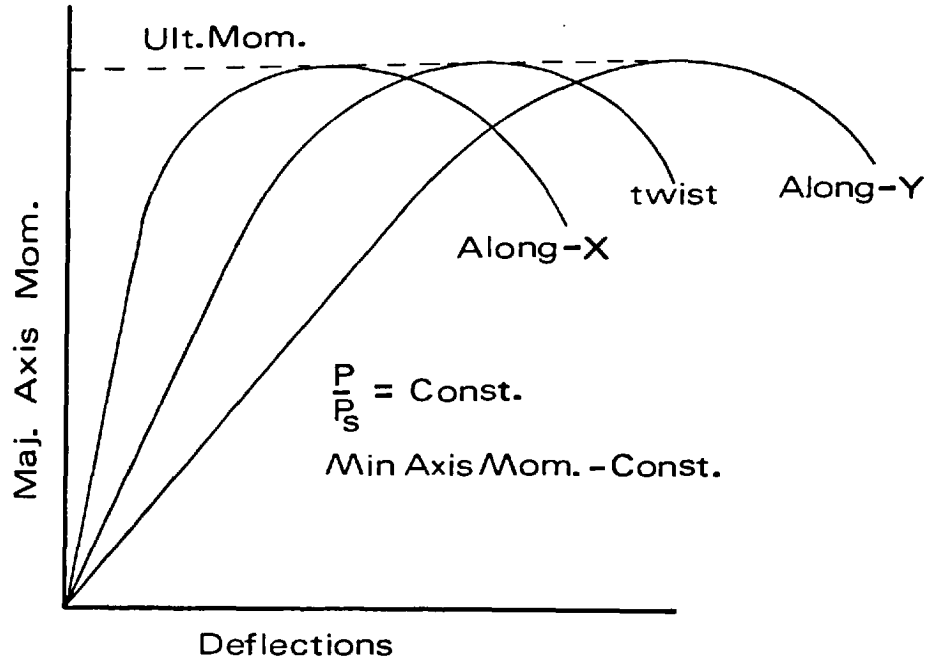


Fig. 4.2 Typical Load-Deflection Plot for a Column in Biaxial Bending Under Constant Axial Thrust

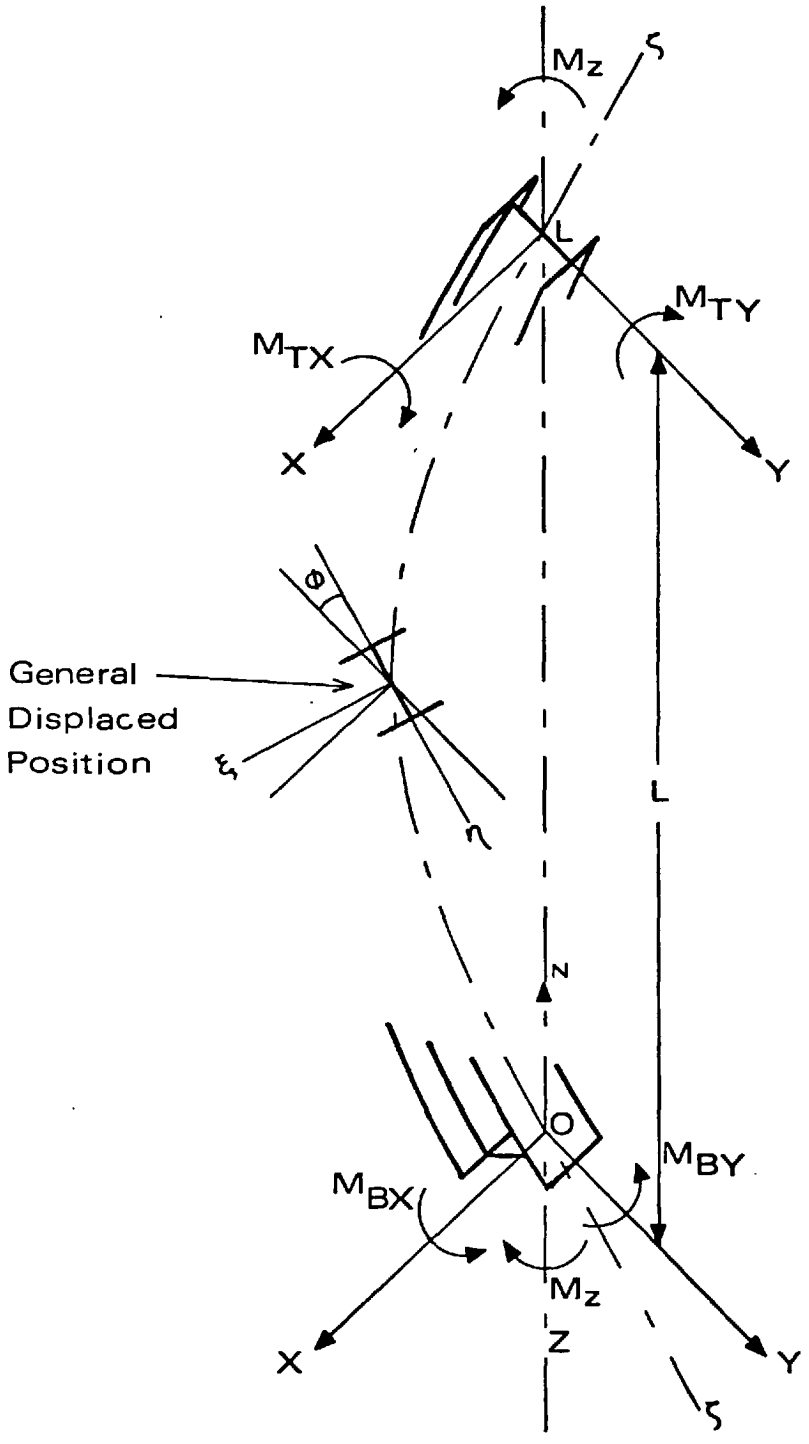


Fig. 4.3 Deformed Configuration of a Column

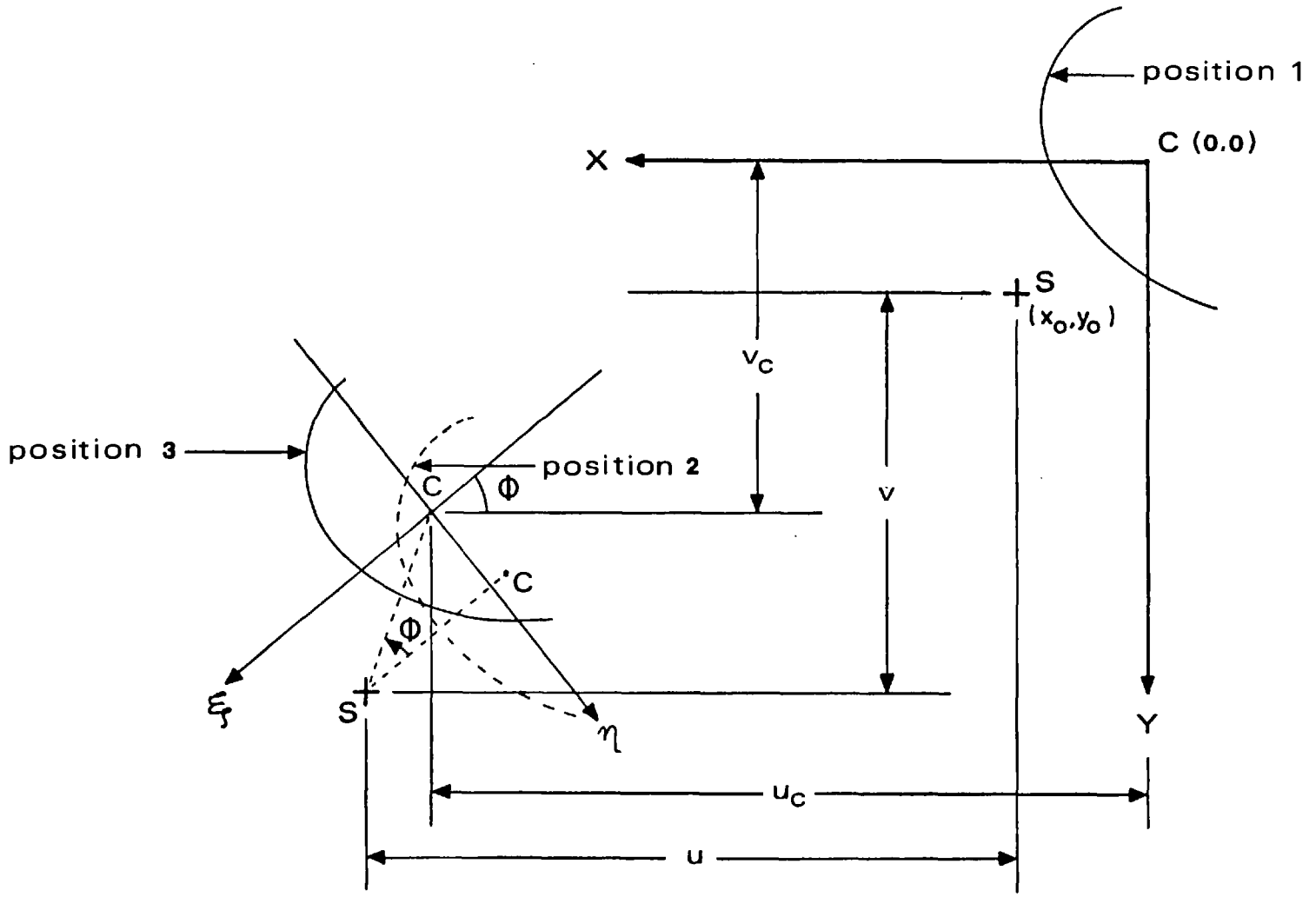


Fig. 4.4 DISPLACEMENTS OF A GENERAL CROSS SECTION

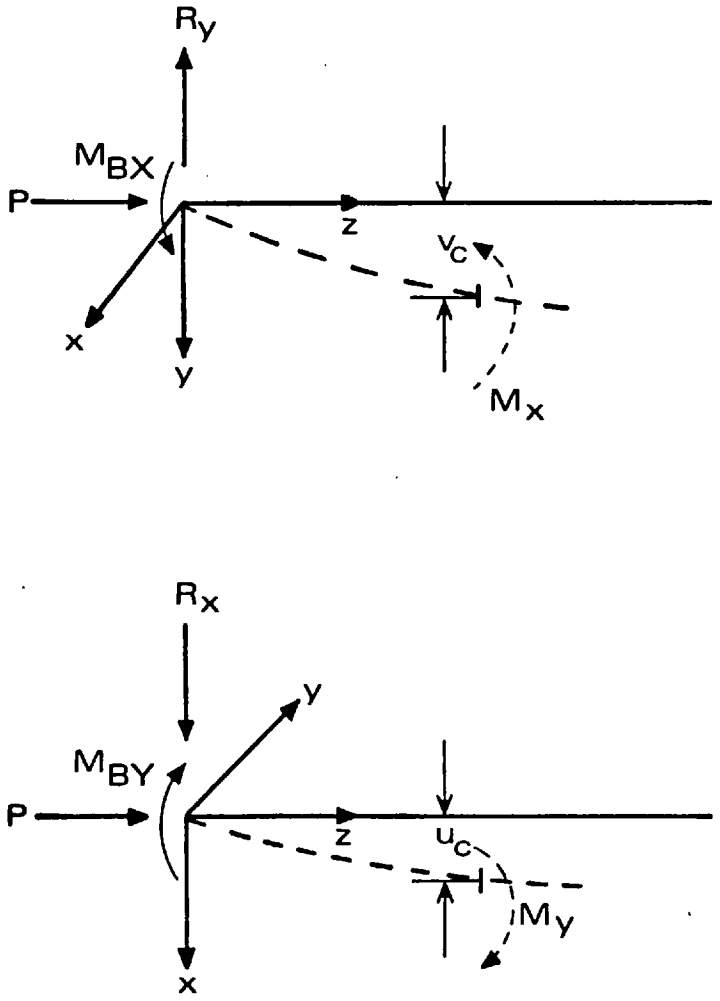


Fig. 4.5 FORCES IN THE Y-Z AND X-Z PLANE

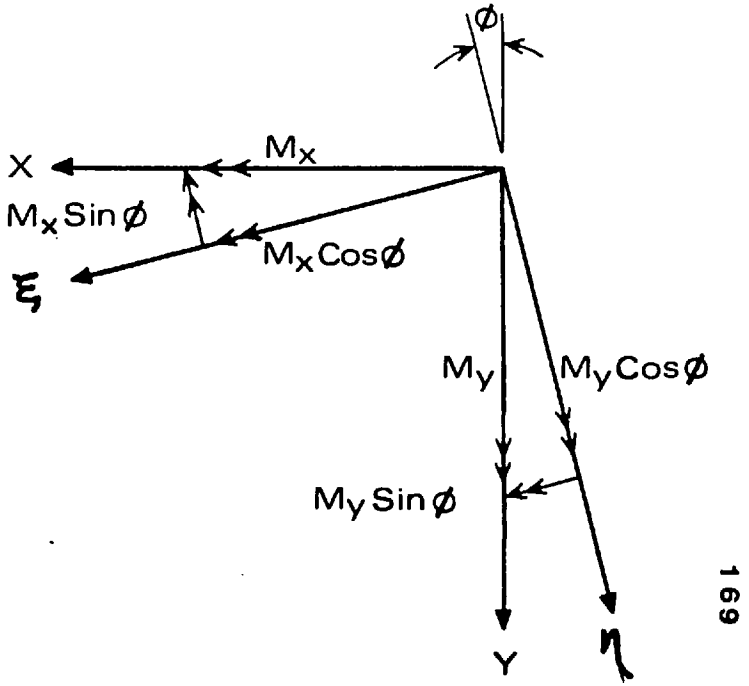


Fig. 4.6 COMPONENTS OF M_X AND M_Y

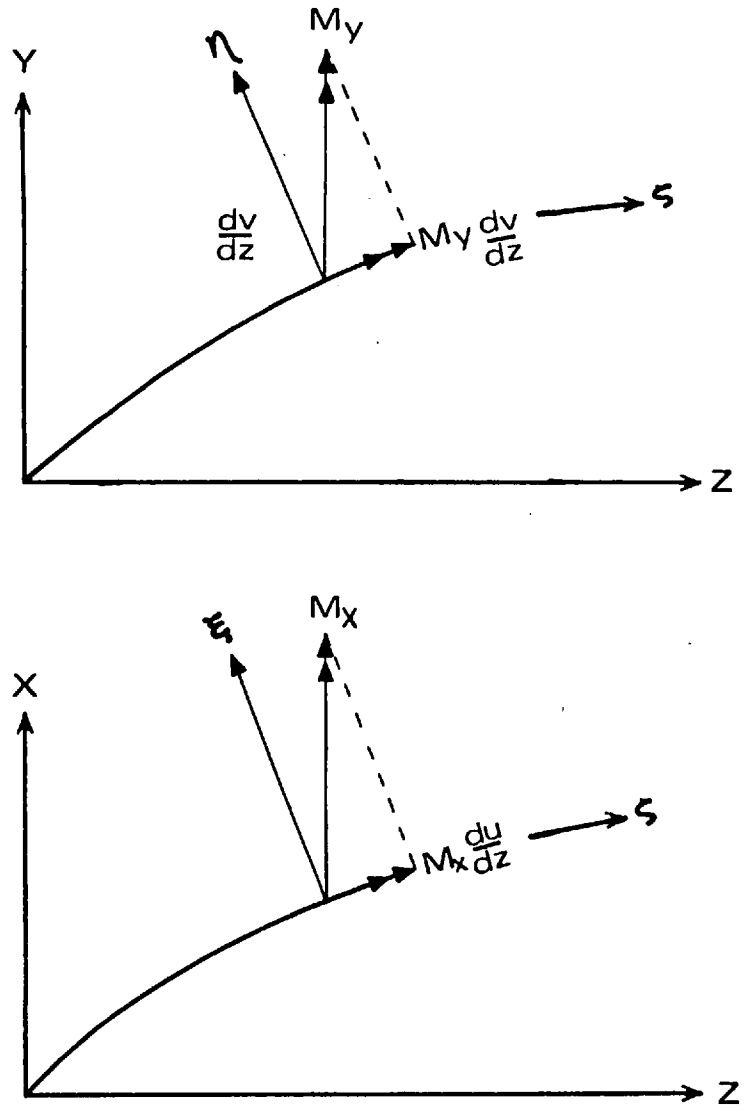


Fig. 4.7 TWISTING DUE TO COMPONENTS OF M_X AND M_Y

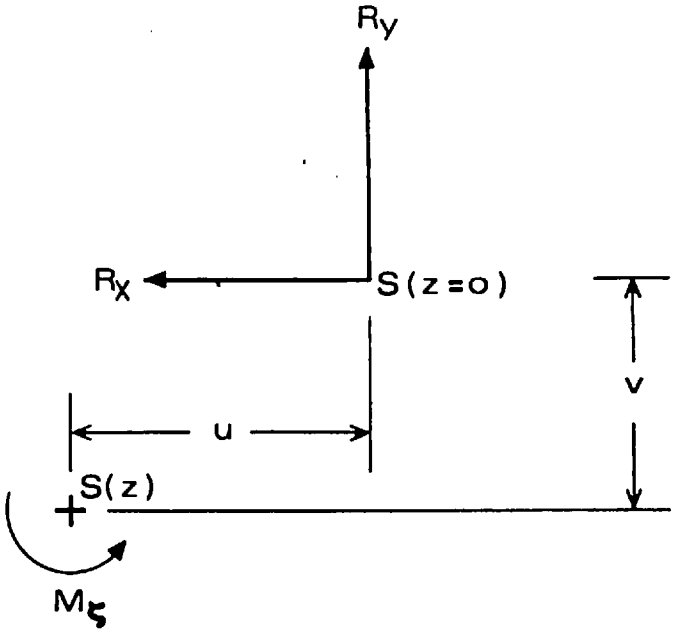


Fig. 4.8 TWISTING DUE TO END SHEARS

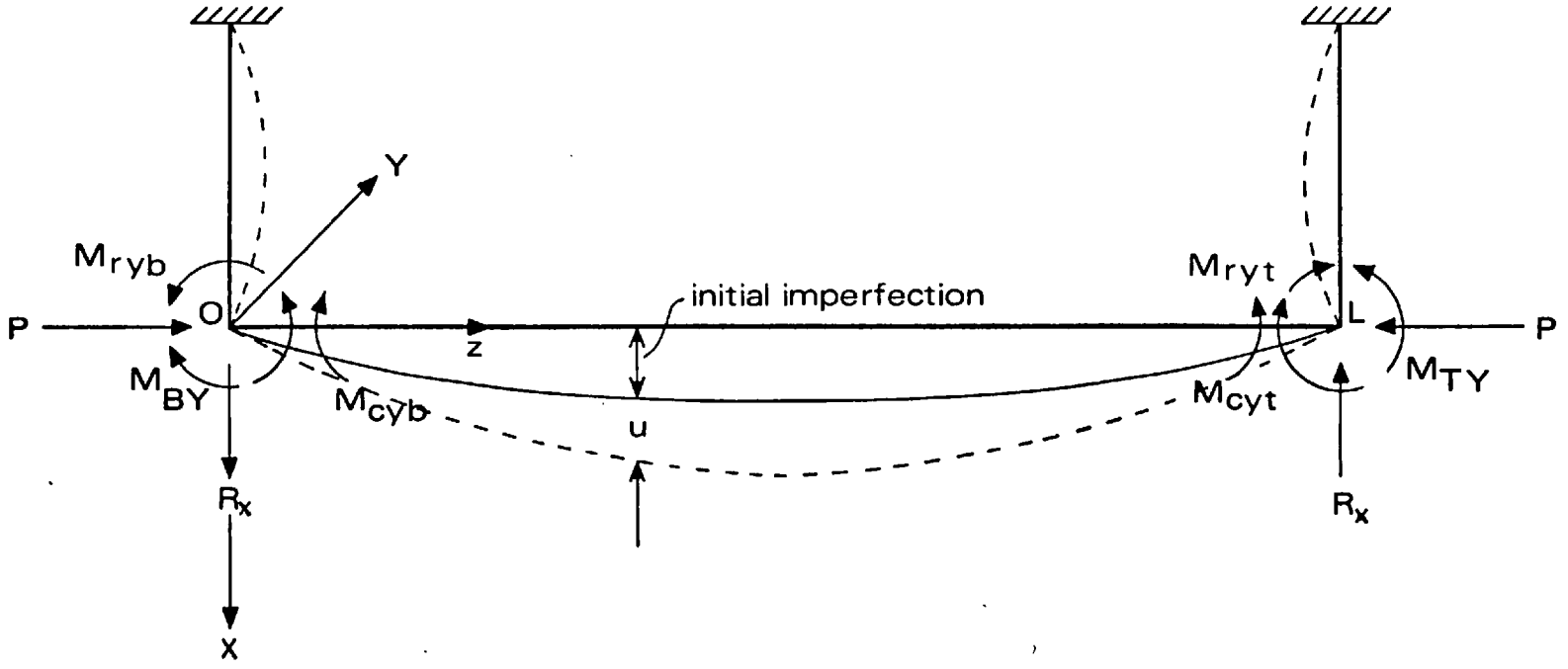


Fig. 4.9 FORCES IN A RESTRAINED COLUMN

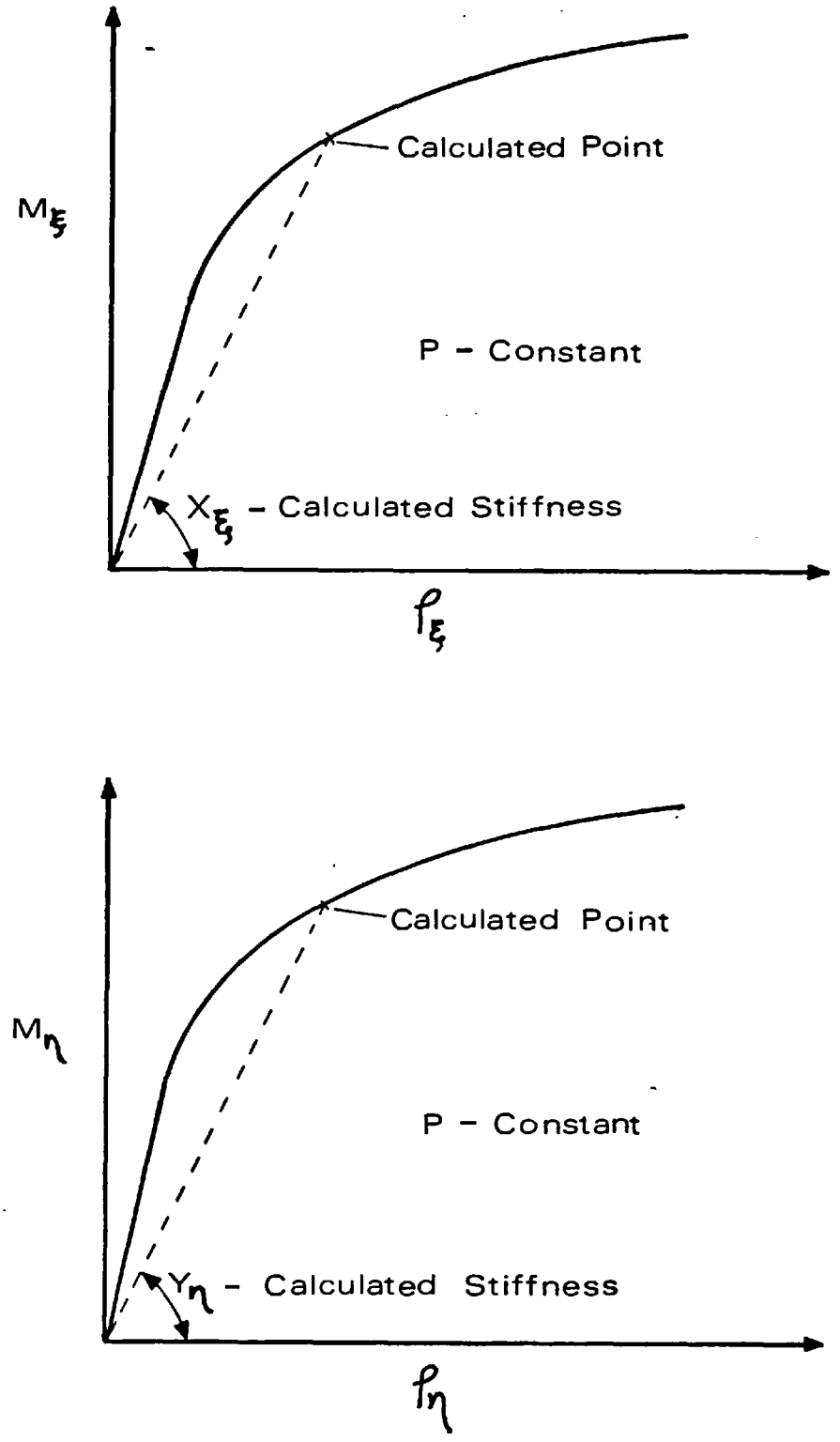


Fig. 5.1 Calculation of Stiffnesses

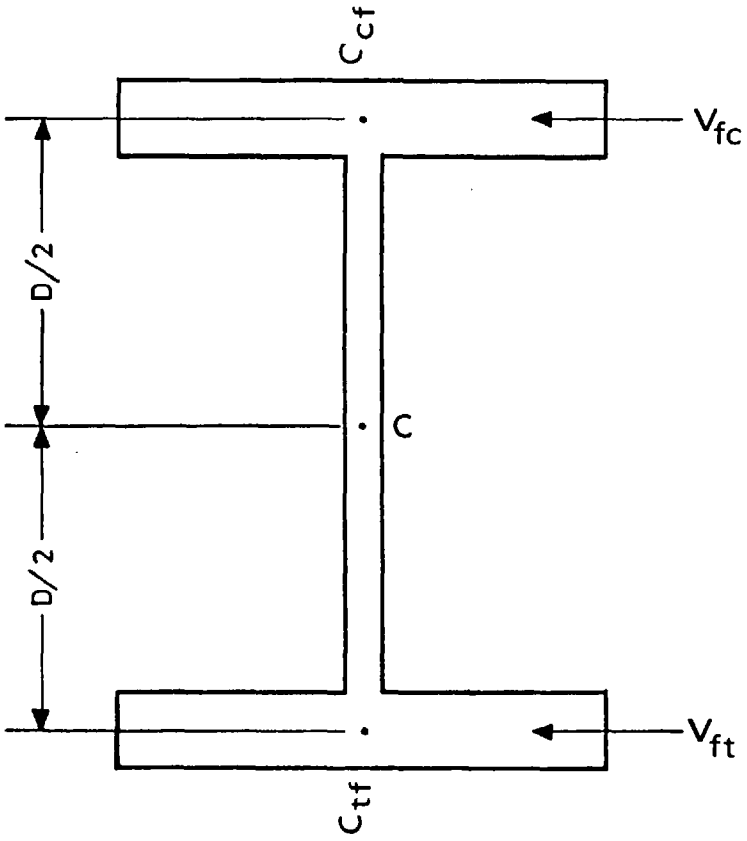


Fig. 5.2 Warping Torque Resistance Of Inelastic Sections

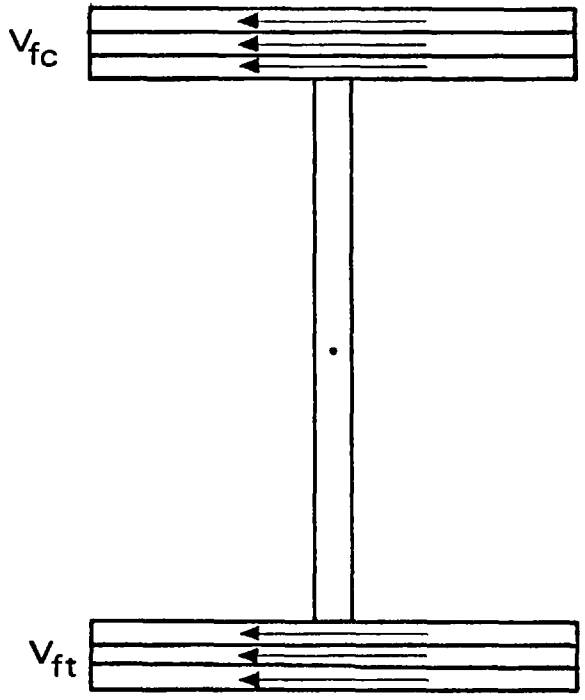


Fig. 5.3 Refinements In Computing Warping Torque Resistance

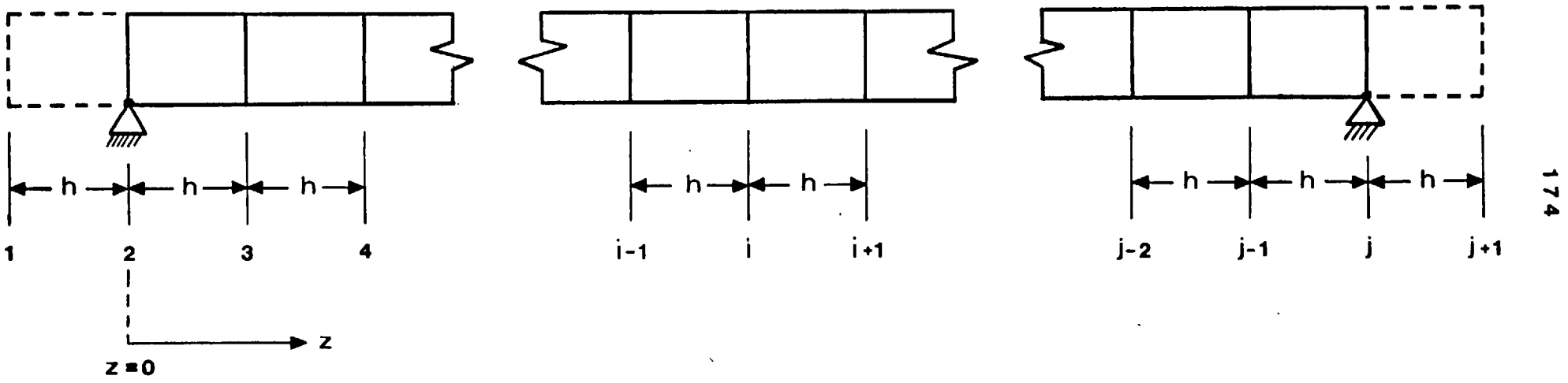


FIG. 5.4 NOTATION FOR FINITE DIFFERENCE EQUATIONS

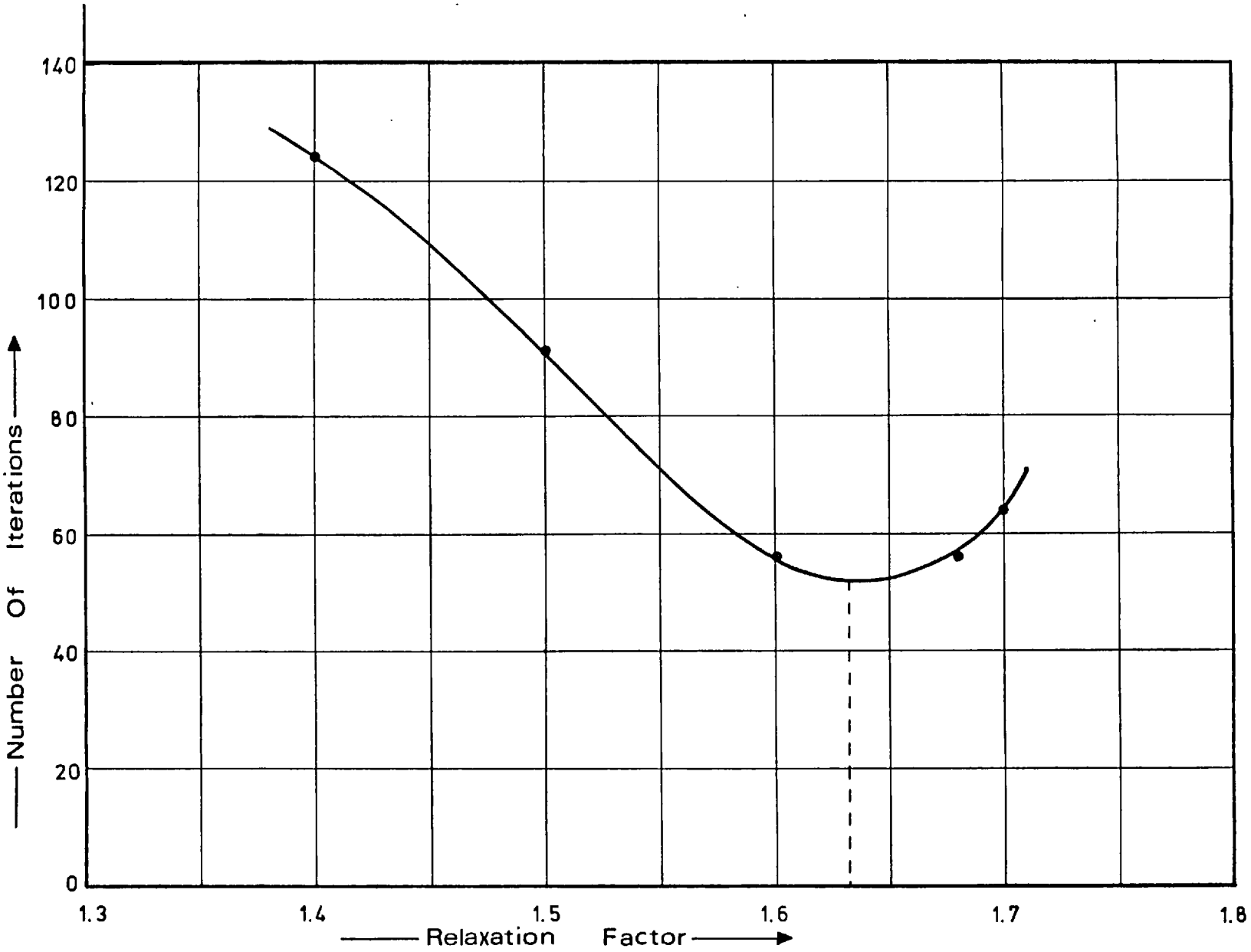


FIG. 5.5 VARIATION OF NUMBER OF ITERATIONS WITH RELAXATION FACTOR

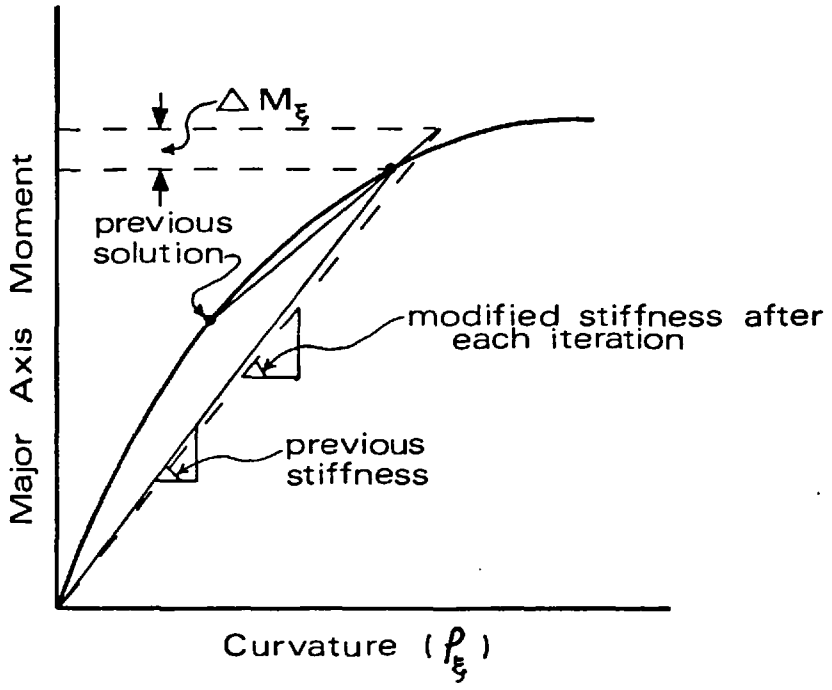


FIG. 5.6 MODIFICATION OF STIFFNESS

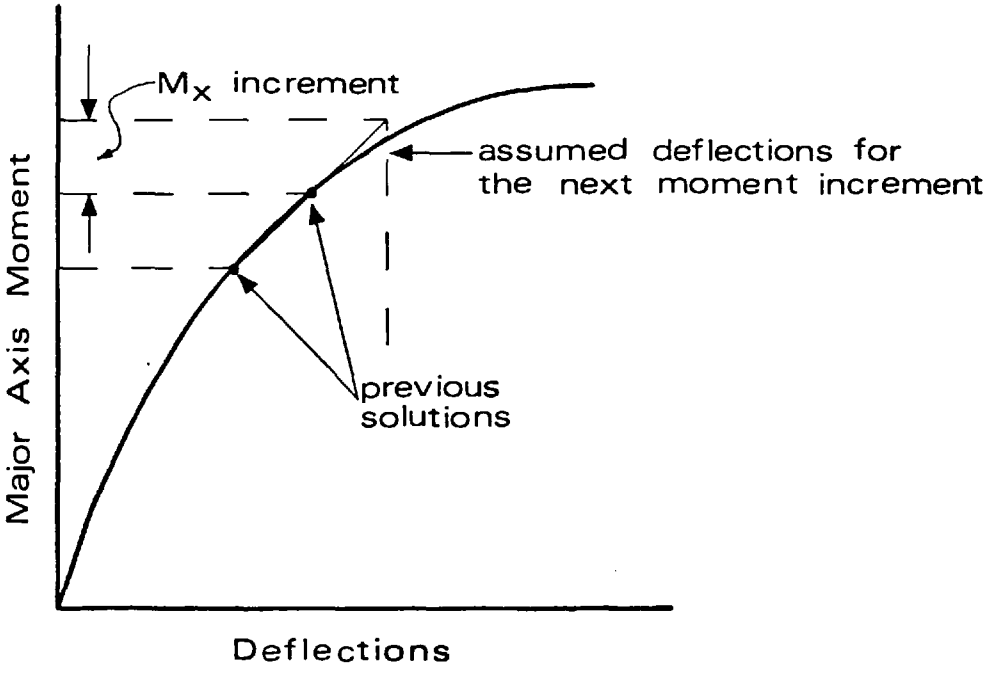


FIG. 5.7 TRIAL DEFLECTIONS FOR INCREMENT OF MOMENT

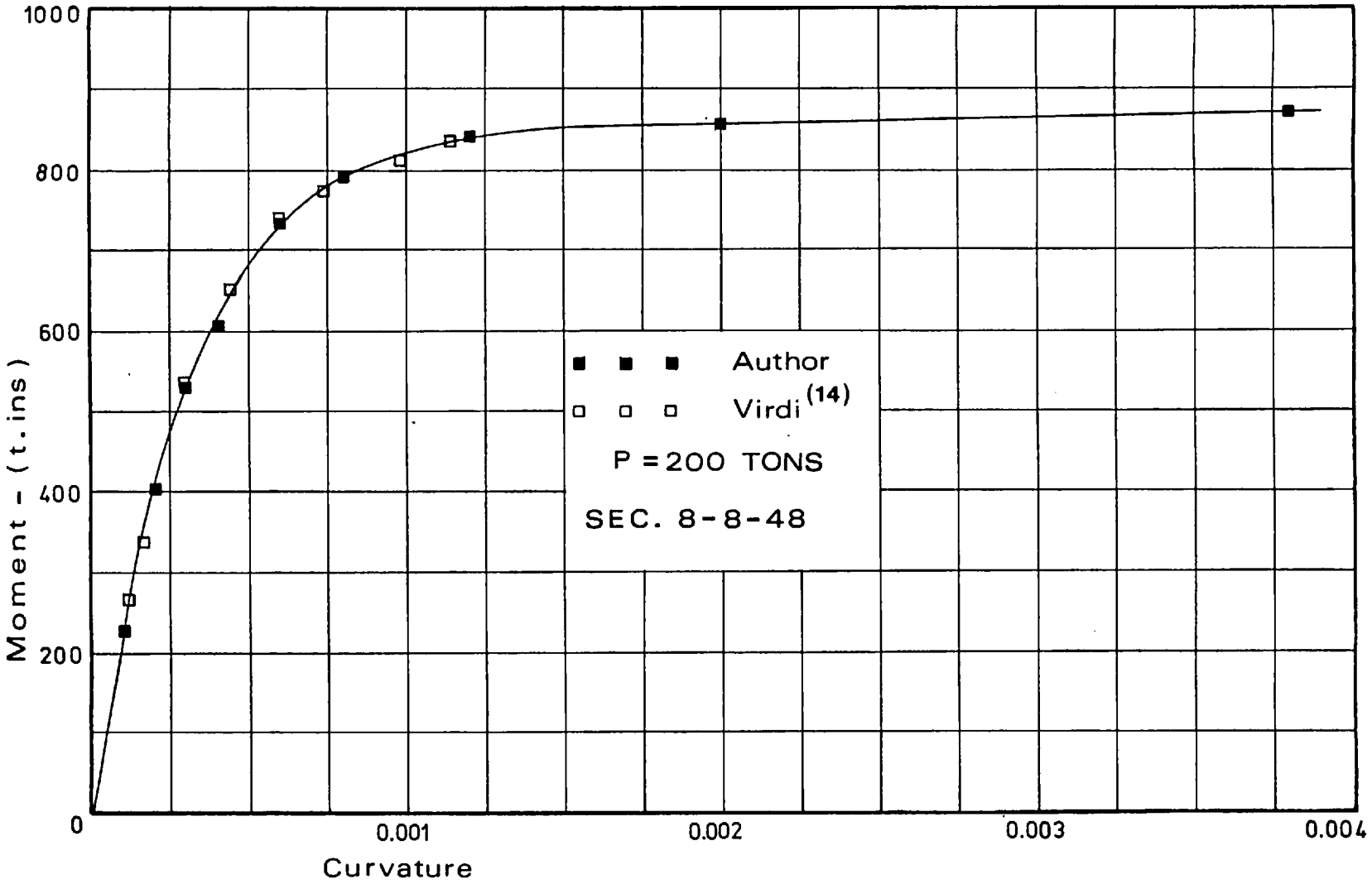
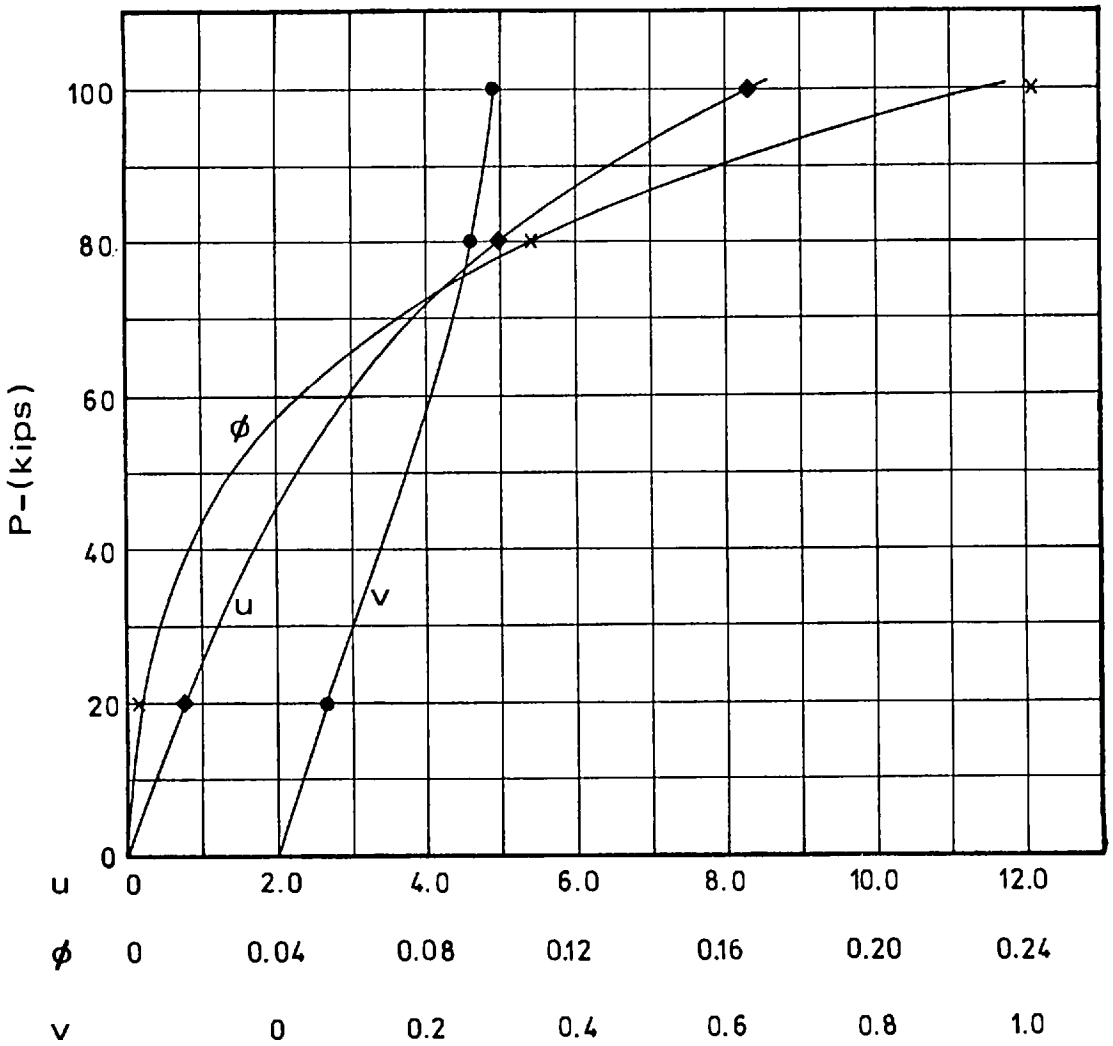


FIG. 6.1 MOMENT - THRUST - CURVATURE RESULTS CHECK



Author's Values Indicated By

x x x ϕ twist

◆ ◆ ◆ u minor axis

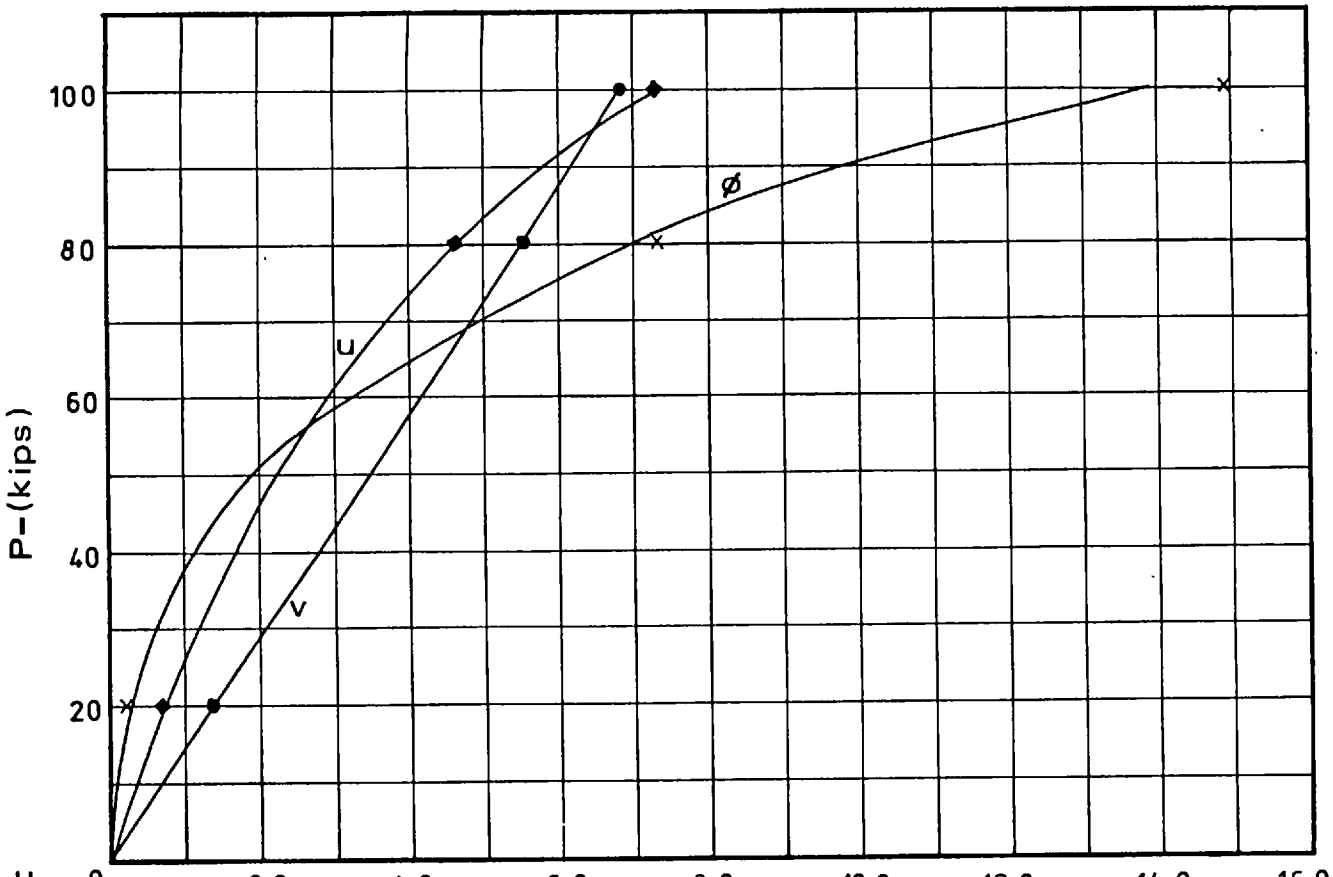
● ● ● v major axis

PROB. 2

Simply Supported

Warping Free

FIG. 6.2 COMPARISON WITH CULVER'S SOLUTION



u	0	2.0	4.0	6.0	8.0	10.0	12.0	14.0	16.0 ins.
ø	0	0.01	0.02	0.03	0.04	0.05	0.06	0.07	0.08 rad.
v	0	0.1	0.2	0.3	0.4	0.5	0.6	0.7	0.8 ins.

Author's Values Indicated By

x x x ø twist

◆ ◆ ◆ u minor axis

● ● ● v major axis

PROB. 4

Simply Supported

Warping Restrained

FIG. 6.3 COMPARISON WITH CULVER'S SOLUTION

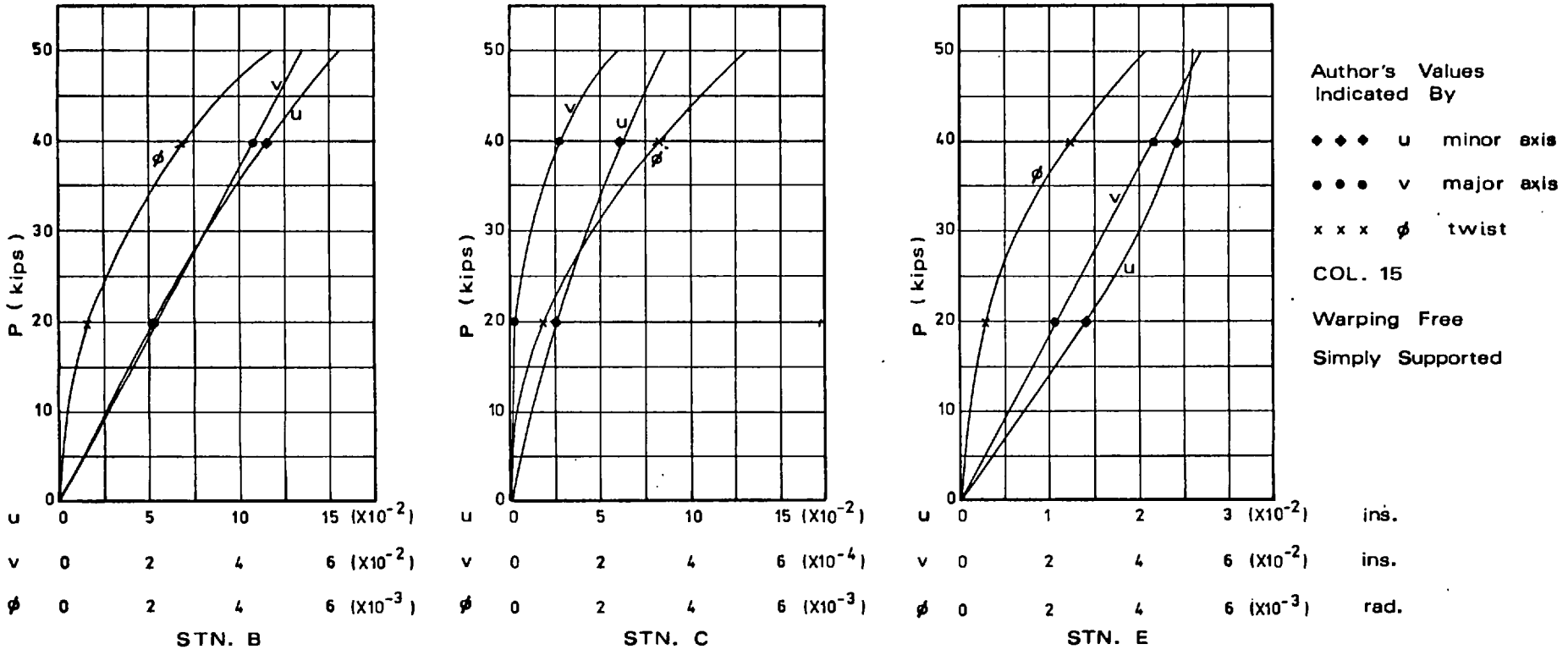


FIG. 6.4 COMPARISON WITH SYAL & SHARMA'S SOLUTION

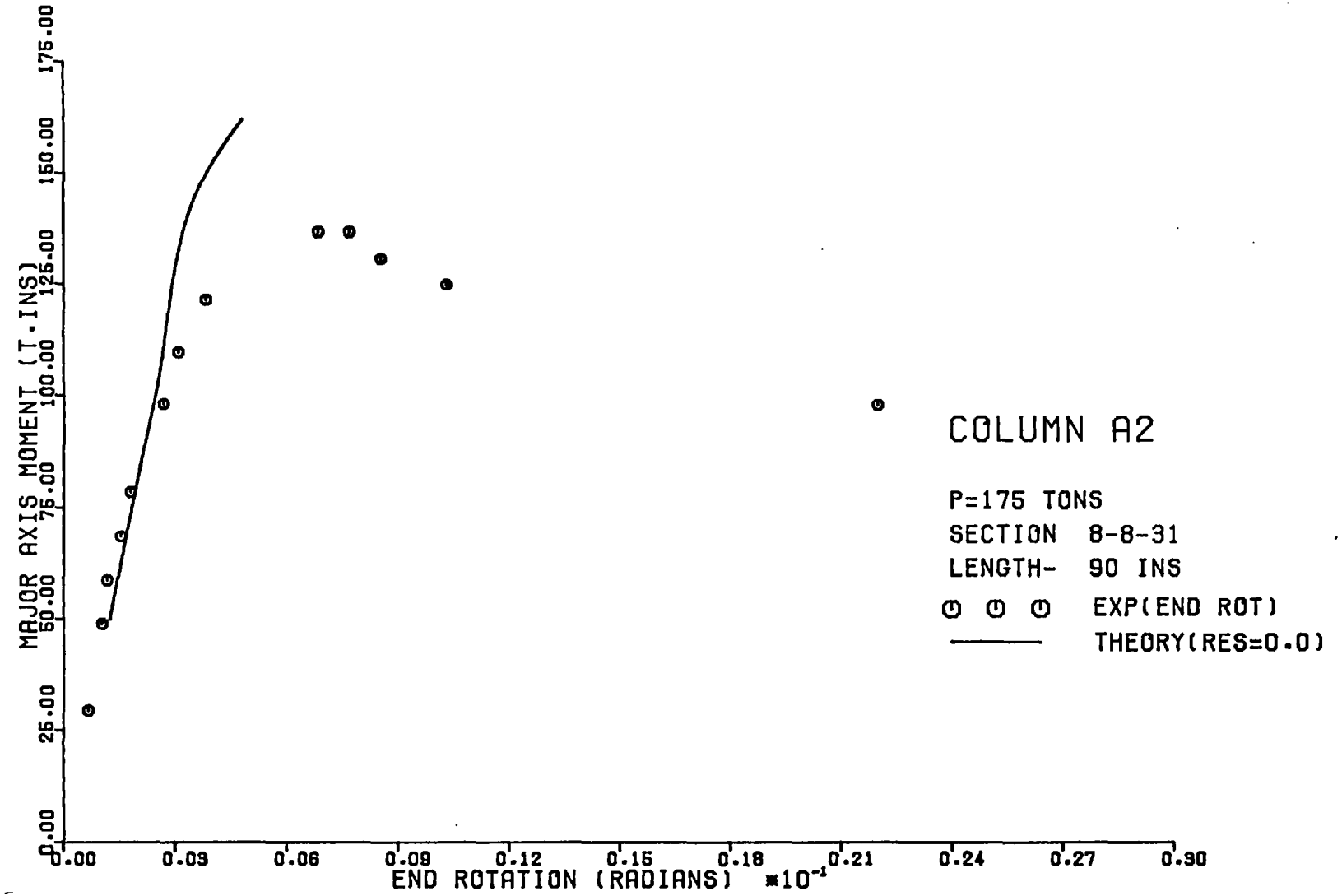


FIG. 6.5 THEORETICAL AND EXPERIMENTAL END ROTATION PLOT

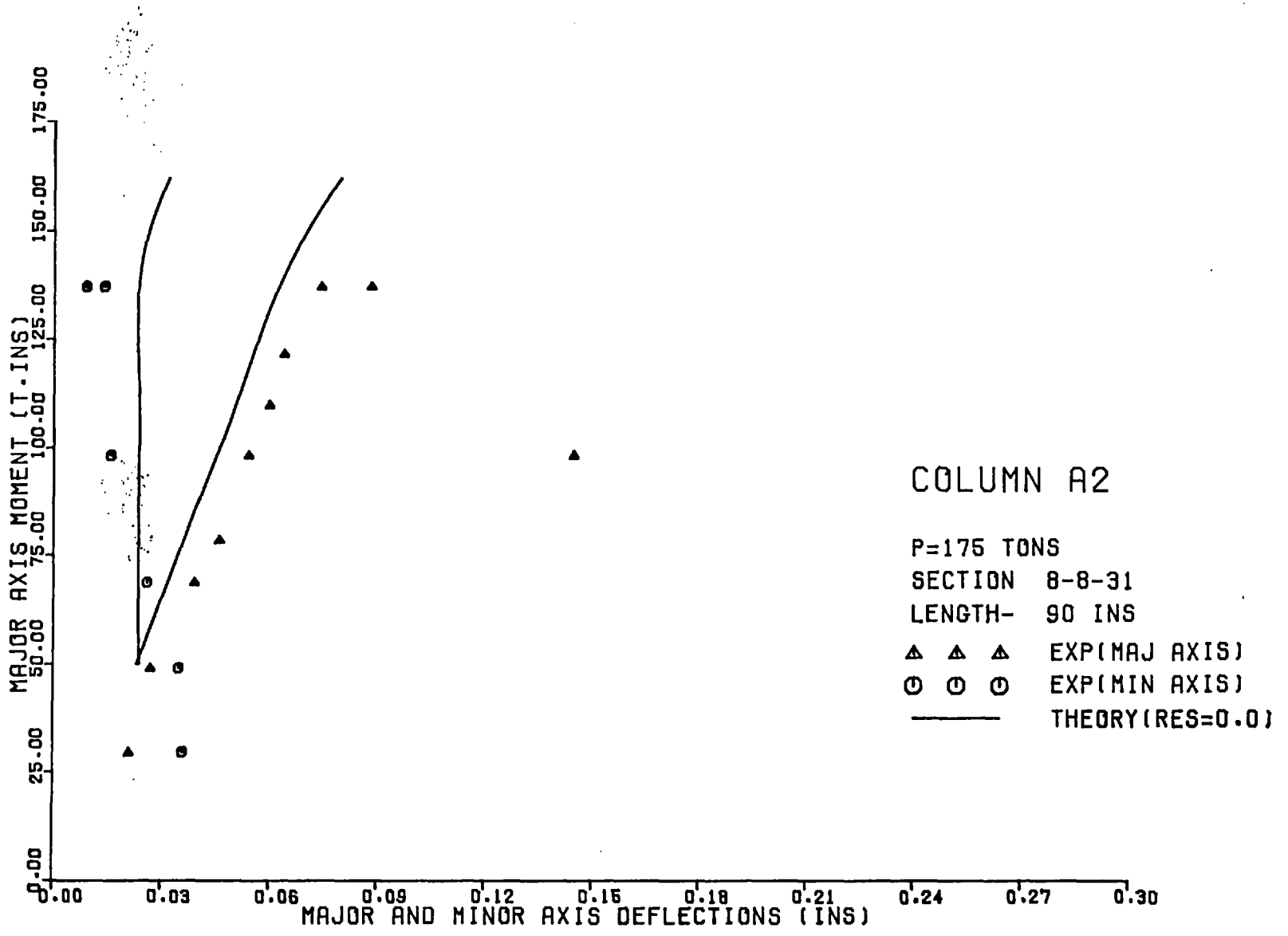


FIG. 6.6 THEORETICAL AND EXPERIMENTAL DEFLECTION PLOT (MID COL. HEIGHT)

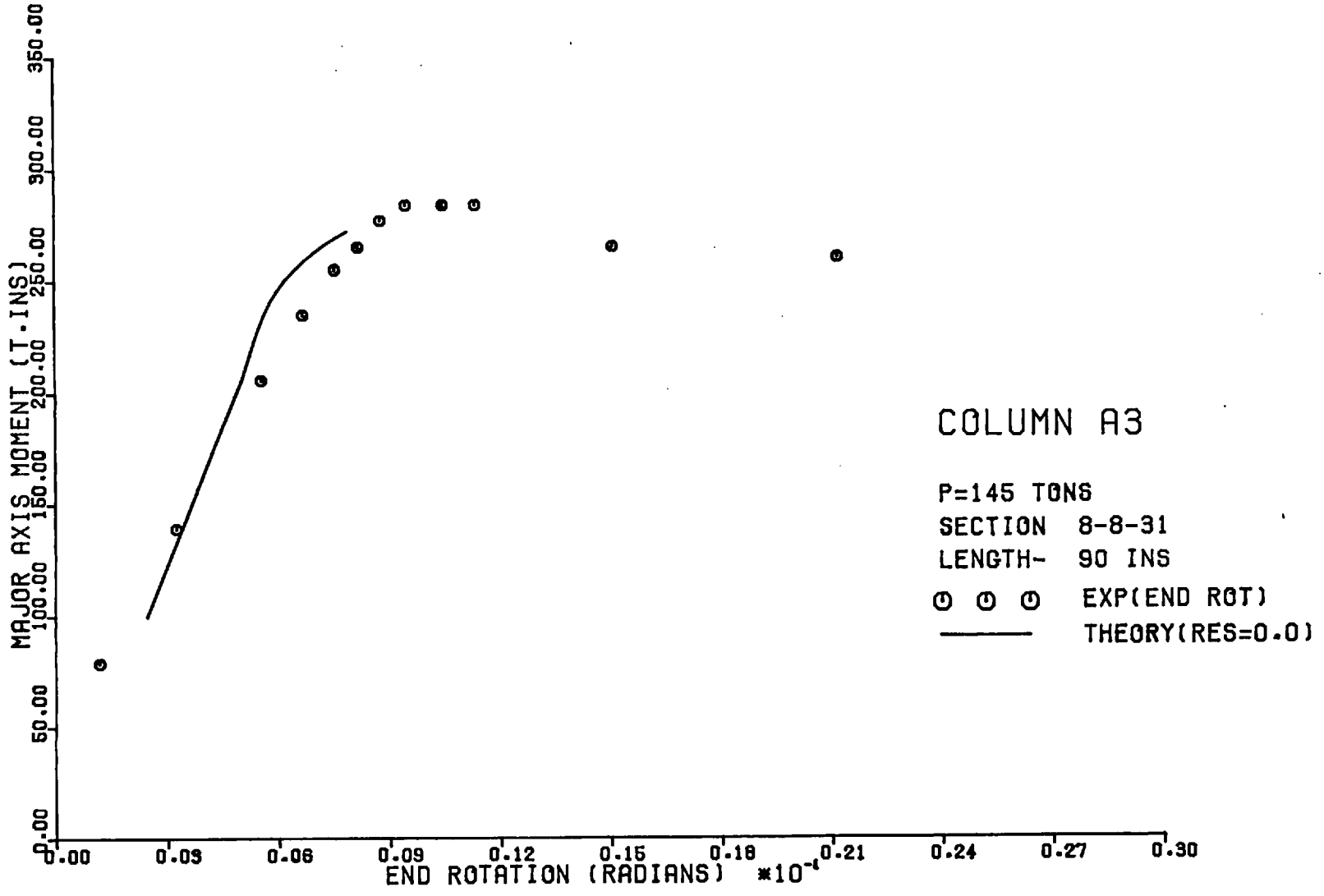


FIG. 6.7 THEORETICAL AND EXPERIMENTAL END ROTATION PLOT

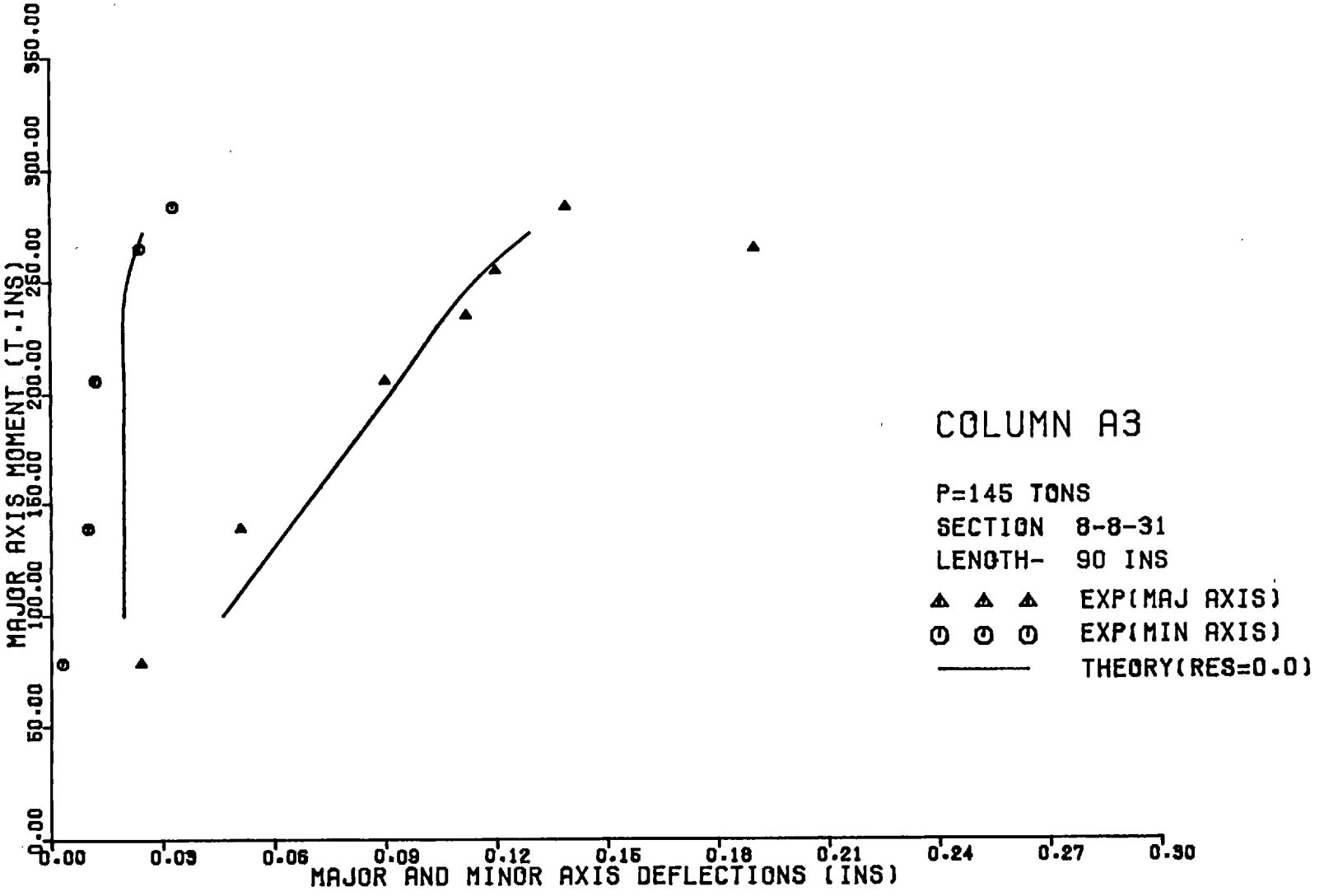


FIG. 6.8 THEORETICAL AND EXPERIMENTAL DEFLECTION PLOT (MID COL. HEIGHT)

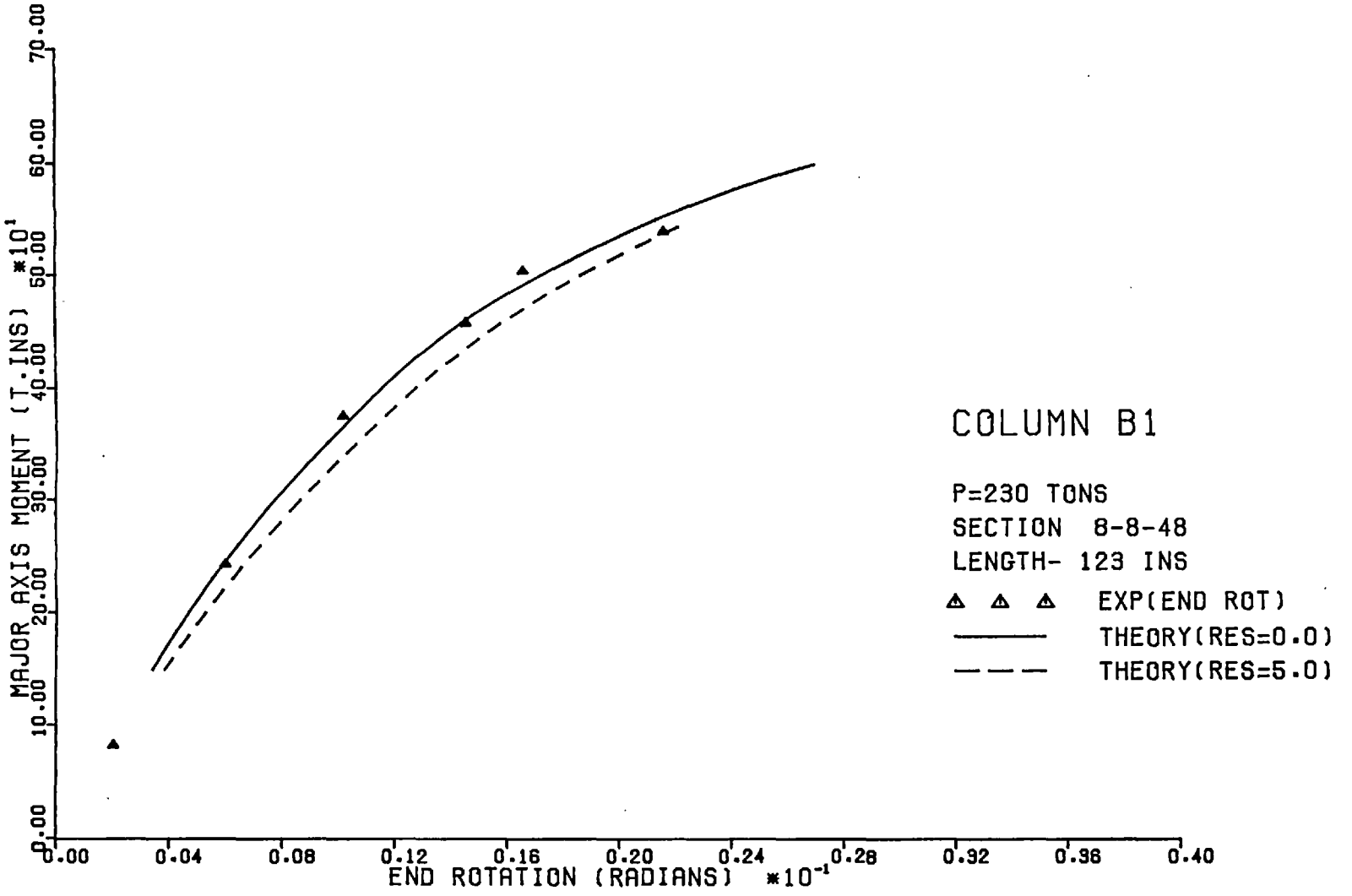


FIG. 6.9 THEORETICAL AND EXPERIMENTAL END ROTATION PLOT

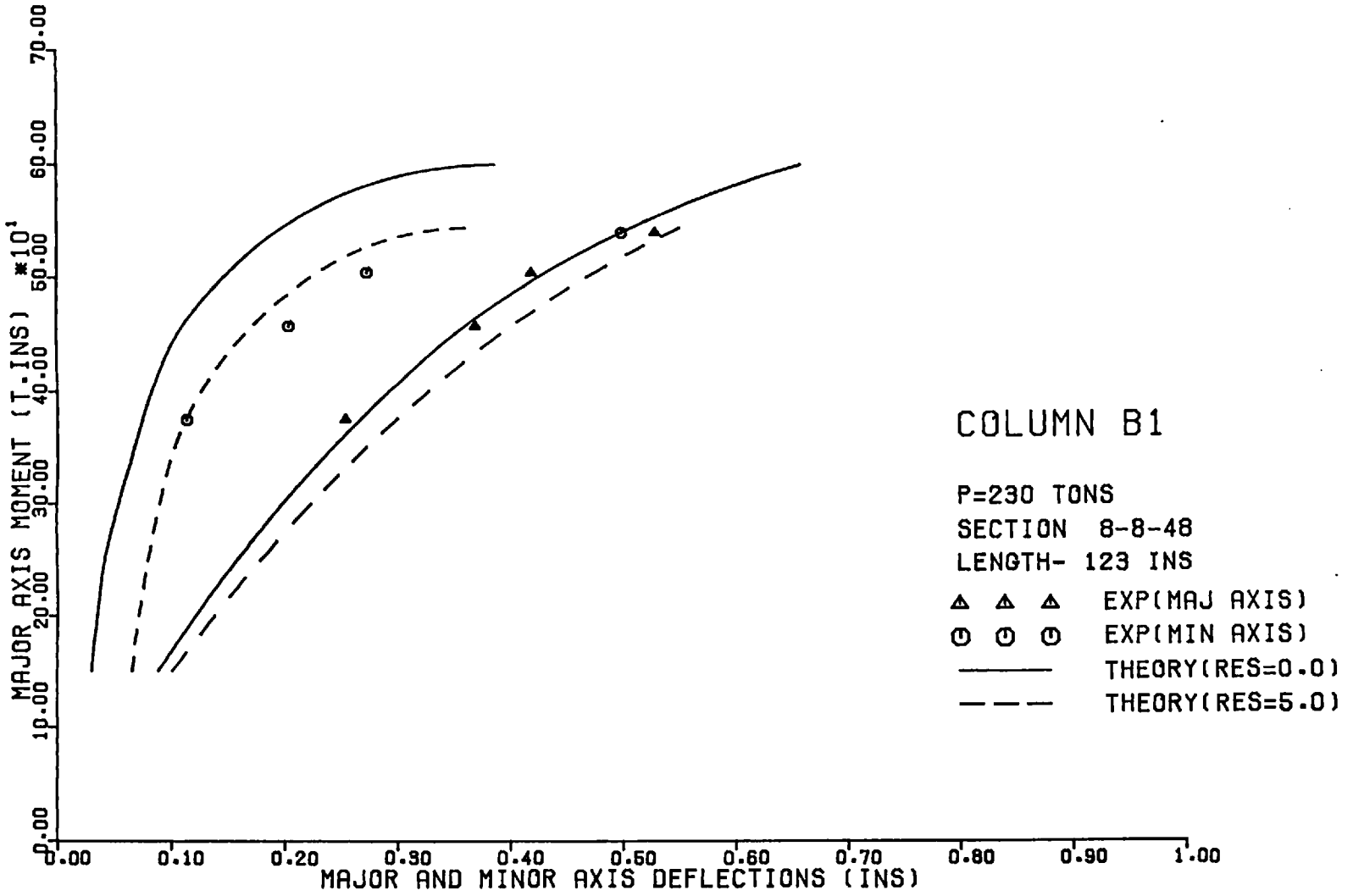


FIG. 6.10 THEORETICAL AND EXPERIMENTAL DEFLECTION PLOT (MID COL. HEIGHT)

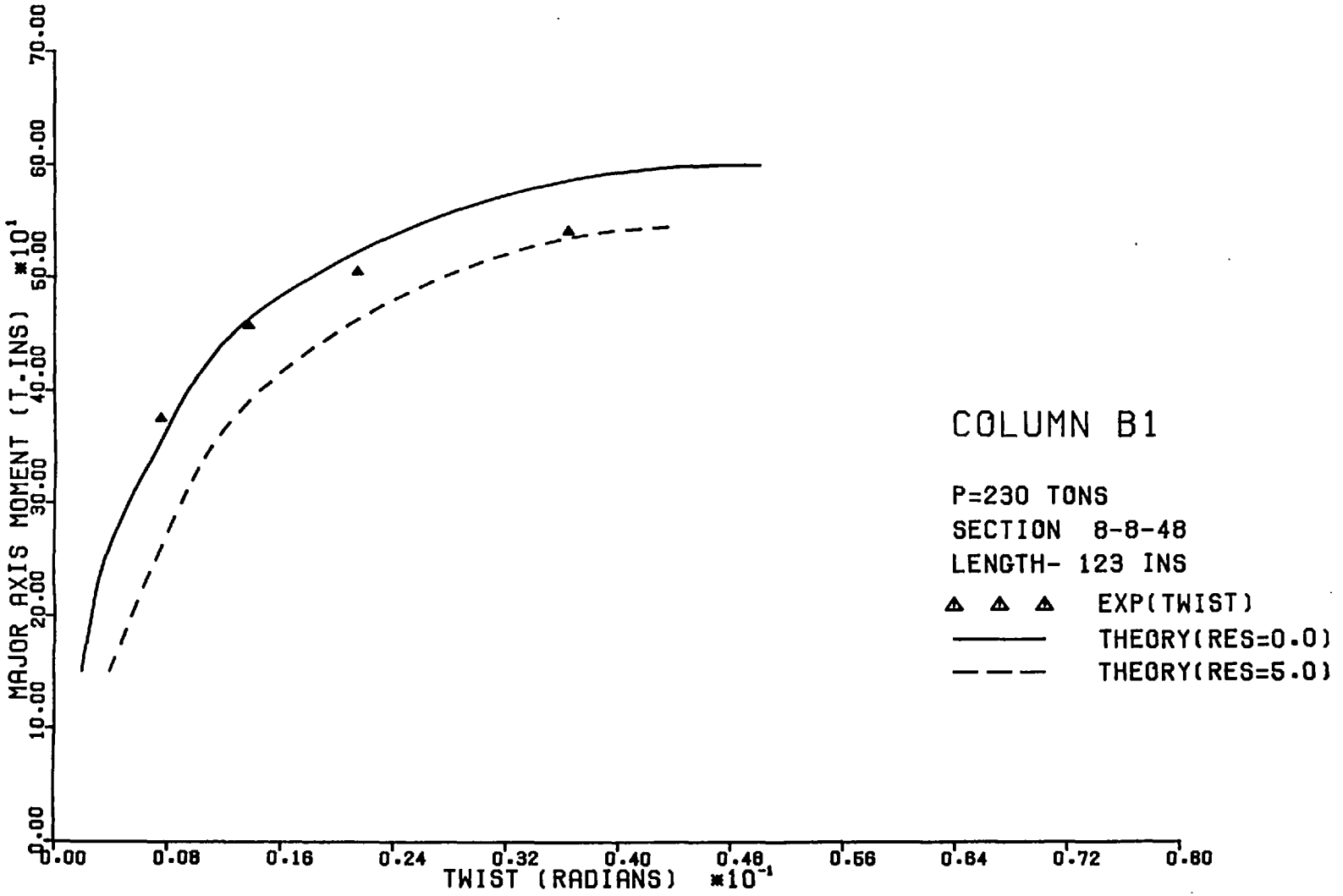


FIG. 6.11 THEORETICAL AND EXPERIMENTAL TWIST PLOT (MID COL. HEIGHT)

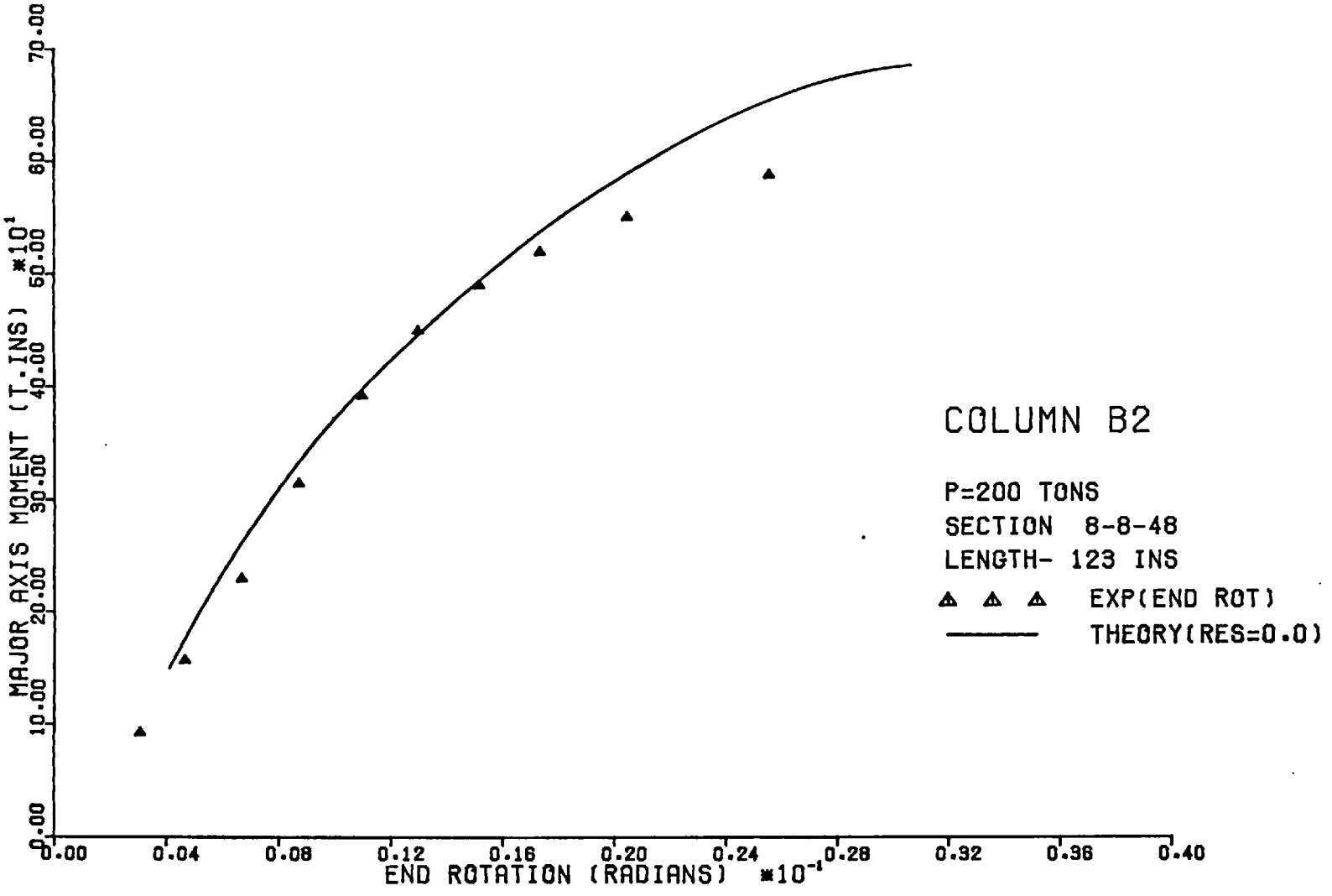


FIG. 6.12 THEORETICAL AND EXPERIMENTAL END ROTATION PLOT

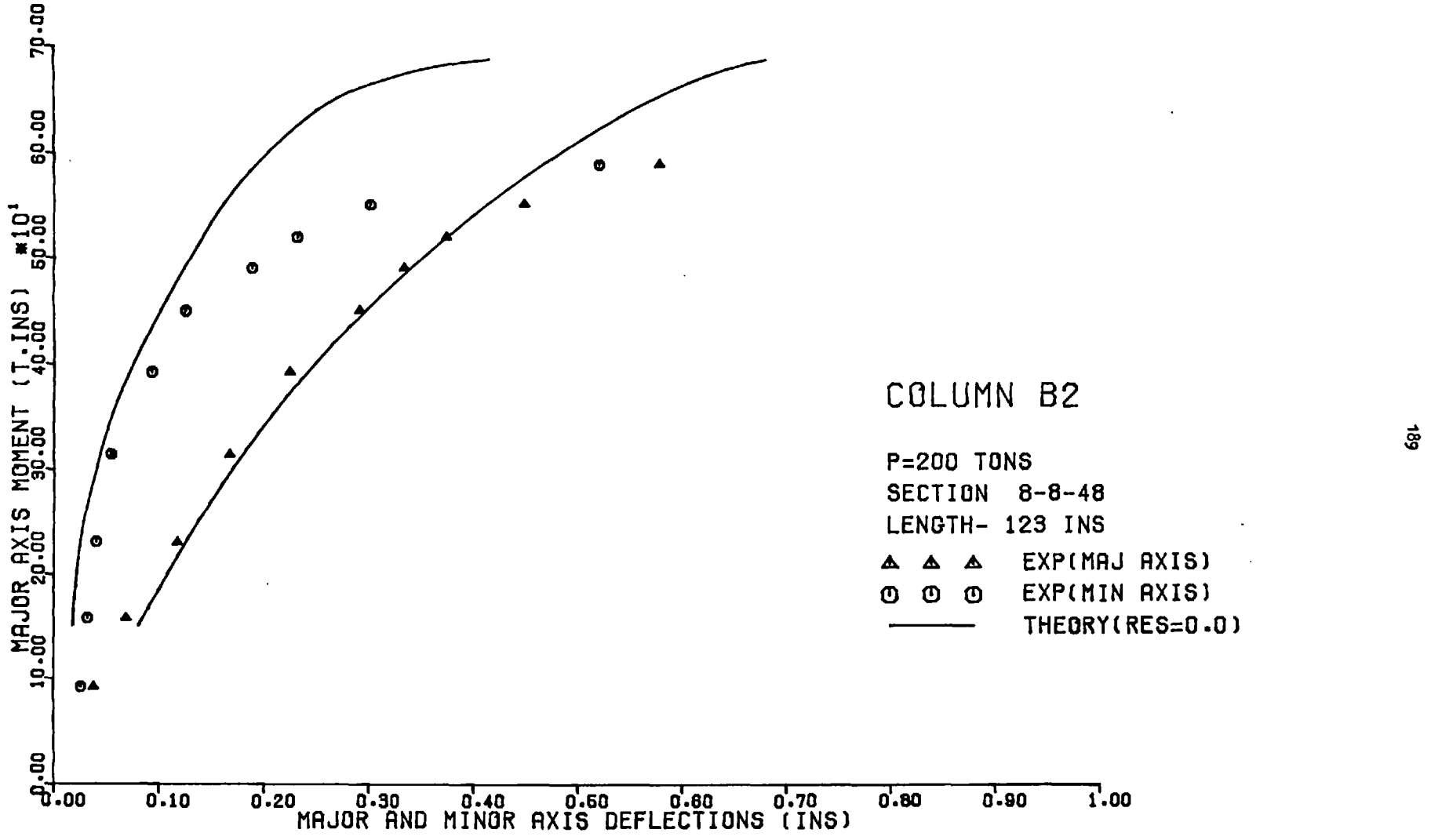


FIG. 6.13 THEORETICAL AND EXPERIMENTAL DEFLECTION PLOT (MID COL. HEIGHT)

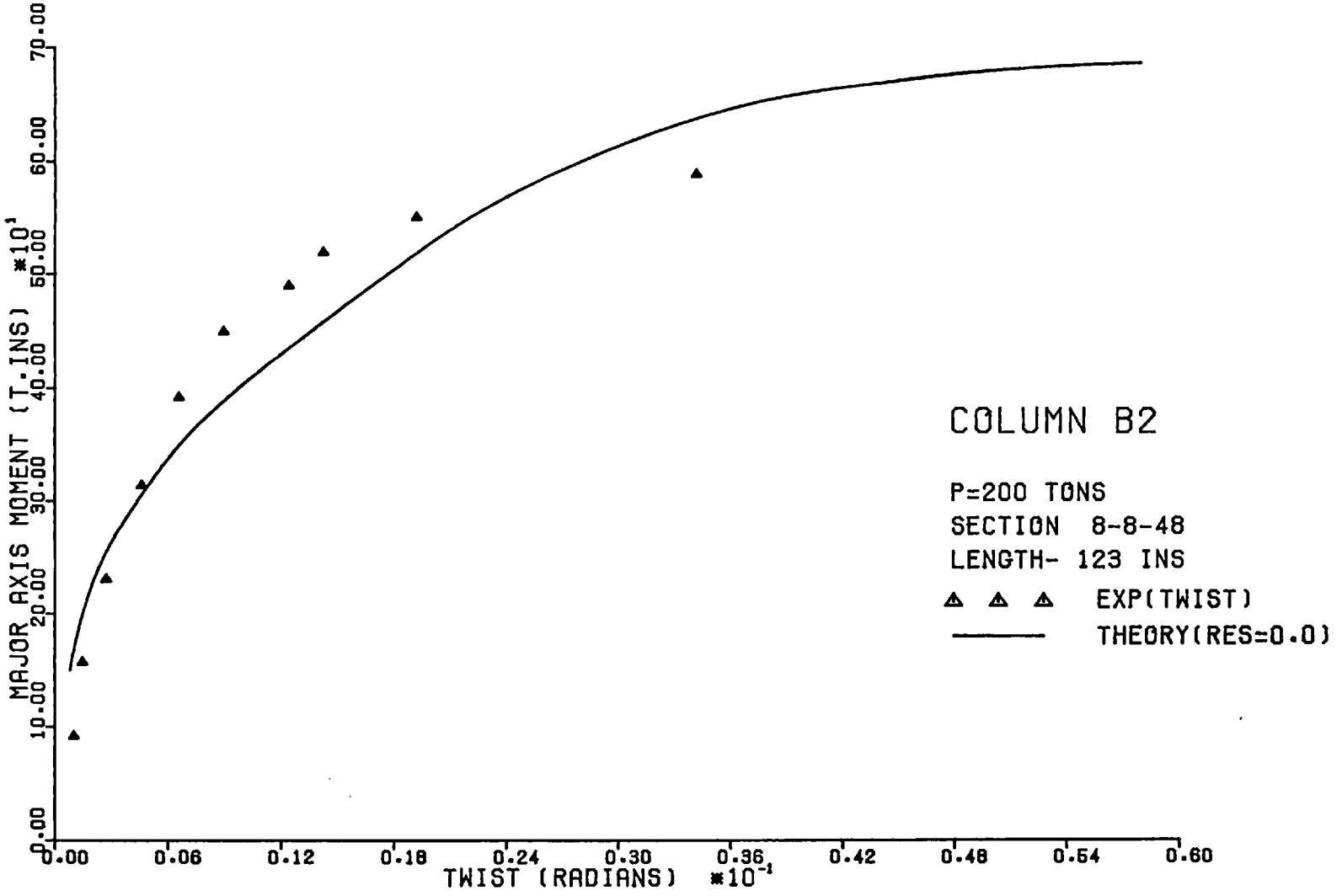


FIG. 6.14 THEORETICAL AND EXPERIMENTAL TWIST PLOT (MID COL. HEIGHT)

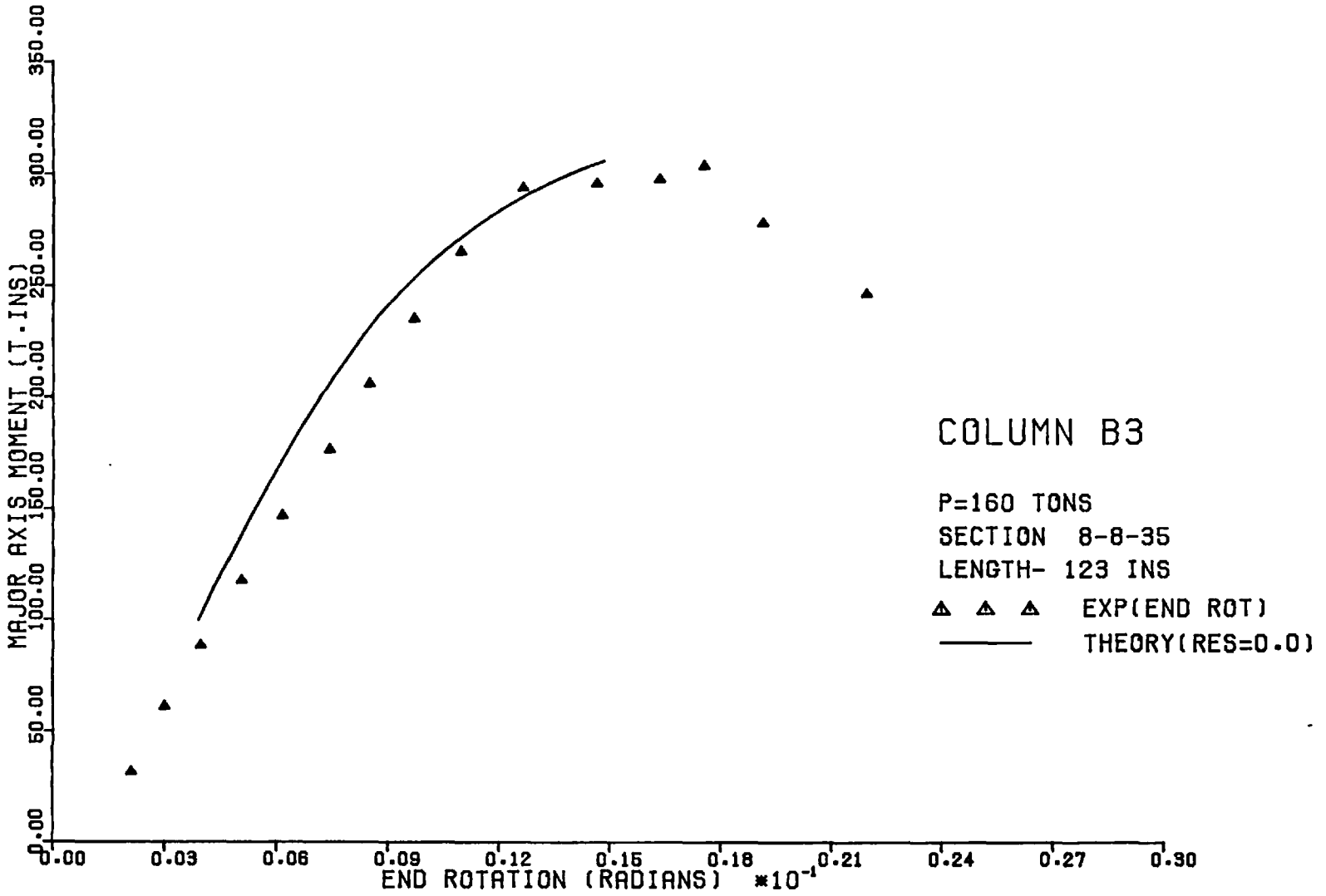


FIG. 6.15 THEORETICAL AND EXPERIMENTAL END ROTATION PLOT

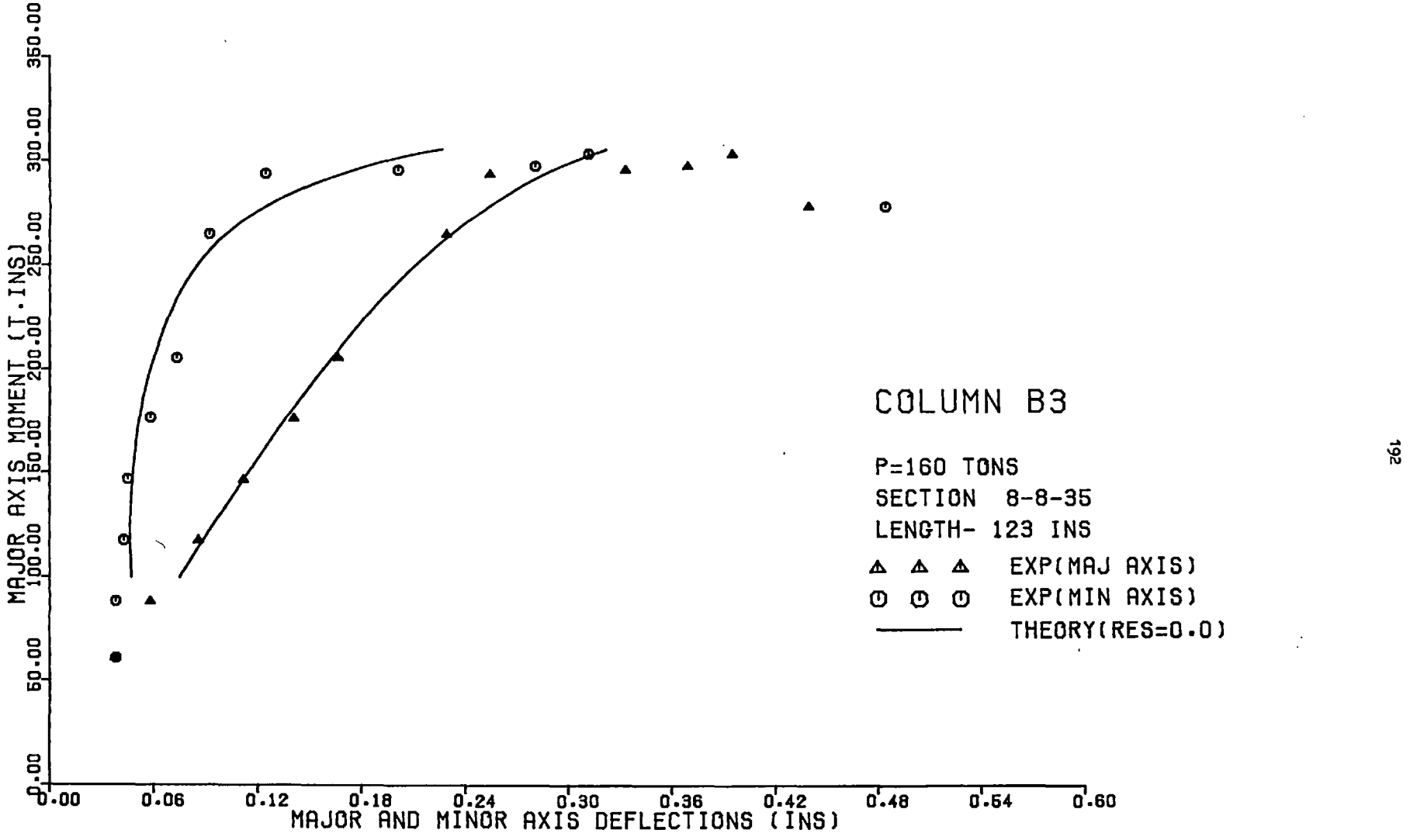


FIG. 6.16 THEORETICAL AND EXPERIMENTAL DEFLECTION PLOT (MID COL. HEIGHT)

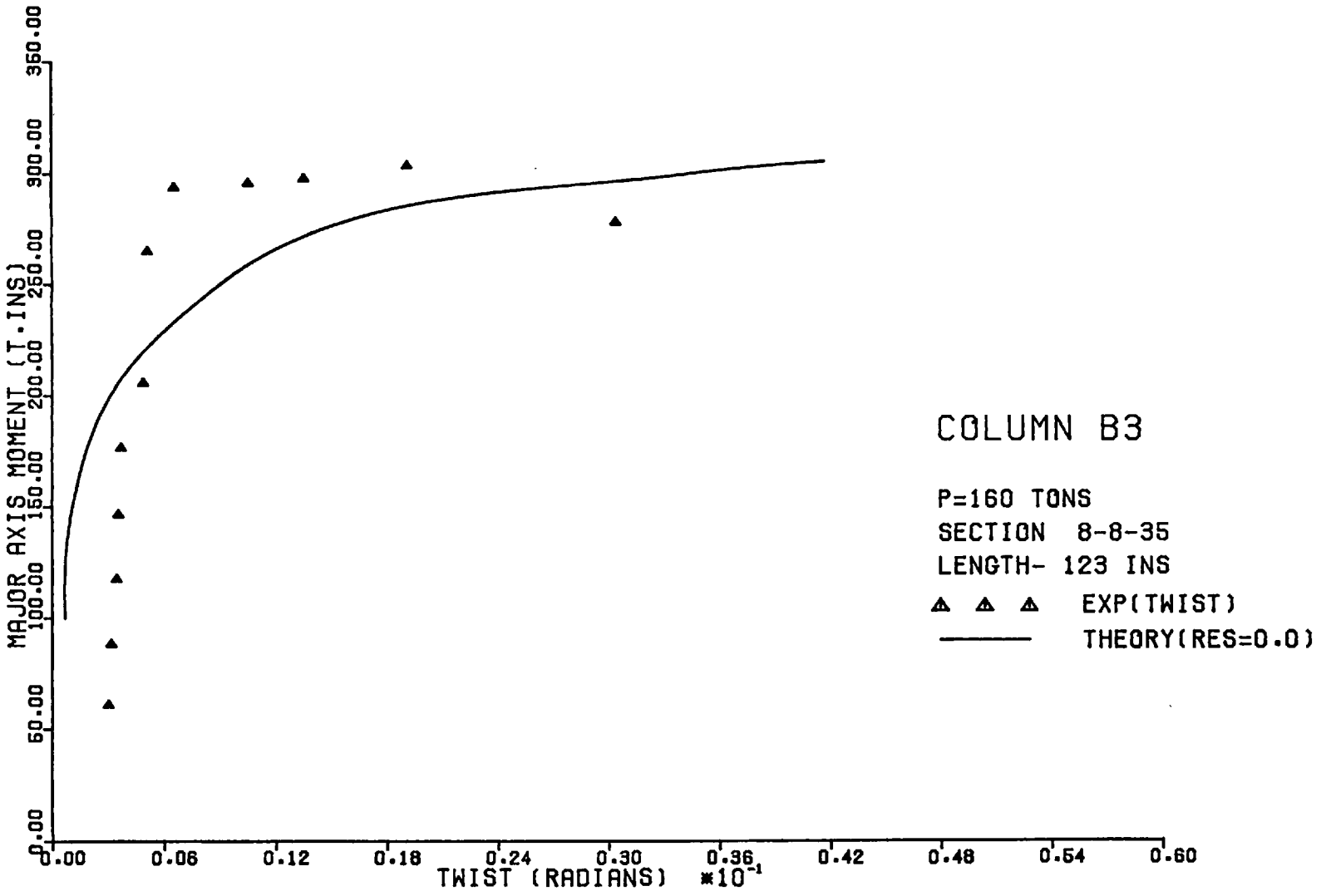


FIG. 6.17 THEORETICAL AND EXPERIMENTAL TWIST PLOT (MID COL. HEIGHT)

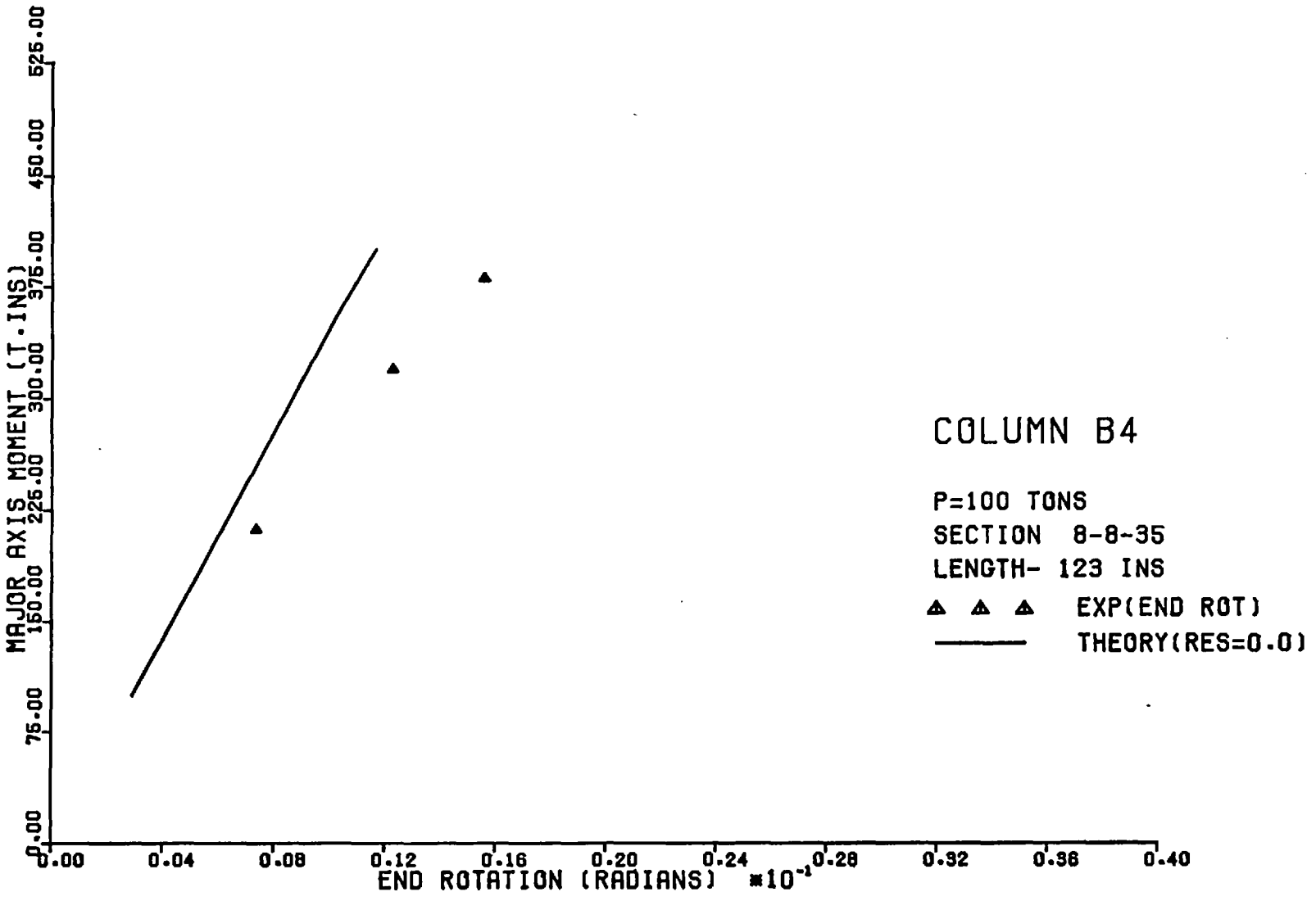


FIG. 6.18 THEORETICAL AND EXPERIMENTAL END ROTATION PLOT

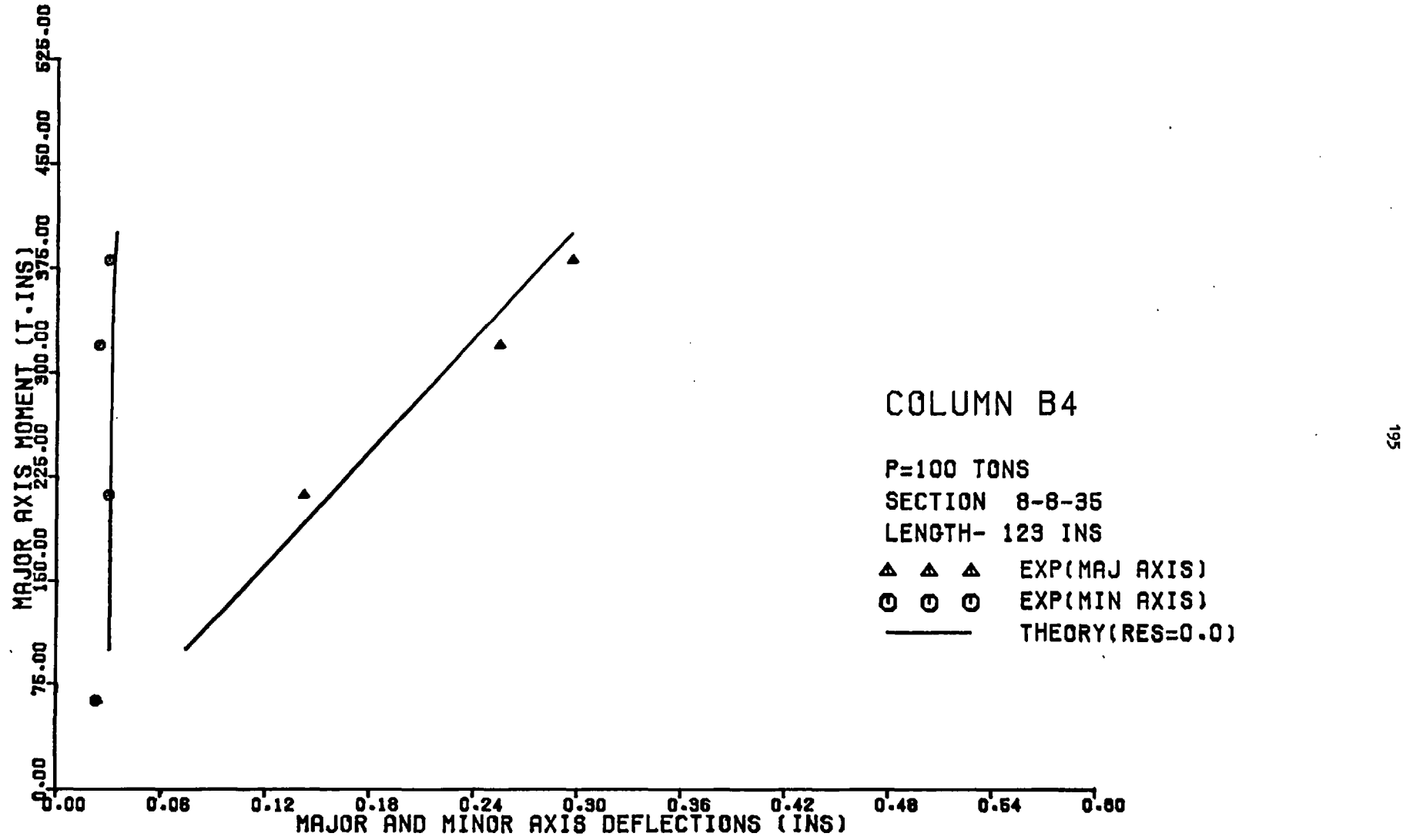


FIG. 6.19 THEORETICAL AND EXPERIMENTAL DEFLECTION PLOT (MID COL. HEIGHT)

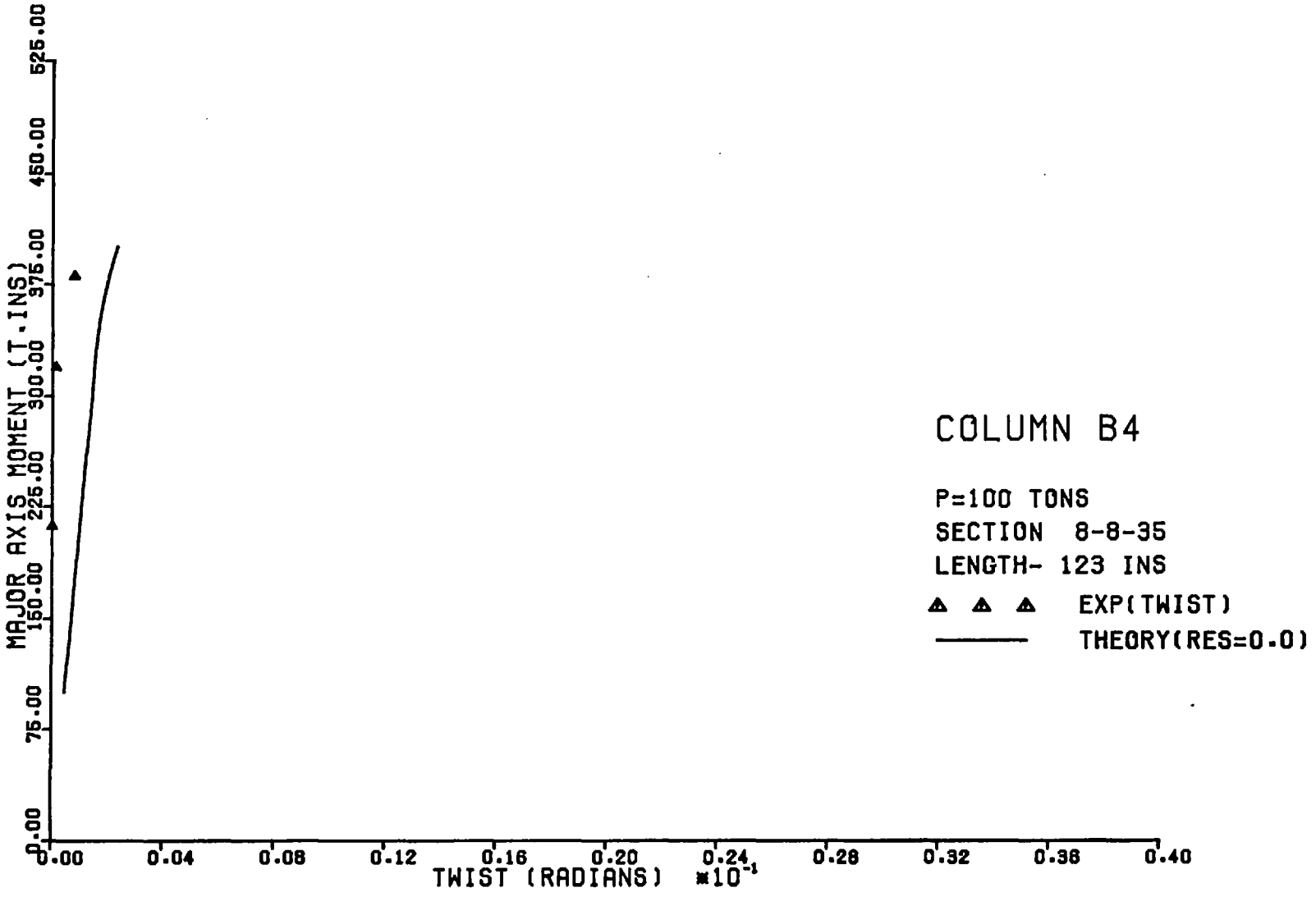


FIG. 6.20 THEORETICAL AND EXPERIMENTAL TWIST PLOT (MID COL. HEIGHT.

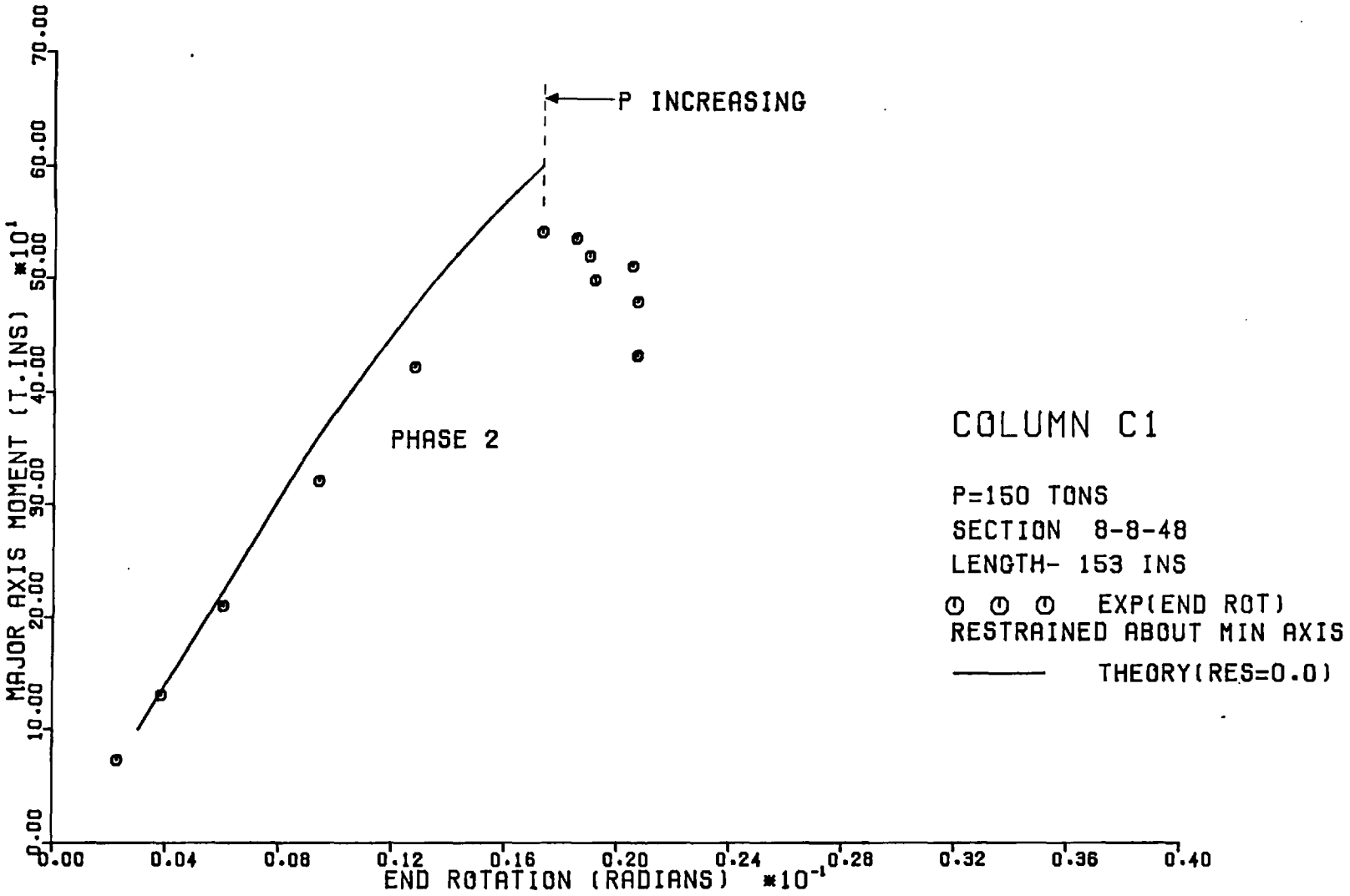


FIG. 6.21 THEORETICAL AND EXPERIMENTAL END ROTATION PLOT

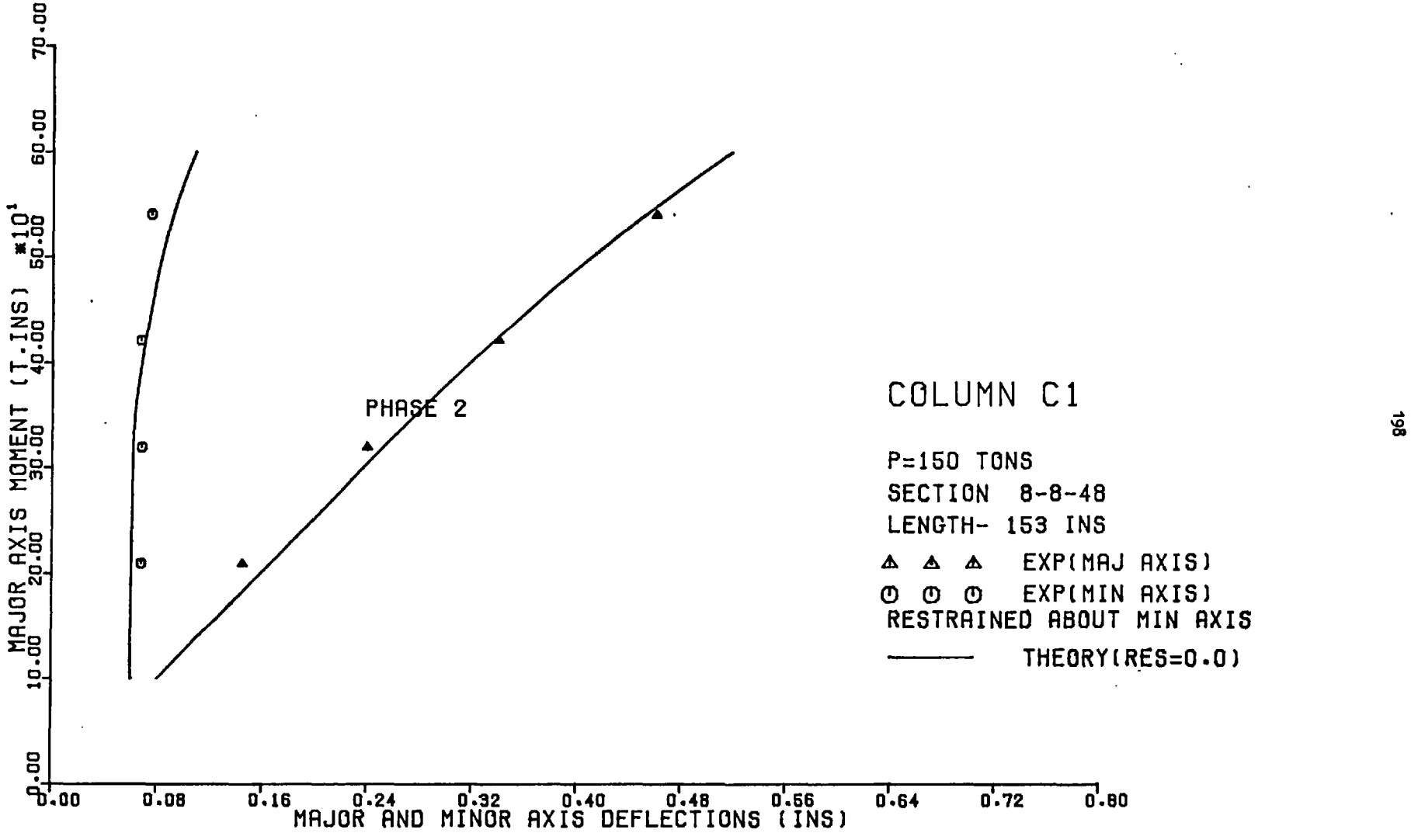


FIG. 6.22 THEORETICAL AND EXPERIMENTAL DEFLECTION PLOT (MID COL. HEIGHT)

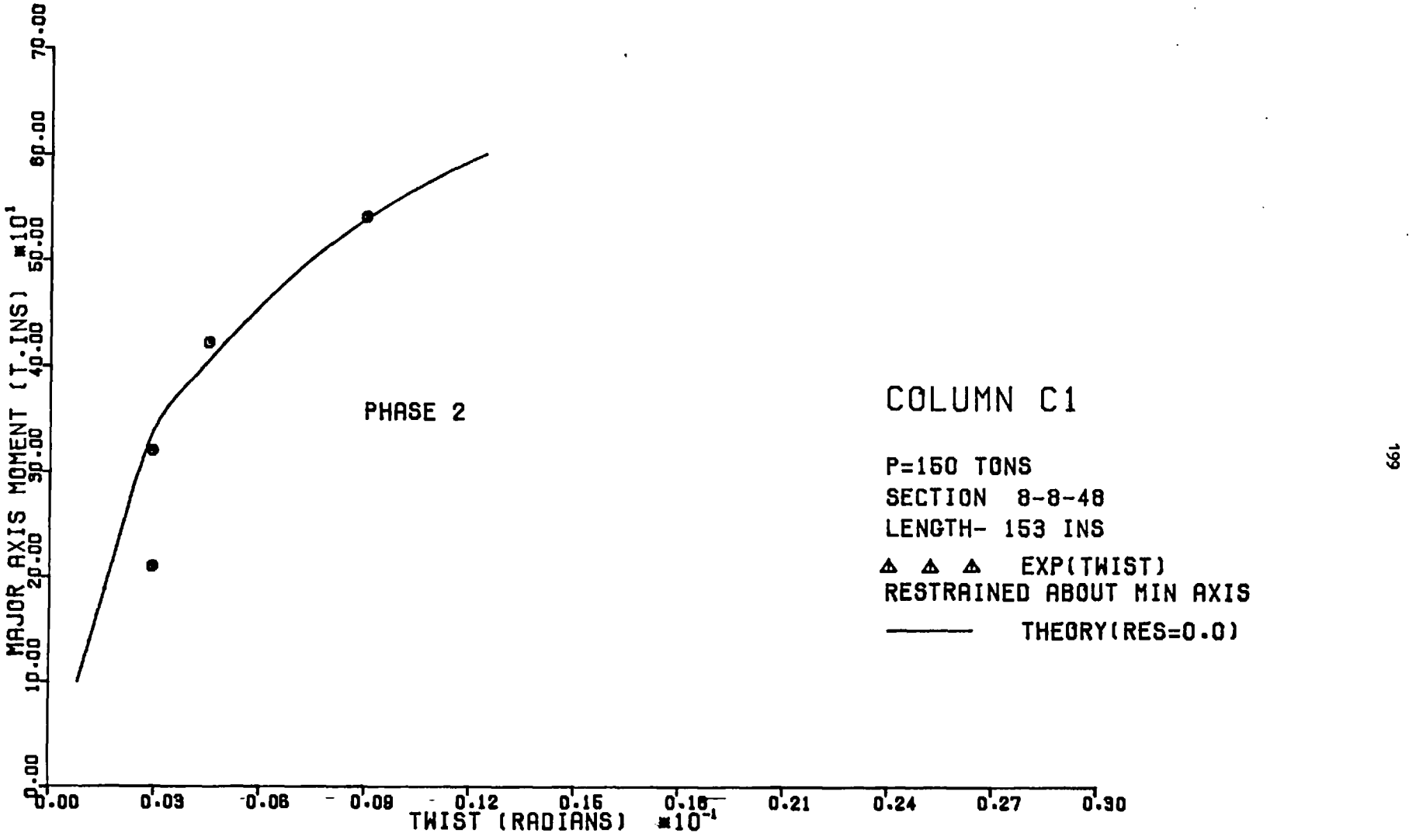


FIG. 6.23 THEORETICAL AND EXPERIMENTAL TWIST PLOT (MID COL. HEIGHT)

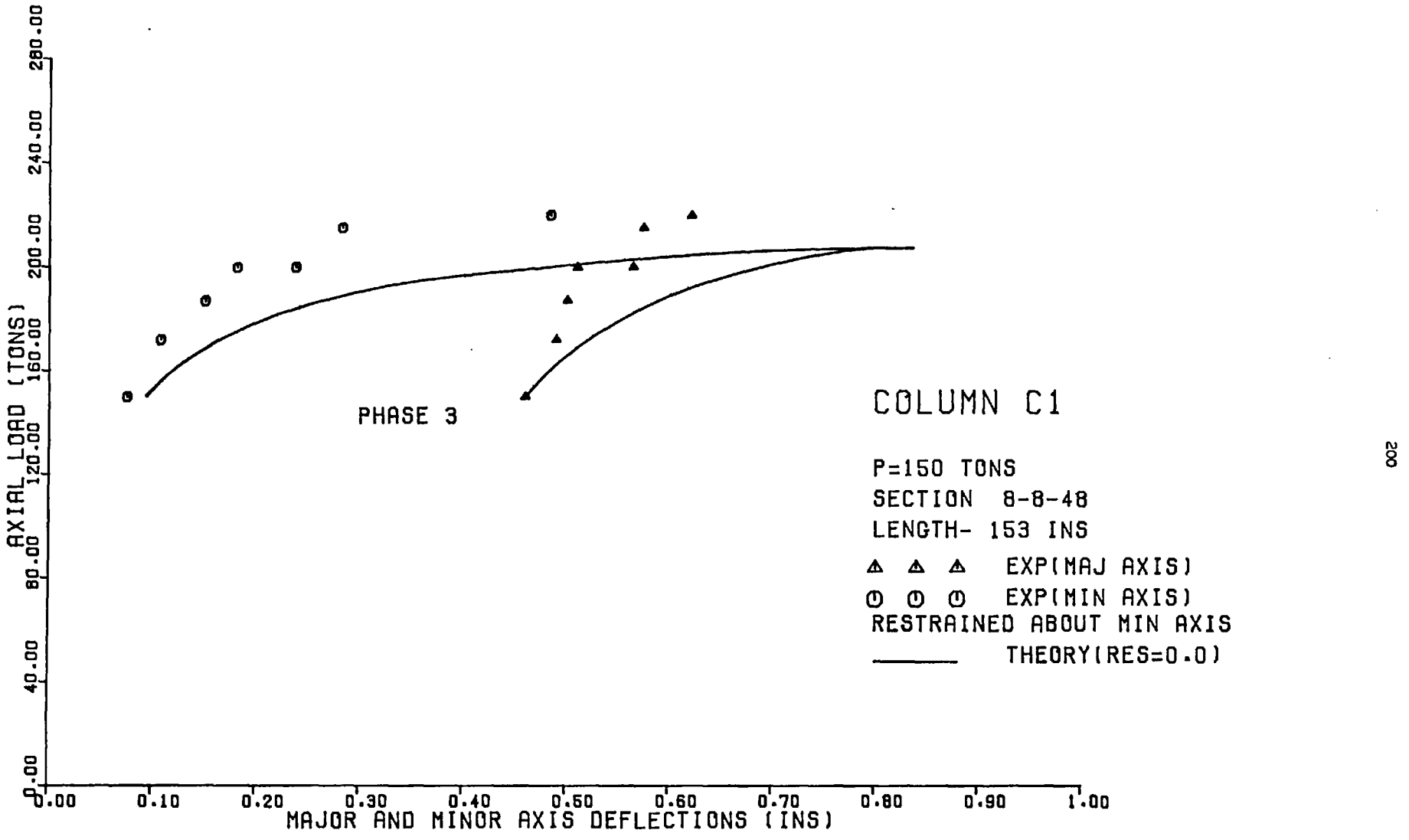


FIG. 6.24 THEORETICAL AND EXPERIMENTAL DEFLECTION PLOT (MID COL. HEIGHT)

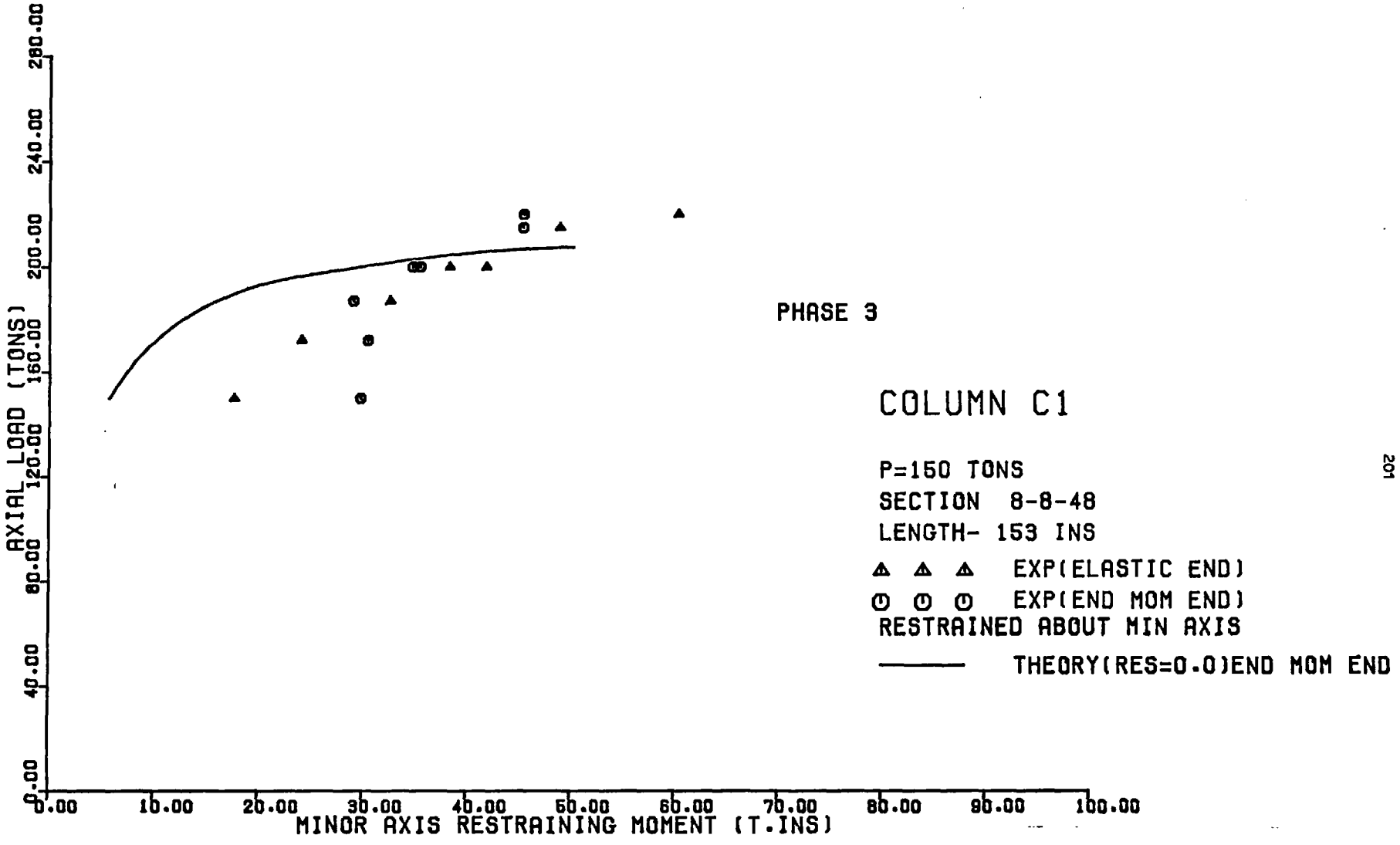


FIG. 6.25 THEORETICAL AND EXPERIMENTAL RESTRAINING MOMENT PLOT

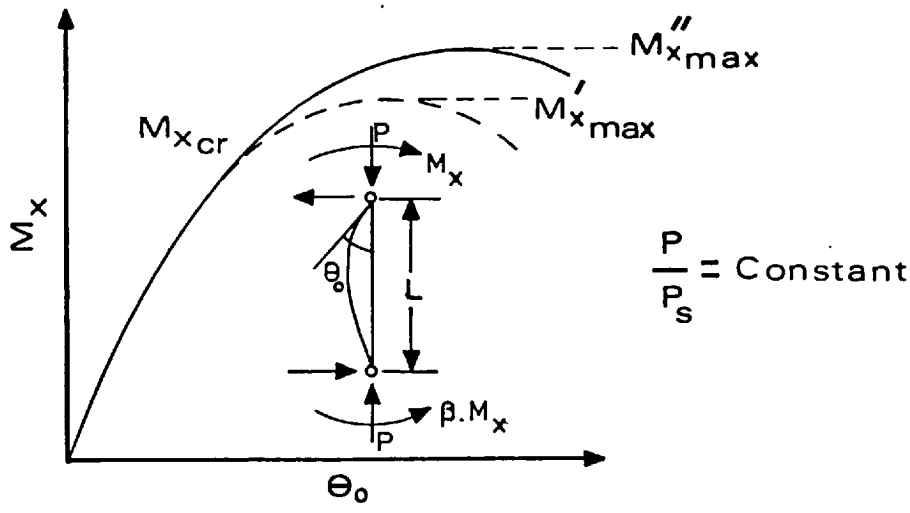


FIG. 7.1a TYPICAL MOMENT END ROTATION CURVE

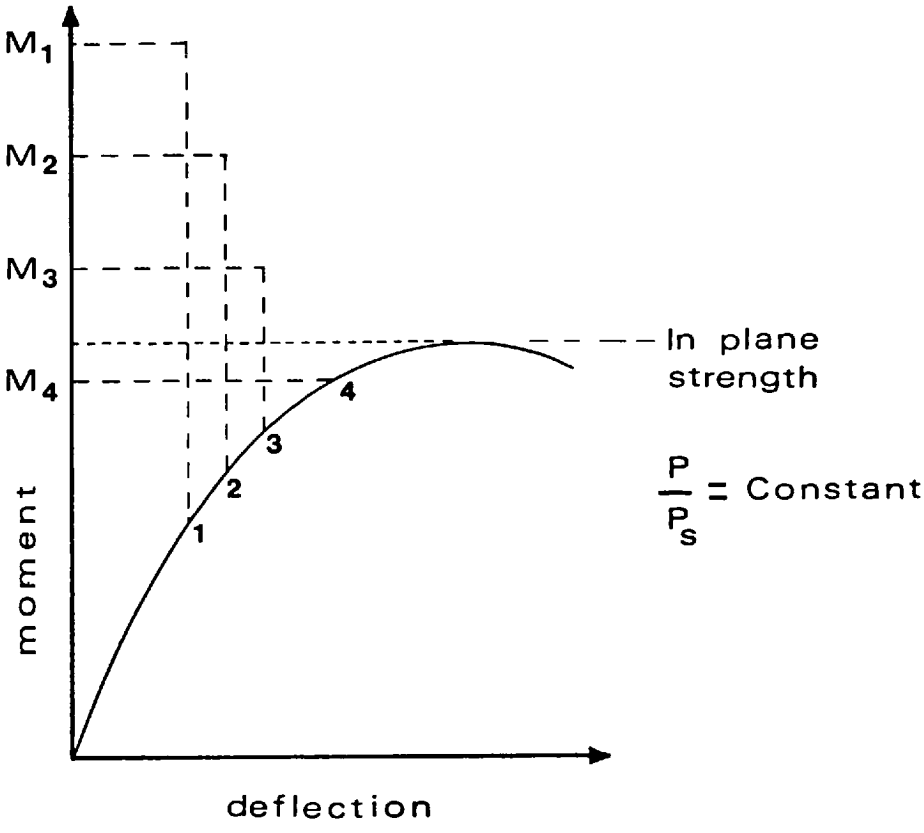


FIG. 7.1b CRITICAL MOMENTS ASSOCIATED WITH IN PLANE BENDING

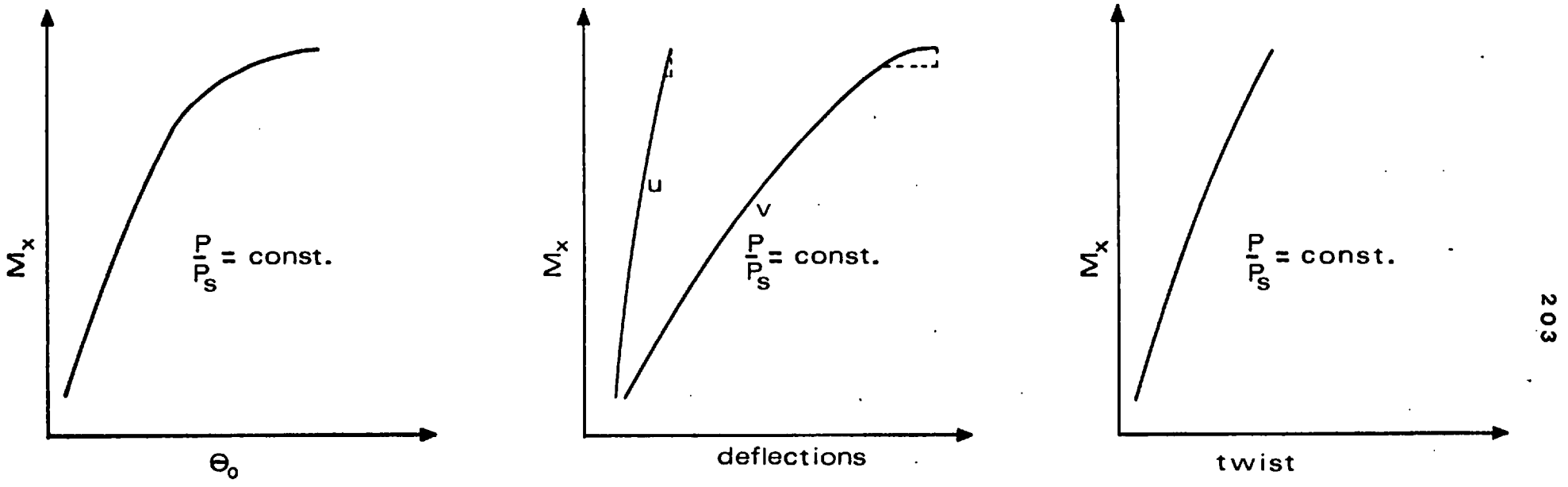


FIG. 7.2 IN PLANE FAILURE CHARACTERISTICS (S/C BENDING)

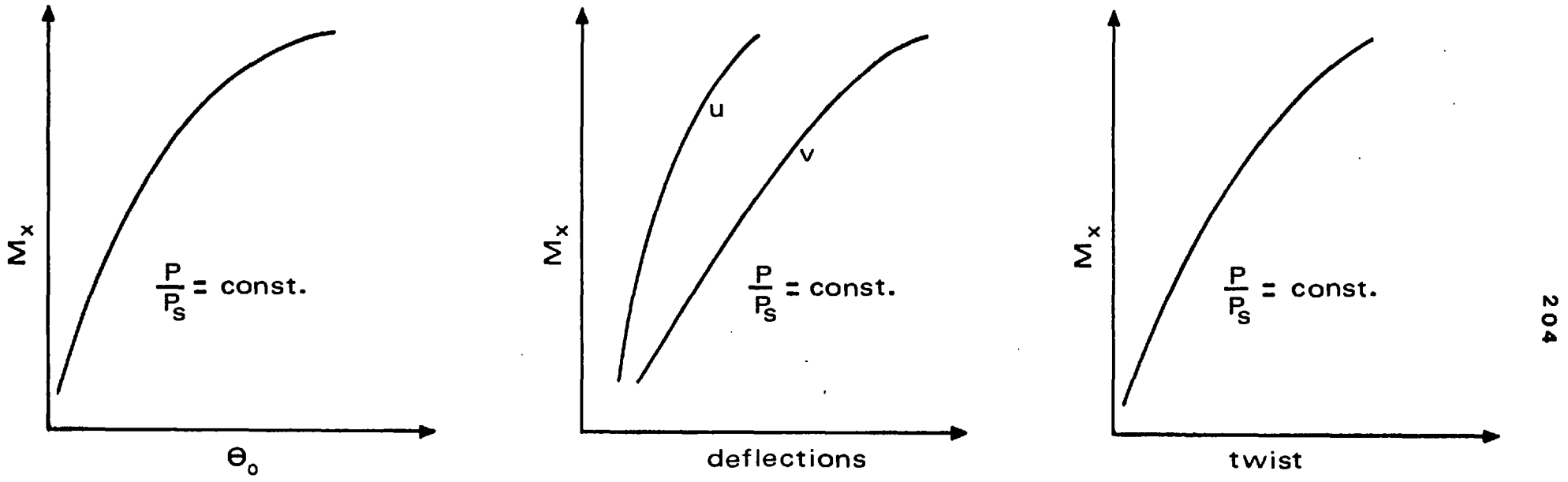


FIG. 7.3 ON THE BOUNDARY OF IN PLANE FAILURE (S/C BENDING)

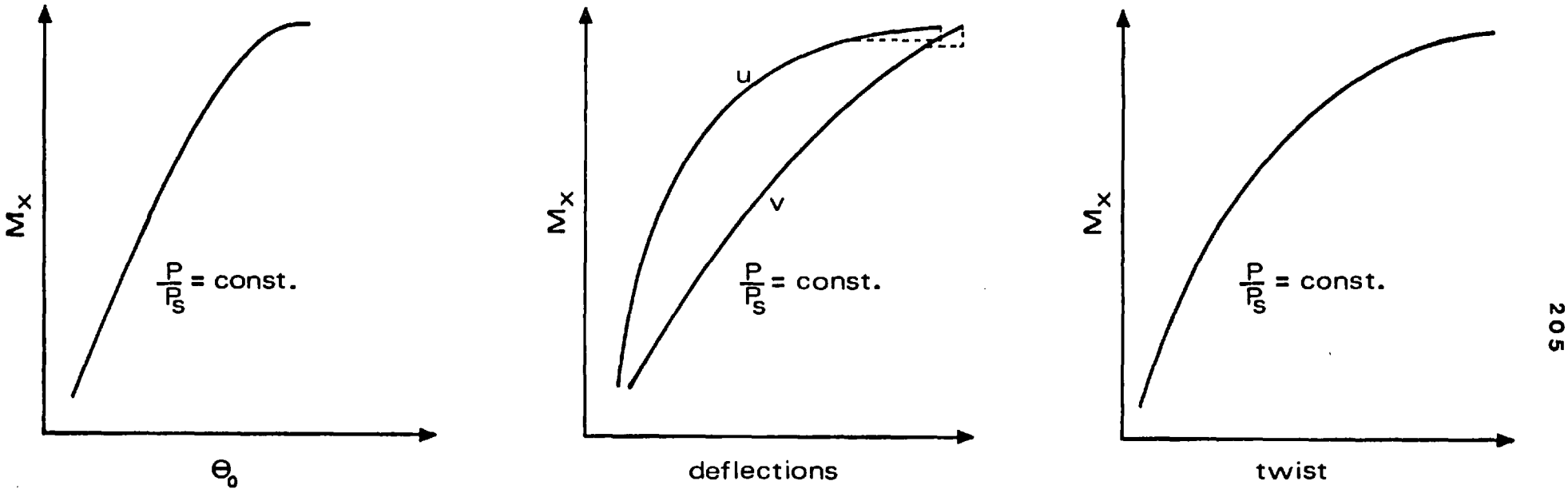


FIG. 7.4 LATERAL TORSIONAL BUCKLING FAILURE CHARACTERISTICS (S/C BENDING)

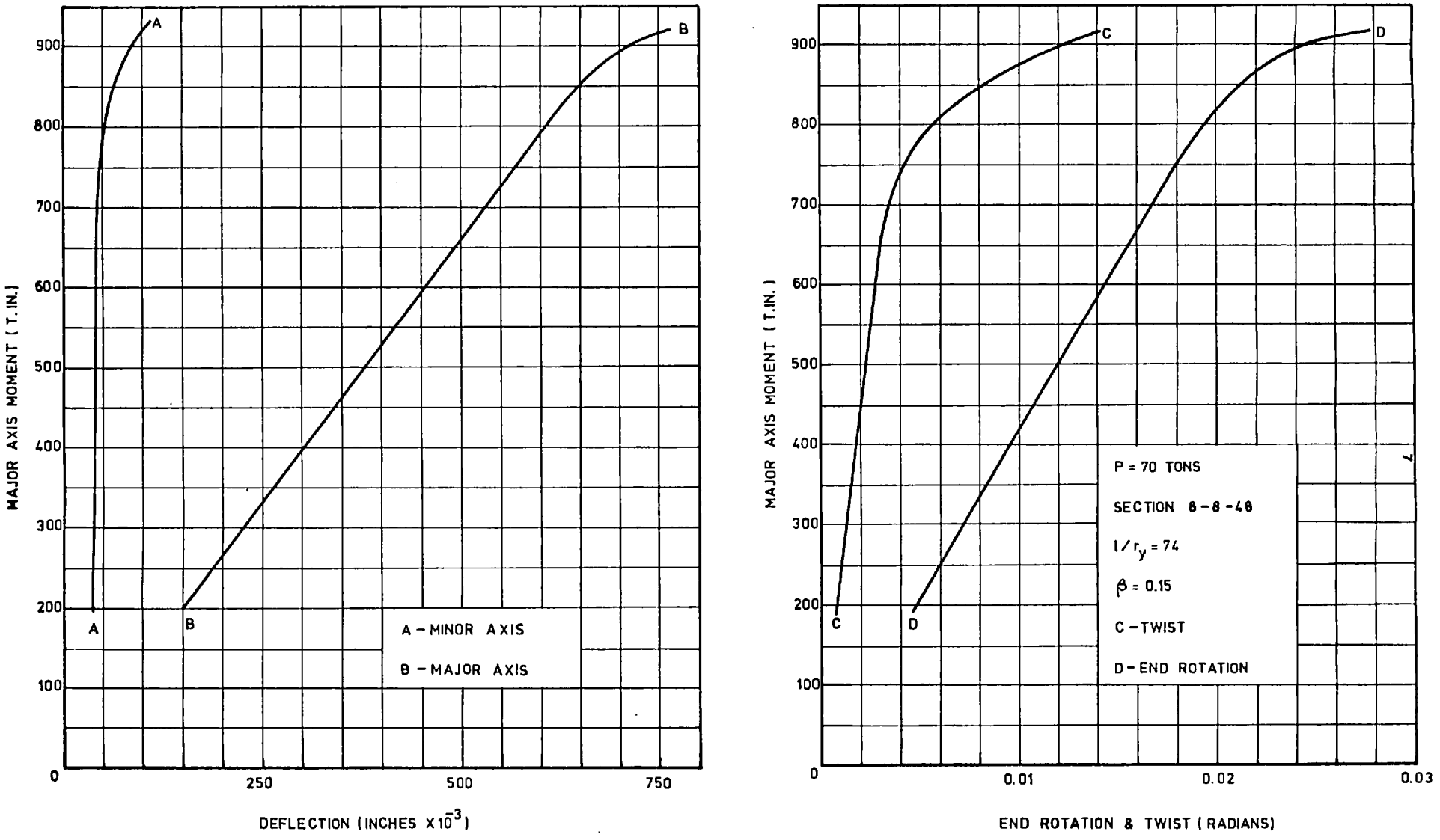


FIG. 7.5 LOAD-DEFLECTION CHARACTERISTICS (PIN ENDED COLUMN)

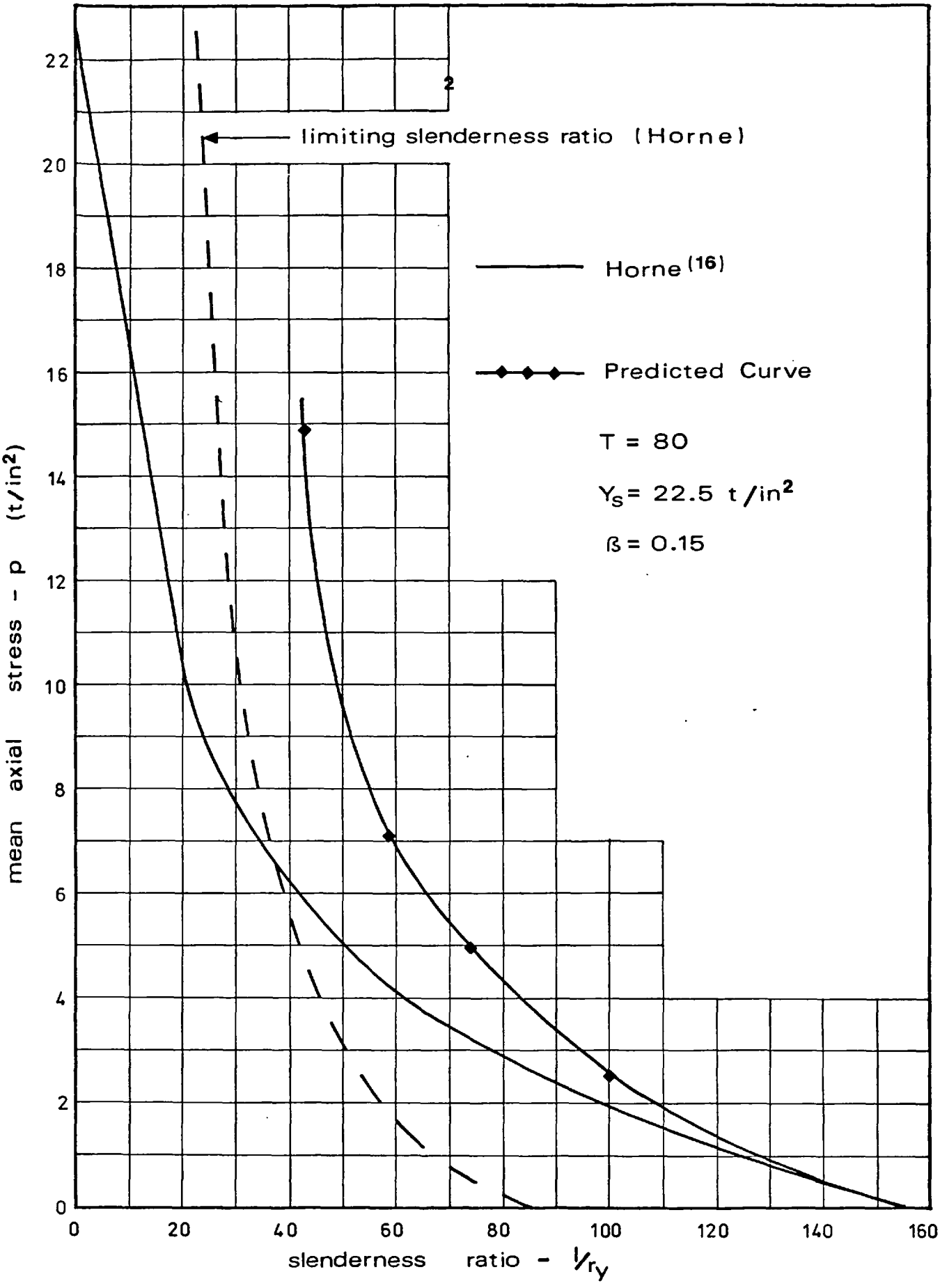


FIG. 7.6 PREDICTED IN PLANE BEHAVIOUR CURVE

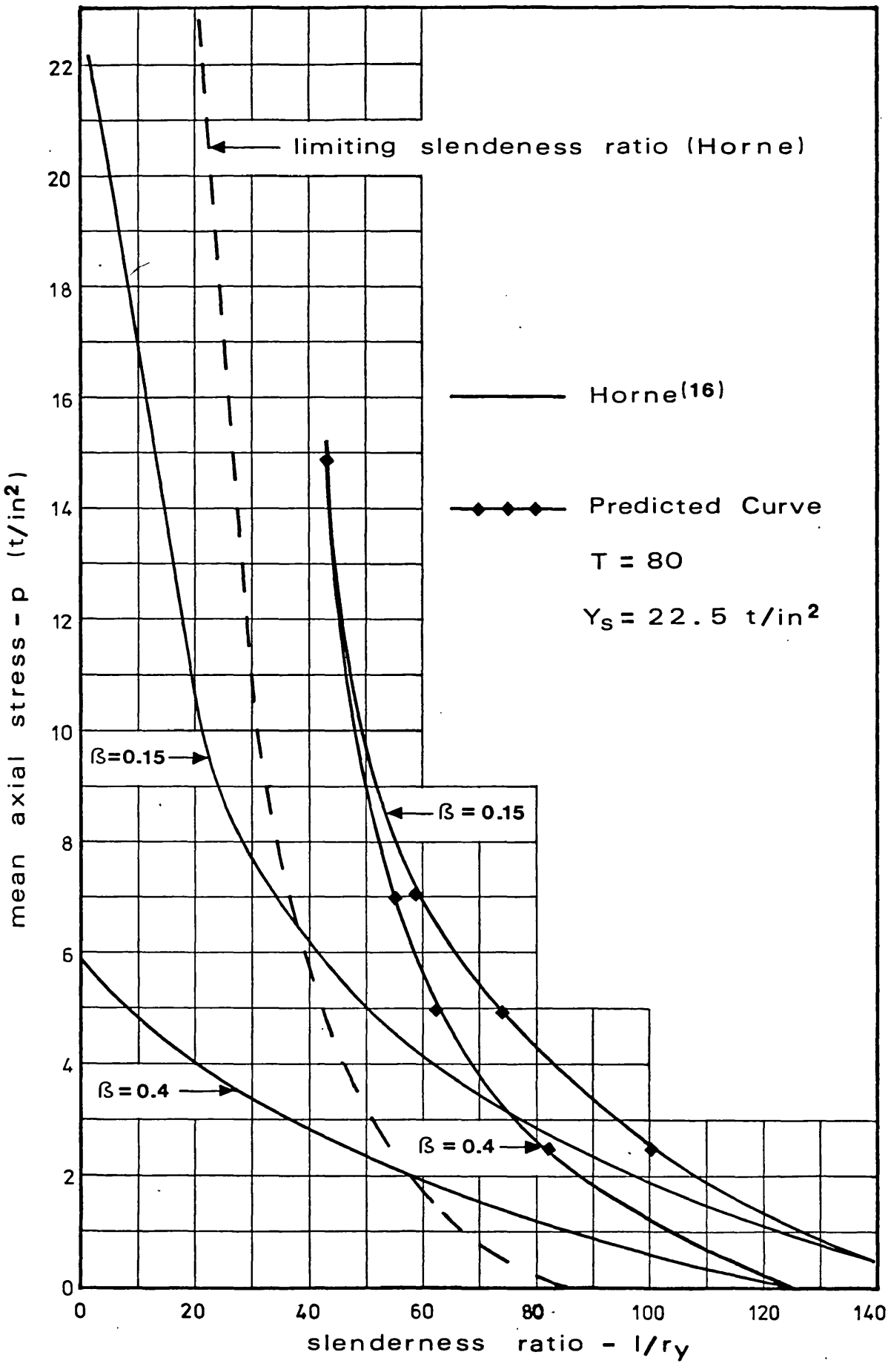


FIG. 7.7 PREDICTED IN PLANE BEHAVIOUR CURVE

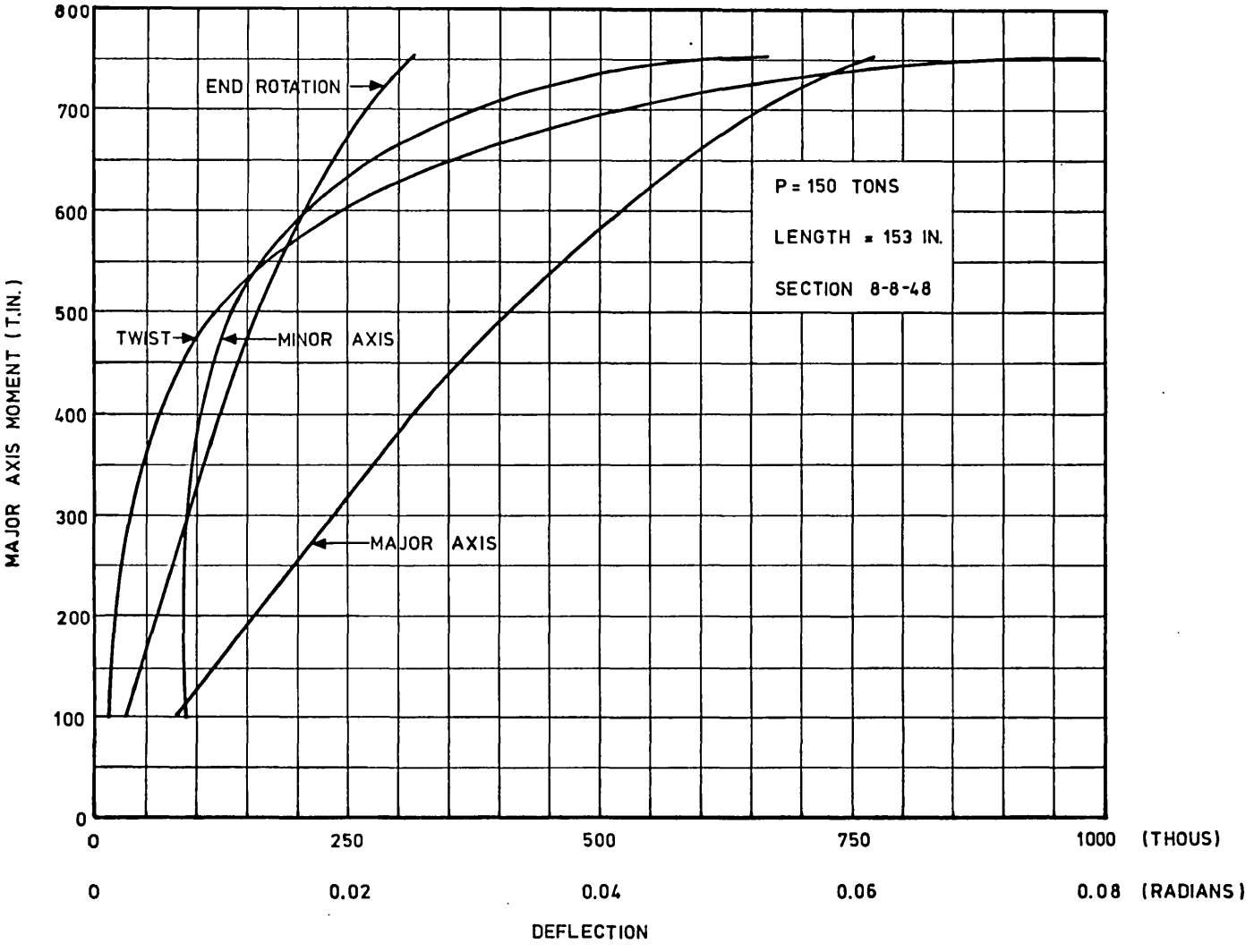


FIG. 7.8 LOAD - DEFLECTION CHARACTERISTICS (PIN ENDED COLUMN)

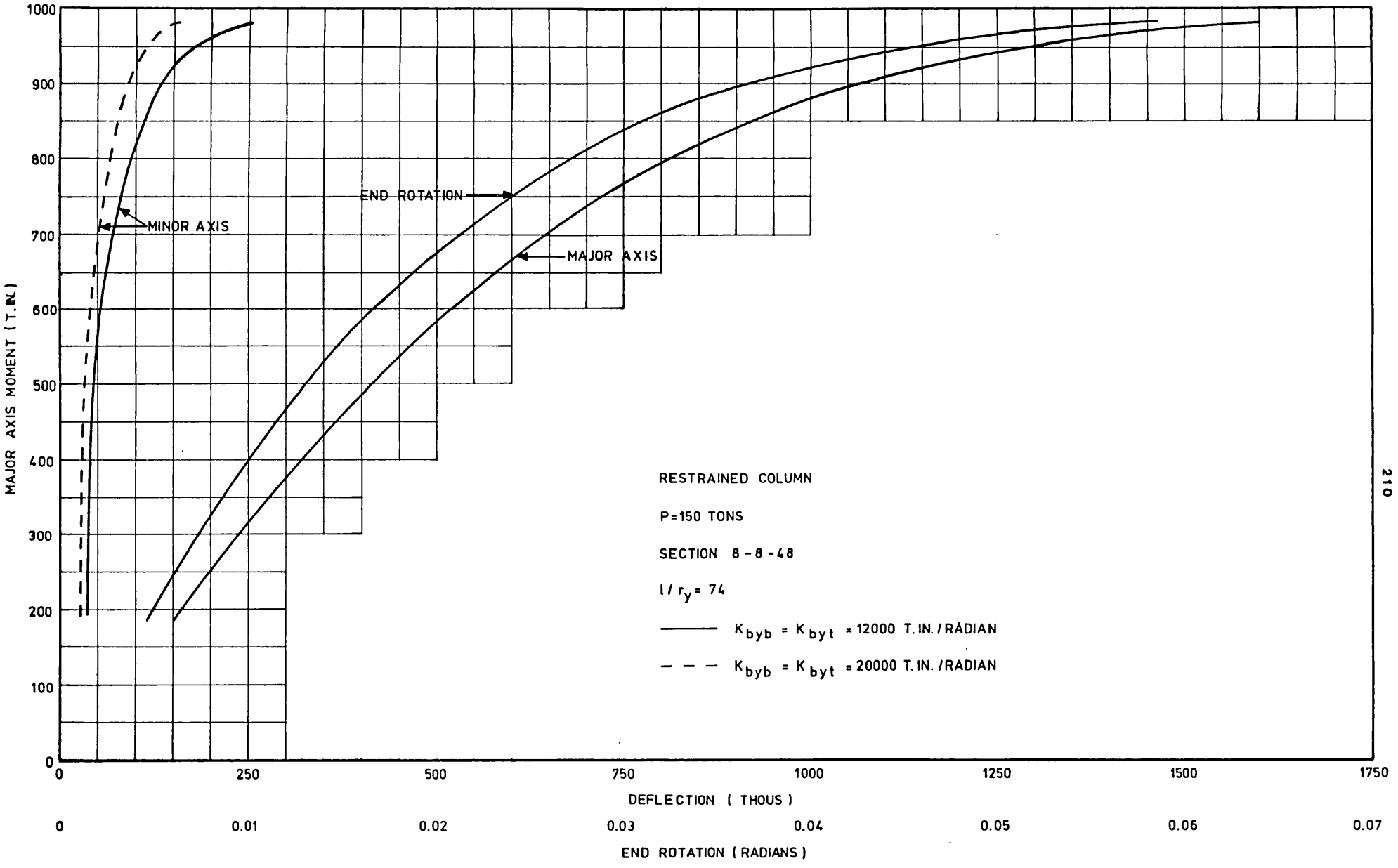


FIG. 7.9 LOAD-DEFLECTION CHARACTERISTICS (RESTRAINED COLUMN)

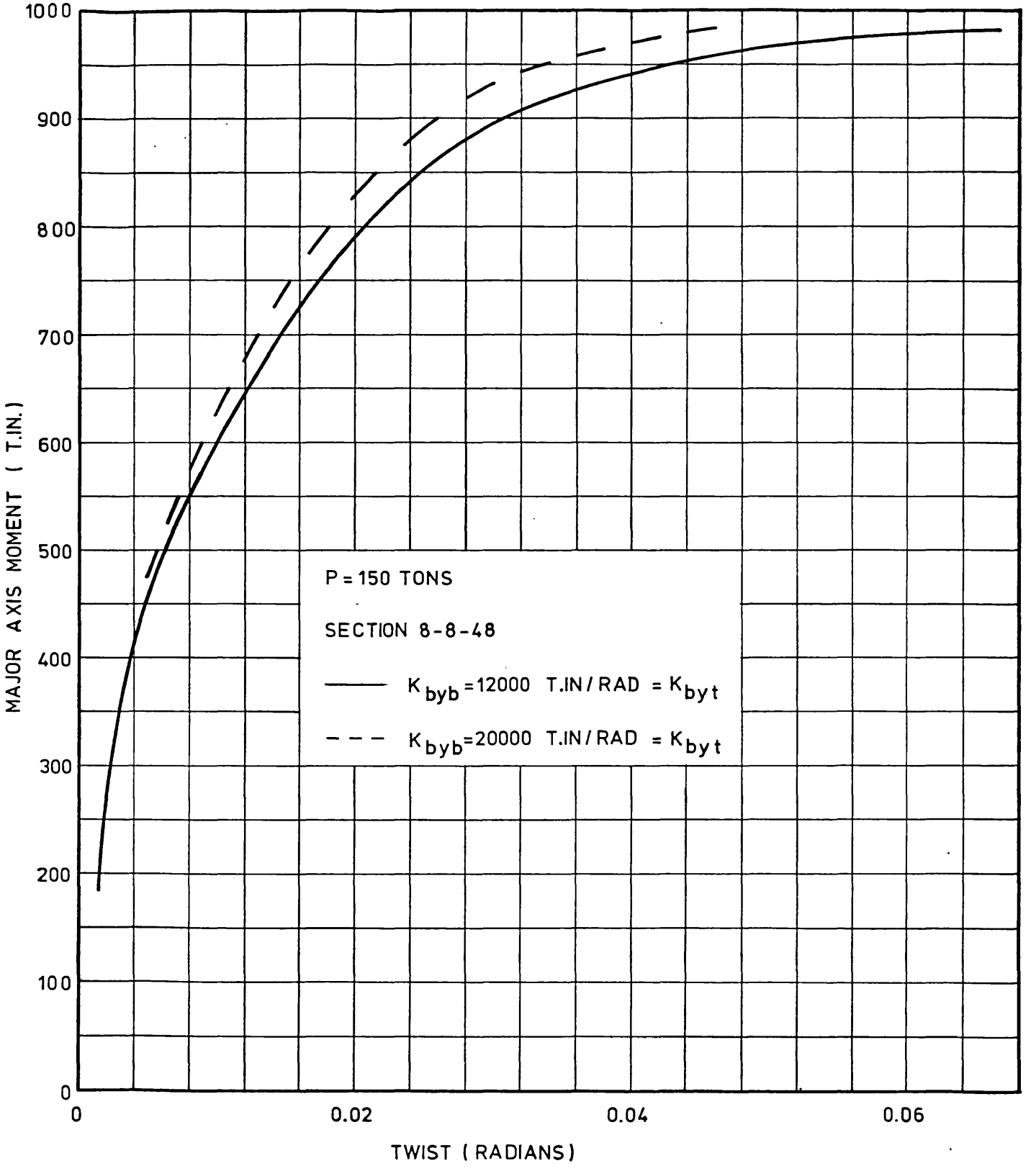


FIG. 7.10 VARIATION OF TWIST WITH MAJOR AXIS MOMENT

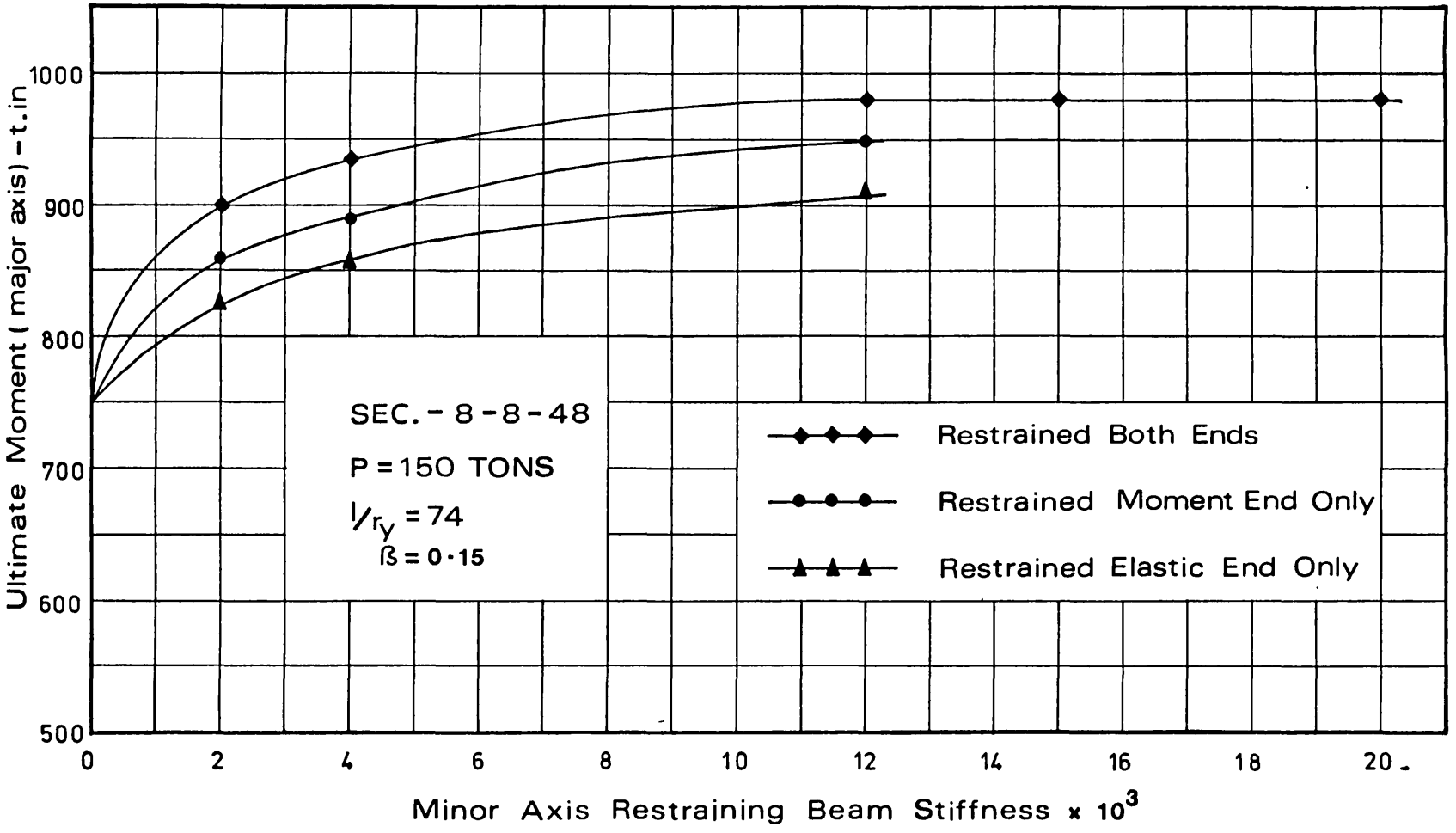
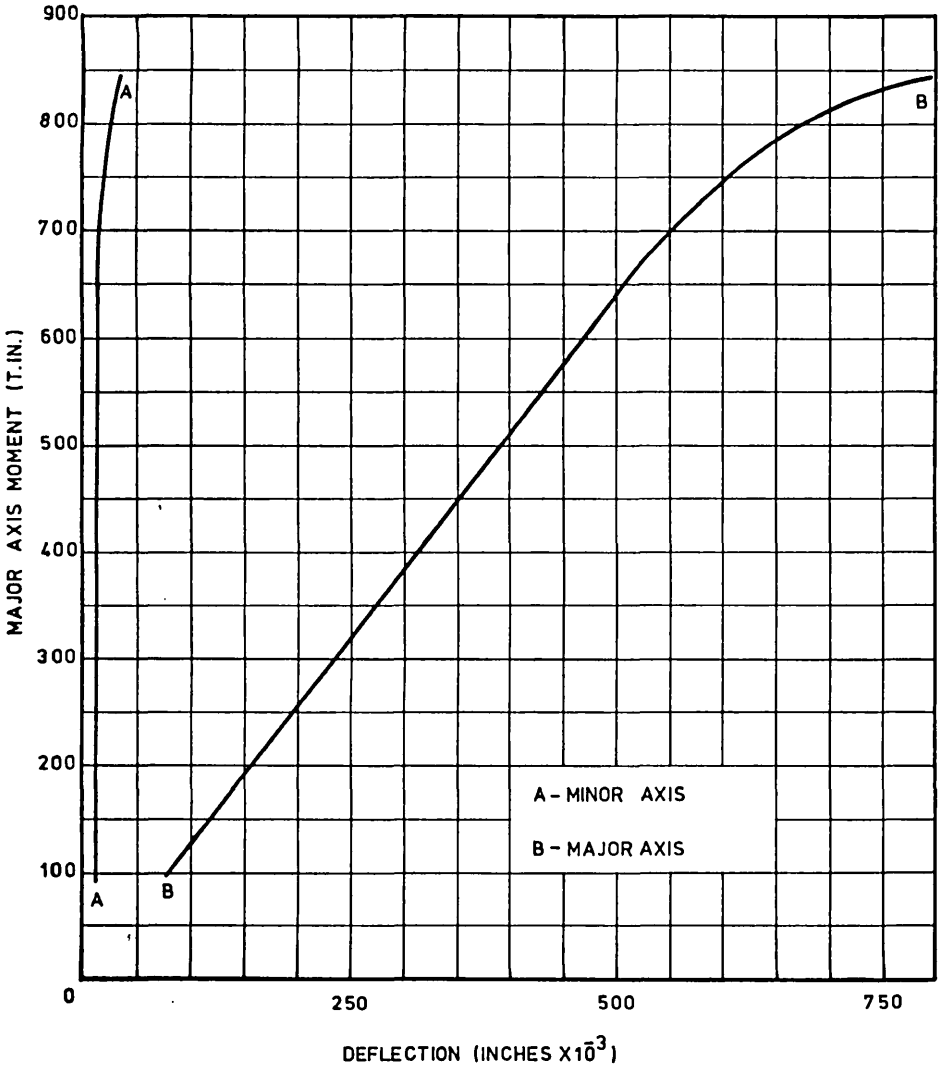


FIG. 7.11 VARIATION OF MAJOR AXIS ULTIMATE MOMENT WITH WEAK AXIS RESTRAINT



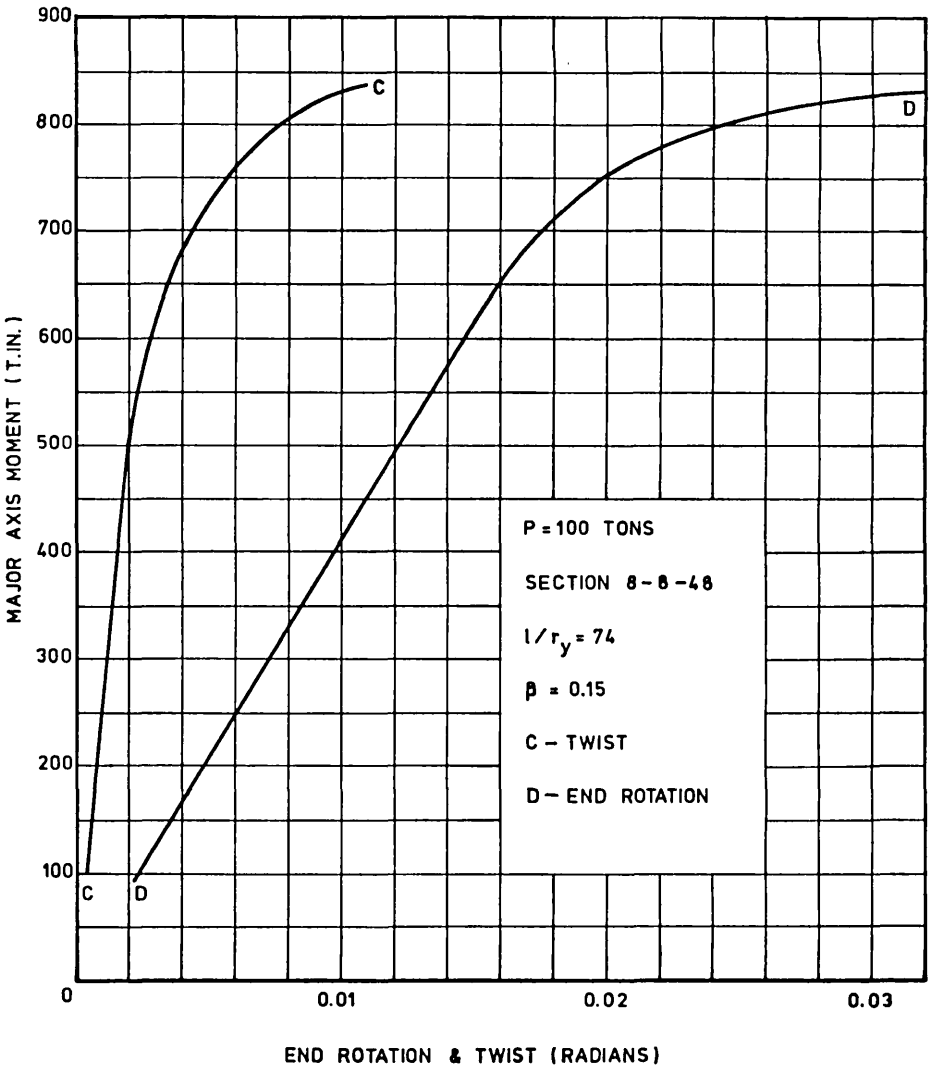


FIG. 7.12 LOAD-DEFLECTION CHARACTERISTICS (RESTRAINED COLUMN)

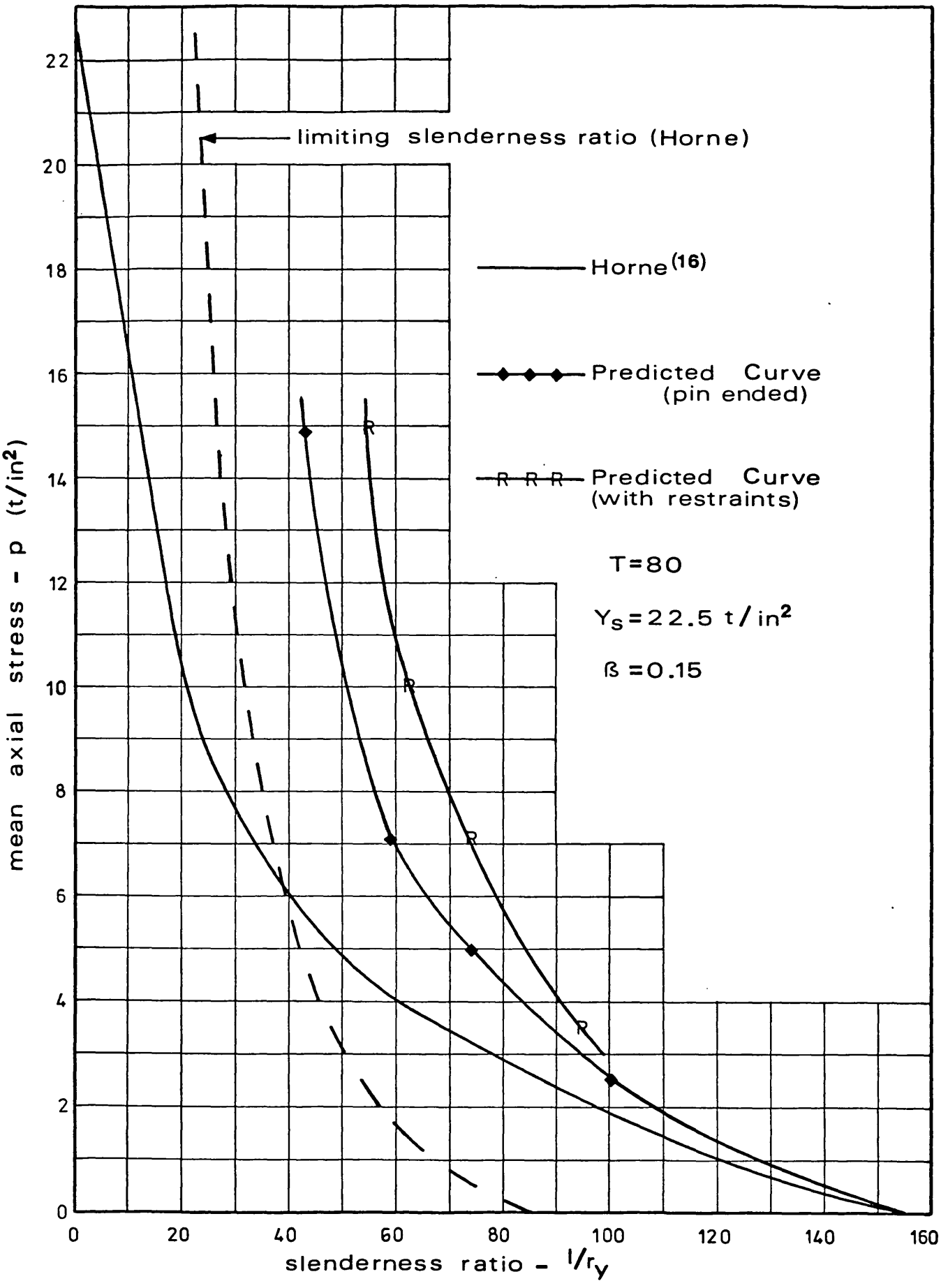


FIG. 7.13 PREDICTED IN PLANE BEHAVIOUR CURVE WITH MINOR AXIS RESTRAINTS

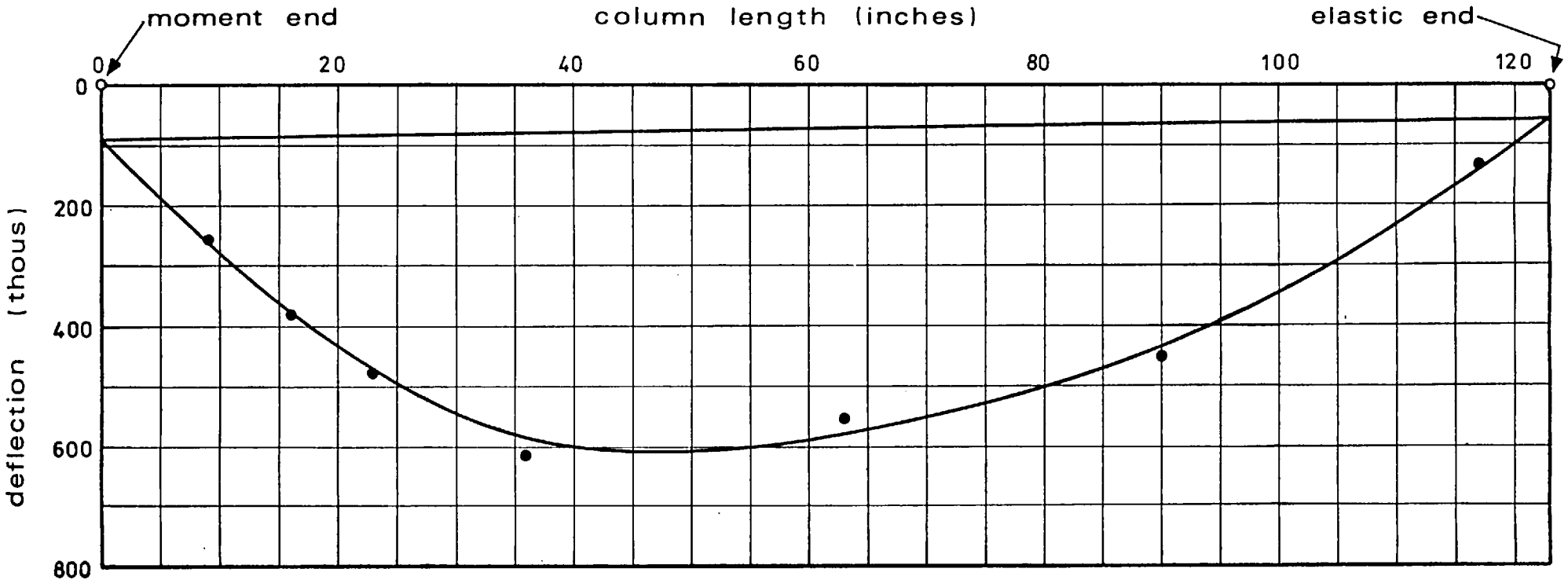


FIG. 7.14 MAJOR AXIS DEFLECTED SHAPE (COLUMN B1)

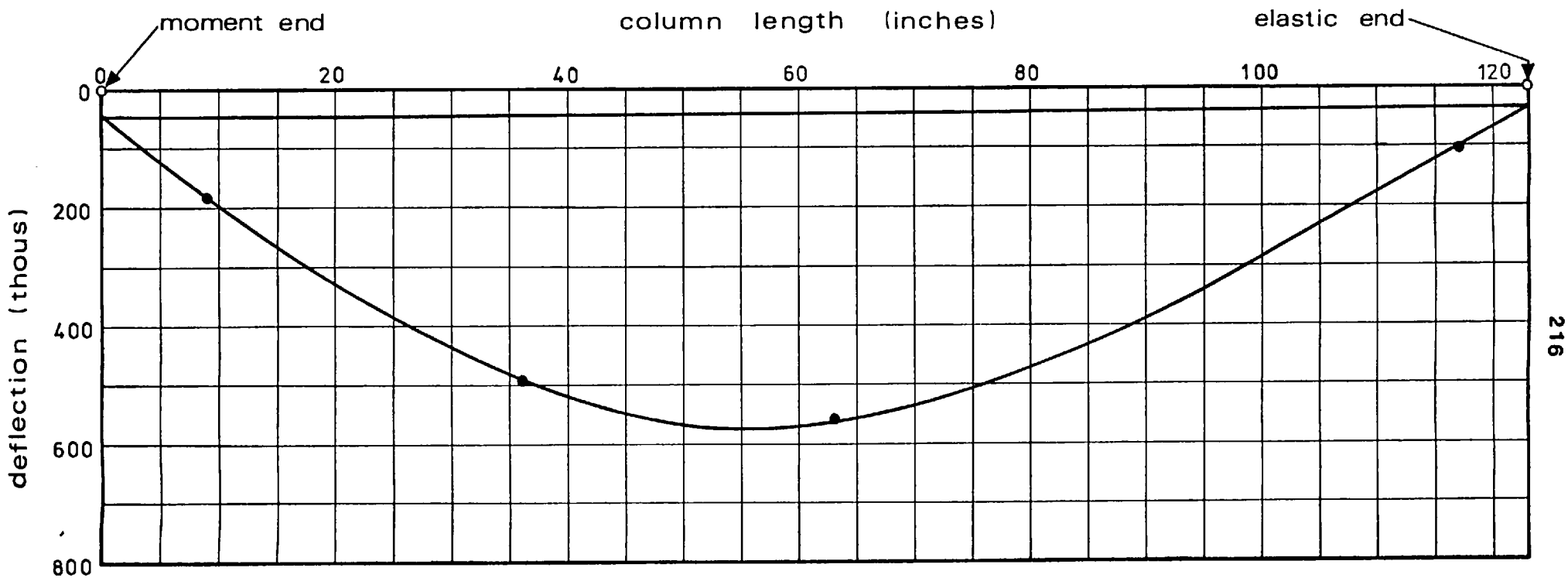


FIG. 7.15 MINOR AXIS DEFLECTED SHAPE (COLUMN B1)